

A Framework for Decentralized Stabilization in Networked Energy Systems: A Passivity-Based Approach

Zur Erlangung des akademischen Grades eines
DOKTORS DER INGENIEURWISSENSCHAFTEN (Dr.-Ing.)
von der KIT-Fakultät für Elektrotechnik und Informationstechnik
des Karlsruher Instituts für Technologie (KIT)
angenommene

DISSERTATION

von
Felix Strehle, M.Sc.
geb. in Aalen

Tag der mündlichen Prüfung:	23. Januar 2024
Hauptreferent:	Prof. Dr.-Ing. Sören Hohmann
Korreferent:	Prof. Dr. Giancarlo Ferrari Trecate

Thanks

To Prof. Hohmann for being an inspiring teacher and introducing a young bachelor student, who had no clue that something like control engineering even existed, to the fascinating world of systems and control. Without your classes, your encouragement to pursue a PhD, and the great support I experienced throughout my time at the IRS, both in professional and personal matters, this journey would not have been possible.

To Prof. Giancarlo “Gianni” Ferrari Trecate for his interest in my work, the fruitful exchanges over the last years, and the assessment of this thesis. Ever since our first meeting at the FEPSET in Champéry back in 2019 with ski lift pitches (and were we made you miss most of an afternoon session – sorry for that!), discussing and working with you has been a pleasant and enriching experience for me.

To the complete IRS team and the NMES group in particular for providing an excellent atmosphere and being more than “just colleagues”. Table soccer, nerdy board game and gaming nights, cooking together, barbecues, race bike tours, hiking, swimming, running, conference trips, traveling together (I probably forgot something) enriched my PhD time with unique experiences beyond systems and control.

To Bertus, Lukas, and Martin for the extraordinary job you did in reviewing this thesis. Further, to Bertus for being an excellent master student, colleague, scientific emergency hotline, occasional host, and friend. To Lukas and Martin for being great supervisors, colleagues, mentors, and friends throughout your IRS times and afterwards.

To Pulkit Nahata for a fruitful collaboration on the AC microgrid topic. To Juan Machado and Michele Cucuzzella for your ideas, your commitment, and the fruitful collaboration over the last two years on the DHN topic. In particular, thank you Juan for providing valuable inspiration and support for Theorem 3.1 and the controllers in Section 6.3.

To my students which supported my research with their passion and great ideas.

To my family for their unconditional support and my friends for complementing my professional life.

To Kathi for your support, your honest feedback, and for providing a positive perspective on things whenever I feel out of options. I am grateful to explore life and the wilderness together with you.

Ulm, November 2023

Abstract

The reliable and secure operation of energy systems is a major cornerstone of modern societies. However, in light of the present strive for a sustainable and climate-neutral energy supply, existing schemes of operating energy systems reach their limits. New operation strategies are required which account for the increasing number of distributed components and more flexible system configurations arising from volatile generation/demand situations and the growing networking between energy systems of different physical domains into networked multi-energy systems.

This thesis presents a new paradigm for the future operation of networked energy systems by providing a passivity-based framework for the decentralized stabilization of voltages, currents, frequencies, pressures, and volume flow rates. The basis of the framework is a unifying system description of various energy systems (DC power systems, AC power systems, district heating networks, and networked multi-energy systems) which combines a graph-based, networked system representation with the domain-unifying modeling approach of port-Hamiltonian systems. The key element and innovation are analytical, equilibrium independent passivity-based conditions that allow to infer asymptotic stability of any feasible networked system equilibrium in a modular manner. Moreover, the conditions are independent of specific technologies, control strategies, and physical domains and thus ensure interoperability between units within and across various networked energy systems. Based on these conditions, decentralized controllers for various energy system actuators (converters, pumps, valves) are developed to asymptotically stabilize desired voltage, current, frequency, pressure, and volume flow rate setpoints. Several case studies validate the theoretical findings and illustrate their advantages. Due to the unifying, decentralized character of the stabilization conditions, the presented framework allows for topology-independent, flexible system configurations in a plug-and-play fashion. In addition, the validity of the stabilization conditions is not limited to the models and controllers proposed in this work. They readily extend to other control solutions, technologies, or altogether new components. This unifying perspective, in particular, paves the way towards realizing holistic system and control solutions for the operation of networked multi-energy systems.

Kurzfassung

Die zuverlässige und sichere Betriebsführung von Energiesystemen ist ein unverzichtbarer Eckpfeiler moderner Gesellschaften. Im Zuge der aktuellen Bestrebungen nach einer nachhaltigen und klimaneutralen Energieversorgung stoßen bestehende Betriebskonzepte jedoch an ihre Grenzen. Insbesondere die steigende Zahl an verteilten Komponenten und flexiblere Systemkonfigurationen, die aus volatilen Erzeugungs-/Verbrauchssituationen sowie aus der zunehmenden Vernetzung von verschiedenen Energiesystemdomänen zu vernetzten Multi-Energiesystemen resultieren, machen neue Betriebsstrategien erforderlich.

Die vorliegende Dissertation präsentiert ein neues Paradigma für den zukünftigen Betrieb vernetzter Energiesysteme basierend auf einem passivitätsbasierten Framework für die dezentrale Stabilisierung von Spannungen, Strömen, Frequenzen, Drücken und Volumenströmen. Grundlage des Frameworks bildet eine vereinheitlichende Systembeschreibung verschiedener Energiesysteme (DC Stromnetze, AC Stromnetze, Fernwärmenetze, vernetzte Multi-Energiesysteme), welche Graphentheorie mit dem generalisierten Modellierungsansatz der port-Hamiltonschen Systeme kombiniert. Die zentrale Innovation und Kernstücke des Frameworks sind analytische, ruhelagenunabhängige Passivitätsbedingungen, welche es erlauben auf modulare Weise Aussagen über die asymptotische Stabilität jeder möglichen Ruhelage eines vernetzten Systems zu machen. Zudem sind die Bedingungen nicht gebunden an Technologien, Regelstrategien oder physikalische Domänen und gewährleisten somit die Interoperabilität zwischen Betriebsmitteln innerhalb verschiedener Energiesysteme sowie über Domänengrenzen hinweg. Ausgehend von den Passivitätsbedingungen werden dezentrale Regler für verschiedene Aktuatoren (Umrichter, Pumpen, Ventile) entwickelt, um gewünschte Spannungs-, Strom-, Frequenz-, Druck- und Volumenstrom-Sollwerte asymptotisch zu stabilisieren. Mehrerer Fallstudien validieren die theoretischen Ergebnisse und veranschaulichen deren Vorteile. Aufgrund des vereinheitlichenden, dezentralen Charakters der passivitätsbasierten Stabilitätsbedingungen ermöglicht das vorgestellte Framework topologieunabhängige, flexible Systemkonfiguration im plug-and-play Stil. Darüber hinaus ist die Gültigkeit der Stabilitätsbedingungen nicht auf die in dieser Arbeit vorgeschlagenen Modelle und Regler beschränkt. Ein Übertrag auf andere Regelungskonzepte, Technologien oder gänzlich neue Komponenten ist problemlos möglich. Diese vereinheitlichende Perspektive bereitet den Weg zur Realisierung ganzheitlicher System- und Steuerungslösungen für den Betrieb vernetzter Multi-Energiesysteme.

Contents

Thanks	I
Abstract	III
Kurzfassung	V
1 Introduction	1
1.1 Research Objective and Contributions	4
1.2 Outline and Notation	5
2 State of Research and Research Questions	9
2.1 Decentralized Stabilization in AC Power Systems	10
2.2 Decentralized Stabilization in DC Power Systems	17
2.3 Decentralized Stabilization in District Heating Networks	21
2.4 Summary	27
3 Methodological Approach	31
3.1 Networked Systems	32
3.2 Equilibrium-Independent Passivity and Stability of Networked Systems ..	33
3.3 Equilibrium-Independent Passivity and Asymptotic Stability of Net- worked Systems Revisited	36
3.4 Equilibrium-Independent Passivity of Port-Hamiltonian Systems	41
4 Passivity-Based Decentralized Stabilization in DC Power Systems	45
4.1 Modeling	46
4.2 Asymptotic Stability Conditions and Control Problems	51
4.3 Passivity-Based Control Design	57
4.4 Simulation	66
4.5 Discussion	74
4.6 Summary and Contributions	77
5 Passivity-Based Decentralized Stabilization in AC Power Systems	79
5.1 Modeling	80
5.2 Asymptotic Stability Conditions and Control Problems	88
5.3 Passivity-Based Control Design	97
5.4 Simulation	106

5.5	Discussion	120
5.6	Summary and Contributions	124
6	Passivity-Based Decentralized Stabilization in District Heating Networks	127
6.1	Modeling	128
6.2	Asymptotic Stability Conditions and Control Problems	143
6.3	Passivity-Based Control Design	149
6.4	Simulation	156
6.5	Discussion	162
6.6	Summary and Contributions	164
7	Towards a Unifying Framework for Decentralized Stabilization in Networked Multi-Energy Systems	167
7.1	Modeling	167
7.2	Stability and Decentralized Stabilization	168
7.3	Asymptotic Stability Conditions	170
7.4	Summary and Contributions	172
8	Conclusion	173
A	Appendices to Chapter 3	177
B	Appendices to Chapters 4 and 5	183
C	Appendices to Chapter 6	189
	Abbreviations and Symbols	194
	List of Figures	201
	List of Tables	203
	References	205
	List of Publications and Supervised Theses	221

1 Introduction

The reliable and secure operation of energy systems is a major cornerstone of modern societies. Over the last decade, policy makers and governments around the globe have set out agendas for a transition towards a sustainable and climate neutral energy supply (see for example He et al. [2020], International Energy Agency [2020], Council and Parliament of the European Union [2021], Parliament of Canada [2021], Deutscher Bundestag [2022], and United States Congress [2022]). This transition is resulting in unprecedented changes in the energy systems and poses fundamental challenges to their operation. Particularly the pervasive integration of distributed renewable energy sources (RESs) into electrical power systems and district heating networks (DHNs) is significantly changing the network structures, system behavior, and system dynamics [Lund et al., 2018; Dörfler and Groß, 2023].

In order to ensure a cost-efficient integration of RESs and the best possible system utilization while retaining a reliable and secure energy supply, it has been widely acknowledged that a higher degree of automation is required with novel operation strategies [Lund et al., 2014; Dörfler et al., 2019; O'Malley et al., 2020; Novitsky et al., 2020; Osiadacz and Chaczykowski, 2020]. In principle, such operation strategies can be broken down into two main tasks: Firstly, the fundamental system variables, i.e., voltages, currents, frequency, pressures, and volume flow rates need to be *stabilized*. This stabilization *forms the grid* over which some flows of energy can then be established.¹ Secondly, generation, transmission, and consumption of energy have to be *coordinated* such that the desired amount of energy is provided in the right place at the right time within the operational constraints and in an economically efficient manner.²

Traditionally, both tasks are organized hierarchically with the stabilization at the lowest control layer serving as the necessary precondition for a subsequent coordination at higher control layers [Gómez-Expósito et al., 2018, p. 380ff.]; [Novitsky et al., 2020; Zhang et al., 2021]; [Kölsch, 2022, Section 2.3]. However, in light of the ongoing energy transition, practical evidence indicates that established stabilization schemes and guarantees become void.

Most notably, this circumstance can be seen in power systems where large, centralized generation plants comprising synchronous machines, considerable rotating masses, and predictable power generation are being replaced by smaller, converter-interfaced, distributed generation units (DGUs) without rotating masses and intermittent power

¹ Formal definitions for decentralized stabilization in electrical power systems, DHNs, and NMESs will be provided in Sections 2.1, 2.2, 2.3, and 7.2.

² See Gómez-Expósito et al. [2018, p. 374ff.], Novitsky et al. [2020], and Nussbaumer et al. [2020, p. 44ff] for more information on energy system operation strategies.

generation. As a consequence, power systems are becoming more distributed with higher numbers of interacting units and are exhibiting increasingly time-varying network topologies. Furthermore, the resulting reduction of rotating masses leads to a reduction of their naturally stabilizing effects on power systems and an increased sensitivity to contingencies [Milano et al., 2018; Dörfler et al., 2019]. On the other hand, compared to synchronous machines, converters are freely configurable actuators with fast dynamics that allow for a wide range of new operation strategies [Milano et al., 2018; Dörfler et al., 2019]. However, if not carefully designed and controlled, converters can exhibit undesired interactions that destabilize power systems (see the discussions in Milano et al. [2018], Farrokhhabadi et al. [2020], Hatziargyriou et al. [2021], and Liu et al. [2022]). The consequences of these developments towards converter-based power systems are, for example, reflected in the increasing costs for grid and system security measures, which include grid stabilizing measures. Over the last decade, they have risen in Germany from around 0.5 billion euro in 2013 to around 4.25 billion euro in 2022 [Bundesverband der Energie- und Wasserwirtschaft, 2023].

From a systems and control perspective, the above developments and challenges point out two main requirements for future power system stabilization:

- The large number of interacting units along with the intermittent nature of RESs call for novel power system stabilization methods that are scalable and allow for flexible system configurations. In other words, it should be possible to easily add or remove subsystems without adapting other controllers, without requiring communication, and without endangering stability—a feature which is commonly referred to in the power system literature as *plug-and-play* capability [Lasseter, 2001; Rivero et al., 2015; Tucci and Ferrari-Trecate, 2020]. From a control engineering perspective, such plug-and-play capabilities are inherently provided by *decentralized* controllers relying only on local information (see Lunze [1992, Figure 1] and Meng et al. [2017, Figure 2]).³
- In addition to increasing numbers of units, the variety of technologies and control strategies that are deployed in power systems is increasing as well. Together with more flexible system configurations, this creates the need to develop not only scalable, decentralized stabilization methods, but in fact aim for a general framework with analytical conditions that ensures decentralized stabilization in power systems across different technologies and control strategies, i.e., interoperability (see also the recent review by Dörfler and Groß [2023]).

Interestingly, similar development trends, challenges, and stabilization requirements can be identified for DHNs. As central element of the sustainable energy transition, DHNs are also undergoing a large-scale integration of distributed RESs such as heat pumps, combined heat and power, waste/biomass-to-energy, solar, and geothermal heat

³ Historically, plug-and-play capability with setpoint offsets has already been provided at power system transmission level by local, i.e., decentralized, control of synchronous machines (droop control). However, it appears that simply transferring established schemes to converter-interfaced units at distribution level does not preserve the plug-and-play feature (see Sections 2.1.1 and 2.2.1 for a detailed discussion).

plants [Lund et al., 2014; Vandermeulen et al., 2018]. Additionally, DHNs increasingly feature intermittent in-feed of excess energy from wind and solar power plants, which cannot be accommodated by the power system. Consequently, similar to power systems, DHNs are starting to exhibit more distributed, flexible system configurations with large numbers of interacting units and an intermittent heat supply. Furthermore, renewable heat sources interface to DHNs via a variety of hydraulic interfaces that comprise freely configurable actuators with fast dynamics, viz. pumps and control valves. Similar to converters, pumps and control valves, if not carefully designed and controlled, can exhibit undesired, destabilizing interactions leading for example to pronounced pressure oscillations [Stræde, 1995; Boysen and Thorsen, 2003; Wang et al., 2017a; Sommer et al., 2019]. Recently, it has also been shown by Lennermo et al. [2014, 2019] that apparent malfunctions of higher-level controllers, which coordinate the thermal power in-feed of distributed heat generation units (DGUs), can in fact be traced back to insufficient hydraulic stabilization, i.e., oscillating network pressures and an insufficient pump control. Thus, following the above argumentation for power systems, there is a similar need to develop a decentralized stabilization framework for DHNs that ensures interoperability across different hydraulic technologies and control strategies by means of analytical design conditions.

In addition to these domain-specific perspectives and needs, there is a broad consensus emerging across different professional disciplines and social groups that aiming for a further networking between energy systems towards integrated, networked multi-energy systems (NMESs) is desirable as it offers technical, economical, strategical, and societal advantages (see for example Geidl [2007], Federal Ministry for Economic Affairs and Energy [2018], O'Malley et al. [2020], Chicco et al. [2020], and The European Commission [2020]).⁴ From systems theory, it is well-known that such an additional networking in general complicates the stabilization problem and thus requires a detailed analysis. In fact, it has been shown by Schäfer et al. [2022] based on the works of Braess et al. [2005] that the widespread assumption of network expansion serving as a universal tool for the energy transition is inherently flawed. Counter-intuitively, network expansion may even reduce system performance.

Thus, besides the need for decentralized, cross-technology stabilization frameworks in individual energy system such as power systems and DHNs, it is desirable to explore the possibilities of decentralized stabilization frameworks that provide interoperability also across different energy system domains.

⁴ Among other things, these advantages comprise robustness and social acceptance due the efficient reuse of existing infrastructure, a more resilient and secure overall energy supply, an overall operational optimization potential at regional/urban level, cost efficiency, the reduction of external dependencies, the strengthening of the competitiveness of national economies as technology leaders, and new market designs with greater consumer empowerment.

1.1 Research Objective and Contributions

The main objective of this thesis is to **develop cross-technology frameworks for the decentralized stabilization in various networked energy systems.**

Apart from decentralized stabilization solutions for power systems, which have been extensively studied in the literature, the problem of decentralized stabilization in DHNs and NMESs as well as unifying, technology-independent stabilization concepts for power systems, DHNs, and NMESs have scarcely been considered. In particular, there exist no decentralized stabilization frameworks that provide analytical, decentralized design conditions ensuring interoperability of different technologies and control strategies within individual energy systems (power systems, DHNs) and across domain borders (NMESs). Motivated by the above-outlined leading role of power systems and DHNs in the sustainable energy transition, the main developments of the thesis will concentrate on electrical DC and AC power systems with converter-interfaced DGUs as well as DHNs. Additionally, first results will be provided on how the findings from electrical power systems and DHNs can be transferred to NMESs.

In a broad sense, the thesis at hand makes the following contributions:

1. Generalized, domain-unifying modeling of networked energy systems:
The development of comprehensive system models for DC power systems, AC power systems, and DHNs. In particular, the models are presented in a generalized form which combines a graph-based, networked system representation with the domain-unifying modeling approach of port-Hamiltonian systems (PHSs). This allows to highlight similarities between the different energy systems and paves the way for a generalized system-theoretical treatment and analysis of NMESs. The results of this thesis are the first to adopt such a generalized perspective in an energy system context and project the generalized effort-flow modeling paradigm onto various networked energy systems.
2. Decentralized, technology- and domain-independent stability conditions:
The development of a decentralized, passivity-based asymptotic stability theorem for general networked system equilibria. In contrast to the results that straightforwardly can be deduced from the literature and whose application to practical problems is severely limited by their strict passivity requirements, the developed theorem allows for relaxed passivity properties (see Chapter 3 for more details). The application of this theorem to DC power systems, AC power systems, DHNs, and NMESs provides decentralized asymptotic stability conditions. Due to their generalized nature, these conditions ensure—independent of specific technologies, control strategies, or physical domains—asymptotic stability of the fundamental system variables (voltages, currents, frequency, pressures, volume flow rates).
3. Parameter specifications and decentralized component controllers:
The development of parameter specifications and decentralized converter, pump,

and valve controllers that ensure the established, decentralized asymptotic stability conditions are met and setpoints with desired voltage, current, frequency, pressure, and volume flow rate values are asymptotically stabilized.

1.2 Outline and Notation

In order to ensure clarity and readability, the outline and notation of the remainder of this thesis are provided in the following.

Outline **Chapter 2** reviews the state of the art as well as emerging trends and challenges regarding the stability and stabilization of AC power systems, DC power system, and DHNs. A special focus is set on works that promote cross-technology, decentralized stabilization concepts. At the end of each section, a discussion of the main insights from the literature review reveals existing gaps and leads to corresponding research questions that are to be addressed in the remainder of this thesis.

Chapter 3 lays the methodological foundation for the passivity-based, decentralized stabilization frameworks put forth in this thesis. Firstly, to allow for a clear, concise presentation of the technical contents and provide the basis for a unifying system description of power systems, DHNs, and NMESs, the notion of an autonomous, networked system is introduced. Subsequently, based on equilibrium-independent passivity (EIP), a general theorem is developed which provides decentralized, sufficient conditions for the asymptotic stability of any feasible equilibrium of such an autonomous, networked system. Finally, the main class of models that is used throughout this thesis, viz. explicit state-space models in input-state-output PHS (ISO-PHS) form, is introduced and its EIP properties are analyzed. Due to their port-based perspective and inherent passivity properties, such PHS models provide a natural starting point for an EIP-based control synthesis and stability analysis of autonomous, networked systems. Additionally, they allow for a generalized, domain-unifying modeling of various networked energy systems.

The specific contributions for the respective energy systems together with validating simulations are elaborated in **Chapter 4** (DC power systems), **Chapter 5** (AC power systems), and **Chapter 6** (DHNs). In each case, a generalized, graph-based model of the energy system in question is presented. Subsequently, decentralized, asymptotic stability conditions are derived by application of the main theorem established in Chapter 3. Finally, parameter specifications for the unactuated subsystems are established and appropriate controller designs for the actuated subsystems are performed to ensure that the previously derived decentralized stability conditions are met.

Chapter 7 combines the insights from the individual energy systems to lay the foundation for a unifying, technology- and domain-independent, decentralized stabilization

framework for integrated NMESs. Definitions for the terms *stability* of and *decentralized stabilization* in NMESs are provided together with decentralized conditions for the asymptotic stability of any feasible NMES equilibrium. This paves the way for the future design of decentralized stabilization solutions in NMESs.

Finally, **Chapter 8** closes the thesis with a conclusive statement on the presented contributions and possible next steps.

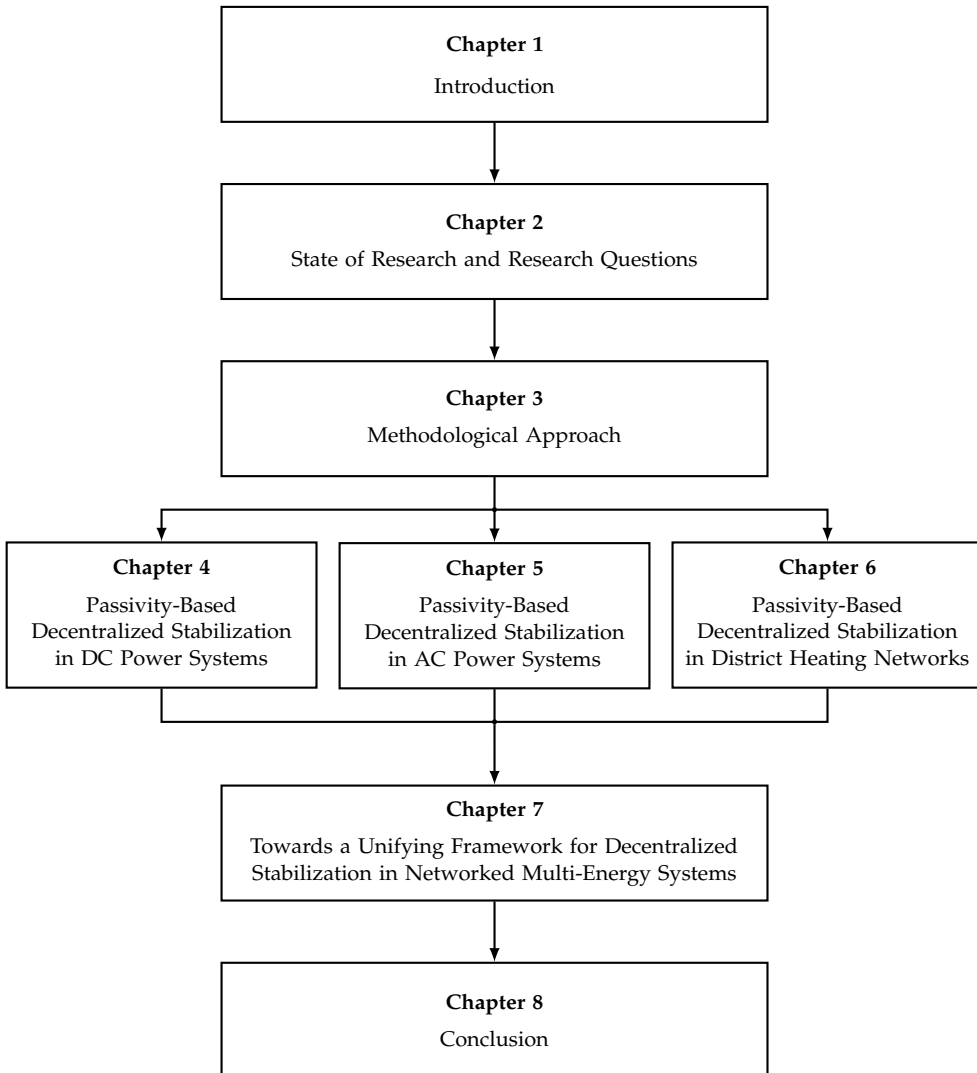


Figure 1.1: Outline of this thesis

Notation The sets of natural and real numbers are denoted by \mathbb{N} and \mathbb{R} , respectively. The sets of positive and strictly positive real numbers are denoted by $\mathbb{R}_{\geq 0}$ and $\mathbb{R}_{> 0}$, respectively. All other sets and spaces are written either in blackboard bold or calligraphic font. The cardinality of a set \mathcal{V} is denoted by $|\mathcal{V}|$. Set subtraction is denoted by “\”, e.g., $\mathbb{R} \setminus \{0\}$ is the set of real numbers without zero.

Vectors and matrices are written in bold font lowercase and uppercase letters, respectively. Let $\mathbf{x} \in \mathbb{R}^n$ be an n -dimensional (column) vector and $\mathbf{A} \in \mathbb{R}^{n \times m}$ be a matrix with n rows and m columns. $\mathbf{0}_n$ and $\mathbf{1}_n$ are n -dimensional vectors of zeros and ones, respectively. Accordingly, $\mathbf{0}_{n \times m}$ is an $n \times m$ matrix of zero entries and \mathbf{I}_n the identity matrix of order n . The transpose of any vector or matrix is denoted by $(\cdot)^\top$. The inverse of a matrix \mathbf{A} , if it exists, is denoted by \mathbf{A}^{-1} . $\mathbf{A} \succ 0$ denotes a positive definite and $\mathbf{A} \succcurlyeq 0$ a positive semidefinite matrix. Conversely, $\mathbf{A} \prec 0$ and $\mathbf{A} \preceq 0$ denote a negative definite and negative semidefinite matrix, respectively. Given $\mathbf{x} \in \mathbb{R}^n$, $\text{diag}(\mathbf{x}) \in \mathbb{R}^{n \times n}$ denotes a diagonal matrix with the elements of \mathbf{x} on the diagonal. The Kronecker product between two matrices \mathbf{A} and \mathbf{C} is denoted by $\mathbf{A} \otimes \mathbf{C}$. The Euclidean norm of a vector \mathbf{x} is given by $\|\mathbf{x}\|$, whereas $\|\mathbf{x}\|_Q$ denotes the Euclidean norm of \mathbf{x} weighted by a symmetric, positive definite matrix \mathbf{Q} , i.e., $\|\mathbf{x}\|_Q = \mathbf{x}^\top \mathbf{Q} \mathbf{x}$. The stacking (concatenation) of some vectors \mathbf{x}_i for all $i \in \mathcal{V}$ is denoted by $\mathbf{x}_\mathcal{V} = \text{stack}(\mathbf{x}_i)_{i \in \mathcal{V}}$.

The notation \bar{x} or $\bar{\mathbf{x}}$ denotes any variable x or vector \mathbf{x} in steady state, whereas x^* or \mathbf{x}^* denotes a desired setpoint or vector of setpoints that is to be established in steady state.

A finite digraph is denoted by $\mathcal{G} = (\mathcal{V}, \mathcal{E})$ with nodes (vertices) \mathcal{V} and edges $\mathcal{E} \subset \mathcal{V} \times \mathcal{V}$. All digraphs in this work are assumed to be without self loop, i.e., for $i \in \mathcal{V}$ it holds that $(i, i) \notin \mathcal{E}$. The incidence matrix $\mathbf{B} \in \mathbb{R}^{|\mathcal{V}| \times |\mathcal{E}|}$ of graph \mathcal{G} is defined by

$$b_{il} = \begin{cases} +1 & \text{if node } i \text{ is the target of edge } l, \\ -1 & \text{if node } i \text{ is the source of edge } l, \\ 0 & \text{otherwise.} \end{cases} \quad (1.1)$$

To provide a clear and intuitive presentation throughout Chapters 4 to 6, the domain-specific variables, i.e., voltages, currents, pressures, and volume flow rates, are used instead of generalized effort and flow variables. However, one can straightforwardly replace the domain variables with their generalized counterparts (see Table A.1) to obtain generalized models, e.g., for composing a generalized NMES model.

2 State of Research and Research Questions

This chapter identifies the research gaps regarding decentralized, cross-technology stabilization frameworks in AC power systems, DC power systems, and DHNs that are to be addressed in this thesis.

The chapter starts with AC power systems in Section 2.1, since they are the only energy systems with a standardized stability definition and standardized control structures. Initially, a short overview of the state of the art as well as emerging trends and challenges regarding the stability and stabilization of AC power systems is provided. To provide clarity for the literature review and the following chapters, a definition for *decentralized stabilization* in AC power systems is established. Subsequently, the state of research regarding decentralized stabilization in AC power systems is reviewed. In line with the overall research objective in Section 1.1, a special focus is set on works that promote unifying stabilization concepts across different technologies. At the end of the section, a concluding discussion identifies the existing research gaps and formulates research questions that are to be addressed in order to establish a decentralized, cross-technology stabilization framework in AC power systems.

DC power systems and DHNs are treated in Sections 2.2 and 2.3 along the same structure as in Section 2.1, i.e., an overview of the state of the art regarding stability and stabilization leads to a decentralized stabilization definition, which is followed by a literature review whose discussion leads to research questions.

Section 2.4 concludes the chapter with an overall summary. This summary leads to the formulation of another research question regarding the decentralized, cross-technology stabilization in NMESs.⁵ Additionally, it motivates the passivity-based approach pursued in the following chapters.

Lastly, note that the state of research regarding decentralized stabilization in power systems and DHNs has evolved significantly during the course of this thesis. In order to provide a clear perspective on the initial state of research, the reviews in Sections 2.1–2.3 only discuss works that have been published prior to the results obtained in this thesis. Works published in parallel and featuring passivity-based approaches to the decentralized stabilization in power systems and DHNs are briefly summarized in an addendum remark along with the publications related to this thesis. A comprehensive discussion of these works is presented at the end of the respective chapters in Sections 4.5, 5.5, and 6.5.

⁵ A brief overview of the few works that contribute towards a system-theoretical treatment of stability and stabilization in NMESs is provided in Section 7.2.

2.1 Decentralized Stabilization in AC Power Systems

AC power systems are the only energy systems with a standardized stability definition and standardized control structures. The accepted definition of the power system community can be found in Kundur et al. [2004] or Hatziargyriou et al. [2021] and reads as follows:

Definition 2.1 (AC power system stability)

Power system stability is the ability of an electric (AC) power system, for a given initial operating condition, to regain a state of operating equilibrium after being subjected to a physical disturbance, with most system variables bounded so that practically the entire system remains intact.

An alternative definition in the context of AC microgrids is given in Farrokhhabadi et al. [2020]:

Definition 2.2 (AC microgrid stability)

Consider an (AC) microgrid which is operating in equilibrium, with state variables taking on appropriate steady-state values satisfying operational constraints, such as acceptable ranges of currents, voltages, and frequency (...). Such a microgrid is stable if, after being subjected to a disturbance, all state variables recover to (possibly new) steady-state values which satisfy operational constraints (...), and without the occurrence of involuntary load shedding.

From a systems and control perspective, the two stability definitions above comprise several control requirements that can be categorized into two main tasks:

- Firstly, desired network equilibria comprising the system variables (currents, voltages, frequency) have to be asymptotically stabilized.
- Secondly, feasibility of such network equilibria within the operational constraints has to be ensured by appropriate coordination of generation, transportation, and consumption.

In state-of-the-art AC power systems, these two tasks are addressed by hierarchical frequency and voltage control structures (see, e.g., Gómez-Expósito et al. [2018, pp. 373ff.], Farrokhhabadi et al. [2020], and Liu et al. [2022]).

The goal of frequency control is to keep the frequency at a nominal value (50 Hz or 60 Hz) by balancing the generated and consumed active power. At the primary frequency control layer, decentralized proportional controllers called droop controllers establish a linear relation between the active power injection and the frequency deviation, called droop slopes. These droop slopes are scaled according to the contribution of each

generation unit to the overall active power generation. This establishes so-called power sharing and ensures that imbalances are picked up by the different generation units according to their nominal power ratings. However, primary frequency control only attenuates the disturbance and stabilizes the frequency at a new equilibrium with steady-state offset from the nominal value. Thus, a secondary frequency control is required to asymptotically reject the disturbance and regulate the frequency to the desired nominal value. It is implemented as a centralized, distributed, or semi-decentralized integral control over a region or control area, respectively. In order to regain the active power balance before the disturbance and possibly provide new setpoints for the secondary frequency control, tertiary frequency control is employed. It is implemented as centralized feedforward solving an optimization problem minimizing some cost function such as economic dispatch or social welfare and satisfying operational constraints (see Milano et al. [2018], Dörfler et al. [2019], Liu et al. [2022], and Gómez-Expósito et al. [2018, p. 382ff] for further details).⁶

The goal of voltage control is to keep the voltage magnitudes at each node of an AC power system within permissible limits around a nominal voltage by balancing the generated and consumed reactive power. Decentralized primary voltage controllers regulate the voltage magnitudes at some nodes to desired reference values by adjusting the excitation system of synchronous machines (so-called automatic voltage regulation), by passive components such as shunt capacitor or inductor banks, or by active flexible AC transmission systems (FACTSs). The secondary voltage controllers then coordinate the decentralized primary voltage controllers in a geographical region by adjusting their setpoints such that the voltage at a chosen pilot node reaches a desired reference value. The tertiary voltage controllers, in turn, centrally coordinate the reference values for the different regional pilot nodes within a larger geographical area such that some optimization criterion, e.g., minimal transmission losses, is fulfilled (see [Gómez-Expósito et al., 2018, p. 405ff] and [Liu et al., 2022, p. 701] for further details).

In the context of converter-based AC power systems considered in this thesis (see Section 1.1), frequency and voltage control must increasingly be shouldered by many smaller converter-interfaced DGUs via appropriate control of their converters [Guerrero et al., 2013; Olivares et al., 2014; Farrokhhabadi et al., 2020]. As these converters effectively form the grid by controlling their output to desired frequency and voltage setpoints, they are referred to as operating in *grid-forming* mode. Conversely, converters that only inject specified currents at network nodes are referred to as operating in *grid-feeding* mode [Rocabert et al., 2012].⁷

In the state-of-the-art hierarchical control structures, the asymptotic stabilization and coordination task are divided over different layers. In particular, decentralized droop control at primary level does not ensure the asymptotic stability of the desired network

⁶ A good illustration over the different timescales and tasks is provided in Milano et al. [2018, Figure 1].

⁷ Note that injecting a specified current at network nodes with a given voltage and frequency is equivalent to injecting a specified active and reactive power.

equilibrium. Instead, droop control only attenuates disturbances and accepts steady-state offsets at the benefit of achieving power sharing. However, a direct transfer of droop control into a converter-based setting does neither provide asymptotic stability of the desired network equilibrium, nor power sharing. Additionally, analytical asymptotic stability statements only exist for simplified AC power system models (see Section 2.1.1 below for a detailed discussion). Furthermore, converters and their controls have very different characteristics when compared to synchronous machines. From a practical perspective, it is thus inefficient and practically problematic to force converters into control structures designed for synchronous machines (see, e.g., the discussions in Olivares et al. [2014], Milano et al. [2018], and Dörfler et al. [2019]).

This thesis therefore proposes to take on a new perspective on stability, stabilization, and coordination of AC power systems closer to systems and control theory. The leading idea is to clearly divide the tasks to achieve AC power system stability into their respective control requirements. At the lowest control layer, *decentralized stabilization* ensures asymptotic stability of the desired network equilibrium comprising the system variables (frequency, voltages, currents) via decentralized controllers. The decentralized realization provides plug-and-play capability and avoids the need for communication or global model knowledge.⁸ This allows for very fast responses and avoids single point of failures, which is favorable in terms of reliability. It also simplifies the control design by decomposing the complex problem of stabilization into more manageable control problems, viz. designing decentralized component controllers. Appropriate tuning of the decentralized controllers via analytical or heuristic design procedures ensures a suitable transient behavior within the permissible frequency, voltage, and current limits. The frequency, voltage, and current setpoints for the decentralized controllers are provided by a higher level control. In order to generate the setpoints and ensure that they constitute a feasible network equilibrium within the operational constraints, the higher level control solves a *feasibility problem* by appropriately *coordinating* generation, transportation, and demand.⁹

For clarity and further reference, decentralized stabilization in AC power systems is defined as follows:

⁸ Note that there is communication with the higher control layer that possibly receives model parameters and measurement values and provides setpoints for the decentralized controllers. However, this communication is not part of the control loop of the decentralized controllers (see, e.g., Meng et al. [2017, Figure 2(d)]).

⁹ For the higher level control, established schemes from secondary frequency and voltage control such as centralized integral control can be employed as well as novel, distributed approaches, e.g., based on multi-agent systems and consensus algorithms (see Dörfler et al. [2019] for an overview).

Definition 2.3 (Decentralized stabilization in AC power systems)

Decentralized stabilization in AC power systems *refers to the basic control task conducted by decentralized controllers at the lowest control layer of a hierarchical stabilization-coordination control structure for AC power systems. It ensures that such AC power system equilibria are asymptotically stabilized that the system frequency as well as voltages and currents of actuated subsystems are at desired setpoints.*

Remark 2.1. *Note that Definition 2.3 covers not only the asymptotic stabilization of the system frequency and voltages, i.e., grid forming, but also current injections, i.e., grid feeding. Current control is considered explicitly here, as while it does not actively contribute to forming a grid, it nevertheless has to be conducted without introducing adverse, destabilizing behavior.*

In the following, approaches that provide decentralized stabilization in converter-based AC power systems are reviewed. Additionally, in line with the overall research objective in Section 1.1, works that promote unifying, cross-technology stabilization concepts are considered.

2.1.1 Literature Review

Approaches to the decentralized frequency and voltage control of converter-based AC power systems are manifold. A recent overview can for example be found in Dörfler et al. [2019]. As a natural starting point and to provide full backward compatibility with traditional AC power systems based on synchronous machines, extensive research effort has been put into developing decentralized solutions that allow to integrating converters into the established hierarchical frequency and voltage control structures.

The most prevalent and developed approaches in this category are converter droop control and extensions thereof (see for example Chandorkar et al. [1993], Guerrero et al. [2011], Guerrero et al. [2013], Zhong [2013], Olivares et al. [2014], Dörfler et al. [2014], Schiffer et al. [2014], and Simpson-Porco et al. [2017]). In fact, as of today, droop control serves as the required standard and unifying concept in AC power system stabilization, as the linear relations between power injections, frequencies, and voltages, i.e., the droop slopes, are written into the grid codes [Dörfler et al., 2019]. Despite its status as the de facto standard, the practical implementation of converter droop controllers typically requires various, additional heuristics [Dörfler et al., 2019]. Furthermore, due to its proportional control structure, droop control shows load-dependent voltage and frequency deviations from the nominal values [Guerrero et al., 2011, 2013; Olivares et al., 2014]. Moreover, droop control establishes two independent single-input single output (SISO) loops for frequency via active power and voltage via reactive power. At transmission level, where synchronous machines are connected, such a decoupling

assumption can be made due to a low R/X ratio. However, at distribution level where DGUs with droop-controlled converters are typically integrated, high R/X ratios create a non-negligible coupling of active power, reactive power, frequency, and voltage. The result is a poor transient performance of droop control and a limited region of attraction for desired operating points. Furthermore, power sharing is no longer achieved [Rocabert et al., 2012; Olivares et al., 2014; Dörfler et al., 2019]. In order to recover power sharing and ensure zero steady-state errors, distributed or centralized secondary controllers are used which necessitate information exchange [Guerrero et al., 2011, 2013; Olivares et al., 2014; Kolluri et al., 2018]. Additionally, rigorous system-theoretic analyses of stability properties of droop-controlled, converter-based AC power systems only exist for simplified, first-order models of the converter dynamics, quasi steady-state network models, and simplified load models [Simpson-Porco et al., 2013; Schiffer et al., 2014; Simpson-Porco et al., 2017]. Thus, droop-controlled converters effectively do not guarantee decentralized stabilization in more realistic, dynamic AC power system setups.

Besides droop control, alternative approaches have been proposed that try to transfer the concept of inertia from synchronous machines to converters by controlling the converters such that they emulate the behavior of synchronous machines (*virtual synchronous machines*) [Beck and Hesse, 2007; D'Arco et al., 2015], emulate the behavior of nonlinear oscillators (*virtual oscillators*) [Johnson et al., 2014; Sinha et al., 2015], or are structurally equivalent to synchronous machines (*matching control*) [Jouini et al., 2016; Monshizadeh et al., 2017; Arghir et al., 2018]. These approaches are unifying in the sense that they establish interoperability between synchronous machines and different converter technologies. Additionally, existing methods and knowledge earned from decades of operating synchronous machine-based AC power systems can be re-used. However, as converters have nearly opposite characteristics when compared to synchronous machines,¹⁰ it seems to be inefficient “to force a converter (a fully actuated, modular, and very fast control system) to behave like a (under-actuated, rigidly controlled, and comparatively slow) synchronous machine that does not make use of the converters’ key resources and strengths” [Milano et al., 2018]. Furthermore, the structural parallels are deceptive and in fact cause problems when used in real AC power systems (see, e.g., the discussions in Olivares et al. [2014], Milano et al. [2018], and Dörfler et al. [2019]).

In recent years, another class of approaches has seen growing interest which is unifying in the sense that it uses the system-theoretical input-output property of passivity and

¹⁰ Synchronous machines have a large inherent energy storage in form of the rotating masses of rotor and turbine which store around 4 s-12 s of nominal power. In comparison, the 10 ms-80 ms of nominal power stored in the DC-side capacitors of converters is three orders of magnitudes smaller and negligible [Jouini et al., 2016, Remark 2]; Dörfler and Groß [2023]. On the other hand, while the AC voltage control performance of synchronous machines is limited by their physical structure (e.g. fixed field inductance) and a complex excitation control with slow-acting over- and under-excitation limiters, converters allow for a much faster actuation in the order of milliseconds, a fully controllable AC voltage, and freedom in control solutions [Milano et al., 2018; Dörfler et al., 2019].

its close link to Lyapunov stability¹¹ to facilitate AC power system stability analysis. Particularly with the advent of PHS theory, pioneering stability results were obtained for AC power systems with synchronous machines, simplified load models [Fiaz et al., 2013; Caliskan and Tabuada, 2014; van der Schaft and Stegink, 2016], quasi steady-state network models [Fiaz et al., 2013; van der Schaft and Stegink, 2016], or single synchronous machines directly connected to a single load [Monshizadeh et al., 2019].¹² For converter-based AC power systems, Avila-Becerril et al. [2017] and Avila-Becerril et al. [2018] use passivity-based control (PBC) designs and PHS theory for voltage stabilization. However, their controllers require knowledge about all line parameters and are thus not decentralized.

Besides the application of passivity techniques on an AC power system level, PBC designs for standalone converters have been thoroughly discussed for example by Perez et al. [2004], Harnefors et al. [2016], Serra et al. [2017], Zhong and Stefanello [2017], and Gui et al. [2018]. While these works provide a detailed analysis and synthesis from a power electronic perspective, they lack an overall system analysis and rely on canonical assumptions such as a stable, stiff grid behaving like a constant voltage source for their stability analyses.

In addition to the above-discussed approaches that have some kind of unifying, cross-technology feature, several other decentralized, droop-free approaches have been proposed in recent years. These approaches usually implement voltage controllers in the dq frame and use open-loop frequency control based on internal oscillators with, e.g., global positioning system (GPS) or Ethernet synchronization to stabilize the system frequency. Etemadi et al. [2012a] conduct a decentralized robust servomechanism design based on a linearized model of a converter-based AC power system comprising linear loads. Rivero et al. [2015], Tucci et al. [2016a], Tucci and Ferrari-Trecate [2017], Sadabadi et al. [2017], and Floriduz et al. [2018] use the concept of neutral interactions from Lunze [1992, p. 170] to design decentralized voltage controllers. However, asymptotic stability of the AC power system equilibrium is only guaranteed under quasi-stationary line approximations and if the solution of linear matrix inequalities states that the plug-in/out of a DGU is feasible. The improved line-independent design algorithm by Tucci and Ferrari-Trecate [2020] is instead always feasible, but still requires quasi-stationary line approximations to prove asymptotic stability. Shafiee-Rad et al. [2021] use a polytopic-type uncertainty approach to design “decentralized” voltage controllers. However, their design and stability proof requires knowledge about the fixed number of overall DGUs, which spoils its true decentralized nature. Furthermore, all the approaches in this paragraph consider load-connected topologies in which loads are always connected at nodes together with DGUs. This significantly limits the possible AC power system configurations.

¹¹ See Section A.1 for more details.

¹² The rationale behind this connection is the fact that every PHS is a passive system. For more details regarding passivity theory, PHSs, and Lyapunov stability see Chapter 3.

2.1.2 Discussion and Research Questions

Considering the literature review in Section 2.1.1, it can be seen that there is no converter control approach that achieves decentralized stabilization as per Definition 2.3. Additionally, there exists no cross-technology, decentralized stabilization concept unifying different AC power system technologies and control strategies. The main feature all the above-discussed works have in common is that they do not provide any decentralized, technology-independent conditions that can ensure asymptotic stability of desired AC power system equilibria. The developed control solutions and asymptotic stability analyses only apply to their specific AC power system models (e.g., with a load-connected topology, a quasi steady-state network, simplified DGU and load models, specific synchronous generator models, etc.). However, no inferences are drawn on how their results can be translated into general system and control design guidelines for decentralized stabilization. In summary, there exists no unifying, cross-technology framework with decentralized, analytical conditions that can serve as normative basis and ensures decentralized stabilization in AC power systems across different technologies and control strategies (see also Farrokhabadi et al. [2020] and Dörfler and Groß [2023]). The discussed passivity-based approaches suggest that passivity theory presents a promising tool to develop such a cross-technology framework. The existing, passivity-based works, however, are not decentralized or remain limited to specific applications and setups (e.g., quasi steady-state networks, simplified loads, AC power systems with synchronous machines).

The present de facto standard to investigate stability and interoperability over different AC power system technologies and control strategies are thus high-fidelity simulations [Farrokhabadi et al., 2020; Dörfler and Groß, 2023]. However, in practice, the required high-fidelity models and detailed information may not always be available due to information barriers (e.g. proprietary information and models). Furthermore, recent results have identified that depending on system topologies, technologies, and control approaches, there are large numbers of very different unfavorable interactions and interdependencies possible [Dörfler and Groß, 2023]. Considering the sheer infinite possibilities of combining system topologies, technologies, and control approaches, it is unrealistic to make reliable design decisions and generalizations based on simulations alone.

Therefore, in order to establish a decentralized, cross-technology stabilization framework in AC power systems, the following two questions need to be answered:

- (Q1.1) How to provide decentralized, analytical conditions that ensure across different technologies and control strategies asymptotic stability of any feasible AC power system equilibrium?
- (Q1.2) How to design, based on the conditions of research question (Q1.1), decentralized converter controllers that asymptotically stabilize the system frequency, desired node voltages, and current injections?

2.2 Decentralized Stabilization in DC Power Systems

While AC is still the prevailing technical standard in electrical power systems, high voltage DC transmission systems and DC distribution systems at low-to-medium voltage levels have attracted rising attention in recent years as they exhibit definite advantages over their AC counterparts. On the one hand, they show higher efficiency, improved power quality, and low system cost. In particular, DC distribution systems reduce the number of converters and thus of lossy DC-AC and AC-DC conversion stages as many DGUs, energy storage systems, and consumer devices (e.g., electric vehicles, household appliances, industrial equipment, lights) directly operate in DC. On the other hand, DC power systems are much simpler to operate as they avoid synchronization issues and the need for controlling frequency and reactive power [Justo et al., 2013; Zhao and Dörfler, 2015; Meng et al., 2017].

In contrast to AC power system stability, however, there exists no standardized definition of DC power system stability and no standardized control structures. Nevertheless, similar to the AC case, the operation of DC power systems can be organized hierarchically to account for different control requirements covering different technical areas, time scales, and physical levels. Overall, the same two main control tasks as in AC power systems have to be fulfilled. That is, asymptotic stabilization of different network equilibria comprising the system variables (voltages, currents)¹³ and coordination to ensure that such network equilibria exist within the operational constraints [Dragičević et al., 2016; Meng et al., 2017].

The hierarchy prevalent in the DC literature is based on the hierarchical AC control structures [Dragičević et al., 2016; Meng et al., 2017]. At the primary control layer, the basic regulation of voltages (grid-forming) and currents (grid-feeding) as well as power sharing are achieved. At the superordinate secondary and tertiary layers, centralized or distributed control strategies are implemented to achieve zero steady-state errors and some possibly optimal, global coordination of generation, transmission, and consumption within the operational constraints.

However, motivated by the lacking performance and analytical stability guarantees of state-of-the-art primary controllers based on DC droop control (see Section 2.2.1 below for a detailed discussion), large parts of the DC power system community have adopted an asymptotic stabilization-coordination hierarchy as discussed in Section 2.1 for AC power systems. In fact, all non-droop based works reviewed below in Section 2.2.1 implicitly or explicitly assume such a hierarchy. That is, they only focus on voltage and current control and outsource all coordination tasks including power sharing to higher level controllers at the secondary and tertiary level.

¹³ Note that this also implies a suitable transient behavior within the permissible voltage and current limits. As for the AC case and in line with control engineering practice, this is ensured by appropriate tuning of the decentralized controllers via analytical or heuristic design procedures.

Following Definition 2.3 for the AC case, decentralized stabilization in DC power systems can be defined as follows:

Definition 2.4 (Decentralized stabilization in DC power systems)

Decentralized stabilization in DC power systems *refers to the basic control task conducted by decentralized controllers at the lowest control layer of a hierarchical stabilization-coordination control structure for DC power systems. It ensures that such DC power system equilibria are asymptotically stabilized that voltages and currents of actuated subsystems are at desired setpoints.*

The following review provides an overview of the current state of research regarding decentralized stabilization solutions in converter-based DC power systems. In line with the overall research objective in Section 1.1, particular attention is given to works that promote unifying, cross-technology concepts.

2.2.1 Literature Review

Inspired by decentralized, droop-based frequency and voltage control in AC power systems, several researchers have focused on adapting converter droop control and extensions thereof for the decentralized voltage stabilization in DC power systems (see Guerrero et al. [2011], Justo et al. [2013], Zhao and Dörfler [2015], Dragičević et al. [2016], Meng et al. [2017] and the references therein). However, similar to its AC counterpart, DC droop control typically requires various, additional heuristics for its practical implementation. Furthermore, it also shows load-dependent voltage deviations from the desired nominal values and propagation of voltage errors along resistive transmission lines [Guerrero et al., 2011; Zhao and Dörfler, 2015; Dragičević et al., 2016]. Moreover, its power sharing accuracy is limited by the specific system setup (e.g., linear loads, quasi-stationary line approximations), the parameters of the system model, and the control parameters [Zhao and Dörfler, 2015; Dragičević et al., 2016; Meng et al., 2017]. Thus, stability results for droop-controlled DC power systems either rely on a secondary control layer with some form of information exchange [Guerrero et al., 2011; Zhao and Dörfler, 2015; Dragičević et al., 2016; Meng et al., 2017] or are limited to small signal analyses of specific topologies [Shafiee et al., 2014]. Additionally, DGU dynamics are often simplified, e.g., to unit gains (see for example Zhao and Dörfler [2015]).

Similar to the AC case, passivity-based approaches for decentralized stabilization have also been explored in DC power systems. Gu et al. [2015] propose to shape converter admittances via voltage feedforward control such that the admittances fulfill desired passivity properties guaranteeing system-wide stability. However, line dynamics are not considered and their passivity analysis in the frequency domain is only admissible for linear SISO systems which hampers the analysis of inherently nonlinear components

such as *constant impedance*¹⁴, *constant current*, *constant power* (ZIP) or exponential loads. Zonetti et al. [2015] propose a unified model for multi-terminal, high-voltage DC transmission systems based on PHS theory and a decentralized proportional-integral (PI) controller for AC/DC voltage source rectifiers to asymptotically stabilize desired output currents and node voltages. Martinelli et al. [2018] explore a nonlinear, passivity-based controller design for voltage stabilization in medium-voltage DC power systems. However, their design is not decentralized as it requires information about line parameters and updating other controllers in the event of plug-in/out operations. Han et al. [2019] propose decentralized voltage and current controllers for DGUs in a load-connected topology with dynamic power lines and linearized ZIP load models. At several places, the authors provide hints regarding passivity interpretations of their results, but do not elaborate further on this. These passivity relations are explored in more detail by Soloperto et al. [2018] and Nahata et al. [2020], whereas Soloperto et al. [2018] is a simplified, preliminary version of Nahata et al. [2020]. Nahata et al. [2020] in particular show that the decentralized, state-feedback controller of Han et al. [2019] (see also Tucci et al. [2018]) indeed passivate DGUs in closed-loop subject to some inequalities for the controller gains and ZIP load model parameters (see Section 4.3.3 for more details).

Besides the application of passivity techniques on a DC power system level, various PBC designs for standalone DC converters have been proposed by the power electronic community (see for example Sira-Ramirez et al. [1997]; Kwasinski and Krein [2007]; Kwasinski and Onwuchekwa [2011]; Zeng et al. [2014]). While these works provide a detailed analysis and synthesis from a power electronic perspective, they lack an overall system analysis and consider only single converters directly connected to a load. Furthermore, the specific controller designs often require system knowledge such as the load parameters [Sira-Ramirez et al., 1997; Kwasinski and Onwuchekwa, 2011; Zeng et al., 2014]. A review of unifying stability criteria for DC distribution systems that are used by the power electronic community can be found, e.g., in Riccobono and Santi [2014] and Gu et al. [2015]. The main drawback all these criteria have in common is that they require a comprehensive overall system model and are thus not decentralized. Impedance- and passivity-based methods, for example, require knowledge about all converter and load impedances in order to make a stability statement. Consequently, it is not possible to a priori and independent of the system configuration provide decentralized control design guidelines that ensure asymptotic stability. Furthermore, besides some Lyapunov-based approaches, all criteria only hold for linear systems.

In addition to decentralized converter control approaches that fall into the unifying category of droop control or passivity methods, several other decentralized approaches to the voltage stabilization in DC power systems have been proposed in recent years. Tucci et al. [2016b] propose a state-feedback voltage controller for DC power systems with general topology. Sadabadi et al. [2018] develop a PI voltage controller for DGUs featuring boost converters. Sadabadi and Shafiee [2020b] propose a robust two-degree-

¹⁴ Note that despite the wording, it is common practice to express the constant impedances (Z) as admittances (Y). For further details, see Appendix B.1.

of-freedom feedback-feedforward controller design for voltage control in DC power systems with constant power loads. The controllers in these three works, however, require information about the impedances of neighboring lines. While scalability is still provided to a certain extent, these controllers are effectively not decentralized. Furthermore, their implementation requires the online solution of an optimization problem. If the problem is infeasible, the plug-in/out operation of the respective DGU is denied, which is cumbersome and impractical. Additionally, the stability statements in these works rely on quasi-stationary line approximations in which the line inductances are neglected. This assumption might be valid in low-voltage DC networks, which are mainly resistive, but does not hold at higher voltage levels where line inductances are significant [Andreasson et al., 2017]. The improved design by Tucci et al. [2018] manages to avoid line information, but retains the issues regarding numerical infeasibility and quasi-stationary line approximations. Zonetti et al. [2019] propose a decentralized voltage controller design based on monotonicity. Their stability statements require quasi-stationary line approximations as well. Additionally, the authors assume that DGU dynamics are simplified to controllable current injections. Sadabadi and Shafiee [2020a] propose a decentralized PI voltage control design for DC microgrids with linear ZI loads. All works in this paragraph consider a load-connected topology in which loads are always connected at nodes together with DGUs. Furthermore, except Sadabadi and Shafiee [2020b] and Nahata et al. [2020], all works consider loads as current disturbances or linear loads and thus disregard the destabilizing effect of exponential loads covering constant power loads.¹⁵ This significantly restricts the possible DC power system configurations.

2.2.2 Discussion and Research Questions

Considering the literature review in Section 2.2.1, it can be seen that the situation is similar to that in AC power systems. While there exists a variety of works that provide decentralized stabilization concepts, the controllers and asymptotic stability analyses proposed in these works only apply to their specific DGU and DC power system models (e.g., with a load-connected topology, linear or simplified loads, small signal models). The only results that are cross-technology and independent of the specific converter-based, closed-loop DGU model are the passivity-, impedance-, and Lyapunov-based stability criteria from the power electronic community summarized in Riccobono and Santi [2014] and Gu et al. [2015]. However, they are not decentralized as they require overall system knowledge (complete system model or overall bus impedance) and with exception of the Lyapunov-based approaches only apply to linear systems. In summary, none of the above-discussed works provide any decentralized, analytical conditions that may serve as basis for a unifying, cross-technology framework for the decentralized stabilization in DC power systems.

¹⁵ The reason behind this destabilizing behavior is the negative incremental impedance of these loads. For further details see Dragičević et al. [2016] and Meng et al. [2017, Equation (8)].

Similar to the AC case, there are again some passivity-based approaches whose results suggest that passivity theory may present a promising tool to develop such a cross-technology framework. The existing works, however, are not decentralized (see Riccobono and Santi [2014] and Martinelli et al. [2018]) or remain limited to specific setups with no line dynamics and linear SISO systems (see Gu et al. [2015]), high-voltage DC transmission systems (see Zonetti et al. [2015]), or DGUs with state-feedback controllers and a load-connected DC power system topology (see Nahata et al. [2020]).

Therefore, the following two questions regarding the decentralized stabilization in DC power systems need to be answered in order to establish a decentralized, cross-technology stabilization framework:

- (Q2.1) How to provide decentralized, analytical conditions that ensure across different technologies and control strategies asymptotic stability of any feasible DC power system equilibrium?
- (Q2.2) How to design, based on the conditions of research question (Q2.1), decentralized converter controllers that asymptotically stabilize desired node voltages and current injections?

2.3 Decentralized Stabilization in District Heating Networks

The operation of DHNs combines two physical domains, viz. hydraulics and thermodynamics. The actual thermal power transferred between heat sources and heat consumers is a product of the temperature and the mass flow of heated water [Krug et al., 2021, Section 2.3]. While controlling the temperature is important for meeting the head demand of consumers and an efficient operation of DHNs [Lund et al., 2014], well-defined, stable hydraulic conditions, i.e., pressures and volume flow rates, are a fundamental requirement for the operation of DHNs [Boysen and Thorsen, 2003; Pan et al., 2016; Novitsky et al., 2020]. The role of pressures and volume flow rates in a hydraulic network in fact shares many similarities with that of voltages and currents in an electrical DC network. When considering that both pressures and voltages represent potential quantities in their respective physical domains,¹⁶ it becomes clear that controlling pressures fulfills the same task of forming the grid that voltage stabilization of grid-forming converters does in electrical DC power systems. In light of the main objective in Section 1.1, the focus in the following is thus on the hydraulic stabilization in DHNs.

Similar to DC power systems, there exists no standardized definition of DHN stability or the term *hydraulic stabilization*. There exist, however, two basic pressure regulation tasks, viz. static and differential pressure control, which are widely used in practice

¹⁶ See Section A.2.1 for further details on formal equivalences between different physical domains and generalized modeling.

and can be understood as hydraulic stabilization. The operating principle behind these pressure controls is motivated by the prevalent configuration of state-of-the-art 2nd and 3rd generation DHNs, which comprise at most a few down to a single main heat source supplying multiple consumers over a hydraulic pipe network.¹⁷ Similar to traditional power system operation, the hydraulics and consequently the thermal power flows are well-understood in such DHN structures. Originating from a few main heat sources with circulation pumps, volume flow rates and thermal power flows, respectively, follow decreasing pressure levels, so-called pressure cones, along the supply pipe layer to the consumer substations and back via the return pipe layer (see for example Nussbaumer et al. [2020, pp. 52–54] and Buffa et al. [2021, Figure 1]). The consumers regulate the volume flow rate and thus the thermal power they receive via control valves. However, as control valves can only induce variable pressure losses, ensuring a proper heat supply requires that each consumer receives a minimum differential pressure ranging from 0.4 bar-1 bar [Nussbaumer et al., 2020, p. 49]. At present, due to the simple structure and well-understood hydraulic conditions, the consumers with the lowest differential pressures between supply and return are known a priori. Consequently, these critical consumer pressures can be observed and controlled centrally by adjusting the main network pumps [Brand et al., 2014; Vandermeulen et al., 2018; Buffa et al., 2021].¹⁸

In addition to differential pressure control, closed hydraulic circuits such as DHNs require at least one pressure holding unit to establish an absolute static pressure (see, e.g., Wang et al. [2017a] and Nussbaumer et al. [2020, pp. 54–55]). While this static pressure does not influence the hydraulic dynamics, which depend only on the differential pressures, it is nevertheless important to avoid pipe bursts or damaging equipment, e.g., by cavitation in the circulation pumps [Nussbaumer et al., 2020, pp. 54–55]; [Sommer et al., 2019; Buffa et al., 2021].

However, in light of the sustainable energy transition and emerging 4th generation DHNs, new strategies and methods of operating, controlling, and analyzing DHNs are required [Lund et al., 2014; Vandermeulen et al., 2018; Novitsky et al., 2020]. Similar to power systems, DHN operation is facing a decentralization with increasing numbers of interacting subsystems and controllable components (pumps, control valves). Primarily, this is due to the integration of renewable DGUs such as heat pumps, combined heat and power, waste/biomass-to-energy, solar, and geothermal heat plants. Additionally, DHNs increasingly feature intermittent in-feed of excess energy from wind and solar power plants, which cannot be accommodated by the power system [Lund et al., 2014; Vandermeulen et al., 2018]. Furthermore, DHN setups in which distributed variable-speed pumps (DVSPs) are installed at every DGU and some (up to all) consumer substations have shown considerable potential to reduce the overall pumping costs for DHNs [Yan et al., 2013; Wang et al., 2017a; Gong et al., 2019].

¹⁷ See Lund et al. [2014] for a comparison and overview of the different DHN generations. The main differences between 2nd, 3rd, and emerging 4th generation DHNs are a trend towards lower temperatures and the integration of distributed, renewable heat sources.

¹⁸ In smaller DHNs, the pump operating points are often even only adjusted by means of offline look-up tables, which are predetermined by a hydraulic network analysis during the DHN design.

Making DHNs more sustainable also comprises improving efficiency. This in turn leads to decreasing water temperatures, decreasing pipe diameters, novel topologies with multiple temperature layers, and frequently changing hydraulic network conditions [Lund et al., 2014; Vandermeulen et al., 2018]. Supply/return temperatures, for example, are decreasing from around $80\text{ }^{\circ}\text{C}$ - $120\text{ }^{\circ}\text{C}$ / $40\text{ }^{\circ}\text{C}$ - $70\text{ }^{\circ}\text{C}$ in 2nd or 3rd generation DHNs to $40\text{ }^{\circ}\text{C}$ - $70\text{ }^{\circ}\text{C}$ / $20\text{ }^{\circ}\text{C}$ - $40\text{ }^{\circ}\text{C}$ in 4th generation DHNs (see Lund et al. [2014], Novitsky et al. [2020], and Nussbaumer et al. [2020, p. 44]). On the one hand, this allows to efficiently integrate renewable heat sources and new consumers (e.g., low-energy buildings). On the other hand, together with decreasing pipe diameters, this reduces the heat distribution losses [Nussbaumer et al., 2020, p. 44]; [Köfinger et al., 2017; Volkova et al., 2020, 2022]. Besides that, different temperature layers can be combined to multi-layer topologies in future DHN to increase efficiency.¹⁹ The return pipes of a 2nd or 3rd generation DHN may then serve as supply for a new low-temperature DHN part. However, such new network structures and operation strategies often require additional booster pumps, i.e., yet more controllable components, at strategic points in pipes and consumers to ensure suitable hydraulic conditions and a proper heat supply.²⁰

In summary, these developments towards more sustainable DHNs lead to an overall increase in complex pressure and volume flow dynamics and interactions between actuators (pumps, valves) on small time scales (see also the discussion in Novitsky et al. [2020]). Similar to interacting converters in power systems, these dynamics and interactions, if not carefully analyzed and understood, can cause serious operational problems such as severe hydraulic oscillations [Yan et al., 2013; Wang et al., 2017a; Sommer et al., 2019]. Furthermore, due to the frequently changing hydraulic conditions caused by increasingly variable volume flow rates and flow reversals [van der Heijde et al., 2017; Mohring et al., 2021], the locations of the critical consumer pressures vary and are not clearly determined [Brand et al., 2014; Hassine and Eicker, 2014]; [Nussbaumer et al., 2020, p. 50].

Similar to power system stabilization, new hydraulic stabilization schemes thus must be able to address an increasing number of interacting units, ensure interoperability across different hydraulic technologies and control strategies, and handle flexible system configurations in which units connect and disconnect in a plug-and-play fashion. Considering the similarities in the development trends, challenges, and stabilization requirements between power systems and DHNs as well as the equivalences between pressures/voltages and volume flow rates/currents, it seems promising to adopt the asymptotic stabilization-coordination hierarchy established in Sections 2.1.2 and 2.2.2 for controlling DHNs. At the lowest control layer, hydraulic network equilibria comprising the hydraulic system variables (pressures, volume flow rates) are asymptotically stabilized by decentralized controllers.²¹ The setpoints for the hydraulic stabilization

¹⁹ See temperature cascading in Köfinger et al. [2017], Nussbaumer et al. [2020, p. 44], Volkova et al. [2020], and Volkova et al. [2022].

²⁰ See De Persis and Kalleøe [2011], Lund et al. [2014], and Nussbaumer et al. [2020, p. 54] for a discussion.

²¹ Recall that in line with control engineering practice, a suitable transient behavior within the permissible pressure and volume flow rate limits is ensured via appropriate tuning of the decentralized controllers.

are provided by higher control layers. Via appropriate coordination of generation, transportation, and demand, these higher layers ensure that suitable hydraulic network equilibria exist within the operational constraints and that these equilibria guarantee a proper heat supply.²²

Following Definitions 2.3 and 2.4 for AC and DC power systems, decentralized stabilization in DHNs is defined as follows:

Definition 2.5 (Decentralized stabilization in DHNs)

Decentralized stabilization in DHNs refers to the basic hydraulic control task conducted by decentralized controllers at the lowest control layer of a hierarchical stabilization-coordination control structure for DHNs. It ensures that such hydraulic DHN equilibria are asymptotically stabilized that pressures and volume flow rates in actuated DHN subsystems are at desired setpoints.

Remark 2.2. *Note that similar to current control in AC and DC power systems, this thesis considers volume flow rate control explicitly as part of the stabilization. This is due to the fact that when volume flow rates are increasingly controlled via pumps instead of via control valves alone, it has to be ensured that these pumps do not introduce adverse, destabilizing behavior.*

In contrast to AC and DC power systems, the following review not only considers the current state of research regarding decentralized stabilization. It also provides a broader overview about hydraulic control approaches that address characteristics of future DHNs such as distributed pumps/producers, topology changes, or plug-and-play operation. This is due to the fact that DHNs have received much less attention by the control community than electrical power systems due to their seemingly simple structures and operating strategies [Novitsky et al., 2020]. In particular, the literature discussing hydraulic control challenges and new hydraulic control methods is scarce and fragmented.

2.3.1 Literature Review

The topic of plug-and-play control in the context of DHNs was first introduced by Knudsen et al. [2008] and Trangbaek et al. [2009]. The authors labeled plug-and-play as the idea of a control system to automatically initialize and reconfigure in the face of varying system topologies due to plug-in/out of a new device. However, the focus of their works is on system identification with least-squares methods to obtain linear, time-invariant, control-design models of the overall DHN hydraulics. Plug-and-play in their understanding refers to updating this overall model automatically in case a

²² Note that temperature control is part of these higher control layers.

new devices is added or removed from the DHN. Their subsequent design of pressure controllers, however, is based on the overall DHN model and thus must be adjusted, whenever changes occur in the DHN.

The pressure regulation in hydraulic networks with topology changes and multiple, distributed pumps has also been addressed by De Persis and Kallæsøe [2011], De Persis et al. [2014], and Scholten et al. [2017b]. The authors consider the problem of controlling the differential pressures over consumers to constant desired setpoints via distributed PI controllers. However, their control strategy is distributed and not decentralized and thus requires information exchange among the controllers to ensure the hydraulic equilibrium is asymptotically stable. Furthermore, the setups considered in these works remain limited to one heat source and require pumps at every producer and consumer. Scholten et al. [2017a] consider temperature and storage volume control for DHNs with a single heat source and simplified hydraulic dynamics in quasi steady state. Trip et al. [2019] address the optimal regulation of storage levels at each node in a simplified DHN. However, the important aspect of pipe friction is neglected.

In contrast to AC and DC power systems, passivity-based approaches for the decentralized stabilization of hydraulics in DHNs have not been investigated in detail. Jensen [2012] provides first elaborations on how the passivity properties of the hydraulic model of a DHN and the negative feedback interconnection of passive systems can be used to design pressure controllers regulating the differential pressure over consumers as in De Persis and Kallæsøe [2011], De Persis et al. [2014], and Scholten et al. [2017b]. However, being based on the model of De Persis and Kallæsøe [2011], the results apply only to a limited class of DHNs as mentioned above, viz. DHNs with only one heat source and pumps at every producer and consumer. Furthermore, the controllers still require information exchange and are thus not decentralized.

Another noteworthy work that contributes towards a passivity-based analysis of DHNs by introducing a PHS model for DHNs is from Hauschild et al. [2020]. In their work, the authors propose a partial differential equation (PDE)-based thermohydraulic, spatially-discretized PHS model of DHNs with a single producer. While being highly detailed and thus suitable, e.g., for validation purposes or optimization techniques, the PDE model is not well-suited for standard system analyses and decentralized control design methods applicable only to ordinary differential equations (ODEs).

In summary, it can be seen that a major limitation of the works of De Persis and Kallæsøe [2011], Jensen [2012], De Persis et al. [2014], Scholten et al. [2017b], and Scholten et al. [2017a] arises from the restriction to DHNs with only a single heat source. The authors justify this limitation by referring to state-of-the-art 2nd and 3rd generation DHNs, which often fulfill this requirement. At the same time, however, they assume pumps at every heat source and every consumer. While this assumption might become reality in some future DHNs, it prevents backward compatibility of the developed solutions to current DHNs as well as to intermediate development stages in which consumers use control valves for volume flow rate regulation. In addition, all works reviewed in this section

only consider DHNs with two temperature layers and symmetric return and supply network topologies. This excludes two practically relevant cases: firstly, current DHNs in which the supply pipes form a meshed network, while the return pipes constitute a tree structure; secondly, future DHNs with multi-layer topologies and temperature cascading. Furthermore, at most static pump models are used and control valves are not considered as actuators (control inputs), although they are in fact one of the main actuators in DHNs (see, e.g., Li et al. [2017, p. 19,29], Vandermeulen et al. [2018], and Nussbaumer et al. [2020, pp. 143–145,151]). Lastly, none of the reviewed works consider pressure holding units necessary for controlling the static DHN pressure.

2.3.2 Discussion and Research Questions

Considering the literature review in Section 2.3.1, it can be seen that the current state of research regarding hydraulic control approaches for DHNs is restricted by substantial model limitations. Overall, there is no dynamic, hydraulic DHN model suitable for control design that encompasses traditional 2nd and 3rd generation DHNs, future 4th generation DHNs as well as intermediate development stages. While some component models exist or can be derived from the literature, there exists no adequate hydraulic DHN model that incorporates all of these components, viz. dynamic pump models, valves as actuators, pressure holding units, and temperature cascading circuits, to represent the relevant DHN subsystems and assemble them in a general topology. General topology hereby means an arbitrary number of producers and consumers connected in a meshed, possibly asymmetric pipe network topology with multiple temperature layers (temperature cascading), distributed pumps at producers, consumers, and pipes, as well as traditional valve-controlled consumers.

Consequently, there are no pressure and volume flow rate, i.e., hydraulic, control approaches that achieve decentralized stabilization as per Definition 2.5 across DHNs of various generations and designs. In particular, there exists no unifying, cross-technology framework with decentralized, analytical, asymptotic stability conditions that can serve as normative basis and ensure decentralized stabilization across different DHN setups, technologies, and control strategies.

Therefore, the following three questions regarding the decentralized stabilization in DHNs need to be answered in order to establish a decentralized, cross-technology stabilization framework:

- (Q3.1) How can the hydraulic dynamics of different DHN generations and setups be modeled for control design purposes?
- (Q3.2) How to provide decentralized, analytical conditions that ensure across different DHN setups, technologies, and control strategies asymptotic stability of any feasible, hydraulic DHN equilibrium?

(Q3.3) How to design, based on the conditions of research question (Q3.2), decentralized pump and valve controllers that asymptotically stabilize desired pressures and volume flow rates?

2.4 Summary

This chapter has provided an overview over the current state of stabilization in AC power systems, DC power systems, and DHNs. Similarities in the development trends of these three energy systems and emerging challenges for their stabilization have been reviewed. Most prominently, the challenges comprise:

- a decentralization with increasing numbers of interacting subsystems and controllable components (converters, pumps, control valves);
- an intermittent energy supply and operation of subsystems demanding plug-and-play capability and flexible system configurations;
- and an overall increase in complex system dynamics and interactions on small time scales.

Based on these insights and the shortcomings of state-of-the-art stabilization schemes, this thesis proposes a new perspective on the hierarchical control of networked energy systems closer to systems and control theory. The leading idea is to clearly separate the tasks to achieve “stability of an energy system” into their respective control requirements, viz. decentralized stabilization at the lowest control layer and coordination at higher control layers.

Considering the current state of research regarding decentralized stabilization and cross-technology stabilization concepts, it has been shown that similar gaps and consequently research questions have to be addressed in order to establish decentralized, cross-technology stabilization frameworks in AC power systems, DC power systems, and DHNs. Apart from the modeling question (Q3.1) for DHNs, the main questions regarding the decentralized, cross-technology stabilization frameworks read as follows:

- How to provide decentralized, analytical conditions that ensure asymptotic stability of any feasible networked energy system equilibrium?
- How to design, based on the decentralized, analytical conditions of the above question, decentralized controllers that asymptotically stabilize desired system variables?

The respective literature reviews in Sections 2.1.1, 2.2.1, and 2.3.1 hint that passivity-based approaches present a promising starting point to address these questions in a unifying, cross-technology manner. Furthermore, for AC and DC power systems, the discussed preliminary works have shown that PHS theory can facilitate the application of passivity methods and the subsequent stability analysis with Lyapunov theory.

Within this thesis, these relations are elaborated. It is shown how a *passivity-based approach together with the energy-focused modeling of physical systems in the PHS framework enables the consistent design of a unifying, cross-technology framework for the decentralized stabilization in various networked energy systems*. While the main focus is on converter-based DC and AC power systems (Chapters 4 and 5) and DHNs (Chapter 6), it is demonstrated that the developed approach can readily be used to answer the following research question related to establishing a unifying, cross-technology stabilization framework for NMESs:

- (Q4.1) How to provide decentralized, analytical conditions that ensure across different technologies, control strategies, and physical domains asymptotic stability of any feasible NMES equilibrium?

2.4.1 Addendum Remark Regarding Parallel Works

At this point, it is important to highlight that the state of research regarding decentralized stabilization in energy systems has significantly evolved compared to its status that lead to the research questions of this thesis. In particular, initially independently from each other and later in some joint works, various research groups have explored passivity-based approaches and designs for providing decentralized, asymptotic stability conditions and decentralized stabilization solutions.

For AC power systems, decentralized, passivity-based stabilization solutions have been proposed by Strehle et al. [2019], Nahata and Ferrari-Trecate [2019], Watson et al. [2019], Spanias and Lestas [2019], Strehle et al. [2020a], Spanias et al. [2020], Ojo et al. [2021], Watson et al. [2021], and Strehle et al. [2022b].

For DC power systems, Cucuzzella et al. [2019a], Strehle et al. [2020a], Strehle et al. [2020b], Cucuzzella et al. [2020], Ferguson et al. [2021], Kosaraju et al. [2021], and Cucuzzella et al. [2023] have considered the problem of decentralized voltage stabilization.

For DHNs, Strehle et al. [2021], Strehle et al. [2022a], Machado et al. [2022a], and Machado et al. [2022b] have provided comprehensive control design models for various multi-producer DHN setups and conducted passivity-based system analyses. Machado et al. [2022a] have further proposed controller designs for the decentralized, hydraulic stabilization in multi-producer setups.

An in-depth discussion and comparison of the above works from other researchers with the results of this thesis is presented at the end of the respective chapters in Sections 4.5, 5.5, and 6.5. The main drawback most of these works share is that they provide model- and technology-specific results only. That is, similar to the works reviewed in Sections 2.1.1 and 2.2.1, their controller designs and asymptotic stability statements only apply to their specific DGU and energy system models. No inferences are drawn on how passivity properties can be used to establish general, decentralized

system and control guidelines for ensuring asymptotic stability.²³ In addition, none of these works investigate similarities between the models and control problems of the various energy systems or explore the possibilities of transferring solutions developed for one energy system to another by using generalized models and concepts. In light of the desired development towards NMESs, it is, however, of great interest to explore such aspects.

²³ An exception are the works of Spanias and Lestas [2019], Spanias et al. [2020], and Watson et al. [2021] for AC power systems.

3 Methodological Approach

The main goal of this thesis is the development of cross-technology frameworks for the decentralized stabilization in various networked energy systems. Following the discussion in Section 2.4, it seems promising to approach such an endeavor by means of passivity methods complemented with a domain-unifying modeling in the PHS framework.

Within this chapter, the methodological groundwork for the passivity-based, decentralized stabilization frameworks is developed. To allow for a clear, concise presentation of the technical contents and provide a basis for the unifying system description of the respective energy systems in Chapters 4 to 7, Section 3.1 first introduces the notion of an autonomous networked system. Subsequently, in Section 3.2, equilibrium-independent passivity (EIP) is introduced. EIP allows for a modular stability analysis of any feasible equilibrium of an autonomous, networked system and thus is a promising tool for answering the research questions of Chapter 2. However, existing EIP theory does not provide any ready theorems with decentralized, asymptotic stability conditions. Thus, in a first step inspired by existing literature, decentralized, EIP-based conditions are deduced which are sufficient for the asymptotic stability of any feasible, autonomous networked system equilibrium. In line with the classical passivity theorems, however, these conditions require strict EIP properties. This restriction introduces a high degree of conservatism and severely limits their practical applicability. Consequently, in Section 3.3, the prior findings are revisited and a theorem is developed which provides relaxed, decentralized asymptotic stability conditions. Throughout Chapters 4 to 7, it will be shown how this theorem can be applied to the respective energy systems. In fact, it will become clear that the relaxed conditions are essential for answering the research questions of Chapter 2, as the restrictive, strict EIP conditions are not applicable.

The chapter is concluded in Section 3.4 with an analysis of the EIP properties of the main class of models that is used throughout this thesis, viz. explicit state-space models in input-state-output PHS (ISO-PHS) form. Due to their port-based perspective and inherent passivity properties, such PHS models provide a natural starting point for an EIP-based control synthesis and stability analysis of networked systems. Additionally, they allow for a generalized, domain-unifying modeling of networked systems that comprise various physical domains.

3.1 Networked Systems

The AC power systems, DC power systems, DHNs, and NMESs considered in this thesis constitute networked systems in which different units are interconnected via some network structure of power lines or pipelines, respectively. From a system-theoretical viewpoint, analyzing and synthesizing such networked systems can be facilitated by means of graph theory (see, e.g., van der Schaft [2017, pp. 76–77]).

Inspired by Pfeifer [2022, Term 2.2], Arcak et al. [2016, p. 13], and van der Schaft [2017, pp. 10,76–77], the notion of an *autonomous, networked system* is introduced to provide a basis for a unifying description of networked energy systems. The following definition combines state-space representations, which are the usual starting point for subsequent stability analyses and controller designs, with a graph-theoretical system description.

Definition 3.1 (Autonomous, networked system)

An autonomous, networked system is a system

$$\dot{\mathbf{x}}(t) = \mathbf{f}(\mathbf{x}(t)) \quad (3.1a)$$

with states $\mathbf{x}(t) \in \mathcal{X} \subseteq \mathbb{R}^n$ and sufficiently smooth mapping $\mathbf{f} : \mathcal{X} \rightarrow \mathcal{X}$ which can be described by a weakly connected digraph $\mathcal{G} = (\mathcal{V}, \mathcal{E})$ without self-loops and $N \in \mathbb{N}$ subsystems on the nodes \mathcal{V} and edges \mathcal{E} . The subsystems are described by

$$\dot{\mathbf{x}}_k(t) = \mathbf{f}_k(\mathbf{x}_k(t), \mathbf{d}_k(t)), \quad \mathbf{z}_k(t) = \mathbf{h}_k(\mathbf{x}_k(t)), \quad k = 1, \dots, N \quad (3.1b)$$

with states $\mathbf{x}_k(t) \in \mathcal{X}_k \subseteq \mathbb{R}^{n_k} \subset \mathcal{X}$, $\mathbf{x}(t) = [\mathbf{x}_1(t), \dots, \mathbf{x}_N(t)]^\top$, interaction (coupling) input $\mathbf{d}_k(t) \in \mathbb{R}^m$, interaction (coupling) output $\mathbf{z}_k(t) \in \mathbb{R}^m$, and sufficiently smooth mappings $\mathbf{f}_k : \mathcal{X}_k \times \mathbb{R}^m \rightarrow \mathcal{X}_k$, $\mathbf{h}_k : \mathcal{X}_k \rightarrow \mathbb{R}^m$. The dynamics of all node and edge subsystems, respectively, are given by

$$\dot{\mathbf{x}}_{\mathcal{V}}(t) = \mathbf{f}_{\mathcal{V}}(\mathbf{x}_{\mathcal{V}}(t), \mathbf{d}_{\mathcal{V}}(t)), \quad \mathbf{z}_{\mathcal{V}}(t) = \mathbf{h}_{\mathcal{V}}(\mathbf{x}_{\mathcal{V}}(t)) \quad (3.1c)$$

$$\dot{\mathbf{x}}_{\mathcal{E}}(t) = \mathbf{f}_{\mathcal{E}}(\mathbf{x}_{\mathcal{E}}(t), \mathbf{d}_{\mathcal{E}}(t)), \quad \mathbf{z}_{\mathcal{E}}(t) = \mathbf{h}_{\mathcal{E}}(\mathbf{x}_{\mathcal{E}}(t)) \quad (3.1d)$$

with $(\cdot)_{\mathcal{V}} = \text{stack}((\cdot)_i)_{i \in \mathcal{V}}$, $(\cdot)_{\mathcal{E}} = \text{stack}((\cdot)_l)_{l \in \mathcal{E}}$, denoting the respective, stacked vectors and mappings of the subsystems. The interconnection structure between the subsystems is given by

$$\begin{bmatrix} \mathbf{d}_{\mathcal{V}}(t) \\ \mathbf{d}_{\mathcal{E}}(t) \end{bmatrix} = \begin{bmatrix} \mathbf{0}_{|\mathcal{V}| \times |\mathcal{V}|} & \mathbf{B} \\ -\mathbf{B}^\top & \mathbf{0}_{|\mathcal{E}| \times |\mathcal{E}|} \end{bmatrix} \otimes \mathbf{I}_m \begin{bmatrix} \mathbf{z}_{\mathcal{V}}(t) \\ \mathbf{z}_{\mathcal{E}}(t) \end{bmatrix} =: \mathbf{M} \begin{bmatrix} \mathbf{z}_{\mathcal{V}}(t) \\ \mathbf{z}_{\mathcal{E}}(t) \end{bmatrix}. \quad (3.1e)$$

where $\mathbf{M} = -\mathbf{M}^\top \in \mathbb{R}^{(mN) \times (mN)}$ is the static, skew-symmetric interconnection matrix and $\mathbf{B} \in \mathbb{R}^{|\mathcal{V}| \times |\mathcal{E}|}$ the incidence matrix of graph \mathcal{G} .

Remark 3.1 (Notation). *In the remainder of this thesis, the time dependence of variables and vectors is only made explicit when it provides clarity, e.g. in some proofs, and is otherwise omitted.*

Remark 3.2. *To simplify the exposition throughout this chapter, Definition 3.1 only considers subsystems (3.1b) with interaction ports $(\mathbf{d}_k, \mathbf{z}_k)$. In particular, this implies that subsystems which are accessible for control via a control port $(\mathbf{u}_k, \mathbf{y}_k)$ with control input $\mathbf{u}_k \in \mathbb{R}^{m_u}$ and corresponding output $\mathbf{y}_k \in \mathbb{R}^{m_y}$, i.e.,*

$$\dot{\mathbf{x}}_k = \tilde{\mathbf{f}}_k(\mathbf{x}_k, \mathbf{u}_k, \mathbf{d}_k), \quad \mathbf{y}_k = \mathbf{h}_{y,k}(\mathbf{x}_k), \quad \mathbf{z}_k = \mathbf{h}_k(\mathbf{x}_k), \quad (3.2)$$

are in closed loop with some controller. Furthermore, note that closing the loop of (3.2) with some controller \mathbf{u}_k does not change the selection of the interaction port pair variables $(\mathbf{d}_k, \mathbf{z}_k)$ (compare (3.2) with (3.1b)). This insight will be relevant later on during the controller designs in Chapters 4 to 6.

Remark 3.3. *Note that in some works from the literature, e.g., van der Schaft [2017, Equation (4.83)], the signs in front of the incidence matrices are reversed compared to (3.1e).*

3.2 Equilibrium-Independent Passivity and Stability of Networked Systems

Passivity is one of the major tools for the analysis of and control design in nonlinear, networked systems. Of particular importance for this thesis is the possibility to provide stability statements of equilibria of autonomous, networked systems in a modular, bottom-up manner [Arcak et al., 2016, p. 17].

With standard passivity theory, stability of the origin $\bar{\mathbf{x}} = \mathbf{0}_n$, $\mathbf{0}_n = \mathbf{f}(\bar{\mathbf{x}})$, of an autonomous, networked system (3.1a) can be investigated by requiring certain passivity properties of the subsystems (3.1b) and posing conditions on the interconnection structure (3.1e).²⁴ However, stability of the origin is typically not of interest in practical applications. Instead, stability of a desired steady-state operating point $\bar{\mathbf{x}} \neq \mathbf{0}_n$ or a range of feasible operating points $\bar{\mathbf{x}}$ within some equilibrium set $\mathcal{X} \subseteq \mathbb{R}^n$ has to be investigated. In such cases, the shifted passivity [van der Schaft, 2017, p. 96] or EIP [Arcak et al., 2016, p. 24–26] property has to be used.

While the basic approach of a modular, EIP-based stability analysis of any feasible equilibrium $\bar{\mathbf{x}} \in \mathcal{X}$ of an autonomous, networked system (3.1a) is similar to that used for the origin (see Appendix A, Lemma A.1), there exist no propositions or theorems

²⁴ A short recapitulation of the technical details behind this idea is provided in Appendix A.

in the literature that are readily applicable to autonomous, networked systems and provide decentralized, asymptotic stability conditions. Inspired by the results of Arcak et al. [2016, Theorem 3.1] and classical passivity theorems, this section provides such decentralized, EIP-based asymptotic stability conditions for any feasible $\bar{\mathbf{x}} \in \bar{\mathcal{X}}$.

To begin with, different notions of EIP are introduced. The following definition combines the results from Arcak et al. [2016, p. 24–26] and Hines et al. [2011, Definitions 1 and 2] with the introduction of a dissipation rate as in Definition A.1 for standard passivity.

Definition 3.2 (EIP, strict EIP, output strict EIP (OSEIP))

Consider a state-space system (3.1b) and suppose there exists a non-empty set $\bar{\mathcal{X}}_k \subseteq \mathbb{R}^{n_k}$, where for every $\bar{\mathbf{x}}_k \in \bar{\mathcal{X}}_k$ there is a unique input $\bar{\mathbf{d}}_k \in \mathbb{R}^m$ such that $\mathbf{0}_{n_k} = \mathbf{f}_k(\bar{\mathbf{x}}_k, \bar{\mathbf{d}}_k)$ and $\bar{\mathbf{z}}_k = \mathbf{h}_k(\bar{\mathbf{x}}_k)$. Then system (3.1b) is **EIP** w.r.t. the supply rate $(\mathbf{d}_k - \bar{\mathbf{d}}_k)^\top (\mathbf{z}_k - \bar{\mathbf{z}}_k)$, if there exists a continuously differentiable, positive semidefinite storage function $S_k : \mathcal{X}_k \times \bar{\mathcal{X}}_k \rightarrow \mathbb{R}_{\geq 0}$, $S_k(\bar{\mathbf{x}}_k, \bar{\mathbf{x}}_k) = 0$, and a positive semidefinite dissipation rate $\psi_k : \mathcal{X}_k \times \bar{\mathcal{X}}_k \rightarrow \mathbb{R}_{\geq 0}$, $\psi_k(\bar{\mathbf{x}}_k, \bar{\mathbf{x}}_k) = 0$, such that $\forall (\mathbf{x}_k, \bar{\mathbf{x}}_k, \mathbf{d}_k) \in \mathcal{X}_k \times \bar{\mathcal{X}}_k \times \mathbb{R}^m$, it holds that

$$\dot{S}_k(\mathbf{x}_k, \bar{\mathbf{x}}_k) = -\psi_k(\mathbf{x}_k, \bar{\mathbf{x}}_k) + (\mathbf{d}_k - \bar{\mathbf{d}}_k)^\top (\mathbf{z}_k - \bar{\mathbf{z}}_k) \leq (\mathbf{d}_k - \bar{\mathbf{d}}_k)^\top (\mathbf{z}_k - \bar{\mathbf{z}}_k). \quad (3.3)$$

Moreover, system (3.1b) is **strictly EIP** w.r.t. the supply rate $(\mathbf{d}_k - \bar{\mathbf{d}}_k)^\top (\mathbf{z}_k - \bar{\mathbf{z}}_k)$ and a continuously differentiable, positive semidefinite storage function $S_k(\bar{\mathbf{x}}_k, \bar{\mathbf{x}}_k)$, if the dissipation rate is positive definite, i.e., $\psi_k(\mathbf{x}_k, \bar{\mathbf{x}}_k) > 0, \forall \mathbf{x}_k \neq \bar{\mathbf{x}}_k, \psi_k(\bar{\mathbf{x}}_k, \bar{\mathbf{x}}_k) = 0$. If $\forall (\mathbf{x}_k, \bar{\mathbf{x}}_k, \mathbf{d}_k) \in \mathcal{X}_k \times \bar{\mathcal{X}}_k \times \mathbb{R}^m$ it holds that

$$\begin{aligned} \dot{S}_k(\mathbf{x}_k, \bar{\mathbf{x}}_k) &= -\psi_k(\mathbf{x}_k, \bar{\mathbf{x}}_k) - (\mathbf{z}_k - \bar{\mathbf{z}}_k)^\top (\boldsymbol{\rho}_k(\mathbf{z}_k) - \boldsymbol{\rho}_k(\bar{\mathbf{z}}_k)) + (\mathbf{d}_k - \bar{\mathbf{d}}_k)^\top (\mathbf{z}_k - \bar{\mathbf{z}}_k) \\ &\leq (\mathbf{d}_k - \bar{\mathbf{d}}_k)^\top (\mathbf{z}_k - \bar{\mathbf{z}}_k) \end{aligned} \quad (3.4)$$

with positive semidefinite dissipation rate $\psi_k : \mathcal{X}_k \times \bar{\mathcal{X}}_k \rightarrow \mathbb{R}_{\geq 0}$, $\psi_k(\bar{\mathbf{x}}_k, \bar{\mathbf{x}}_k) = 0$ and strictly monotone function $\boldsymbol{\rho}_k(\mathbf{z}_k) : \mathbb{R}^m \rightarrow \mathbb{R}^m$, $(\mathbf{z}_k - \bar{\mathbf{z}}_k)^\top (\boldsymbol{\rho}_k(\mathbf{z}_k) - \boldsymbol{\rho}_k(\bar{\mathbf{z}}_k)) > 0, \forall \mathbf{z}_k \neq \bar{\mathbf{z}}_k$, then system (3.1b) is **output strictly EIP (OSEIP)** w.r.t. the supply rate $(\mathbf{d}_k - \bar{\mathbf{d}}_k)^\top (\mathbf{z}_k - \bar{\mathbf{z}}_k)$ and a continuously differentiable, positive semidefinite storage function $S_k(\bar{\mathbf{x}}_k, \bar{\mathbf{x}}_k)$.

Remark 3.4 (Notation). When referring to EIP properties, the addition “w.r.t. the supply rate (...) and (...) storage function $S_k(\mathbf{x}_k, \bar{\mathbf{x}}_k)$ ” is commonly omitted in the literature. However, for clarity, the additional information regarding the supply rate and the properties of the storage function are provided throughout this thesis except when explicitly clear from the context, e.g, in a technical argument with repetitive reference to the same EIP property.

Remark 3.5 (Wording). EIP is also termed “shifted passivity with respect to any constant input $\bar{\mathbf{d}}$ and corresponding equilibrium $\bar{\mathbf{x}}$ ” by van der Schaft [2017, p. 169] or “passivity of incremental systems” by Bürger et al. [2014] and Jayawardhana et al. [2007]. On the other

hand, “incremental passivity” as defined by Stan and Sepulchre [2007] and van der Schaft [2017, p. 94–95], i.e., passivity with respect to two arbitrary state trajectories $\mathbf{x}_1(t)$, $\mathbf{x}_2(t)$, is more general than EIP, where one of the trajectories is an equilibrium $\bar{\mathbf{x}}$ [Hines et al., 2011; Simpson-Porco, 2019]. However, this makes incremental passivity also harder to verify. Within this thesis, the denotation EIP is used as the author believes it provides the clearest understanding of the passivity property it describes, i.e., passivity independent of an explicit equilibrium point.

In line with the stability analysis of the origin in Lemma A.1, (asymptotic) stability of any feasible equilibrium $\bar{\mathbf{x}} \in \bar{\mathcal{X}}$ of the autonomous, networked system (3.1a) can now be investigated by requiring certain EIP properties of the subsystems (3.1b) and using the skew symmetry of the interconnection structure (3.1e). The following proposition is inspired by Arcak et al. [2016, Theorem 3.1].

Proposition 3.1 (Equilibrium-independent stability of networked systems)

Consider an autonomous, networked system as in Definition 3.1. Assume (3.1a) admits equilibria within a non-empty equilibrium set $\bar{\mathcal{X}}$, i.e., $\bar{\mathbf{x}} \in \bar{\mathcal{X}}$. If each subsystem (3.1b) is EIP w.r.t. the supply rate $(\mathbf{d}_k - \bar{\mathbf{d}}_k)^\top (\mathbf{z}_k - \bar{\mathbf{z}}_k)$ and a continuously differentiable, positive definite storage function $S_k(\mathbf{x}_k, \bar{\mathbf{x}}_k) > 0, \forall \mathbf{x}_k \neq \bar{\mathbf{x}}_k, S_k(\bar{\mathbf{x}}_k, \bar{\mathbf{x}}_k) = 0$, then any equilibrium $\bar{\mathbf{x}} \in \bar{\mathcal{X}}$ is stable. If each subsystem (3.1b) is strictly EIP w.r.t. the supply rate $(\mathbf{d}_k - \bar{\mathbf{d}}_k)^\top (\mathbf{z}_k - \bar{\mathbf{z}}_k)$ and a continuously differentiable, positive definite storage function, $S_k(\mathbf{x}_k, \bar{\mathbf{x}}_k)$, then any equilibrium $\bar{\mathbf{x}} \in \bar{\mathcal{X}}$ is asymptotically stable.

Proof:

The proof follows a similar reasoning as that of Lemma A.1. Choose the storage function $S : \mathcal{X} \times \bar{\mathcal{X}} \rightarrow \mathbb{R}_{\geq 0}$ of the autonomous, networked system (3.1a) as the sum of the subsystem storage functions $S(\mathbf{x}, \bar{\mathbf{x}}) = \sum_{k=1}^N S_k(\mathbf{x}_k, \bar{\mathbf{x}}_k)$. Since each $S_k(\mathbf{x}_k, \bar{\mathbf{x}}_k)$ is continuously differentiable and positive definite, $S(\mathbf{x}, \bar{\mathbf{x}})$ is continuously differentiable and positive definite. Due to the skew symmetry of the interconnection structure (3.1e), it holds that $(\mathbf{d} - \bar{\mathbf{d}})^\top (\mathbf{z} - \bar{\mathbf{z}}) = (\mathbf{z} - \bar{\mathbf{z}})^\top \mathbf{M}(\mathbf{z} - \bar{\mathbf{z}}) = 0$. Thus, the time derivative of $S(\mathbf{x}, \bar{\mathbf{x}})$ is given by

$$\dot{S}(\mathbf{x}, \bar{\mathbf{x}}) = - \sum_{k=1}^N \psi_k(\mathbf{x}_k, \bar{\mathbf{x}}_k) \leq 0, \quad \forall \mathbf{x} \in \mathcal{X}, \quad (3.5)$$

which makes $S(\mathbf{x}, \bar{\mathbf{x}})$ a Lyapunov function for any feasible equilibrium $\bar{\mathbf{x}} \in \bar{\mathcal{X}}$ and proves its stability (see van der Schaft [2017, p. 44]). From strict EIP of each subsystem (3.1b), it follows that

$$\dot{S}(\bar{\mathbf{x}}, \bar{\mathbf{x}}) = 0, \quad \dot{S}(\mathbf{x}, \bar{\mathbf{x}}) = - \sum_{i=1}^N \psi_k(\mathbf{x}_k, \bar{\mathbf{x}}_k) < 0, \quad \forall \mathbf{x} \neq \bar{\mathbf{x}}, \quad (3.6)$$

which proves asymptotic stability of any feasible equilibrium $\bar{\mathbf{x}} \in \bar{\mathcal{X}}$ (see van der Schaft [2017, p. 44]). \square

Remark 3.6. Note that in order to directly infer stability statements from passivity/EIP properties as done in Proposition 3.1 and Lemma A.1, the storage functions S_k are required to be positive definite (see also Khalil [2002, Lemma 6.6]). In general, this additional requirement is needed, since the passivity/EIP properties introduced in Definitions 3.2 and A.1 only require positive semidefinite storage functions. In case of standard passivity, alternatively to requiring positive definite storage functions, additional detectability conditions can be posed on the subsystems to infer stability of the origin [Sepulchre et al., 1997, pp. 48-50]. However, in practice, the positive definiteness requirement is typically used as it is not restrictive. In particular, when storage functions are proposed based on energy considerations of the subsystem models (3.1b), they are often quadratic functions of the form $S_k(\mathbf{x}_k) = \frac{1}{2}\mathbf{x}_k^\top \mathbf{Q}_k \mathbf{x}_k$, $\mathbf{Q}_k \succ 0$, which are naturally positive definite (see for example Sections 4.2.2, 5.2.2, and 6.2.2).

3.3 Equilibrium-Independent Passivity and Asymptotic Stability of Networked Systems Revisited

Proposition 3.1 gives decentralized, analytical conditions that allow to infer asymptotic stability of any feasible equilibrium $\bar{\mathbf{x}} \in \bar{\mathcal{X}}$ of an autonomous, networked system (3.1). In principle, it thus provides a general answer to the research questions (Q1.1), (Q2.1), (Q3.2), and (Q4.1).

However, asymptotic stability can only be deduced directly in case *all* subsystems are strictly EIP, i.e., *all* dissipation rates $\psi_k(\mathbf{x}_k, \bar{\mathbf{x}}_k)$ have to be positive definite functions that satisfy $\psi_k(\mathbf{x}_k, \bar{\mathbf{x}}_k) > 0, \forall \mathbf{x}_k \neq \bar{\mathbf{x}}_k, \psi_k(\bar{\mathbf{x}}_k, \bar{\mathbf{x}}_k) = 0$. In other words, every state variable in each subsystem state vector \mathbf{x}_k is required to appear in the dissipation rate, as only then $\psi_k(\mathbf{x}_k, \bar{\mathbf{x}}_k) = 0$ implies $\mathbf{x}_k \equiv \bar{\mathbf{x}}_k$. In practice, this means that every state variable in \mathbf{x}_k must be subject to some direct damping, e.g., via a serial or parallel resistor in electrical systems or friction in hydraulic systems. However, in many applications including the various networked energy systems considered in this thesis, this requirement cannot be fulfilled in all subsystems (see for example Sections 4.3, 5.3, 6.2.2, and 6.3).

Thus, milder decentralized conditions are sought that allow to infer asymptotic stability of any feasible equilibrium $\bar{\mathbf{x}} \in \bar{\mathcal{X}}$ of an autonomous, networked system (3.1). For standard passivity, the strict passivity requirement that each subsystem has to fulfill in order to prove asymptotic stability can be relaxed by requiring additional invariance arguments or detectability/observability conditions (see, e.g., Sepulchre et al. [1997, pp. 48–50] or Khalil [2002, pp.243–250]). For the feedback interconnection of two passive subsystems, for example, OSP and zero-state observability (ZSO) (see Definition 3.3) are sufficient to proof asymptotic stability of the origin [Khalil, 2002, Theorem 6.3].

Definition 3.3 (Zero-state observability [van der Schaft, 2017, Definition 3.2.11])

A state-space system (3.1b) is zero-state observable (ZSO), if $\mathbf{d}_k(t) = \mathbf{0}_m$, $\mathbf{z}_k(t) = \mathbf{0}_m$, $\forall t \geq 0$ implies $\mathbf{x}_k(t) = \mathbf{0}_{n_k}$.

However, there exists no theorem within EIP theory that provides similarly relaxed, decentralized conditions to infer asymptotic stability of any feasible equilibrium $\bar{\mathbf{x}} \in \bar{\mathcal{X}}$ of an autonomous, networked system (3.1). Thus, inspired by classical passivity results and preliminary works in the EIP context by Hines et al. [2011], Bürger et al. [2014], and Simpson-Porco [2019], a general theorem is proposed which combines EIP, OSEIP, equilibrium-independent observability (EIO), and confined dynamics arguments to prove asymptotic stability of any feasible $\bar{\mathbf{x}} \in \bar{\mathcal{X}}$. The main idea behind the theorem is as follows: firstly, the EIP properties of the subsystems and their positive definite storage functions are combined to prove stability of $\bar{\mathbf{x}}$. Subsequently, the specific digraph representation of an autonomous, networked system, particularly its skew-symmetric interconnection structure, OSEIP, EIO, and confined dynamics arguments are used to modularize the asymptotic convergence analysis via the Invariance principle and prove asymptotic stability of $\bar{\mathbf{x}}$.

Definition 3.4 (Equilibrium-independent observability (EIO) [Simpson-Porco, 2019, Definition 4.1])

Consider a state-space system (3.1b) and suppose there exists a non-empty set $\bar{\mathcal{X}}_k \subseteq \mathbb{R}^{n_k}$, where for every $\bar{\mathbf{x}}_k \in \bar{\mathcal{X}}_k$ there is a unique input $\bar{\mathbf{d}}_k \in \mathbb{R}^m$ such that $\mathbf{0}_{n_k} = \mathbf{f}_k(\bar{\mathbf{x}}_k, \bar{\mathbf{d}}_k)$ and $\bar{\mathbf{z}}_k = \mathbf{h}_k(\bar{\mathbf{x}}_k)$. Then (3.1b) is equilibrium-independent observable (EIO), if $\mathbf{d}_k(t) = \bar{\mathbf{d}}_k$, $\mathbf{z}_k(t) = \bar{\mathbf{z}}_k$, $\forall t \geq 0$ implies $\mathbf{x}_k(t) = \bar{\mathbf{x}}_k$.

Theorem 3.1 (Equilibrium-independent asymptotic stability of networked systems)

Consider an autonomous, networked system as in Definition 3.1. Assume (3.1a) admits equilibria within a non-empty equilibrium set $\bar{\mathcal{X}} \subseteq \mathbb{R}^n$, i.e., $\bar{\mathbf{x}} \in \bar{\mathcal{X}}$. Then any equilibrium $\bar{\mathbf{x}} \in \bar{\mathcal{X}}$ is asymptotically stable, if the following four conditions hold:

- (i) Each edge subsystem $l \in \mathcal{E}$ is OSEIP w.r.t. the supply rate $(\mathbf{d}_l - \bar{\mathbf{d}}_l)^\top (\mathbf{z}_l - \bar{\mathbf{z}}_l)$ and a continuously differentiable, positive definite storage function $S_l(\mathbf{x}_l, \bar{\mathbf{x}}_l) > 0, \forall \mathbf{x}_l \neq \bar{\mathbf{x}}_l, S_l(\bar{\mathbf{x}}_l, \bar{\mathbf{x}}_l) = 0$.
- (ii) Each edge subsystem $l \in \mathcal{E}$ is either EIO or such that no solution other than $\mathbf{x}_l = \bar{\mathbf{x}}_l$ can stay in $\mathbb{E}_l = \{\mathbf{x}_l \in \mathcal{X}_l \subseteq \mathbb{R}^{n_l} \mid \dot{S}_l(\mathbf{x}_l, \bar{\mathbf{x}}_l) = 0, \mathbf{d}_l = \bar{\mathbf{d}}_l\}$ for all time.
- (iii) Each node subsystem $i \in \mathcal{V}$ is EIP w.r.t. the supply rate $(\mathbf{d}_i - \bar{\mathbf{d}}_i)^\top (\mathbf{z}_i - \bar{\mathbf{z}}_i)$ and a continuously differentiable, positive definite storage function $S_i(\mathbf{x}_i, \bar{\mathbf{x}}_i) > 0, \forall \mathbf{x}_i \neq \bar{\mathbf{x}}_i, S_i(\bar{\mathbf{x}}_i, \bar{\mathbf{x}}_i) = 0$.
- (iv) Each node subsystem $i \in \mathcal{V}$ is such that no solution other than $\mathbf{x}_i = \bar{\mathbf{x}}_i$ can stay in $\mathbb{E}_i = \{\mathbf{x}_i \in \mathcal{X}_i \subseteq \mathbb{R}^{n_i} \mid \dot{S}_i(\mathbf{x}_i, \bar{\mathbf{x}}_i) = 0, \mathbf{d}_i = \bar{\mathbf{d}}_i\}$ for all time.

Furthermore, the asymptotic stability statement continues to hold when the conditions for the node and edge subsystems are interchanged.

Proof:

Choose the storage function $S : \mathcal{X} \times \bar{\mathcal{X}} \rightarrow \mathbb{R}_{\geq 0}$ of the autonomous, networked system (3.1a) as the sum of the subsystem storage functions $S(\mathbf{x}, \bar{\mathbf{x}}) = \sum_{k=1}^N S_k(\mathbf{x}_k, \bar{\mathbf{x}}_k)$. Since each $S_k(\mathbf{x}_k, \bar{\mathbf{x}}_k)$ is continuously differentiable and positive definite per conditions (i) and (iii), $S(\mathbf{x}, \bar{\mathbf{x}})$ is continuously differentiable and positive definite. Due to the skew symmetry of the interconnection structure (3.1e), it holds that $(\mathbf{z} - \bar{\mathbf{z}})^\top (\mathbf{d} - \bar{\mathbf{d}}) = (\mathbf{z} - \bar{\mathbf{z}})^\top \mathbf{M}(\mathbf{z} - \bar{\mathbf{z}}) = 0$. Thus, with the OSEIP and EIP properties from conditions (i) and (iii), the time derivative of $S(\mathbf{x}, \bar{\mathbf{x}})$ satisfies

$$\dot{S}(\mathbf{x}, \bar{\mathbf{x}}) = \sum_{i \in \mathcal{V}} \dot{S}_i(\mathbf{x}_i, \bar{\mathbf{x}}_i) - \sum_{l \in \mathcal{E}} \dot{S}_l(\mathbf{x}_l, \bar{\mathbf{x}}_l) \quad (3.7a)$$

$$= - \sum_{k \in \mathcal{V} \cup \mathcal{E}} \psi_k(\mathbf{x}_k, \bar{\mathbf{x}}_k) - \sum_{l \in \mathcal{E}} (\mathbf{z}_l - \bar{\mathbf{z}}_l)^\top (\boldsymbol{\rho}_l(\mathbf{z}_l) - \boldsymbol{\rho}_l(\bar{\mathbf{z}}_l)) \leq 0, \quad \forall \mathbf{x} \in \mathcal{X}, \quad (3.7b)$$

which makes $S(\mathbf{x}, \bar{\mathbf{x}})$ a Lyapunov function for any feasible equilibrium $\bar{\mathbf{x}} \in \bar{\mathcal{X}}$ and proves its stability (see van der Schaft [2017, p. 44]).

Furthermore, as $t \rightarrow \infty$, every solution $\mathbf{x}(t)$ starting in \mathcal{X} converges to the largest invariant set \mathbb{M} contained in

$$\mathbb{E} = \{\mathbf{x} \in \mathcal{X} \mid \dot{S}(\mathbf{x}, \bar{\mathbf{x}}) = 0\}. \quad (3.8)$$

Due to its invariance, set \mathbb{M} can be found by considering only those solutions $\mathbf{x}(t)$ of (3.1a) which start in \mathbb{E} and evolve with their dynamics constraint to \mathbb{E} .

From (3.7), condition (i), and condition (iii), it follows that set \mathbb{E} in (3.8) can equivalently be characterized by $\dot{S}_i(\mathbf{x}_i, \bar{\mathbf{x}}_i) = 0$, $i \in \mathcal{V}$, and $\dot{S}_l(\mathbf{x}_l, \bar{\mathbf{x}}_l) = 0$, $l \in \mathcal{E}$. Due to the OSEIP of the edge subsystems (see condition (i)), $\dot{S}_l(\mathbf{x}_l, \bar{\mathbf{x}}_l) = 0$ implies $\mathbf{z}_l \equiv \bar{\mathbf{z}}_l$ for all $l \in \mathcal{E}$ and thus $\mathbf{z}_{\mathcal{E}} \equiv \bar{\mathbf{z}}_{\mathcal{E}}$. Due to the interconnection structure (3.1e), $\mathbf{z}_{\mathcal{E}} \equiv \bar{\mathbf{z}}_{\mathcal{E}}$ implies $\mathbf{d}_{\mathcal{V}} \equiv \bar{\mathbf{d}}_{\mathcal{V}}$. From $\mathbf{d}_{\mathcal{V}} \equiv \bar{\mathbf{d}}_{\mathcal{V}}$, $\dot{S}_i(\mathbf{x}_i, \bar{\mathbf{x}}_i) = 0$, and the confined node dynamics behavior in condition (iv), it follows that $\mathbf{x}_{\mathcal{V}} \equiv \bar{\mathbf{x}}_{\mathcal{V}}$, which in turn implies $\mathbf{z}_{\mathcal{V}} \equiv \bar{\mathbf{z}}_{\mathcal{V}}$. Due to the interconnection structure (3.1e), $\mathbf{z}_{\mathcal{V}} \equiv \bar{\mathbf{z}}_{\mathcal{V}}$ implies $\mathbf{d}_{\mathcal{E}} \equiv \bar{\mathbf{d}}_{\mathcal{E}}$. With $\mathbf{d}_{\mathcal{E}} \equiv \bar{\mathbf{d}}_{\mathcal{E}}$ and $\mathbf{z}_{\mathcal{E}} \equiv \bar{\mathbf{z}}_{\mathcal{E}}$ established, the EIO property or the confined dynamics behavior of the edge subsystems in condition (ii) implies $\mathbf{x}_{\mathcal{E}} \equiv \bar{\mathbf{x}}_{\mathcal{E}}$. Consequently, the largest invariant set contained in (3.8) is $\mathbf{x} = \bar{\mathbf{x}} = [\bar{\mathbf{x}}_{\mathcal{V}}, \bar{\mathbf{x}}_{\mathcal{E}}]^{\top} \in \bar{\mathcal{X}}$. Thus, any feasible equilibrium $\bar{\mathbf{x}} \in \bar{\mathcal{X}}$ is asymptotically stable.

In case the conditions for the node and edge subsystem are interchanged, the proof follows analogously by appropriately swapping the indices $(\cdot)_i$, $(\cdot)_l$ and $(\cdot)_{\mathcal{E}}$, $(\cdot)_{\mathcal{V}}$, respectively. \square

Remark 3.7. Note that in Theorem 3.1, the EIO property is only added as alternative for the edge subsystems (see condition (ii)), since it does not add any limitation on the other subsystem conditions. In contrast, adding EIO as an alternative property in the node condition (iv) alone would not yield a working proof. After establishing $\mathbf{d}_{\mathcal{V}} \equiv \bar{\mathbf{d}}_{\mathcal{V}}$, the argument would stop since $\mathbf{z}_{\mathcal{V}} \equiv \bar{\mathbf{z}}_{\mathcal{V}}$ would be needed to infer $\mathbf{x}_{\mathcal{V}} \equiv \bar{\mathbf{x}}_{\mathcal{V}}$ and continue the proof. A possibility to establish $\mathbf{z}_{\mathcal{V}} \equiv \bar{\mathbf{z}}_{\mathcal{V}}$ in \mathbb{E} would be to require the node subsystems to be OSEIP instead of EIP. However, this adds more conservativeness. The confined dynamics requirement in condition (iv), on the other hand, only needs $\mathbf{d}_{\mathcal{V}} \equiv \bar{\mathbf{d}}_{\mathcal{V}}$ to make the $\mathbf{x}_{\mathcal{V}} \equiv \bar{\mathbf{x}}_{\mathcal{V}}$ statement. Additionally, when applying the conditions from Theorem 3.1 to a given autonomous networked system model, the confined dynamics requirement makes not only use of $\mathbf{d}_i \equiv \bar{\mathbf{d}}_i$, but also considers any confinements arising from $\dot{S}_i(\mathbf{x}_i, \bar{\mathbf{x}}_i) = 0$. That is, states in \mathbf{x}_i that experience direct damping and thus appear in $\dot{S}_i(\mathbf{x}_i, \bar{\mathbf{x}}_i)$ via the dissipation rate (see (3.7b)) can be set to zero in \mathbb{E} . Experience gained by applying the conditions of Theorem 3.1 throughout Chapters 4 to 6 indicate that this often largely simplifies the confined dynamics and allows for a much more direct and simple analysis compared to establishing EIO.

As a last step within this section, the results of Proposition 3.1 and Theorem 3.1 are combined. The resulting corollary accounts for the fact that if some subsystem (3.1b) at a node or edge k of an autonomous, networked system (3.1a) is strictly EIP w.r.t. the supply rate $(\mathbf{d}_k - \bar{\mathbf{d}}_k)^{\top}(\mathbf{z}_k - \bar{\mathbf{z}}_k)$ and a continuously differentiable, positive definite storage function $S_k(\mathbf{x}_k, \bar{\mathbf{x}}_k)$, it can readily be integrated into the asymptotic stability proof of Theorem 3.1.

Corollary 3.1 (Theorem 3.1 with some strictly EIP subsystems)

Consider an autonomous, networked system as in Definition 3.1. Assume (3.1a) admits equilibria within a non-empty equilibrium set $\bar{\mathcal{X}} \subseteq \mathbb{R}^n$, i.e., $\bar{\mathbf{x}} \in \bar{\mathcal{X}}$. Furthermore, define $\mathcal{V} = \mathcal{V}_{\text{Th}} \cup \mathcal{V}_{\text{SEIP}}$, $\mathcal{E} = \mathcal{E}_{\text{Th}} \cup \mathcal{E}_{\text{SEIP}}$, and assume some subsystems $k \in \mathcal{V}_{\text{Th}} \cup \mathcal{E}_{\text{Th}}$ fulfill the conditions of Theorem 3.1, while others given by $k \in \mathcal{V}_{\text{SEIP}} \cup \mathcal{E}_{\text{SEIP}}$ are strictly EIP w.r.t. the supply rate $(\mathbf{d}_k - \bar{\mathbf{d}}_k)^\top (\mathbf{z}_k - \bar{\mathbf{z}}_k)$ and a continuously differentiable, positive definite storage function $S_k(\mathbf{x}_k, \bar{\mathbf{x}}_k) > 0, \forall \mathbf{x}_k \neq \bar{\mathbf{x}}_k, S_k(\bar{\mathbf{x}}_k, \bar{\mathbf{x}}_k) = 0$. Then any equilibrium $\bar{\mathbf{x}} \in \bar{\mathcal{X}}$ is asymptotically stable.

Proof:

The proof is similar to that of Theorem 3.1. The main difference is that in case of strict EIP, it holds for the respective subsystems that $\dot{S}_i(\mathbf{x}_i, \bar{\mathbf{x}}_i) = 0$ and $\dot{S}_l(\mathbf{x}_l, \bar{\mathbf{x}}_l) = 0$ directly imply $\mathbf{x}_i \equiv \bar{\mathbf{x}}_i$ and $\mathbf{x}_l \equiv \bar{\mathbf{x}}_l$, respectively. Furthermore, $\mathbf{x}_i \equiv \bar{\mathbf{x}}_i$ and $\mathbf{x}_l \equiv \bar{\mathbf{x}}_l$ imply $\mathbf{z}_i \equiv \bar{\mathbf{z}}_i$ and $\mathbf{z}_l \equiv \bar{\mathbf{z}}_l$, respectively. Consequently, either from OSEIP in condition (i) of Theorem 3.1 or from strict EIP, it follows that $\mathbf{z}_\mathcal{E} \equiv \bar{\mathbf{z}}_\mathcal{E}$ and thus $\mathbf{d}_\mathcal{V} \equiv \bar{\mathbf{d}}_\mathcal{V}$. Then, either from condition (iv) of Theorem 3.1 or from strict EIP, it follows that $\mathbf{x}_\mathcal{V} \equiv \bar{\mathbf{x}}_\mathcal{V}$, which in turn implies $\mathbf{z}_\mathcal{V} \equiv \bar{\mathbf{z}}_\mathcal{V}$. Lastly, either from condition (ii) of Theorem 3.1 or strict EIP, it follows that $\mathbf{x}_\mathcal{E} \equiv \bar{\mathbf{x}}_\mathcal{E}$. \square

3.3.1 Discussion

By requiring each subsystem to be strictly EIP, decentralized conditions for the asymptotic stability of any feasible networked system equilibrium can be deduced (see Proposition 3.1). This strict EIP requirement, however, is of limited practical use as it often cannot be fulfilled in real networked systems (see for example the various networked energy system models in Sections 4.3, 4.3, 6.2.2, and 6.3).

Theorem 3.1 remedies this limitation and demonstrates that less restricting EIP and OSEIP properties together with a confined dynamics requirement suffice for proving asymptotic stability of any feasible networked system equilibrium in a modular manner. The main innovation of the theorem lies in a full modularization of the two-step procedure which is commonly used when proving asymptotic stability of equilibria by means of non-strict passivity properties (see, e.g., Sepulchre et al. [1997, pp. 43,50]). In this procedure, firstly, stability of the/any equilibrium is established by generating a composite Lyapunov function V from the storage functions of the subsystems and combining their passivity/EIP properties to show negative semidefiniteness of \dot{V} . In absence of strict passivity/EIP, however, the second step towards an asymptotic stability statement cannot directly be conducted in a modular way. Instead, the Invariance Principle is applied to the overall system dynamics. In the proof of Theorem 3.1, this second step is also modularized by combining the skew-symmetric interconnection structure of autonomous, networked systems with EIP, OSEIP, EIO, and confined dynamics

properties of the subsystems. The generality of the decentralized, asymptotic stability conditions in Theorem 3.1, which are applicable to general, nonlinear state-space subsystems of the form (3.1b), provides a solid, system-theoretical foundation for realizing flexible networked system configurations comprising different technologies, control strategies, and physical domains. The local, decentralized nature furthermore allows for time-varying network topologies in which subsystems can connect and disconnect in a plug-and-play fashion.

Throughout Chapters 4 to 7, it will be shown how these beneficial features can be used to lay the foundation for decentralized stabilization frameworks in various networked energy systems. It will become evident that the relaxed EIP and OSEIP properties are in fact essential for proving asymptotic stability of any feasible equilibrium in AC power systems, DC power systems, DHNs, and NMESs, and thus for answering research questions (Q1.1), (Q2.1), (Q3.2), and (Q4.1).

3.4 Equilibrium-Independent Passivity of Port-Hamiltonian Systems

The representation of explicit state-space models (see (3.1b) or (3.2)) in PHS form provides a clear perspective on which input-output ports are accessible for control and over which ports subsystems interact with each other in a network structure. Furthermore, the passivity properties with respect to these ports and the Hamiltonian as a storage function are directly visible. This makes PHS representations the natural starting point or desired closed-loop form of many PBC designs (see, e.g., Ortega and García-Canseco [2004]; Jayawardhana et al. [2007]; Donaire and Junco [2009] and van der Schaft [2017, Chapter 7]) and facilitates a subsequent EIP-based stability analysis. Moreover, the generalized, power- and energy-based perspective underlying PHS modeling allows to describe different physical domains in a formally equivalent way and thus provides the basis for the analysis and control synthesis of multi-domain physical systems. In the context of this thesis, the domain-unifying nature of the PHS framework together with the notion of an autonomous, networked system are used to provide a unifying system description of the various networked energy systems, to transfer control solutions between energy systems, and formulate the NMES results in Chapter 7.

For a recapitulation of the concept of generalized modeling, which underlies PHSs theory, and basic ISO-PHS definitions, the reader is referred to Appendix A. Of particular interest within this thesis is the following subclass of ISO-PHSs, which is used to model the different subsystems within the networked energy systems. It combines aspects of a linear ISO-PHS with that of an ISO-PHS with nonlinear resistive structure.²⁵

²⁵ Note that the term *nonlinear* in the context of the resistive structure does not refer to a nonlinearity with respect to \mathbf{x} , which can already occur in expressions of the form $\mathbf{R}(\mathbf{x})\frac{\partial H(\mathbf{x})}{\partial \mathbf{x}}$. Instead, the nonlinearity refers to the so-called resistive port variables. For a detailed discussion see van der Schaft and Jeltsema [2014, p. 24] and Pfeifer [2022, pp. 28–29].

Definition 3.5 (Partially linear ISO-PHS with nonlinear resistive structure)

A partially linear ISO-PHS with nonlinear resistive structure is an explicit state-space model of the form

$$\dot{\mathbf{x}} = [\mathbf{J} - \mathbf{R}] \frac{\partial H}{\partial \mathbf{x}}(\mathbf{x}) - \mathcal{R} \left(\frac{\partial H}{\partial \mathbf{x}}(\mathbf{x}) \right) + \mathbf{G}(\mathbf{x})\mathbf{u} + \mathbf{K}\mathbf{d}, \quad (3.9a)$$

$$\mathbf{y} = \mathbf{G}^\top(\mathbf{x}) \frac{\partial H(\mathbf{x})}{\partial \mathbf{x}}, \quad (3.9b)$$

$$\mathbf{z} = \mathbf{K}^\top \frac{\partial H(\mathbf{x})}{\partial \mathbf{x}}, \quad (3.9c)$$

$$H(\mathbf{x}) = \frac{1}{2} \mathbf{x}^\top \mathbf{Q} \mathbf{x}, \quad (3.9d)$$

with \mathbf{x} , $\frac{\partial H}{\partial \mathbf{x}}(\mathbf{x})$, (\mathbf{u}, \mathbf{y}) , (\mathbf{d}, \mathbf{z}) as in Definition A.2. The Hamiltonian $H(\mathbf{x})$ is a quadratic, positive definite function with $\mathbf{Q} = \mathbf{Q}^\top \succ 0$. The matrices $\mathbf{J}, \mathbf{R} \in \mathbb{R}^{n \times n}$, $\mathbf{J} = -\mathbf{J}^\top$, $\mathbf{R} = \mathbf{R}^\top \succcurlyeq 0$, and $\mathbf{K} \in \mathbb{R}^{n \times m}$ are constant. The matrix $\mathbf{G}(\mathbf{x}) \in \mathbb{R}^{n \times m_u}$ is state-dependent. The nonlinear damping function $\mathcal{R} \left(\frac{\partial H}{\partial \mathbf{x}}(\mathbf{x}) \right) : \mathbb{R}^n \rightarrow \mathbb{R}^n$ is monotone w.r.t. $\frac{\partial H}{\partial \mathbf{x}}(\mathbf{x})$ and satisfies $\mathcal{R}(\mathbf{0}_n) = \mathbf{0}_n$ such that $\left(\frac{\partial H}{\partial \mathbf{x}}(\mathbf{x}) \right)^\top \mathcal{R} \left(\frac{\partial H}{\partial \mathbf{x}}(\mathbf{x}) \right) \geq 0$ for all $\frac{\partial H}{\partial \mathbf{x}}(\mathbf{x}) \in \mathbb{R}^n$ (cf. Rockafellar and Wets [1998, Definition 12.1]).

In the sequel, during the modeling of the DC power systems, AC power systems, and DHNs in Sections 4.1, 5.1, and 6.1, it is shown that each of the subsystems within the respective energy system can be represented as an ISO-PHS of the form (3.9). Thus, to facilitate the technical arguments in the remainder of this thesis, the EIP properties of the ISO-PHS (3.9) are analyzed in the following lemma.

Lemma 3.1 (EIP properties of ISO-PHS (3.9))

The ISO-PHS (3.9) is EIP w.r.t. the supply rate $(\mathbf{u} - \bar{\mathbf{u}})^\top (\mathbf{y} - \bar{\mathbf{y}}) + (\mathbf{d} - \bar{\mathbf{d}})^\top (\mathbf{z} - \bar{\mathbf{z}})$ and the shifted Hamiltonian as continuously differentiable, positive definite storage function

$$S(\mathbf{x}, \bar{\mathbf{x}}) = \frac{1}{2} (\mathbf{x} - \bar{\mathbf{x}})^\top \mathbf{Q} (\mathbf{x} - \bar{\mathbf{x}}) = \frac{1}{2} \|\mathbf{x} - \bar{\mathbf{x}}\|_Q^2, \quad (3.10)$$

if $\mathbf{G}(\mathbf{x})$ is constant, i.e., $\mathbf{G}(\mathbf{x}) = \mathbf{G}$. If additionally

$$\tilde{\mathcal{R}} \left(\frac{\partial H}{\partial \mathbf{x}}(\mathbf{x}) \right) := \mathbf{R} \frac{\partial H}{\partial \mathbf{x}}(\mathbf{x}) + \mathcal{R} \left(\frac{\partial H}{\partial \mathbf{x}}(\mathbf{x}) \right) \quad (3.11)$$

is strictly monotone w.r.t. $\frac{\partial H}{\partial \mathbf{x}}(\mathbf{x})$, then (3.9) is strictly EIP.

Proof:

In order to show EIP, let $\mathbf{G}(\mathbf{x}) = \mathbf{G}$ be constant in (3.9). Then, let \mathbf{u} and \mathbf{d} be fixed to arbitrary equilibrium values $\bar{\mathbf{u}}$ and $\bar{\mathbf{d}}$ with associated $\bar{\mathbf{y}}$, $\bar{\mathbf{z}}$, and $\bar{\mathbf{x}}$. Since $\bar{\mathbf{x}}$ satisfies

$$\mathbf{0} = [\mathbf{J} - \mathbf{R}] \frac{\partial H}{\partial \mathbf{x}}(\bar{\mathbf{x}}) - \mathcal{R} \left(\frac{\partial H}{\partial \mathbf{x}}(\bar{\mathbf{x}}) \right) + \mathbf{G}\bar{\mathbf{u}} + \mathbf{K}\bar{\mathbf{d}}, \quad (3.12)$$

the ISO-PHS (3.9) can equivalently be written as

$$\dot{\mathbf{x}} = [\mathbf{J} - \mathbf{R}] \left(\frac{\partial H}{\partial \mathbf{x}}(\mathbf{x}) - \frac{\partial H}{\partial \mathbf{x}}(\bar{\mathbf{x}}) \right) - [\mathcal{R} \left(\frac{\partial H}{\partial \mathbf{x}}(\mathbf{x}) \right) - \mathcal{R} \left(\frac{\partial H}{\partial \mathbf{x}}(\bar{\mathbf{x}}) \right)] + \mathbf{G}(\mathbf{u} - \bar{\mathbf{u}}) + \mathbf{K}(\mathbf{d} - \bar{\mathbf{d}}), \quad (3.13a)$$

$$\mathbf{y} - \bar{\mathbf{y}} = \mathbf{G}^\top \left(\frac{\partial H}{\partial \mathbf{x}}(\mathbf{x}) - \frac{\partial H}{\partial \mathbf{x}}(\bar{\mathbf{x}}) \right), \quad (3.13b)$$

$$\mathbf{z} - \bar{\mathbf{z}} = \mathbf{K}^\top \left(\frac{\partial H}{\partial \mathbf{x}}(\mathbf{x}) - \frac{\partial H}{\partial \mathbf{x}}(\bar{\mathbf{x}}) \right). \quad (3.13c)$$

By introducing $\tilde{\mathcal{R}} \left(\frac{\partial H}{\partial \mathbf{x}}(\mathbf{x}) \right)$ as in (3.11), (3.13a) can be rewritten as

$$\dot{\mathbf{x}} = \mathbf{J} \left(\frac{\partial H}{\partial \mathbf{x}}(\mathbf{x}) - \frac{\partial H}{\partial \mathbf{x}}(\bar{\mathbf{x}}) \right) - \left[\tilde{\mathcal{R}} \left(\frac{\partial H}{\partial \mathbf{x}}(\mathbf{x}) \right) - \tilde{\mathcal{R}} \left(\frac{\partial H}{\partial \mathbf{x}}(\bar{\mathbf{x}}) \right) \right] + \mathbf{G}(\mathbf{u} - \bar{\mathbf{u}}) + \mathbf{K}(\mathbf{d} - \bar{\mathbf{d}}). \quad (3.14)$$

For the time derivative of $S(\mathbf{x}, \bar{\mathbf{x}})$ in (3.10), it holds that

$$\begin{aligned} \dot{S}(\mathbf{x}, \bar{\mathbf{x}}) = & - \underbrace{\left(\frac{\partial H}{\partial \mathbf{x}}(\mathbf{x}) - \frac{\partial H}{\partial \mathbf{x}}(\bar{\mathbf{x}}) \right)^\top \left[\tilde{\mathcal{R}} \left(\frac{\partial H}{\partial \mathbf{x}}(\mathbf{x}) \right) - \tilde{\mathcal{R}} \left(\frac{\partial H}{\partial \mathbf{x}}(\bar{\mathbf{x}}) \right) \right]}_{\psi(\mathbf{x}, \bar{\mathbf{x}})} \\ & + \underbrace{(\mathbf{x} - \bar{\mathbf{x}})^\top \mathbf{Q}^\top \mathbf{G}^\top}_{(\mathbf{y} - \bar{\mathbf{y}})^\top} (\mathbf{u} - \bar{\mathbf{u}}) + \underbrace{(\mathbf{x} - \bar{\mathbf{x}})^\top \mathbf{Q}^\top \mathbf{K}^\top}_{(\mathbf{z} - \bar{\mathbf{z}})^\top} (\mathbf{d} - \bar{\mathbf{d}}). \end{aligned} \quad (3.15)$$

Since per definition $\mathbf{R} \succcurlyeq 0$ and $\mathcal{R} \left(\frac{\partial H}{\partial \mathbf{x}}(\mathbf{x}) \right)$ is monotone w.r.t. $\frac{\partial H}{\partial \mathbf{x}}(\mathbf{x})$, $\tilde{\mathcal{R}} \left(\frac{\partial H}{\partial \mathbf{x}}(\mathbf{x}) \right)$ is also monotone w.r.t. $\frac{\partial H}{\partial \mathbf{x}}(\mathbf{x})$ such that

$$\left(\frac{\partial H}{\partial \mathbf{x}}(\mathbf{x}) - \frac{\partial H}{\partial \mathbf{x}}(\bar{\mathbf{x}}) \right)^\top \left[\tilde{\mathcal{R}} \left(\frac{\partial H}{\partial \mathbf{x}}(\mathbf{x}) \right) - \tilde{\mathcal{R}} \left(\frac{\partial H}{\partial \mathbf{x}}(\bar{\mathbf{x}}) \right) \right] \geq 0, \quad \forall \frac{\partial H}{\partial \mathbf{x}}(\mathbf{x}) \in \mathbb{R}^n, \quad (3.16)$$

and consequently $\psi(\mathbf{x}, \bar{\mathbf{x}}) \geq 0$. Thus, according to Definition 3.2, the ISO-PHS (3.9) with $\mathbf{G}(\mathbf{x}) = \mathbf{G}$ is EIP w.r.t. the supply rate $(\mathbf{u} - \bar{\mathbf{u}})^\top (\mathbf{y} - \bar{\mathbf{y}}) + (\mathbf{d} - \bar{\mathbf{d}})^\top (\mathbf{z} - \bar{\mathbf{z}})$ and the continuously differentiable, positive definite storage function (3.10).

If $\tilde{\mathcal{R}} \left(\frac{\partial H}{\partial \mathbf{x}}(\mathbf{x}) \right)$ is strictly monotone w.r.t. $\frac{\partial H}{\partial \mathbf{x}}(\mathbf{x})$, i.e.,

$$\left(\frac{\partial H}{\partial \mathbf{x}}(\mathbf{x}) - \frac{\partial H}{\partial \mathbf{x}}(\bar{\mathbf{x}}) \right)^\top \left[\tilde{\mathcal{R}} \left(\frac{\partial H}{\partial \mathbf{x}}(\mathbf{x}) \right) - \tilde{\mathcal{R}} \left(\frac{\partial H}{\partial \mathbf{x}}(\bar{\mathbf{x}}) \right) \right] > 0, \quad \forall \frac{\partial H}{\partial \mathbf{x}}(\mathbf{x}) \neq \frac{\partial H}{\partial \mathbf{x}}(\bar{\mathbf{x}}), \quad (3.17)$$

it follows that $\psi(\mathbf{x}, \bar{\mathbf{x}}) > 0$ for all $\mathbf{x} \neq \bar{\mathbf{x}}$. Thus, the ISO-PHS (3.9) with $\mathbf{G}(\mathbf{x}) = \mathbf{G}$ is strictly EIP. \square

Remark 3.8. If $\mathbf{R} \succ 0$ or $\mathcal{R} \left(\frac{\partial H}{\partial \mathbf{x}}(\mathbf{x}) \right)$ is strictly monotone w.r.t. $\frac{\partial H}{\partial \mathbf{x}}(\mathbf{x})$, i.e.,

$$\left(\frac{\partial H}{\partial \mathbf{x}}(\mathbf{x}) - \frac{\partial H}{\partial \mathbf{x}}(\bar{\mathbf{x}}) \right)^\top \left[\mathcal{R} \left(\frac{\partial H}{\partial \mathbf{x}}(\mathbf{x}) \right) - \mathcal{R} \left(\frac{\partial H}{\partial \mathbf{x}}(\bar{\mathbf{x}}) \right) \right] > 0, \quad \forall \frac{\partial H}{\partial \mathbf{x}}(\mathbf{x}) \neq \frac{\partial H}{\partial \mathbf{x}}(\bar{\mathbf{x}}), \quad (3.18)$$

the strict monotonicity requirement of $\tilde{\mathcal{R}}$ in Lemma 5.2 is directly fulfilled.

Remark 3.9. *Note that while the standard passivity properties of ISO-PHS models of the form (A.5) or (3.9) can readily be verified (see, e.g., Duindam et al. [2009, p. 108] or Pfeifer [2022, Remark 2.27]), this is in general not the case for their EIP properties. The reason for this is the state dependence of the matrices (see, e.g., van der Schaft [2017, pp.136–137]). Lemma 3.1 thus provides a remedy for the relevant use cases that will appear within this thesis.*

Remark 3.10. *Note that since the Hamiltonian (3.9d) is a quadratic, positive definite function, its shifted version directly qualifies as a positive definite storage function. This property will be used throughout Chapters 4 to 6, since the various networked energy system models only comprise linear storage elements which always lead to quadratic Hamiltonians.*

This concludes the outline of the methodological approach. In the following, the concepts introduced in this chapter are used to answer the research questions formulated in Chapter 2 and develop cross-technology frameworks for the decentralized stabilization in DC power systems, AC power systems, DHNs, and NMESs.

In contrast to the order of appearance in the literature discussion in Chapter 2, the following presentation starts with DC power systems. As outlined in Section 2.2, DC power systems are on the rise over the last decades due to technological improvements and their advantages over their AC counterparts. In particular, the treatment of DC power systems is simpler than that of AC power systems as the system frequency, reactive power, and the consideration of electrical three-phase systems in a coupled dq frame are avoided. This simplifies the system modeling, stability analysis, and controller design and thus motivates DC power systems as the starting point for developing the ideas put forth in this thesis.

4 Passivity-Based Decentralized Stabilization in DC Power Systems

In this chapter, the graph-based description of a networked system, PHS modeling, and the EIP-based asymptotic stability theorem from Chapter 3 are used to develop a cross-technology framework for the decentralized stabilization of voltages and currents in DC power systems.

Firstly, Section 4.1 presents a graph-based, networked system description of the considered DC power systems along the lines of Definition 3.1. In particular, following Section 3.4, the subsystems at the nodes and edges of the DC power system digraph are modeled in a generalized manner as ISO-PHSs to facilitate the subsequent derivation of decentralized, technology-independent, asymptotic stability conditions and the PBC design.

Based on the model, Section 4.2 demonstrates how the passivity-based approach of Theorem 3.1 and Corollary 3.1 provides a direct answer to research question (Q2.1). Subsequently, the unactuated subsystems are shown to fulfill the derived, decentralized asymptotic stability conditions under parameter requirements. Lastly, the main control problems related to answering research question (Q2.2) are formulated.

In Section 4.3, the formulated control problems are addressed. Decentralized, passivity-based current and voltage controllers for the actuated DGU subsystems are designed. Additionally, the unifying, cross-technology nature of the established decentralized stabilization framework is showcased. By example of the voltage controller of Nahata et al. [2020] it is demonstrated how decentralized control solutions available in the literature are readily compatible with the decentralized asymptotic stability conditions derived in Section 4.2.

Subsequently, Section 4.4 presents simulation scenarios to validate the findings of the prior sections.

Sections 4.5 and 4.6 conclude this chapter with a discussion and summary of the main contributions. In particular, the main results are compared to the passivity-based works published in parallel to this thesis (see Section 2.4).²⁶

²⁶ Preliminary results leading to the content of this chapter have been published in the conference papers [Strehle et al., 2020a; Strehle et al., 2020b].

4.1 Modeling

In this section, the model of the considered DC power systems is established along the lines of Definition 3.1. Firstly, in Section 4.1.1, the DC power system setup is outlined and formally described as a digraph. Afterwards, in Sections 4.1.2 and 4.1.3, the subsystems on the nodes (DGUs, loads) and the edges (power lines) are modeled as explicit state-space systems in the form of ISO-PHSs (3.9). Lastly, the interconnection structure of the subsystems is formalized via the incidence matrix of the digraph in Section 4.1.4.

4.1.1 System Setup

This chapter considers DC power systems comprising DGUs, loads, and power lines that are connected in flexible, time-varying system configurations. Such DC power systems can be described by a weakly connected digraph $\mathcal{G} = (\mathcal{V}, \mathcal{E})$ without self-loops as illustrated in Figure 4.1 with subsystems on the nodes \mathcal{V} and edges \mathcal{E} . The nodes \mathcal{V} are partitioned into two sets: $\mathcal{D} = \{1, \dots, D\}$, $D \geq 1$, represents the DGUs, which may each supply a local load, and $\mathcal{L} = \{D + 1, \dots, D + L\}$, $L \geq 1$, represents load nodes without DGUs. The edges $\mathcal{E} = \mathcal{P} = \{1, \dots, P\}$, $P \geq 1$, represent power lines. The edge orientation represents the arbitrary reference direction of positive line currents. Furthermore, the digraph \mathcal{G} is completely specified by its incidence matrix $\mathbf{B} \in \mathbb{R}^{|\mathcal{V}| \times |\mathcal{E}|}$ with elements b_{il} (cf. (1.1)).

In the following, the models of the DGUs and loads on the nodes \mathcal{V} and the power lines on the edges \mathcal{E} of a DC power system digraph are presented.

4.1.2 Subsystems on Nodes

DGUs The circuit diagram of a DGU at any node $i \in \mathcal{D}$ in the DC power system is shown in the left dashed frame of Figure 4.2. The DGU comprises a DC voltage source, a voltage-source converter (VSC), and a series *RLC* filter with parameters $R_i, L_i, C_i > 0$. The DC voltage source represents an RES (e.g., a photovoltaic power plant), a storage device or a combination thereof. The losses in the VSC and filter are lumped together in R_i . The VSC is modeled by a time-averaged model commonly employed for control design (see for example Chiniforoosh et al. [2010] and Schiffer et al. [2016]).²⁷ The DC

²⁷ The average model is motivated by the fact that the switching frequencies of converters are typically very high (2 kHz-20 kHz) compared to the other system dynamics and sufficiently suppressed by RLC filters.

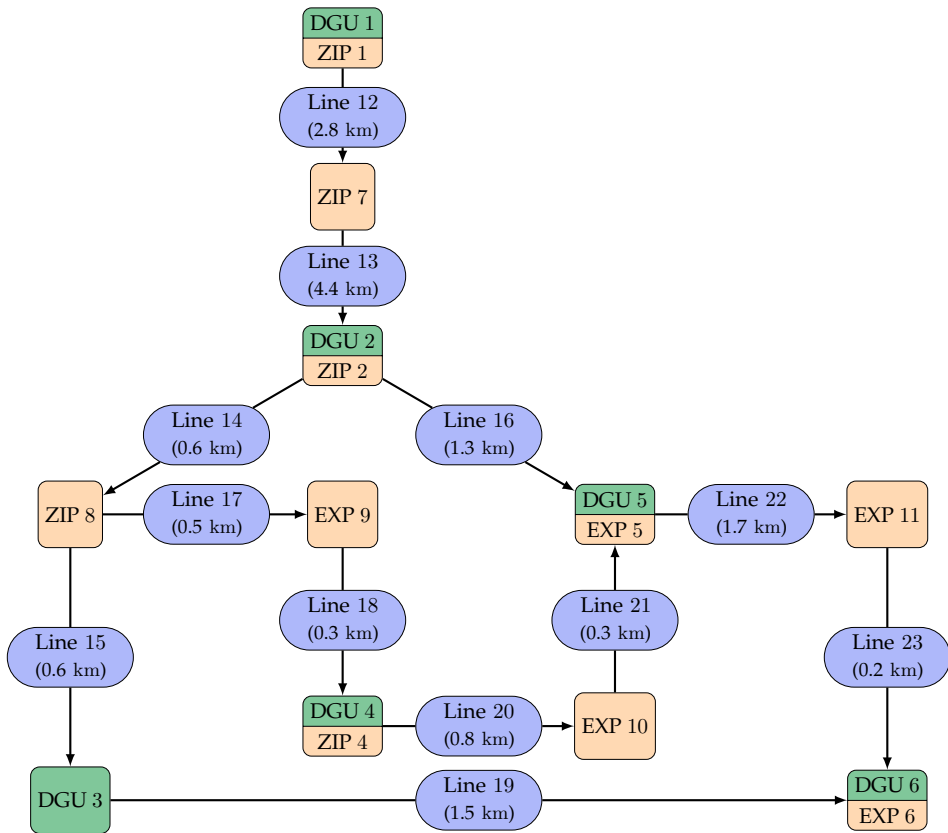


Figure 4.1: Digraph representation of Feeder 1 of the medium-voltage CIGRE AC benchmark network from Strunz et al. [2014, Figure 6.5] as DC power system comprising ZIP and exponential loads; DGUs are added at nodes $i \in \mathcal{D} = \{1, 2, 3, 4, 5, 6\}$.

source together with the averaged VSC model is assumed to form an ideal voltage source $V_{S,i}$ that supplies sufficient power at all times.²⁸

The current $I_{N,i}$ is the net-current injected into the DC power system which equals the accumulated incoming and outgoing line currents. Furthermore, each DGU may supply a local load described by a voltage-dependent current sink $I_{L,i}(V_i)$.

From Kirchhoff's current law (KCL) and Kirchhoff's voltage law (KVL), the dynamics for each DGU $i \in \mathcal{D}$ follow as

$$\begin{aligned} L_i \dot{I}_i &= -R_i I_i + V_{S,i} - V_i \\ C_i \dot{V}_i &= I_i - I_{L,i}(V_i) - I_{N,i}, \end{aligned} \quad (4.1a)$$

²⁸ Implicitly or explicitly, the ideal voltage source assumption is commonly made in the literature without any further discussion (see, e.g., all works reviewed in Section 2.2.1 and the parallel works focusing on DC power systems mentioned in Section 2.4.1). In the discussion in Section 4.5, its practical implications will be illuminated.

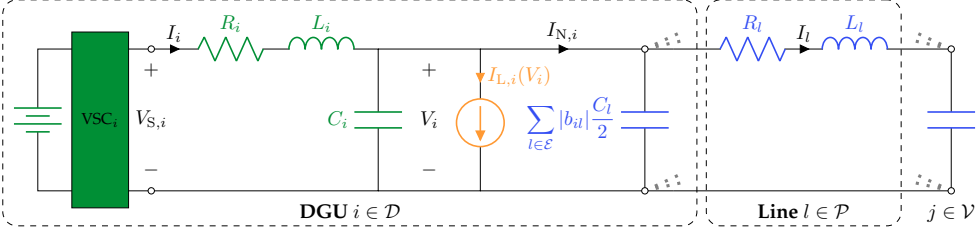


Figure 4.2: Circuit diagram of a DGU $i \in \mathcal{D}$ comprising a DC voltage source, a VSC with control input $V_{S,i}$, and a series RLC filter (green) connected to Π -model power lines (blue) and a local DC load represented by a voltage-dependent current sink $I_{L,i}(V_i)$ (orange). The line capacitances C_l are considered to be part of the respective subsystems at the nodes.

with $I_i, V_{S,i}, I_{N,i} \in \mathbb{R}$, $V_i \geq 0$, $I_{L,i} : \mathbb{R}_{\geq 0} \rightarrow \mathbb{R}$, and parameters $R_i, L_i, C_i > 0$. In order to write (4.1) as an ISO-PHS model, the following assumption has to be made:

Assumption 4.1 (Monotonicity of DC load current functions)

The load current function $I_{L,i}(V_i)$ is monotonically increasing and satisfies $I_{L,i}(0) = 0$.

Remark 4.1. In Section 4.2.2, conditions on the load parameters will be established such that Assumption 4.1 holds. It will be shown that ensuring the monotonicity property is equivalent to providing parameter specifications under which the load model is EIP.

Given Assumption 4.1, the DGU model (4.1) can be written as an ISO-PHS of the form (3.9) with state and co-state vectors

$$\mathbf{x}_i = \begin{bmatrix} L_i I_i \\ C_i V_i \end{bmatrix}, \quad \frac{\partial H_i}{\partial \mathbf{x}_i}(\mathbf{x}_i) = \begin{bmatrix} I_i \\ V_i \end{bmatrix}, \quad (4.1b)$$

control port pair

$$u_i = V_{S,i}, \quad y_i = I_i, \quad (4.1c)$$

uncontrolled interaction (coupling) port pair

$$d_i = -I_{N,i} = \sum_{l \in \mathcal{E}} b_{il} I_l, \quad z_i = V_i, \quad (4.1d)$$

matrices

$$\mathbf{J}_i = \begin{bmatrix} 0 & -1 \\ 1 & 0 \end{bmatrix}, \quad \mathbf{R}_i = \begin{bmatrix} R_i & 0 \\ 0 & 0 \end{bmatrix}, \quad \mathbf{G}_i = \begin{bmatrix} 1 \\ 0 \end{bmatrix}, \quad \mathbf{K}_i = \begin{bmatrix} 0 \\ 1 \end{bmatrix}, \quad \mathbf{Q}_i = \begin{bmatrix} \frac{1}{L_i} & 0 \\ 0 & \frac{1}{C_i} \end{bmatrix}, \quad (4.1e)$$

and nonlinear damping function

$$\mathcal{R}_i \left(\frac{\partial H_i}{\partial \mathbf{x}_i}(\mathbf{x}_i) \right) = \begin{bmatrix} 0 \\ I_{L,i}(V_i) \end{bmatrix}. \quad (4.1f)$$

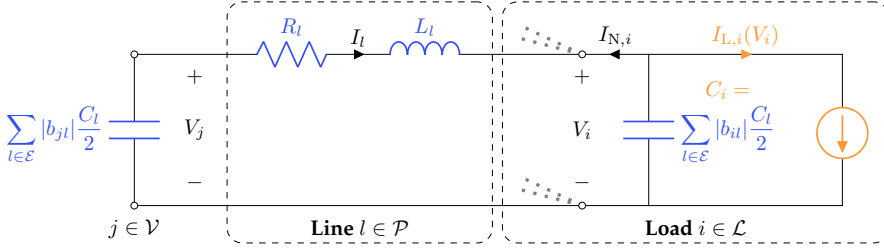


Figure 4.3: Circuit diagram of a load node $i \in \mathcal{L}$ comprising a nonlinear static ZIP or exponential load represented by a voltage-dependent current sink $I_{L,i}(V_i)$ (orange) connected to Π -model power lines (blue). The capacitance C_i is the sum of the parallel capacitances of the lines connecting to the load node.

Remark 4.2. In this thesis, the specific current-voltage relation $I_{L,i}(V_i)$ of a local load is either given by (4.2f) or (4.2g). In case a DGU does not supply a local load, $I_{L,i}(V_i) = 0$ and $\mathcal{R}_i \left(\frac{\partial H_i}{\partial x_i}(x_i) \right) = \mathbf{0}_2$.

Load nodes The circuit diagram of a DC load node $i \in \mathcal{L}$ along with connecting power lines is shown in Figure 4.3. The load is modeled as a voltage-dependent current sink representing a nonlinear static DC load. From KCL, the dynamic equation for each load node $i \in \mathcal{L}$ follows as

$$C_i \dot{V}_i = -I_{L,i}(V_i) - I_{N,i}, \quad (4.2a)$$

with $I_{N,i} \in \mathbb{R}$, $V_i \geq 0$, $I_{L,i} : \mathbb{R}_{\geq 0} \rightarrow \mathbb{R}$, and capacitance $C_i > 0$.

Under Assumption 4.1, the load node model (4.2) can be written as an ISO-PHS of the form (3.9) with state and co-state

$$x_i = C_i V_i, \quad \frac{\partial H_i}{\partial x_i}(x_i) = V_i, \quad (4.2b)$$

uncontrolled interaction (coupling) port pair

$$d_i = -I_{N,i} = \sum_{l \in \mathcal{E}} b_{il} I_l, \quad z_i = V_i, \quad (4.2c)$$

scalars

$$J_i = 0, \quad R_i = 0, \quad G_i = 0, \quad K_i = 1, \quad Q_i = \frac{1}{C_i}, \quad (4.2d)$$

and nonlinear damping function

$$\mathcal{R}_i \left(\frac{\partial H_i}{\partial x_i}(x_i) \right) = I_{L,i}(V_i). \quad (4.2e)$$

The nonlinear damping function (4.2e) is specified by the nonlinear, static current-voltage relation of the respective DC load models. In this thesis, the prevalent nonlinear,

static *ZIP* and *exponential* load models are considered (see Appendix B.1). For voltages above 0.7 times the nominal voltage $V_0 > 0$, i.e., $V_i \geq 0.7 V_0$, ZIP and exponential DC loads are modeled by the power equations (B.3a) and (B.4a), respectively. For $V_i < 0.7 V_0$, they behave like constant impedances (B.5a).

To obtain the current-voltage relation in (4.2e), the power equations (B.3a), (B.4a), and (B.5a) are divided by the respective node voltage V_i . This yields the ZIP load current relation

$$I_{L,i}(V_i) = \begin{cases} Y_{P,i}V_i + I_{P,i} + \frac{P_{P,i}}{V_i}, & V_i \geq 0.7 V_0, \\ \tilde{Y}_{P,i}V_i, & V_i < 0.7 V_0, \end{cases} \quad (4.2f)$$

with ZIP parameters $Y_{P,i}, I_{P,i}, P_{P,i} \geq 0$, $\tilde{Y}_{P,i} = Y_{P,i} + \frac{I_{P,i}}{0.7 V_0} + \frac{P_{P,i}}{(0.7 V_0)^2}$, and the exponential load current relation

$$I_{L,i}(V_i) = \begin{cases} P_{0,i} \frac{V_i^{n_{P,i}-1}}{V_0^{n_{P,i}}}, & V_i \geq 0.7 V_0, \\ \tilde{Y}_{P,i}V_i, & V_i < 0.7 V_0, \end{cases} \quad (4.2g)$$

with nominal power consumption $P_{0,i} \geq 0$, voltage index $n_{P,i} \geq 0$, and admittance $\tilde{Y}_{P,i} = \frac{P_{0,i} 0.7^{n_{P,i}}}{(0.7 V_0)^2}$.

4.1.3 Subsystems on Edges

Power lines The model of a DC power line at any edge $l \in \mathcal{P}$ is given by the Π -equivalent model of a transmission line [Kundur, 1994, pp. 201–207] with $C_l, R_l, L_l > 0$ as illustrated in Figures 4.2 and 4.3. The capacitances on both sides of the line are considered to be included in the equivalent capacitance C_i of the respective node subsystem $i \in \mathcal{V}$. This avoids dependent storages (i.e. parallel capacitances in this case) and thus dependent states. From KVL, the dynamic equation of each power line $l \in \mathcal{E}$ follows as

$$L_l \dot{I}_l = -R_l I_l - \sum_{i \in \mathcal{V}} b_{il} V_i, \quad (4.3a)$$

with $I_l \in \mathbb{R}$, $V_i \geq 0$, and parameters $R_l, L_l > 0$. Equation (4.3a) can be written as a linear ISO-PHS of the form (3.9) with state and co-state

$$x_l = L_l I_l, \quad \frac{\partial H_l}{\partial x_l}(x_l) = I_l, \quad (4.3b)$$

uncontrolled interaction (coupling) port pair

$$d_l = - \sum_{i \in \mathcal{V}} b_{il} V_i, \quad z_l = I_l, \quad (4.3c)$$

and scalars

$$J_l = 0, \quad R_l = R_l, \quad G_l = 0, \quad K_l = 1, \quad Q_l = \frac{1}{L_l}. \quad (4.3d)$$

Note that (4.3) has no control port (u_l, y_l) .

4.1.4 Interconnection Structure

The interconnection of the DGU and load subsystems on the nodes $i \in \mathcal{V}$ with the power line subsystems on the edges $l \in \mathcal{E}$ is clearly defined by the interaction (coupling) ports (4.1d), (4.2c), (4.3c) arising from their respective PHS representations. In particular, it holds that

$$d_i = \sum_{l \in \mathcal{E}} b_{il} I_l = \sum_{l \in \mathcal{E}} b_{il} z_l, \quad (4.4a)$$

$$d_l = - \sum_{i \in \mathcal{V}} b_{il} V_i = - \sum_{i \in \mathcal{V}} b_{il} z_i, \quad (4.4b)$$

and (cf. (3.1e) with $m = 1$)

$$\begin{bmatrix} \mathbf{d}_{\mathcal{V}} \\ \mathbf{d}_{\mathcal{E}} \end{bmatrix} = \begin{bmatrix} \mathbf{0}_{|\mathcal{V}| \times |\mathcal{V}|} & \mathbf{B} \\ -\mathbf{B}^{\top} & \mathbf{0}_{|\mathcal{E}| \times |\mathcal{E}|} \end{bmatrix} \begin{bmatrix} \mathbf{z}_{\mathcal{V}} \\ \mathbf{z}_{\mathcal{E}} \end{bmatrix} =: \mathbf{M} \begin{bmatrix} \mathbf{z}_{\mathcal{V}} \\ \mathbf{z}_{\mathcal{E}} \end{bmatrix} \quad (4.5)$$

with $(\cdot)_{\mathcal{V}} = \text{stack}((\cdot)_i)_{i \in \mathcal{V}}$ and $(\cdot)_{\mathcal{E}} = \text{stack}((\cdot)_l)_{l \in \mathcal{E}}$ denoting the respective, stacked vectors of the subsystems.

4.2 Asymptotic Stability Conditions and Control Problems

With the DC power system formalized as a digraph and its model established, research questions (Q2.1) and (Q2.2) can now formally be addressed. Firstly, in Section 4.2.1, decentralized asymptotic stability conditions are derived by application of Theorem 3.1 and Corollary 3.1. Subsequently, in Section 4.2.2, parameter requirements for the unactuated power line and load subsystems are established such that the derived, decentralized stability conditions are met. Lastly, in Section 4.2.3, the remaining control problems for the actuated DGU subsystems are formulated. Their solution in Section 4.3 will provide answers to research question (Q2.2).

4.2.1 Decentralized Asymptotic Stability Conditions

As a first step, note that the DC power system model outlined in Section 4.1 is similar to that of an autonomous, networked system given in Definition 3.1. So far, however, the control ports (u_i, y_i) of the DGUs at nodes $i \in \mathcal{D}$ are open, i.e., the DGU models are of the form (3.2). In order to conduct an equilibrium stability analysis, it is thus assumed that each DGU is in closed loop with some controller (see Remark 3.2).

Then, by direct application of Theorem 3.1 and Corollary 3.1 to the now autonomous DC power system model, decentralized, analytical conditions can be obtained, which,

if satisfied, ensure asymptotic stability of any feasible DC power system equilibrium $\bar{\mathbf{x}}_{\text{DC}} = \text{stack}(\bar{\mathbf{x}}_k)_{k \in \mathcal{V} \cup \mathcal{E}}$. The vectors $\bar{\mathbf{x}}_k$ are the respective equilibrium state vectors of the subsystems that are proportional to the steady-state voltages and currents of the DC power system (cf. (4.1b), (4.2b), (4.3b)).²⁹

Theorem 4.1 (Decentralized, asymptotic stability conditions for DC power systems)

Consider an autonomous DC power system as described in Section 4.1 with some controller u_i at each DGU $i \in \mathcal{D}$. Any feasible equilibrium $\bar{\mathbf{x}}_{\text{DC}} = \text{stack}(\bar{\mathbf{x}}_k)_{k \in \mathcal{V} \cup \mathcal{E}}$ of such an autonomous DC power system is asymptotically stable, if the following two conditions hold:

(DC 1) each subsystem at a node $i \in \mathcal{V}$ is

- strictly EIP w.r.t. the supply rate $(d_i - \bar{d}_i)(z_i - \bar{z}_i)$ and a continuously differentiable, positive definite storage function $S_i(\mathbf{x}_i, \bar{\mathbf{x}}_i)$, or
- EIP w.r.t. the supply rate $(d_i - \bar{d}_i)(z_i - \bar{z}_i)$ and a continuously differentiable, positive definite storage function $S_i(\mathbf{x}_i, \bar{\mathbf{x}}_i)$, and such that no solution other than $\mathbf{x}_i(t) = \bar{\mathbf{x}}_i$ can stay in $\mathbb{E}_i = \{\mathbf{x}_i \in \mathcal{X}_i \subseteq \mathbb{R}^{n_i} \mid \dot{S}_i(\mathbf{x}_i, \bar{\mathbf{x}}_i) = 0, d_i = \bar{d}_i\}$ for all time.

(DC 2) each subsystem at an edge $l \in \mathcal{E}$ is

- strictly EIP w.r.t. the supply rate $(d_l - \bar{d}_l)(z_l - \bar{z}_l)$ and a continuously differentiable, positive definite storage function $S_l(\mathbf{x}_l, \bar{\mathbf{x}}_l)$, or
- OSEIP w.r.t. the supply rate $(d_l - \bar{d}_l)(z_l - \bar{z}_l)$ and a continuously differentiable, positive definite storage function $S_l(\mathbf{x}_l, \bar{\mathbf{x}}_l)$, and either EIO or such that no solution other than $\mathbf{x}_l(t) = \bar{\mathbf{x}}_l$ can stay in $\mathbb{E}_l = \{\mathbf{x}_l \in \mathcal{X}_l \subseteq \mathbb{R}^{n_l} \mid \dot{S}_l(\mathbf{x}_l, \bar{\mathbf{x}}_l) = 0, d_l = \bar{d}_l\}$ for all time.

Proof:

The proof follows directly by application of Theorem 3.1 and Corollary 3.1 to the DC power system model established in Section 4.1 with some controller u_i at each DGU $i \in \mathcal{D}$. □

The conditions (DC 1) and (DC 2) of Theorem 4.1 answer research question (Q2.1). Next, it has to be ensured that the DGU and load subsystems fulfill (DC 1) and the power line subsystems fulfill (DC 2).

²⁹ Note that $\bar{\mathbf{x}}_k$ for $k \in \mathcal{D}$ possibly implies a slight abuse of notation, as in the case of dynamic DGU controllers the original state vector \mathbf{x}_k from (4.1b) is augmented by additional controller states.

4.2.2 Properties of the Unactuated Systems

For the unactuated subsystems without control ports, i.e, load nodes $i \in \mathcal{L}$ (see (4.2)) and power lines $l \in \mathcal{P}$ (see (4.3)), requirements on the model parameters have to be established such that conditions (DC 1) and (DC 2) are satisfied.

Load Nodes

Under Assumption 4.1, each load node $i \in \mathcal{L}$ can be represented as an ISO-PHS of form (3.9) with $G_i(x_i) = G_i = 0$ (see (4.2d)). According to Lemma 3.1, the load node model (4.2) is thus EIP w.r.t. the supply rate $(d_i - \bar{d}_i)(z_i - \bar{z}_i)$ and the shifted Hamiltonian as continuously differentiable, positive definite storage function $S_i(x_i, \bar{x}_i) = \frac{1}{2} \|x_i - \bar{x}_i\|_{Q_i}^2$. So far, however, it has not been investigated under which conditions Assumption 4.1 holds.

In the following proposition, necessary and sufficient conditions are provided that ensure each load node $i \in \mathcal{L}$ fulfills Assumption 4.1 and condition (DC 1). Furthermore, in the proof, it will be shown that ensuring EIP is in fact equivalent to fulfilling the monotonicity property from Assumption 4.1.

Proposition 4.1 (EIP and confined dynamics behavior of ZIP and exponential DC loads)

Consider a load node $i \in \mathcal{L}$ described by (4.2). If and only if

- for ZIP loads with (4.2f), it holds that

$$Y_{P,i} - \frac{P_{P,i}}{V_i^2} \geq 0, \quad V_i \geq 0.7 V_0. \quad (4.6)$$

- for exponential loads with (4.2g), it holds that

$$n_{P,i} - 1 \geq 0, \quad V_i \geq 0.7 V_0, \quad (4.7)$$

then Assumption 4.1 is fulfilled and (4.2a) is EIP w.r.t. the supply rate $(d_i - \bar{d}_i)(z_i - \bar{z}_i)$ and the continuously differentiable, positive definite storage function

$$S_i(x_i, \bar{x}_i) = \frac{1}{2} \|x_i - \bar{x}_i\|_{Q_i}^2 \quad (4.8)$$

for any (feasible) equilibrium pair (\bar{d}_i, \bar{z}_i) and associated equilibrium state

$$\bar{x}_i = C_i \bar{V}_i. \quad (4.9)$$

Furthermore, no solution other than $x_i(t) = \bar{x}_i$ as in (4.9) can stay in $\mathbb{E}_i = \{x_i \in \mathcal{X}_i \subseteq \mathbb{R} \mid \dot{S}_i(x_i, \bar{x}_i) = 0, d_i = \bar{d}_i\}$ for all time.

Proof:

In order to show that the load model (4.2) is EIP w.r.t. the supply rate $(d_i - \bar{d}_i)(z_i - \bar{z}_i)$ and the continuously differentiable, positive definite storage function $S_i(x_i, \bar{x}_i)$ in (4.8), let d_i be fixed to an arbitrary equilibrium value \bar{d}_i with associated equilibrium values $\bar{z}_i = \bar{V}_i$ and $\bar{x}_i = C_i \bar{V}_i$ (cf. (4.2b), (4.2c)) for the interaction output and state, respectively. Since \bar{x}_i satisfies $-\mathcal{R}_i\left(\frac{\partial H_i}{\partial x_i}(x_i)\right) + \bar{d}_i = 0$, the load model (4.2) can equivalently be written as

$$\dot{x}_i = - \left[\mathcal{R}_i\left(\frac{\partial H_i}{\partial x_i}(x_i)\right) - \mathcal{R}_i\left(\frac{\partial H_i}{\partial x_i}(\bar{x}_i)\right) \right] + K_i(d_i - \bar{d}_i). \quad (4.10)$$

For the time derivative of $S_i(x_i, \bar{x}_i)$ in (4.8), it holds that

$$\begin{aligned} \dot{S}_i(x_i, \bar{x}_i) = & - \underbrace{\left(\frac{\partial H_i}{\partial x_i}(x_i) - \frac{\partial H_i}{\partial x_i}(\bar{x}_i) \right) \left[\mathcal{R}_i\left(\frac{\partial H_i}{\partial x_i}(x_i)\right) - \mathcal{R}_i\left(\frac{\partial H_i}{\partial x_i}(\bar{x}_i)\right) \right]}_{\psi_i(x_i, \bar{x}_i)} \\ & + \underbrace{\left(\frac{\partial H_i}{\partial x_i}(x_i) - \frac{\partial H_i}{\partial x_i}(\bar{x}_i) \right)}_{(z_i - \bar{z}_i)} K_i(d_i - \bar{d}_i). \end{aligned} \quad (4.11)$$

Following Definition 3.2, the load model (4.2) is EIP, if and only if

$$\psi_i(x_i, \bar{x}_i) \stackrel{(4.2)}{=} (V_i - \bar{V}_i) (I_{L,i}(V_i) - I_{L,i}(\bar{V}_i)) \geq 0. \quad (4.12)$$

Note that according to Rockafellar and Wets [1998, Definition 12.1], (4.12) is the definition of a monotonically increasing, differentiable mapping $I_{L,i} : \mathbb{R} \rightarrow \mathbb{R}$. Thus, (4.12) is fulfilled, if and only if the load current function $I_{L,i}(V_i)$ is monotonically increasing, i.e., if and only if $\frac{dI_{L,i}(V_i)}{dV_i} \geq 0$ (see Rockafellar and Wets [1998, Proposition 12.3]). Additionally, $I_{L,i}(0) = 0$ holds (see (4.2f) and (4.2g)). Thus, fulfilling Assumption 4.1 and ensuring EIP are equivalent.

For the ZIP current-voltage function (4.2f), the derivative condition is given by

$$\frac{dI_{L,i}(V_i)}{dV_i} = \begin{cases} Y_{P,i} - \frac{P_{P,i}}{V_i^2} \geq 0, & V_i \geq 0.7 V_0, \\ \tilde{Y}_{P,i} = Y_{P,i} + \frac{I_{P,i}}{0.7 V_0} + \frac{P_{P,i}}{(0.7 V_0)^2} \geq 0, & V_i < 0.7 V_0. \end{cases} \quad (4.13)$$

Since $Y_{P,i}, I_{P,i}, P_{P,i}, V_0 \geq 0$ per definition, $\tilde{Y}_{P,i} \geq 0$ is always fulfilled. Thus, only the condition for $V_i \geq 0.7 V_0$ poses a restriction on the load parameters (see (4.6)).

For the exponential current-voltage function (4.2g), the derivative condition is given

by

$$\frac{dI_{L,i}(V_i)}{dV_i} = \begin{cases} (n_{P,i} - 1)P_{0,i} \frac{V_i^{n_{P,i}-2}}{V_0^{n_{P,i}}} \geq 0, & V_i \geq 0.7 V_0, \\ \tilde{Y}_{P,i} = \frac{P_{0,i} 0.7^{n_{P,i}}}{(0.7 V_0)^2} \geq 0, & V_i < 0.7 V_0. \end{cases} \quad (4.14)$$

Since $P_{0,i}, n_{P,i} \geq 0$ and $V_0 > 0$ per definition, $\tilde{Y}_{P,i} \geq 0$ is always fulfilled and only the condition for $V_i \geq 0.7 V_0$ poses restrictions on the load parameters. With $P_{0,i}, n_{P,i} \geq 0$ and $V_i \geq 0.7 V_0 > 0$, (4.14) holds if and only if (4.7).

Lastly, it is proven that conditions (4.6) and (4.7), respectively, also imply that no solution other than \bar{x}_i as in (4.9) can stay in $\mathbb{E}_i = \{x_i \in \mathcal{X}_i \subseteq \mathbb{R} \mid \dot{S}_i(x_i, \bar{x}_i) = 0, d_i = \bar{d}_i\}$ for all time. From (4.11), it follows that set \mathbb{E}_i is characterized by $\psi_i(x_i, \bar{x}_i) = 0$, which either directly implies $V_i = \bar{V}_i$ or $I_{L,i}(V_i) - I_{L,i}(\bar{V}_i) = 0$. For the latter, consider the evolution of a solution of (4.10) starting in \mathbb{E}_i . Confine the dynamics (4.10) to \mathbb{E}_i for any future time by inserting $\mathcal{R}_i \left(\frac{\partial H_i}{\partial x_i}(x_i) \right) - \mathcal{R}_i \left(\frac{\partial H_i}{\partial x_i}(\bar{x}_i) \right) = 0$ and $d_i = \bar{d}_i$. This yields $\dot{x}_i \equiv 0$, which implies $V_i \equiv \bar{V}_i$ and $x_i \equiv \bar{x}_i$, respectively. Thus, no solution other than \bar{x}_i as in (4.9) can stay in \mathbb{E}_i for all time. \square

Remark 4.3. The ZIP load condition (4.6) is most restrictive on the ratio between $Y_{P,i}$ and $P_{P,i}$ at the lower voltage bound $V_i = 0.7 V_0$, where

$$0.49 V_0^2 Y_{P,i} \geq P_{P,i} \quad (4.15)$$

has to be fulfilled. Thus, to ensure that some load node $i \in \mathcal{L}$ fulfills (DC 1) for all voltages $V_i \geq 0$, condition (4.15) has to be fulfilled.

Remark 4.4. From (4.6) and (4.15), it can be seen that loads whose constant power share $P_{P,i}$ becomes too large compared to the constant impedance share $Y_{P,i}$ violate the derived load conditions and thus prevent statements about the asymptotic stability of any DC power system equilibrium \bar{x}_{DC} . This is in line with power engineering practice and provides insights into the destabilizing effect of constant power loads mentioned in the literature (see, e.g., Dragičević et al. [2016] and Meng et al. [2017, Equation (8)]). Similarly, it can be seen from (4.7) that exponential loads must not behave too much like constant power loads ($n_{P,i} = 0$ for constant power load behavior).

Remark 4.5. Note that if (4.13) and (4.14), respectively, hold strictly, the load current function $I_{L,i}(V_i)$ is strictly monotonically increasing, i.e., $\frac{dI_{L,i}(V_i)}{dV_i} > 0$ (see Rockafellar and Wets [1998, Proposition 12.3]) and the load model is thus strictly EIP.

Power Lines

The DC power line models (4.3) can be represented as linear ISO-PHS models with constant matrices and positive definite dissipation $R_l > 0$ (see (4.3d)). According to Lemma 3.1, the power line models (4.3) are thus strictly EIP w.r.t. the supply rate $(d_l - \bar{d}_l)(z_l - \bar{z}_l)$ and the shifted Hamiltonian as continuously differentiable, positive definite storage function $S_l(x_l, \bar{x}_l) = \frac{1}{2} \|x_l - \bar{x}_l\|_{Q_l}^2$. Consequently, they satisfy condition (DC 2) for all model parameters.

4.2.3 Control Problems

For the actuated DGU subsystems $i \in \mathcal{D}$, decentralized controllers for the VSCs are to be designed such that the closed-loop systems satisfy condition (DC 1). Furthermore, the respective closed-loop equilibrium state vectors $\hat{x}_i, i \in \mathcal{D}$, should be such that desired node voltages $\bar{V}_i = V_i^* > 0$ and current injections $\bar{I}_i = I_i^* > 0$ are established in steady state (see research question (Q2.2)).

In particular, recall from Section 2.2 that the operating modes of VSCs can be separated into grid-forming voltage control and grid-feeding current control (see also Rocabert et al. [2012]). Consequently, in the following, the set of DGUs with VSCs stabilizing voltage setpoints V_i^* is denoted by $i \in \mathcal{D}_{\text{form}}$. Conversely, the set of DGUs with VSCs stabilizing the injected currents to setpoints I_i^* is denoted by $i \in \mathcal{D}_{\text{feed}}$.

In order to achieve decentralized stabilization in DC power systems as per Definition 2.4 and provide answers to research question (Q2.2), the following control problem is left to be addressed:

Problem 4.1 (Decentralized voltage and current control)

Consider DGUs $i \in \mathcal{D}$ described in open loop by (4.1). For the VSC in each DGU $i \in \mathcal{D}$, design decentralized controllers of the form

$$\dot{x}_{c,i} = f_{c,i}(x_i, x_{c,i}), \quad u_i = V_{S,i} = \hat{u}_i(x_i, x_{c,i}) \quad (4.16)$$

with controller state $x_{c,i} \in \mathbb{R}$ such that the resulting closed-loop system fulfills (DC 1). Furthermore, the respective closed-loop equilibrium state vector $\hat{x}_i = [\bar{x}_i, \bar{x}_{c,i}]^\top$ shall fulfill the following characteristics:

- (a) For each grid-feeding DGU $i \in \mathcal{D}_{\text{feed}}$, $\bar{I}_i = I_i^* > 0$ in \bar{x}_i .
- (b) For each grid-forming DGU $i \in \mathcal{D}_{\text{form}}$, $\bar{V}_i = V_i^* > 0$ in \bar{x}_i .

Remark 4.6. *In line with the hierarchical control structure discussed in Section 2.2.2, the setpoints V_i^* and I_i^* are assumed to be known and specified by a higher-level control ensuring that these setpoints constitute feasible DC power system equilibria \bar{x}_{DC} within the operational constraints.*

4.3 Passivity-Based Control Design

In this section, Problem 4.1 is addressed. In Sections 4.3.1 and 4.3.2, current and voltage controllers are designed for the VSCs such that the closed-loop DGU models fulfill the requirements in Problem 4.1. To showcase the unifying nature of the derived decentralized stability conditions, Section 4.3.3 demonstrates by example of the voltage controller proposed by Nahata et al. [2020] that decentralized, passivity-based controllers which are available in the literature are compatible with condition (DC 1).

4.3.1 Current Controller

The goal of current controllers in grid-feeding DGUs $i \in \mathcal{D}_{\text{feed}}$ is to asymptotically stabilize closed-loop DGU equilibria $\tilde{x}_i = [L_i I_i^*, C_i \bar{V}_i, \bar{x}_{c,i}]^\top$ containing some desired VSC output current $I_i^* > 0$ (see Problem 4.1 (a)). As $I_i = y_i$ is the natural passive control output of the open-loop DGU model (see (4.1c)), a standard PI controller working on $y_i^* - y_i = I_i^* - I_i$ can stabilize any equilibrium value \tilde{x}_i while preserving EIP of the closed-loop system with respect to the supply rate $(d_i - \bar{d}_i)(z_i - \bar{z}_i)$ (cf. Jayawardhana et al. [2007]). In the present case of grid-feeding DGUs $i \in \mathcal{D}_{\text{feed}}$, it can be shown that a standard PI current controller also suffices to ensure the additional confined dynamics requirement posed by (DC 1).

Proposition 4.2 (Current controller for grid-feeding DGUs)

Consider a grid-feeding DGU $i \in \mathcal{D}_{\text{feed}}$ described in open loop by (4.1). Assume the local ZIP or exponential load (4.1f) fulfills the conditions of Proposition 4.1. Assign the control input $u_i = V_{S,i}$ with the PI controller

$$Q_{I,i} \dot{r}_i = -(I_i - I_i^*), \quad (4.17a)$$

$$u_i = -k_{P,i}(I_i - I_i^*) + r_i, \quad (4.17b)$$

where $I_i^* > 0$ is a desired current setpoint and $k_{P,i}, Q_{1,i} > 0$ are control parameters. Then, the closed-loop DGU system can be written as

$$\frac{d}{dt} \underbrace{\begin{bmatrix} L_i I_i \\ C_i V_i \\ Q_{1,i} r_i \end{bmatrix}}_{\hat{\mathbf{x}}_i} = \underbrace{\begin{bmatrix} -R_i I_i - k_{P,i}(I_i - I_i^*) + r_i - V_i \\ I_i - I_{L,i}(V_i) \\ -(I_i - I_i^*) \end{bmatrix}}_{\hat{\mathbf{f}}_i(\hat{\mathbf{x}}_i)} + \underbrace{\begin{bmatrix} 0 \\ 1 \\ 0 \end{bmatrix}}_{\hat{\mathbf{K}}_i} d_i, \quad (4.18a)$$

$$z_i = V_i. \quad (4.18b)$$

Moreover, (4.18) is EIP w.r.t. the supply rate $(d_i - \bar{d}_i)(z_i - \bar{z}_i)$ and the continuously differentiable, positive definite storage function

$$\hat{S}_i(\hat{\mathbf{x}}_i, \bar{\mathbf{x}}_i) = \frac{1}{2} \|\hat{\mathbf{x}}_i - \bar{\mathbf{x}}_i\|_{\hat{\mathbf{Q}}_i}^2, \quad (4.19a)$$

$$\hat{\mathbf{Q}}_i = \text{diag} \left(\frac{1}{L_i}, \frac{1}{C_i}, \frac{1}{Q_{1,i}} \right), \quad (4.19b)$$

for any (feasible) equilibrium pair (\bar{d}_i, \bar{z}_i) and associated equilibrium state vector

$$\bar{\mathbf{x}}_i = [L_i I_i^*, C_i \bar{V}_i, Q_{1,i} \bar{r}_i]^\top. \quad (4.20)$$

Furthermore, no solution other than $\hat{\mathbf{x}}_i = \bar{\mathbf{x}}_i$ as in (4.20) can stay in $\mathbb{E}_i = \{\hat{\mathbf{x}}_i \in \hat{\mathcal{X}}_i \subseteq \mathbb{R}^3 \mid \hat{S}_i(\hat{\mathbf{x}}_i, \bar{\mathbf{x}}_i) = 0, d_i = \bar{d}_i\}$ for all time.

Proof:

Writing the closed-loop DGU model as in (4.18) directly follows by inserting the PI controller (4.17) into the open-loop DGU model (4.1).

In order to show that (4.18) is EIP w.r.t. the supply rate $(d_i - \bar{d}_i)(z_i - \bar{z}_i)$ and the continuously differentiable, positive definite storage function (4.19), let d_i be fixed to an arbitrary equilibrium value \bar{d}_i with associated equilibrium values \bar{z}_i and $\bar{\mathbf{x}}_i$ for the interaction output and state, respectively. Since $\bar{\mathbf{x}}_i$ satisfies $\hat{\mathbf{f}}_i(\bar{\mathbf{x}}_i) + \hat{\mathbf{K}}_i \bar{d}_i = \mathbf{0}_3$, the closed-loop DGU model (4.18) can equivalently be written as

$$\dot{\hat{\mathbf{x}}}_i = \hat{\mathbf{f}}_i(\hat{\mathbf{x}}_i) - \hat{\mathbf{f}}_i(\bar{\mathbf{x}}_i) + \hat{\mathbf{K}}_i (d_i - \bar{d}_i) \quad (4.21a)$$

$$\stackrel{(4.18)}{\stackrel{(4.20)}{=}} \begin{bmatrix} -R_i(I_i - I_i^*) - k_{P,i}(I_i - I_i^*) + (r_i - \bar{r}_i) - (V_i - \bar{V}_i) \\ (I_i - I_i^*) - (I_{L,i}(V_i) - I_{L,i}(\bar{V}_i)) \\ -(I_i - I_i^*) \end{bmatrix} + \begin{bmatrix} 0 \\ 1 \\ 0 \end{bmatrix} (d_i - \bar{d}_i), \quad (4.21b)$$

$$z_i - \bar{z}_i = V_i - \bar{V}_i. \quad (4.21c)$$

For the time derivative of $\hat{S}_i(\hat{\mathbf{x}}_i, \bar{\mathbf{x}}_i)$ in (4.19), it holds that

$$\dot{\hat{S}}_i(\hat{\mathbf{x}}_i, \bar{\mathbf{x}}_i) = \underbrace{(\hat{\mathbf{x}}_i - \bar{\mathbf{x}}_i)^\top \hat{\mathbf{Q}}_i^\top (\hat{\mathbf{f}}_i(\hat{\mathbf{x}}_i) - \hat{\mathbf{f}}_i(\bar{\mathbf{x}}_i))}_{-\hat{\psi}_i(\hat{\mathbf{x}}_i, \bar{\mathbf{x}}_i)} + \underbrace{(\hat{\mathbf{x}}_i - \bar{\mathbf{x}}_i)^\top \hat{\mathbf{Q}}_i^\top \hat{\mathbf{K}}_i}_{(z_i - \bar{z}_i)} (d_i - \bar{d}_i). \quad (4.22)$$

With (4.18), (4.19), and (4.20), the dissipation rate can be written as

$$\hat{\psi}_i(\hat{\mathbf{x}}_i, \bar{\mathbf{x}}_i) = (R_i + k_{P,i})(I_i - I_i^*)^2 + (V_i - \bar{V}_i)(I_{L,i}(V_i) - I_{L,i}(\bar{V}_i)). \quad (4.23)$$

Under the load conditions of Proposition 4.1 and since $R_i, k_{P,i} > 0$, it holds that $\hat{\psi}_i(\hat{\mathbf{x}}_i, \bar{\mathbf{x}}_i) \geq 0$. Thus, according to Definition 3.2, the closed-loop DGU model (4.18) is EIP w.r.t. the supply rate $(d_i - \bar{d}_i)(z_i - \bar{z}_i)$ and the continuously differentiable, positive definite storage function (4.19).

Lastly, it is proven that no solution other than $\bar{\mathbf{x}}_i$ as in (4.20) can stay in $\mathbb{E}_i = \{\hat{\mathbf{x}}_i \in \hat{\mathcal{X}}_i \subseteq \mathbb{R}^3 \mid \dot{\hat{S}}_i(\hat{\mathbf{x}}_i, \bar{\mathbf{x}}_i) = 0, d_i = \bar{d}_i\}$ for all time. From (4.22), it follows that set \mathbb{E}_i is characterized by

$$\hat{\psi}_i(\hat{\mathbf{x}}_i, \bar{\mathbf{x}}_i) \equiv 0 \stackrel{(4.23)}{\implies} I_i \equiv I_i^*. \quad (4.24)$$

Now consider the evolution of a solution of (4.21) starting in \mathbb{E}_i . Confine the dynamics (4.21) to \mathbb{E}_i for any future time by inserting (4.24). This yields the set of equations

$$\begin{aligned} 0 &= (r_i - \bar{r}_i) - (V_i - \bar{V}_i), \\ C_i \dot{V}_i &= I_{L,i}(V_i) - I_{L,i}(\bar{V}_i), \\ Q_{I,i} \dot{r}_i &= 0, \end{aligned} \quad (4.25)$$

whose unique solution is $V_i \equiv \bar{V}_i, r_i \equiv \bar{r}_i$. Thus, no solution other than $\bar{\mathbf{x}}_i$ as in (4.20) can stay in \mathbb{E}_i for all time. \square

In case a grid-feeding DGU $i \in \mathcal{D}_{\text{feed}}$ does not supply a local load, i.e., $I_{L,i}(V_i) = 0$ (see Remark 4.2), the statements of Proposition 4.2 still hold. The following corollary summarizes this insight.

Corollary 4.1 (Current control of grid-feeding DGUs without local loads)

Consider a grid-feeding DGU $i \in \mathcal{D}_{\text{feed}}$ that does not supply a local load, i.e., its open-loop model is given by (4.1) with $I_{L,i}(V_i) = 0$. Assign the control input with the PI controller as in Proposition 4.2. Then the closed-loop DGU system is given by (4.18) with $I_{L,i}(V_i) = 0$. Moreover, all statements from Proposition 4.2 regarding the EIP properties of the closed loop and its dynamics confined to set \mathbb{E}_i hold.

Proof:

The proof is identical to that of Proposition 4.2 except with $I_{L,i}(V_i) = I_{L,i}(\bar{V}_i) = 0$ in the respective equations. \square

4.3.2 Voltage Controller

The goal of voltage controllers in grid-forming DGUs $i \in \mathcal{D}_{\text{form}}$ is to asymptotically stabilize DGU equilibria $\hat{\mathbf{x}}_i = [L_i \bar{I}_i, C_i V_i^*, \bar{x}_{c,i}]^\top$ containing some desired node voltage $V_i^* > 0$ (see Problem 4.1 (b)). However, the node voltage is the passive interaction output $z_i = V_i$ (see (4.1d)) whose corresponding input d_i is not accessible as control input. Thus, a standard PI controller as for the current controller in Section 4.3.1 does not directly ensure EIP of the closed-loop with respect to the supply rate $(d_i - \bar{d}_i)(z_i - \bar{z}_i)$.

In order to meet the requirements for grid-forming DGUs $i \in \mathcal{D}_{\text{form}}$ stated in Problem 4.1, a voltage controller is proposed based on a design combining algebraic IDA-PBC from Ortega and García-Canseco [2004] and integral action from Donaire and Junco [2009].

Proposition 4.3 (Voltage controller for grid-forming DGUs)

Consider a grid-forming DGU $i \in \mathcal{D}_{\text{form}}$ described in open loop by (4.1). Assume the local ZIP or exponential load (4.1f) fulfills the conditions of Proposition 4.1. Assign the control input $u_i = V_{S,i}$ as

$$Q_{1,i} \dot{r}_i = V_i - V_i^*, \quad (4.26a)$$

$$u_i = V_i^* + (R_i - \hat{R}_i)I_i - \hat{R}_i r_i + \frac{L_i}{Q_{1,i}}(V_i^* - V_i), \quad (4.26b)$$

where $V_i^* > 0$ is a desired voltage setpoint and $\hat{R}_i, Q_{1,i} > 0$ are control parameters. Then, with the change of coordinates from I_i to

$$\chi_i := I_i + r_i, \quad (4.27)$$

the closed-loop DGU system can be written as

$$\frac{d}{dt} \underbrace{\begin{bmatrix} L_i \chi_i \\ C_i V_i \\ Q_{1,i} r_i \end{bmatrix}}_{\hat{\mathbf{x}}_i} = \underbrace{\begin{bmatrix} -\hat{R}_i \chi_i - (V_i - V_i^*) \\ \chi_i - r_i - I_{L,i}(V_i) \\ V_i - V_i^* \end{bmatrix}}_{\hat{\mathbf{f}}_i(\hat{\mathbf{x}}_i)} + \underbrace{\begin{bmatrix} 0 \\ 1 \\ 0 \end{bmatrix}}_{\hat{\mathbf{K}}_i} d_i, \quad (4.28a)$$

$$z_i - \bar{z} = V_i - V_i^*. \quad (4.28b)$$

Moreover, (4.28) is EIP w.r.t. the supply rate $(d_i - \bar{d}_i)(z_i - \bar{z}_i)$ and the continuously differentiable, positive definite storage function

$$\hat{S}_i(\hat{\mathbf{x}}_i, \bar{\mathbf{x}}_i) = \frac{1}{2} \|\hat{\mathbf{x}}_i - \bar{\mathbf{x}}_i\|_{\hat{Q}_i}^2, \quad (4.29a)$$

$$\hat{Q}_i = \text{diag} \left(\frac{1}{L_i}, \frac{1}{C_i}, \frac{1}{Q_{1,i}} \right) \quad (4.29b)$$

for any (feasible) equilibrium pair (\bar{d}_i, \bar{z}_i) and associated equilibrium state

$$\bar{\hat{x}}_i = [L_i \bar{\chi}_i, C_i V_i^*, Q_{1,i} \bar{r}_i]^\top. \quad (4.30)$$

Furthermore, no solution other than $\hat{x}_i = \bar{\hat{x}}_i$ as in (4.30) can stay in $\mathbb{E}_i = \{\hat{x}_i \in \hat{\mathcal{X}}_i \subseteq \mathbb{R}^3 \mid \hat{S}_i(\hat{x}_i, \bar{\hat{x}}_i) = 0, d_i = \bar{d}_i\}$ for all time.

Proof:

Firstly, it is illustrated how to assign desired closed-loop dynamics (4.28) according to IDA-PBC and systematically derive the coordinate transformation (4.27). Following the IDA-PBC design methodology from Ortega and García-Canseco [2004], the directly actuated current dynamics (see (4.1a)) are assigned a desired damping $\hat{R}_i > 0$ and the Hamiltonian is shifted such that it contains a term $C_i(V_i - V_i^*)$ implying a minimum at the desired voltage setpoint V_i^* . Additionally, following Donaire and Junco [2009], an integrator state (4.26a) is added to guarantee zero steady-state voltage errors. Subsequently, by introducing a new coordinate χ_i , the resulting DGU dynamics in closed-loop (see (4.28a)) can be written in the form of an ISO-PHS (3.9)

$$\frac{d}{dt} \begin{bmatrix} L_i \chi_i \\ C_i V_i \\ Q_{1,i} r_i \end{bmatrix} = \begin{bmatrix} -\hat{R}_i & -1 & 0 \\ 1 & 0 & -1 \\ 0 & 1 & 0 \end{bmatrix} \begin{bmatrix} \chi_i \\ V_i - V_i^* \\ r_i \end{bmatrix} - \begin{bmatrix} 0 \\ I_{L,i}(V_i) \\ 0 \end{bmatrix} + \begin{bmatrix} 0 \\ 1 \\ 0 \end{bmatrix} d_i. \quad (4.31)$$

The specific coordinate transformation (4.27) is found by matching the voltage dynamics, which are not directly actuated, in closed-loop (4.28a) (see also (4.31)) and open-loop (4.1a). This yields

$$\chi_i - r_i - I_{L,i}(V_i) + d_i = I_i - I_{L,i}(V_i) + d_i, \quad (4.32)$$

$$\Leftrightarrow \chi_i = I_i + r_i, \quad (4.33)$$

as in (4.27). In order to derive the controller (4.26b), compute $L_i \dot{\chi}_i$ to get

$$L_i \dot{\chi}_i \stackrel{(4.27)}{=} L_i \dot{I}_i + L_i \dot{r}_i \stackrel{(4.1a)}{=} \stackrel{(4.26a)}{=} -R_i I_i - V_i + u_i + L_i \frac{1}{Q_{1,i}} (V_i - V_i^*). \quad (4.34)$$

By matching (4.34) with the assigned $L_i \dot{\chi}_i$ dynamics in (4.28a) (see also (4.31)), i.e.,

$$-\hat{R}_i \chi_i - (V_i - V_i^*) \stackrel{(4.27)}{=} -\hat{R}_i I_i - \hat{R}_i r_i - (V_i - V_i^*) = -R_i I_i - V_i + u_i + L_i \frac{1}{Q_{1,i}} (V_i - V_i^*), \quad (4.35)$$

and rearranging, the control law (4.26b) is obtained.

Next, it is shown that (4.28) is EIP w.r.t. the supply rate $(d_i - \bar{d}_i)(z_i - \bar{z}_i)$ and the continuously differentiable, positive definite storage function (4.29). Following the same reasoning as in the proof of Proposition 4.2, the closed-loop DGU model (4.28) can

equivalently be written as

$$\dot{\hat{\mathbf{x}}}_i = \hat{\mathbf{f}}_i(\hat{\mathbf{x}}_i) - \hat{\mathbf{f}}_i(\bar{\mathbf{x}}_i) + \hat{\mathbf{K}}_i(d_i - \bar{d}_i) \quad (4.36a)$$

$$\stackrel{(4.28)}{=} \stackrel{(4.30)}{=} \begin{bmatrix} \hat{R}_i(\chi_i - \bar{\chi}_i) - (V_i - V_i^*) \\ (\chi_i - \bar{\chi}_i) - (r_i - \bar{r}_i) - (I_{L,i}(V_i) - I_{L,i}(V_i^*)) \\ V_i - V_i^* \end{bmatrix} + \begin{bmatrix} 0 \\ 1 \\ 0 \end{bmatrix} (d_i - \bar{d}_i), \quad (4.36b)$$

$$z_i - \bar{z}_i = V_i - \bar{V}_i. \quad (4.36c)$$

For the time derivative of $\hat{S}_i(\hat{\mathbf{x}}_i, \bar{\mathbf{x}}_i)$ in (4.29), it holds that

$$\dot{\hat{S}}_i(\hat{\mathbf{x}}_i, \bar{\mathbf{x}}_i) = \underbrace{(\hat{\mathbf{x}}_i - \bar{\mathbf{x}}_i)^\top \hat{\mathbf{Q}}_i^\top (\hat{\mathbf{f}}_i(\hat{\mathbf{x}}_i) - \hat{\mathbf{f}}_i(\bar{\mathbf{x}}_i))}_{-\hat{\psi}_i(\hat{\mathbf{x}}_i, \bar{\mathbf{x}}_i)} + \underbrace{(\hat{\mathbf{x}}_i - \bar{\mathbf{x}}_i)^\top \hat{\mathbf{Q}}_i^\top \hat{\mathbf{K}}_i}_{(z_i - \bar{z}_i)} (d_i - \bar{d}_i). \quad (4.37)$$

With (4.28), (4.29), and (4.30), the dissipation rate can be written as

$$\hat{\psi}_i(\hat{\mathbf{x}}_i, \bar{\mathbf{x}}_i) = \hat{R}_i(\chi_i - \bar{\chi}_i)^2 + (V_i - V_i^*) (I_{L,i}(V_i) - I_{L,i}(V_i^*)). \quad (4.38)$$

Under the load conditions of Proposition 4.1 and since $\hat{R}_i > 0$, it holds that $\hat{\psi}_i(\hat{\mathbf{x}}_i, \bar{\mathbf{x}}_i) \geq 0$. Thus, according to Definition 3.2, the closed-loop DGU model (4.28) is EIP w.r.t. the supply rate $(d_i - \bar{d}_i)(z_i - \bar{z}_i)$ and the continuously differentiable, positive definite storage function (4.29).

Lastly, it is proven that no solution other than $\bar{\mathbf{x}}_i$ as in (4.30) can stay in $\mathbb{E}_i = \{\hat{\mathbf{x}}_i \in \hat{\mathcal{X}}_i \subseteq \mathbb{R}^3 \mid \dot{\hat{S}}_i(\hat{\mathbf{x}}_i, \bar{\mathbf{x}}_i) = 0, d_i = \bar{d}_i\}$ for all time. From (4.37), it follows that set \mathbb{E}_i is characterized by

$$\hat{\psi}_i(\hat{\mathbf{x}}_i, \bar{\mathbf{x}}_i) \equiv 0 \stackrel{(4.38)}{\implies} \chi_i \equiv \bar{\chi}_i. \quad (4.39)$$

Now consider the evolution of a solution of (4.36) starting in \mathbb{E}_i . Confine the dynamics (4.36) to \mathbb{E}_i for any future time by inserting (4.39). This yields the set of equations

$$\begin{aligned} 0 &= -(V_i - V_i^*), \\ C_i \dot{V}_i &= -(r_i - \bar{r}_i) - (I_{L,i}(V_i) - I_{L,i}(V_i^*)), \\ Q_{1,i} \dot{r}_i &= (V_i - V_i^*), \end{aligned} \quad (4.40)$$

whose unique solution is $V_i \equiv V_i^*$, $r_i \equiv \bar{r}_i$. Thus, no solution other than $\bar{\mathbf{x}}_i$ as in (4.30) can stay in \mathbb{E}_i for all time. \square

Remark 4.7. Note that the controller (4.26) is composed of a setpoint feedforward V_i^* , a static state feedback proportional to I_i for damping assignment, and a PI term acting on the control error $V_i^* - V_i$ to ensure zero steady-state errors under parameter uncertainties and unknown, steady-state interaction inputs $\bar{d}_i = -\bar{I}_{N,i}$. All these building blocks are available as industrial standard, off-the-shelf control functions.

Similar to current-controlled, grid-feeding DGUs (see Corollary 4.1), the statements about voltage-controlled, grid-forming DGUs in Proposition 4.3 remain valid in case the DGUs do not supply a local load, i.e., $I_{L,i}(V_i) = 0$ (see Remark 4.2). The following corollary summarizes this insight.

Corollary 4.2 (Voltage control of grid-forming DGUs without local loads)

Consider a grid-forming DGU $i \in \mathcal{D}_{\text{form}}$ that does not supply a local load, i.e., its open-loop model is given by (4.1) with $I_{L,i}(V_i) = 0$. Assign the control input and coordinate transformation as in Proposition 4.2. Then the closed-loop DGU system is given by (4.28) with $I_{L,i}(V_i) = 0$. Moreover, all statements from Proposition 4.3 regarding the EIP properties of the closed loop and its dynamics confined to set \mathbb{E}_i hold.

Proof:

The proof is identical to that of Proposition 4.3 except with $I_{L,i}(V_i) = I_{L,i}(\bar{V}_i) = 0$ in the respective equations. \square

In Appendix B.2, it is shown how the results of the voltage control design from Proposition 4.3 can be generalized for a passivity-based output control of linear second-order systems. On the one hand, the generalized results will be used in the sequel to transfer the insights from the DC voltage control design to controlling pumps in DHNs (see Section 6.3.1). On the other hand, due to the simple structure of the resulting controller (see Remark 4.7) and the ubiquity of linear second-order systems in practical control engineering problems, the generalization presents an interesting result for promoting passivity-based control in practical control problems.

4.3.3 Voltage Controller of Nahata et al. [2020]

In this last control design section, it is shown by example of the voltage controller proposed by Nahata et al. [2020] that decentralized controllers in the literature are readily compatible with the decentralized stability conditions of Theorem 4.1.

For the subsequent elaborations, note that Nahata et al. [2020] model DGUs with the permuted version of the co-state vector $\frac{\partial H_i}{\partial \mathbf{x}_i}(\mathbf{x}_i)$ (4.1b) as actual state vector, i.e., $\mathbf{x}_i = [V_i, I_i]^\top$. To allow for a transparent cross-referencing, this model perspective is used in the following proposition.

Proposition 4.4 (Voltage controller of Nahata et al. [2020])

Consider a grid-forming DGU $i \in \mathcal{D}_{\text{form}}$ described in open loop by (4.1). Assume the local ZIP or exponential load (4.1f) fulfills the conditions of Proposition 4.1. Assign the control input $u_i = V_{S,i}$ according to Nahata et al. [2020] as

$$\dot{r}_i = -(V_i - V_i^*), \quad (4.41a)$$

$$u_i = k_{1,i}V_i + k_{2,i}I_i + k_{3,i}r_i, \quad (4.41b)$$

with voltage setpoint $V_i^* > 0$ and control parameters

$$k_{1,i} < 1, \quad k_{2,i} < R_i, \quad 0 < k_{3,i} < \frac{1}{L_i}(k_{1,i} - 1)(k_{2,i} - R_i). \quad (4.42)$$

Then, the closed-loop DGU system can be written as

$$\frac{d}{dt} \underbrace{\begin{bmatrix} V_i \\ I_i \\ r_i \end{bmatrix}}_{\hat{\mathbf{x}}_i} = \underbrace{\begin{bmatrix} \frac{1}{C_i}I_i - \frac{1}{C_i}I_{L,i}(V_i) \\ \alpha_i V_i + \beta_i I_i + \gamma_i r_i \\ -(V_i - V_i^*) \end{bmatrix}}_{\hat{\mathbf{f}}_i(\hat{\mathbf{x}}_i)} + \underbrace{\begin{bmatrix} \frac{1}{C_i} \\ 0 \\ 0 \end{bmatrix}}_{\hat{\mathbf{K}}_i} d_i, \quad (4.43a)$$

$$z_i = V_i, \quad (4.43b)$$

with

$$\alpha_i = \frac{k_{1,i} - 1}{L_i}, \quad \beta_i = \frac{k_{2,i} - R_i}{L_i}, \quad \gamma_i = \frac{k_{3,i}}{L_i}. \quad (4.43c)$$

Moreover, (4.43) is EIP w.r.t. the supply rate $(d_i - \bar{d}_i)(z_i - \bar{z}_i)$ and the continuously differentiable, positive definite storage function

$$\hat{S}_i(\hat{\mathbf{x}}_i, \bar{\mathbf{x}}_i) = \frac{1}{2} \|\hat{\mathbf{x}}_i - \bar{\mathbf{x}}_i\|_{\hat{\mathbf{Q}}_i}^2, \quad (4.44a)$$

$$\hat{\mathbf{Q}}_i = \begin{bmatrix} C_i & 0 & 0 \\ 0 & \frac{\beta_i}{\omega_i} & \frac{\gamma_i}{\omega_i} \\ 0 & \frac{\gamma_i}{\omega_i} & \frac{\alpha_i \gamma_i}{\omega_i} \end{bmatrix}, \quad (4.44b)$$

$$\omega_i = \gamma_i - \alpha_i \beta_i, \quad (4.44c)$$

for any (feasible) equilibrium pair (\bar{d}_i, \bar{z}_i) and associated equilibrium state

$$\bar{\mathbf{x}}_i = [V_i^*, \bar{I}_i, \bar{r}_i]^\top. \quad (4.45)$$

Lastly, no solution other than $\hat{\mathbf{x}}_i = \bar{\mathbf{x}}_i$ as in (4.45) can stay in $\mathbb{E}_i = \{\hat{\mathbf{x}}_i \in \hat{\mathcal{X}}_i \subseteq \mathbb{R}^3 \mid \hat{S}_i(\hat{\mathbf{x}}_i, \bar{\mathbf{x}}_i) = 0, d_i = \bar{d}_i\}$ for all time.

Proof:

Writing the closed-loop DGU model as in (4.43) directly follows by inserting the state-feedback controller (4.41) into the open-loop DGU model (4.1) and rewriting with states as in Nahata et al. [2020].

In order to show that (4.43) is EIP w.r.t. the supply rate $(d_i - \bar{d}_i)(z_i - \bar{z}_i)$ and the continuously differentiable, positive definite storage function (4.44), the same reasoning as in the proof of Proposition 4.2 is used. In particular, the closed-loop DGU model (4.43) can equivalently be written as (cf. Nahata et al. [2020, Equation (25)])

$$\dot{\hat{\mathbf{x}}}_i = \hat{\mathbf{f}}_i(\hat{\mathbf{x}}_i) - \hat{\mathbf{f}}_i(\bar{\mathbf{x}}_i) + \hat{\mathbf{K}}_i(d_i - \bar{d}_i) \quad (4.46a)$$

$$\stackrel{(4.43)}{=} \stackrel{(4.45)}{\left[\begin{array}{c} \frac{1}{C_i}(I_i - \bar{I}_i) - \frac{1}{C_i}(I_{L,i}(V_i) - I_{L,i}(V_i^*)), \\ \alpha_i(V_i - V_i^*) + \beta_i(I_i - \bar{I}_i) + \gamma_i(r_i - \bar{r}_i) \\ -(V_i - V_i^*) \end{array} \right]} + \left[\begin{array}{c} \frac{1}{C_i} \\ 0 \\ 0 \end{array} \right] (d_i - \bar{d}_i), \quad (4.46b)$$

$$z_i - \bar{z}_i = V_i - \bar{V}_i. \quad (4.46c)$$

For the time derivative of $\hat{S}_i(\hat{\mathbf{x}}_i, \bar{\mathbf{x}}_i)$ in (4.44), it holds that

$$\dot{\hat{S}}_i(\hat{\mathbf{x}}_i, \bar{\mathbf{x}}_i) = \underbrace{(\hat{\mathbf{x}}_i - \bar{\mathbf{x}}_i)^\top \hat{\mathbf{Q}}_i^\top (\hat{\mathbf{f}}_i(\hat{\mathbf{x}}_i) - \hat{\mathbf{f}}_i(\bar{\mathbf{x}}_i))}_{-\hat{\psi}_i(\hat{\mathbf{x}}_i, \bar{\mathbf{x}}_i)} + \underbrace{(\hat{\mathbf{x}}_i - \bar{\mathbf{x}}_i)^\top \hat{\mathbf{Q}}_i^\top \hat{\mathbf{K}}_i}_{(z_i - \bar{z}_i)} (d_i - \bar{d}_i). \quad (4.47)$$

With (4.43), (4.44), and (4.45), the dissipation rate can be written as (cf. Nahata et al. [2020, Equation (37)])

$$\hat{\psi}_i(\hat{\mathbf{x}}_i, \bar{\mathbf{x}}_i) = \frac{(\beta_i(I_i - \bar{I}_i) + \gamma_i(r_i - \bar{r}_i))^2}{\omega} + (V_i - V_i^*)(I_{L,i}(V_i) - I_{L,i}(V_i^*)). \quad (4.48)$$

If the control parameters $k_{1,i}, k_{2,i}, k_{3,i}$, satisfy (4.42) (see the proof of Theorem 2 in Nahata et al. [2020], particularly (41)) and the load conditions of Proposition 4.1 hold, it follows that $\hat{\psi}_i(\hat{\mathbf{x}}_i, \bar{\mathbf{x}}_i) \geq 0$. Thus, according to Definition 3.2, the closed-loop DGU model (4.43) is EIP w.r.t. the supply rate $(d_i - \bar{d}_i)(z_i - \bar{z}_i)$ and the continuously differentiable, positive definite storage function (4.44).

Lastly, it is proven that no solution other than $\bar{\mathbf{x}}_i$ as in (4.30) can stay in $\mathbb{E}_i = \{\hat{\mathbf{x}}_i \in \hat{\mathcal{X}}_i \subseteq \mathbb{R}^3 \mid \dot{\hat{S}}_i(\hat{\mathbf{x}}_i, \bar{\mathbf{x}}_i) = 0, d_i = \bar{d}_i\}$ for all time. From (4.47), it follows that set \mathbb{E}_i is characterized by (cf. Nahata et al. [2020, Equation (44)])

$$\hat{\psi}_i(\hat{\mathbf{x}}_i, \bar{\mathbf{x}}_i) \equiv 0 \stackrel{(4.48)}{\implies} \beta_i(I_i - \bar{I}_i) \equiv -\gamma_i(r_i - \bar{r}_i). \quad (4.49)$$

Now consider the evolution of a solution of (4.36) starting in \mathbb{E}_i . Confine the dynamics (4.36) to \mathbb{E}_i for any future time by inserting (4.49). This yields the set of equations

$$\dot{V}_i = -\frac{\gamma_i}{C_i \beta_i}(r_i - \bar{r}_i) - \frac{1}{C_i}(I_{L,i}(V_i) - I_{L,i}(V_i^*)), \quad (4.50a)$$

$$-\frac{\gamma_i}{\beta_i} \dot{r}_i = \alpha_i(V_i - V_i^*), \quad (4.50b)$$

$$\dot{r}_i = -(V_i - V_i^*). \quad (4.50c)$$

From (4.50b) and (4.50c) follows that $\alpha_i \beta_i (V_i - V_i^*) = \gamma_i (V_i - V_i^*)$. Following the explanations around Nahata et al. [2020, Equation (48)], this can only hold if $V_i \equiv V_i^*$, which implies by (4.50a) that $r_i \equiv \bar{r}_i$ and by (4.49) that $I_i \equiv \bar{I}_i$. Thus, no solution other than $\bar{\hat{x}}_i$ as in (4.45) can stay in \mathbb{E}_i for all time. \square

Remark 4.8. *Compared to the voltage controller (4.26) in Proposition 4.3, the voltage control law (4.41) by Nahata et al. [2020] is more restrictive on the choice of control parameters that are required to fulfill condition (DC 1). While the controller (4.26) only requires positive control parameters $\hat{R}_i, Q_{1,i} > 0$, the control parameters of (4.41) must fulfill the three inequality conditions given by (4.42). On the other hand, the voltage controller (4.41) of Nahata et al. [2020] comprises individual gains for the voltage V_i , the current I_i , and the integral voltage error r_i , while the voltage controller (4.26) only has two control parameters for the three terms containing V_i, I_i , and r_i .*

4.4 Simulation

This section demonstrates the validity of the presented unifying stabilization framework via two simulative case studies. In particular, the stability properties of ZIP and exponential loads under the conditions of Proposition 4.1 as well as the stabilizing properties, plug-and-play capabilities, and disturbance rejection behavior of the voltage and current controllers from Propositions 4.2 and 4.3 are shown.

The first scenario in Section 4.4.2 focuses on plug-and-play operations of DGUs and flexible, time-varying system configurations. The second scenario in Section 4.4.3 investigates whether different setpoints for the controlled node voltages and VSC output currents can be asymptotically stabilized and disturbances arising from load variations be rejected. In order to highlight the unifying nature of the presented, EIP-based stabilization framework, both scenarios are complemented with a DGU controlled by the voltage controller of Nahata et al. [2020] (see Proposition 4.4). Additionally, both scenarios are simulated with an uncertainty on the DGU filter parameters to evaluate the disturbance rejection capabilities of the controllers against parameter uncertainties.

4.4.1 General Simulation Setup

For the simulations, a DC power system based on the topology of Feeder 1 of the CIGRE medium-voltage AC benchmark network from Strunz et al. [2014, Figure 6.5] and Farrokhhabadi et al. [2018, pp. 42ff] is implemented in MATLAB/SIMULINK using

SIMSCAPE components.³⁰ In order to adequately assess the control schemes proposed in this chapter, the network is modified in two ways (see Figure 4.1):

- The connection to the high-voltage transmission network at node 1 is resolved. Instead, DGUs are added at nodes $i \in \mathcal{D} = \{1, 2, 3, 4, 5, 6\}$ with the proposed current controller (4.17) at DGUs $i \in \mathcal{D}_{\text{feed}} = \{3, 5, 6\}$, the proposed voltage controller (4.26) at DGUs $i \in \mathcal{D}_{\text{PBC}} = \{2, 4\}$, and the voltage controller (4.41) from Nahata et al. [2020] at DGU $i \in \mathcal{D}_{\text{N20}} = \{1\}$.
- Instead of only exponential loads as in Farrokhhabadi et al. [2018, pp. 42ff], ZIP loads are connected at nodes $i \in \mathcal{L}_{\text{ZIP}} = \{1, 2, 4, 7, 8\}$, while exponential loads remain at nodes $i \in \mathcal{L}_{\text{EXP}} = \{5, 6, 9, 10, 11\}$.

The network, DGU filter, and electrical line parameters used in the simulations are summarized in Table 4.1. They are in line with typical values (see, e.g., Tucci et al. [2016b], Han et al. [2019], and Cucuzzella et al. [2023]). In both scenarios, the RLC filters of all DGUs are parameterized identically with nominal values as in Table 4.1. These nominal values are used in all DGU controllers (4.17), (4.26), and (4.41), while the actual implemented filter parameters have a +10 % offset to evaluate the disturbance rejection capabilities of the controllers against parameter uncertainties. The resulting effective cut-off frequency of the RLC filters is thus $f_{\text{cut}} = \frac{1}{\sqrt{L_i C_i}} = 80 \text{ Hz}$.

The parameters of the controllers are summarized in Table 4.1 as well. The DGU references used in the controllers are set as in Table 4.2 to yield reasonable network situations.

The load parameters are given in Tables 4.3 and 4.4. The exponential load parameters are taken from Farrokhhabadi et al. [2018, pp. 42,45] and adapted to the DC case. That is, only the active power values are used. Additionally, the overall power demand of the loads is scaled down from originally 1 MW to 19 kW to account for the lower network voltage of $V_0 = 380 \text{ V}$ compared to the original $V_0 = 20 \text{ kV}$. The ZIP load parameters then follow from the exponential load parameters in Farrokhhabadi et al. [2018, pp. 42,45] via the equivalence transformation in Farrokhhabadi et al. [2018, Equation (38)] with $Z^p = \frac{5}{7}$, $I^p = \frac{1}{7}$, $P^p = \frac{1}{7}$. The parameters of each load satisfy the conditions of Proposition 4.1 for all voltages $V_i \geq 0$. For the ZIP loads, this means that the condition from Remark 4.3 is fulfilled.

³⁰ The SIMSCAPE toolbox extends SIMULINK with tools for modeling and simulating multi-domain physical systems. It allows to textually create physical component models based on physical ports and generalized effort and flow variables (see www.mathworks.com/help/simscape).

Table 4.1: Simulation parameters for the DC power system simulation

Network	$V_0 = 380 \text{ V}$
DGU filters (4.1)	$R_i = 0.2 \Omega, L_i = 1.8 \text{ mH}, C_i = 2.2 \text{ mF}$
Electrical lines (4.3)	$R_l = 0.1 \Omega/\text{km}, L_l = 2 \mu\text{H}/\text{km}, C_l = 151.2 \text{ nF}/\text{km}$ length $\in [0.24; 4.42] \text{ km}$ (see Figure 4.1)
Current controller (4.17), $i \in \mathcal{D}_{\text{feed}}$	$k_{P,i} = 0.1, Q_{1,i}^{-1} = 15$
Voltage controller (4.26), $i \in \mathcal{D}_{\text{PBC}}$	$\hat{R}_i = 0.4, Q_{1,i}^{-1} = 200$
Voltage controller (4.41), $i \in \mathcal{D}_{\text{N20}}$	$k_{1,i} = 0.3, k_{2,i} = 0.05, k_{3,i} = 40$

Table 4.2: Voltage and current setpoints of the DGUs. For Scenario A in Section 4.4.2, only the base values are used. For Scenario B in Section 4.4.3 featuring load and setpoint changes, the values vary at the indicated times.

DGU	i	1 (blue)	2 (red)	3 (yellow)	4 (purple)	5 (turquoise)	6 (black)
base	V_i^* (V)	385	383	–	383	–	–
$t = 15 \text{ s}$	V_i^* (V)	386	384	–	384	–	–
base	I_i^* (A)	–	–	3	–	5	6
$t = 20 \text{ s}$	I_i^* (A)	–	–	4	–	6	7

Table 4.3: ZIP load parameters. For Scenario A in Section 4.4.2, only the base values are used. For Scenario B in Section 4.4.3 featuring load and setpoint changes, the values vary at the indicated times.

	i		1	2	4	7	8
base	$Y_{P,i}$	(mS)	7.9	10.3	5.5	5.5	6.2
$t = 1 \text{ s}$	$Y_{P,i}$	(mS)	11.8	15.4	8.2	8.2	9.2
base	$I_{P,i}$	(A)	0.6	0.78	0.416	0.416	0.468
$t = 1 \text{ s}$	$I_{P,i}$	(A)	0.9	1.17	0.624	0.624	0.702
base	$P_{P,i}$	(W)	228	296.4	158	158	177.8
$t = 1 \text{ s}$	$P_{P,i}$	(W)	342	444.6	237	237	266.7

Table 4.4: Exponential load parameters. For Scenario A in Section 4.4.2, only the base values are used. For Scenario B in Section 4.4.3 featuring load and setpoint changes, the base values are ramped up from $t = 5$ s to the final value at $t = 10$ s.

	i		5	6	9	10	11
base	$P_{0,i}$	(W)	1720	889	967	1383	1520
$t = 10$ s	$P_{0,i}$	(W)	2579	1334	1451	2075	2280
base	$n_{P,i}$		1.5	1.5	1.5	1.5	1.5
$t = 10$ s	$n_{P,i}$		1.5	1.5	1.5	1.5	1.5

4.4.2 Scenario A: Plug-and-Play

This scenario features disconnecting and connecting DGUs and power lines in order to validate the decentralized nature of the stability conditions (DC 1) and (DC 2). At the indicated times, the following events occur (see Figure 4.1 for the network):

- $t = 5$ s: DGU 4 disconnects.
- $t = 10$ s: Power lines 17 and 19 disconnect.
- $t = 15$ s: DGU 4 reconnects.
- $t = 20$ s: DGU 5 disconnects.
- $t = 25$ s: Power lines 17 and 19 reconnect.
- $t = 30$ s: DGU 5 reconnects.

During the complete scenario, the DGU setpoints as well as the load parameters remain at the base values provided in Tables 4.2, 4.3, and 4.4.

The results of the simulation are given in Figures 4.4–4.7. The colored lines represent the node voltages V_i and filter currents I_i of the voltage- and current-controlled DGUs $i \in \mathcal{D} = \{1, 2, 3, 4, 5, 6\}$ with colors as per Table 4.2. Additionally, all uncontrolled node voltages as well as all uncontrolled filter, load, and line currents are given in grey. The deviations of controlled node voltages V_i , $i \in \{1, 2, 4\}$, and controlled filter currents I_i , $i \in \{3, 5, 6\}$, from their setpoints in Table 4.2 are given in % with respect to the nominal voltage $V_0 = 380$ V and the average amplitude of the current setpoints $I_0 = 4.67$ A, respectively.

The maximum voltage errors at the voltage-controlled DGU nodes $i \in \{1, 2, 4\}$ remain within a 0.46 % (1.75 V) band around their desired setpoints (see Figure 4.4). At the latest 0.25 s after an event, the controlled node voltages settle to within a 0.005 % (0.02 V) band (see Figure 4.6). The uncontrolled node voltages show similar deviation magnitudes and converge similarly fast to their corresponding steady-state values. Overall, the

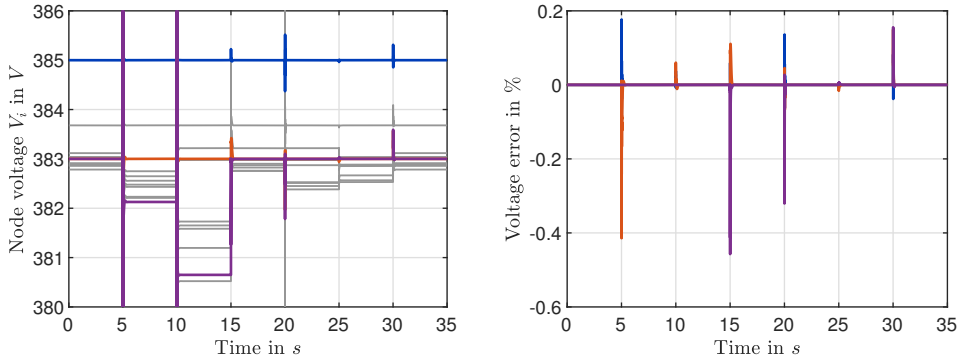


Figure 4.4: Scenario A: node voltages V_i with uncontrolled nodes in grey. The colors of the voltage-controlled DGU nodes $i \in \{1, 2, 4\}$ and their setpoints are given in Table 4.2. The voltage errors are given in % w.r.t. the nominal voltage $V_0 = 380$ V.

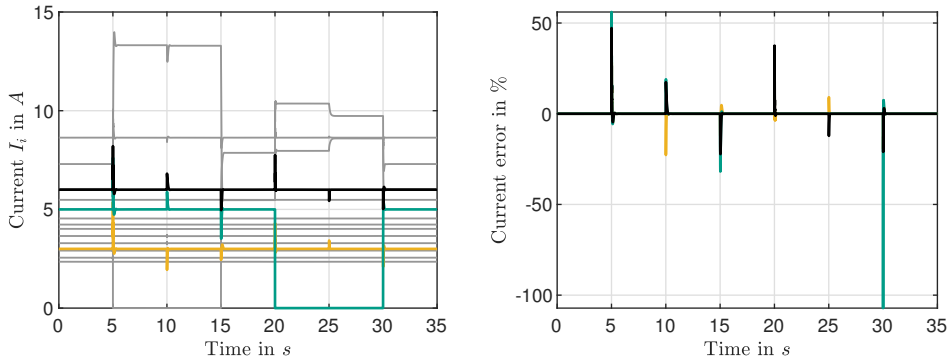


Figure 4.5: Scenario A: filter currents I_i and load currents $I_{L,i}$ with uncontrolled currents in grey. The colors of the current-controlled DGUs $i \in \{3, 5, 6\}$ and their setpoints are given in Table 4.2. The current errors are given in % w.r.t. the average amplitude of the currents setpoints $I_0 = 4.67$ A.

voltages thus stay well within a 5% band around the nominal voltage.³¹ Note that between $t = 5$ s – 15 s, the voltage at node 4 (purple line) is not controlled since DGU 4 is disconnected. Consequently, during that period, the voltage error is set to zero.

The filter current errors at the current-controlled DGU nodes $i \in \{3, 5, 6\}$ show peaks during the events of around 50% (2.3 A) except for a larger peak at $t = 30$ s of approximately 107% (5 A) which lasts for around 20 ms (see Figure 4.5). At the latest 0.4 s after an event, the controlled filter currents settle to within a 0.06% (0.003 A) band around their desired setpoints (see Figure 4.6). The uncontrolled filter, load, and line currents converge similarly fast to their corresponding steady-state values (see Figures 4.5 and 4.7). Note that between $t = 5$ s – 15 s and $t = 20$ s – 30 s, DGU 4 and DGU 5, respectively,

³¹ The AC power system standard EN 50160 defines a nominal voltage range of $\pm 5\%$ around the nominal voltage for fast voltage transients in low-voltage networks. In absence of any comparable norm for DC power systems, the 5% measure is transferred to the DC case for orientation.

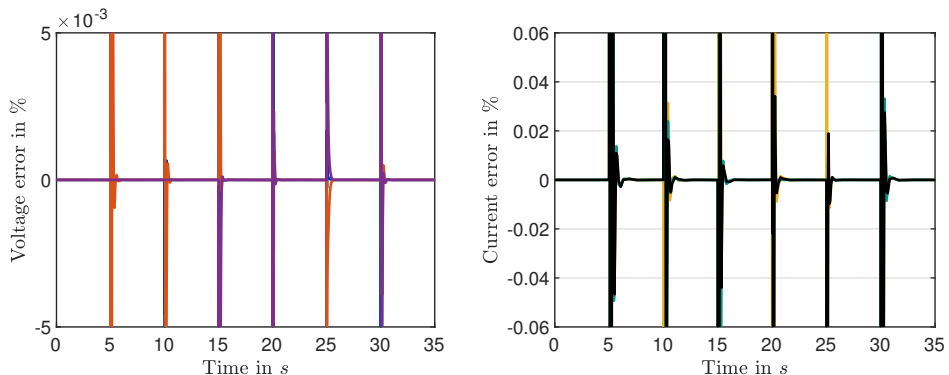


Figure 4.6: Scenario A: zoomed in errors of the controlled node voltages V_i , $i \in \{1, 2, 4\}$, and the controlled filter currents I_i , $i \in \{3, 5, 6\}$, with colors as per Table 4.2.

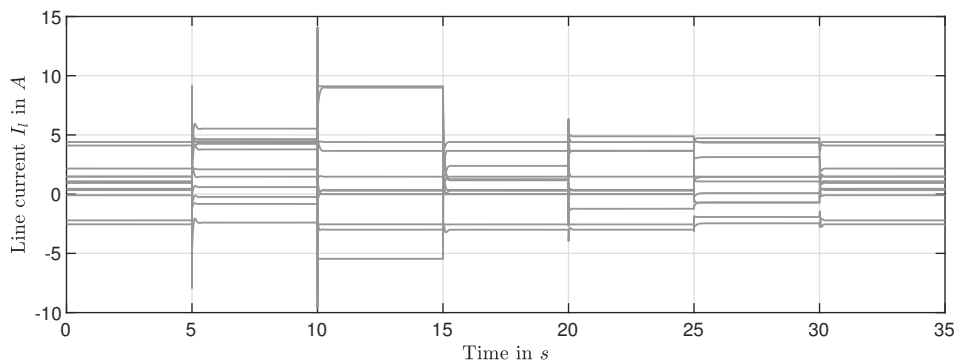


Figure 4.7: Scenario A: line currents I_l , $l \in \mathcal{P} = \{12, \dots, 23\}$.

are disconnected and their filter currents as well as the current error for DGU 5 are thus set to zero.

The reason for the seemingly high current peak at $t = 30$ s is the abrupt setpoint change caused by the reconnection of DGU 5. While the setpoint undergoes a step change from 0 A to 5 A, the actual current is subject to the RLC filter and controller dynamics. As illustrated in the left part of Figure 4.5, there is thus no real peak, but instead merely a large difference between desired setpoint and measured current. Furthermore, the overshoot of I_5 remains below 8% (0.37 A).

In summary, the results confirm the statements of Theorem 4.1 and demonstrate that all node voltages and currents and thus all states of the system (see (4.1b), (4.2b), (4.3b)) can be asymptotically stabilized throughout the complete scenario despite flexible system configurations with plug-and-play operations and topology changes. Furthermore, the integral parts of the proposed controllers ensure zero steady-state errors in the presence of parameter uncertainties which naturally occur in practice.

4.4.3 Scenario B: Setpoint and Load Changes

This scenario features changes in the voltage and current setpoints of the DGU controllers to investigate whether the asymptotic stability guarantee given by Theorem 4.1 is indeed independent of the specific equilibrium values. In addition to parameter uncertainties, load variations in form of step changes and ramps are simulated to further evaluate the disturbance rejection capabilities of the proposed controllers. At the indicated times, the following events occur (see Figure 4.1 for the network):

- $t = 1$ s: All ZIP loads $i \in \mathcal{L}_{\text{ZIP}} = \{1, 2, 4, 7, 8\}$ increase their demand by 50 %.
- $t = 5$ s – 10 s: All exponential loads $i \in \mathcal{L}_{\text{EXP}} = \{5, 6, 9, 10, 11\}$ increase their demand by 50 %.
- $t = 15$ s: All voltage setpoints V_i^* , $i \in \mathcal{D} = \{1, 2, 4\}$ are increased by 1 V.
- $t = 20$ s: All current setpoints I_i^* , $i \in \mathcal{D} = \{3, 5, 6\}$ are increased by 1 A.

The DGU setpoints as well as the load parameters before and after the changes are summarized in Tables 4.2, 4.3, and 4.4.

The results of the simulation are given in Figures 4.8–4.11. The colored lines represent the node voltages V_i and filter currents I_i of the voltage- and current-controlled DGUs $i \in \mathcal{D} = \{1, 2, 3, 4, 5, 6\}$ with colors as per Table 4.2. Additionally, all uncontrolled node voltages as well as all uncontrolled filter, load, and line currents are given in grey. The deviations of controlled node voltages V_i , $i \in \{1, 2, 4\}$, and controlled filter currents I_i , $i \in \{3, 5, 6\}$, from their setpoints in Table 4.2 are given in % with respect to the nominal voltage $V_0 = 380$ V and the average amplitude of the current setpoints $I_0 = 5.17$ A, respectively.

The maximum voltage errors at the voltage-controlled DGU nodes $i \in \{1, 2, 4\}$ remain within a 0.63 % (2.4 V) band around their desired setpoints (see Figure 4.8). At the latest 0.18 s after an event, the controlled node voltages settle to within a 0.005 % (0.02 V) band (see Figure 4.10). The uncontrolled node voltages show similar deviation magnitudes and converge similarly fast to their corresponding steady-state values. During the load ramps between $t = 5$ s – 10 s, the maximum voltage errors stay within a 0.15 % (0.57 V) band. As in Scenario A, the voltages throughout Scenario B stay well within a 5 % band around the nominal voltage.

The maximum current errors at the current-controlled DGU nodes $i \in \{3, 5, 6\}$ remain within a 40.1 % (2.07 A) band (see Figure 4.9). Except during the load ramps between $t = 5$ s – 10 s, the controlled filter currents settle to within a 0.06 % (0.003 A) band around their desired setpoints after at most 0.32 s (see Figure 4.10). The uncontrolled filter, load, and line currents converge similarly fast to their corresponding steady-state values (see Figures 4.9 and 4.11). During the load ramps between $t = 5$ s – 10 s, the maximum current errors remain below 0.2 % (0.01 A) (see Figure 4.10).

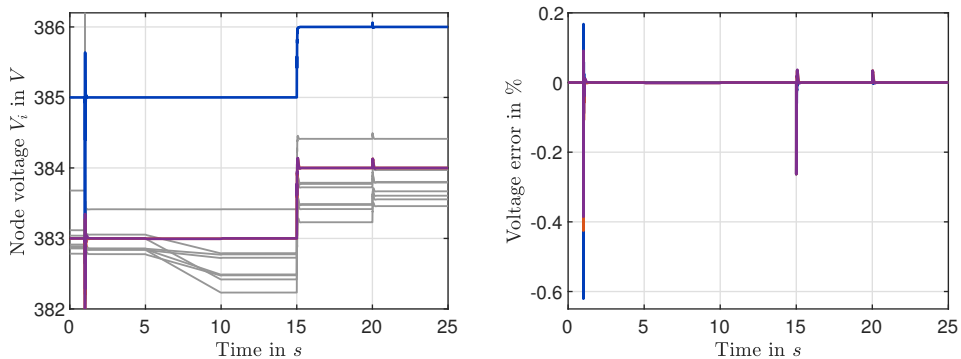


Figure 4.8: Scenario B: node voltages V_i with uncontrolled nodes on grey. The colors of the voltage-controlled DGU nodes $i \in \{1, 2, 4\}$ and their setpoints are given in Table 4.2. The voltage errors are given in % w.r.t. the nominal voltage $V_0 = 380$ V.

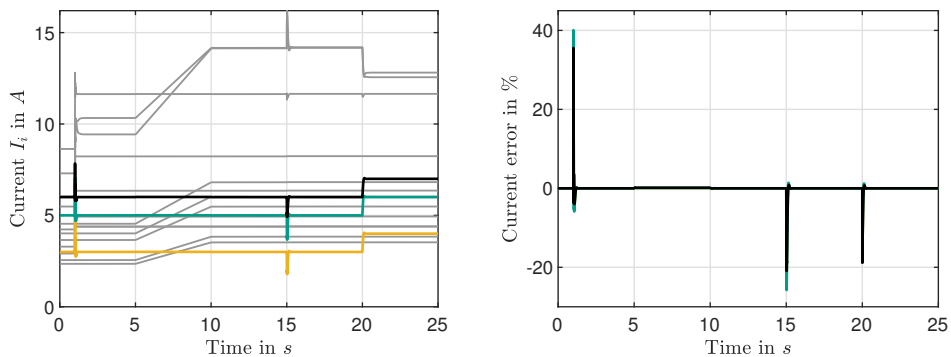


Figure 4.9: Scenario B: filter currents I_i and load currents $I_{L,i}$ with uncontrolled currents in grey. The colors of the current-controlled DGU nodes $i \in \{3, 5, 6\}$ and their setpoints are given in Table 4.2. The current errors are given in % w.r.t. the average amplitude of the currents setpoints $I_0 = 5.17$ A.

In summary, the results confirm the statements of Theorem 4.1 and demonstrate that the asymptotically stabilizing properties of the controllers (4.17), (4.26), and (4.41) are indeed independent of the specific voltage and currents setpoints. Furthermore, although not a specific focus of the controller designs, constant disturbances arising from unknown load demands and parameter uncertainties can be fully rejected by the integral parts of the controllers. Additionally, the integrators are sufficiently fast to reject the time-varying disturbances caused by the load ramps to negligible values.

This concludes the presentation and validation of the unifying stabilization framework for DC power systems. In the next section, the presented model, decentralized stability conditions, and controller designs are discussed with respect to the main research questions (Q2.1) and (Q2.2). Additionally, the results from this chapter are compared to those of the passivity-based works that have been published in parallel to this thesis (see Section 2.4.1).

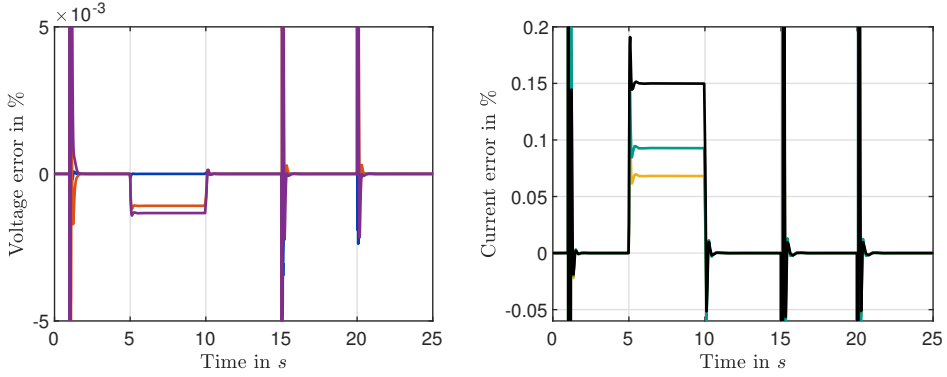


Figure 4.10: Scenario B: zoomed in errors of the controlled node voltages V_i , $i \in \{1, 2, 4\}$, and the controlled filter currents I_i , $i \in \{3, 5, 6\}$, with colors as per Table 4.2.

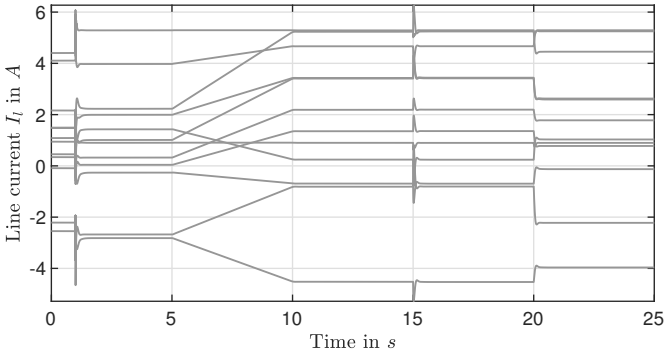


Figure 4.11: Scenario B: line currents I_l , $l \in \mathcal{P} = \{12, \dots, 23\}$.

4.5 Discussion

Theorem 4.1 and Propositions 4.1, 4.2, 4.3, are the main results of this chapter. Together, these results establish a cross-technology framework for the decentralized stabilization of voltages and currents in DC power systems.

Theorem 4.1 answers research question (Q2.1) and provides two decentralized analytical conditions (DC 1) and (DC 2) that are sufficient for ensuring asymptotic stability of any feasible DC power system equilibrium. The conditions (DC 1) and (DC 2) are *unifying* conditions that provide model- and technology-independent system and control design requirements for the decentralized stabilization in flexible DC power system configurations. Other subsystems (e.g., for different loads or with more detailed converter models, different converter topologies and technologies with output filters different than RLC, as well as altogether new units) can thus readily be integrated into the presented DC power system model. Then, following the steps taken in this chapter, requirements on

the model parameters and/or appropriate control laws can be developed to ensure (DC 1) and (DC 2) are met.

Propositions 4.1, 4.2 and 4.3 provide explicit parameter requirements and control solutions for ensuring the conditions of Theorem 4.1 are met for the DC power system described in Section 4.1. The passivity-based voltage controller for grid-forming DGUs $i \in \mathcal{D}_{\text{form}}$ and the passivity-based current controller for grid-feeding DGUs $i \in \mathcal{D}_{\text{feed}}$ in particular provide two explicit solutions for research question (Q2.2). However, due to the technology-independent nature of the decentralized stabilization conditions, research question (Q2.2) allows for a variety of decentralized control solutions as illustrated by example of the voltage controller from Nahata et al. [2020] in Proposition 4.4. From a practical engineering perspective, this is appealing as it creates a large, technology-neutral solution space to the problem of DC power system stabilization.

A further practically appealing aspect is that despite the complex methodological concepts underlying the conditions (DC 1) and (DC 2), the controllers required to enforce these conditions are simple and use standard, off-the-shelf control functions: a PI current controller (see (4.17)); a combination of setpoint feedforward, static state feedback, and PI term for the voltage controller (see (4.26) and Remark 4.7); and a state feedback voltage controller in Nahata et al. [2020] (see (4.41)). Furthermore, note that each of the control inputs $u_i = V_{S,i}$ is in fact a function of the duty cycle δ_i of the VSC and the DC voltage $V_{\text{DC},i}$ supplied by the DC voltage source, i.e., a RES, a storage device or a combination thereof (see Section 4.1.2). For a practical implementation of any control law u_i , the duty cycle δ_i can be obtained from u_i . For a buck VSC, for example, the relation is given by $u_i = V_{S,i} = \delta_i V_{\text{DC},i}$.

For a proper functioning of the controllers and a stabilization-coordination hierarchy as proposed in Section 2.2.2, it is crucial that the combination of DC voltage source and VSC behaves approximately like an ideal voltage source $V_{S,i}$ (see Section 4.1.2). In practice, this has three implications: firstly, sufficient short-term energy buffer (battery storage, supercapacitors, headroom on generation, or a combination thereof) must be available at the input-side of each VSC to provide sufficient power for a time scale of seconds to a few minutes (see also Matevosyan et al. [2019]).³² For example, for the 380 V DC power system from Section 4.4 with an overall demand of approximately 15 kW, a 50% demand increase of all loads equals 7.5 kW. Depending on the communication rate with the coordination layer and assuming no headroom for the DGU generation, stored energy of 1.875 kW h for a 15 min communication interval, 0.125 kW h for a 1 min interval, and 0.021 kW h for a 10 s interval must be available.

Secondly, the combination of short-term energy storage and VSC must have sufficient peak power capability to realize the control inputs provided by the controllers. For both scenarios from Section 4.4, for example, the maximum power peaks are in the range of 3 kW to 4 kW, which equals peak currents of 7.9 A to 10.5 A. Practical experience

³² The exact duration depends on the computing speed of and communication interval with the coordination layer.

indicates that integrated energy storage architectures combining batteries and supercapacitors are promising solutions for providing both, fast, high-power transients as well as sufficient short-term energy storage [Matevosyan et al., 2019; Rocabert et al., 2019].

Thirdly, several seconds to a few minutes after a disturbance, the coordination layer has to intervene and reschedule the setpoints according to the present generation-demand situation. In the last few years, first coordination schemes that operate on such smaller time-scales have been developed for example by Zhao and Dörfler [2015], Cucuzzella et al. [2019b], Malan et al. [2022], and Nahata et al. [2022].

4.5.1 Comparison with Parallel Works

As outlined in Section 2.4, during the time of this thesis, several other research groups have explored independently from each other the possibilities of using passivity techniques to provide decentralized stability conditions and controller designs for DC power systems.

The main feature this works have in common is that they do not provide any unifying, model- and technology-independent, decentralized asymptotic stability conditions comparable to those in Theorem 4.1. Instead, they focus on developing decentralized, passivity-based controllers for specific VSC types and DC power system models. The different passivity properties of the subsystem models are then merely used to facilitate the stability statement. However, no inferences are drawn on how the passivity properties can be translated into general system and control design guidelines.

In detail, Cucuzzella et al. [2019a], Cucuzzella et al. [2020], Kosaraju et al. [2021], and Cucuzzella et al. [2023] propose decentralized voltage controllers for DC power systems with different VSC types (buck, boost, buck-boost, Cúk). Their stability analysis and controller designs are based on new passivity notions in which the storage functions require the first-order time derivatives of the voltages [Cucuzzella et al., 2020, 2023] or the voltages and currents [Cucuzzella et al., 2019a; Kosaraju et al., 2021] of the VSCs.³³ The ZIP load condition in Cucuzzella et al. [2019a, Assumption 1] and Cucuzzella et al. [2023, Remark 2] are similar to the condition in (4.6).

Ferguson et al. [2021] use the PHS framework to develop two decentralized PBC schemes for voltage stabilization in DC power systems with dynamic power lines, ZIP loads with unknown parameters, and other unknown time-varying disturbances. In Ferguson et al. [2023], the same authors devise a linear, decentralized, passivity-based voltage controller which injects additional damping to relax the ZIP load conditions commonly required to proof asymptotic stability in DC power systems (see (4.6), Cucuzzella et al. [2019a, Assumption 1], and Cucuzzella et al. [2023, Remark 2]).

³³ The new types of storage functions are so-called Krasovskii-type storage functions [Cucuzzella et al., 2019a] (see Kosaraju et al. [2019] and Khalil [2002, p. 183] for further details) and mixed-potential storage functions [Cucuzzella et al., 2020; Kosaraju et al., 2021; Cucuzzella et al., 2023].

Overall, the results of this chapter are thus the first to provide a unifying, model- and technology-independent framework for the decentralized stabilization in DC power systems. As illustrated by example of the voltage controller of Nahata et al. [2020] in Section 4.3.3, the large, technology-neutral solution space arising from a decentralized, passivity-based stabilization framework allows the results of different researchers to positively complement each other. Instead of creating a black and white situation with opposing solutions, different foci and insights can contribute together towards the overall goal of addressing the stabilization challenges emerging along the transformation towards sustainable energy systems. In this spirit, the models and decentralized controller for different VSC types in Cucuzzella et al. [2019a] and Kosaraju et al. [2021] as well as the advanced control techniques used by Ferguson et al. [2021], Cucuzzella et al. [2023], and Ferguson et al. [2023] to improve the control performance present promising extensions to the model and controllers developed in this chapter.

In addition to this main benefit, the specific DC power system model and controller designs presented in this chapter extend the above-discussed works in several other directions. Firstly, the considered DC power system setup preserves the original network structure and does not require a load-connected topology in which the loads are mapped to the DGU terminals. Additionally, instead of merely focusing on the grid-forming voltage control, the problem of current control in grid-feeding DGUs is considered explicitly. Lastly, detailed ZIP and exponential load models are introduced with a practically-motivated two-tier behavior for voltages below and above $0.7 V_0$, respectively.³⁴

4.6 Summary and Contributions

The sustainable energy transition challenges power system stabilization with large numbers of interacting units that feature an increasing variety of technologies and control strategies. To make the stabilization task manageable, allow for flexible system configurations in a plug-and-play fashion, and ensure interoperability between units, this chapter establishes a passivity-based framework that ensures the decentralized stabilization of voltages and currents in DC power systems in a unifying manner across different technologies and control strategies. The results of this chapter are the first to provide such a decentralized, cross-technology stabilization framework for DC power systems. In summary, the main contributions of this chapter are:

- a generalized networked system model for DC power systems which combines graph theory with PHS modeling (Section 4.1);
- decentralized, EIP-based conditions that provide model- and technology-independent system and control design requirements for ensuring asymptotic stability of any feasible DC power system equilibrium (Theorem 4.1);

³⁴ Note that Ferguson et al. [2023] consider a similar two-tier load behavior, although only for ZIP loads.

- parameter specifications and decentralized converter controllers that ensure the EIP-based asymptotic stability conditions are met and desired voltage and current setpoints are asymptotically stabilized (Propositions 4.1, 4.2, and 4.3).

Together, these contributions answer the research questions (Q2.1) and (Q2.2) formulated in Section 2.2.2. Simulation studies based on a CIGRE benchmark network demonstrate the functionality of the developed decentralized stabilization framework and illustrate its unifying nature.

5 Passivity-Based Decentralized Stabilization in AC Power Systems

In the previous chapter, a cross-technology framework for the decentralized stabilization in DC power systems has been presented. The central elements of this framework are a generalized, graph-based DC power system model and decentralized, model- and technology-independent conditions based on EIP that ensure asymptotic stability of any feasible DC power system equilibrium. Motivated by the unifying, model- and technology-independent nature of these results, this chapter pursues a similar approach for developing a decentralized, cross-technology framework for the decentralized stabilization of voltages, currents, and the system frequency in AC power systems. In addition to profiting from a transfer of the main principles and ideas, this procedure provides a first assessment to what extent a passivity-based approach can also provide interoperability across different energy systems.³⁵

Following the outline of Chapter 4, Section 5.1 first presents a graph-based, networked system description of the considered AC power system model along the lines of Definition 3.1. The subsystems at the nodes and edges are modeled in a generalized manner as ISO-PHSs to facilitate the subsequent derivation of decentralized, technology-independent, asymptotic stability conditions and the PBC design.

Based on the model, Section 5.2 shows how the passivity-based approach of Theorem 3.1 and Corollary 3.1 can also be used to answer research question (Q1.1). Subsequently, parameter requirements for the unactuated subsystems are derived such that they fulfill the established, decentralized asymptotic stability conditions. Lastly, the main control problems related to answering research question (Q1.2) are formulated.

In Section 5.3, the formulated control problems are addressed. Decentralized, passivity-based controllers for the actuated DGU subsystems are designed to asymptotically stabilize desired setpoints for the system frequency, node voltages, and current injections. Additionally, the unifying, cross-technology nature of the established decentralized stabilization framework is shown by example of the voltage controller proposed by Nahata and Ferrari-Trecate [2019].

Subsequently, Section 5.4 presents simulation scenarios to validate the findings of the prior sections.

³⁵ Note that while both DC and AC power systems are physically based on the electrical domain, the AC power system case is technically not a straightforward extension of the DC case. In particular, the system frequency and electrical three-phase signals considerably complicate the system analysis and control synthesis.

Sections 5.5 and 5.6 conclude this chapter with a discussion and summary of the main contributions. In particular, the main results are compared to the passivity-based works published in parallel to this thesis (see Section 2.4).³⁶

5.1 Modeling

In this section, the model of the considered AC power systems is established along the lines of Definition 3.1. Firstly, in Section 5.1.1, the AC power system setup is outlined and formally described as a digraph. Subsequently, in Sections 5.1.2 and 5.1.3, the three main subsystems *DGU*, *load*, and *power line* are modeled as explicit state-space system in the form of ISO-PHSs (3.9). Lastly, the interconnection structure of the subsystems is formalized via the incidence matrix of the digraph in Section 5.1.4.

5.1.1 System Setup

This chapter considers AC power systems comprising DGUs, loads, and power lines that are connected in flexible, time-varying system configurations. Such AC power systems can be described by a weakly connected digraph $\mathcal{G} = (\mathcal{V}, \mathcal{E})$ without self-loops as illustrated in Figure 5.1 with subsystems on the nodes \mathcal{V} and edges \mathcal{E} . The nodes \mathcal{V} are partitioned into two sets: $\mathcal{D} = \{1, \dots, D\}$, $D \geq 1$, represents the DGUs, which may each supply a local load, and $\mathcal{L} = \{D + 1, \dots, D + L\}$, $L \geq 1$, represents load nodes without DGUs. The edges $\mathcal{E} = \mathcal{P} = \{1, \dots, P\}$, $P \geq 1$, represent the power lines. The orientation of the edges represents the arbitrary reference direction of positive line currents. Furthermore, the digraph \mathcal{G} is completely specified by its incidence matrix $B \in \mathbb{R}^{|\mathcal{V}| \times |\mathcal{E}|}$ with elements b_{il} (cf. (1.1)).

Following standard practice and the pertinent literature (see, e.g., Etemadi et al. [2012a], Glover et al. [2012, p. 74–75], Rivero et al. [2015], Schiffer et al. [2016], Baimel et al. [2017], and Gómez-Expósito et al. [2018, pp.280–281]), the following assumption is made throughout this chapter:

Assumption 5.1 (Balanced three-phase signals)

Three-phase electrical signals are balanced and thus without a zero-sequence.

Under Assumption 5.1, electrical three-phase signals can be fully represented by two-dimensional vectors

$$\mathbf{x}^{\text{dq}}(t) = \begin{bmatrix} x^{\text{d}}(t) \\ x^{\text{q}}(t) \end{bmatrix} \in \mathcal{X}^{\text{dq}} \subseteq \mathbb{R}^2 \quad (5.1)$$

³⁶ Preliminary results leading to the content of this chapter have been published in the conference papers [Strehle et al., 2019; Strehle et al., 2020a] and the journal article [Strehle et al., 2022b].

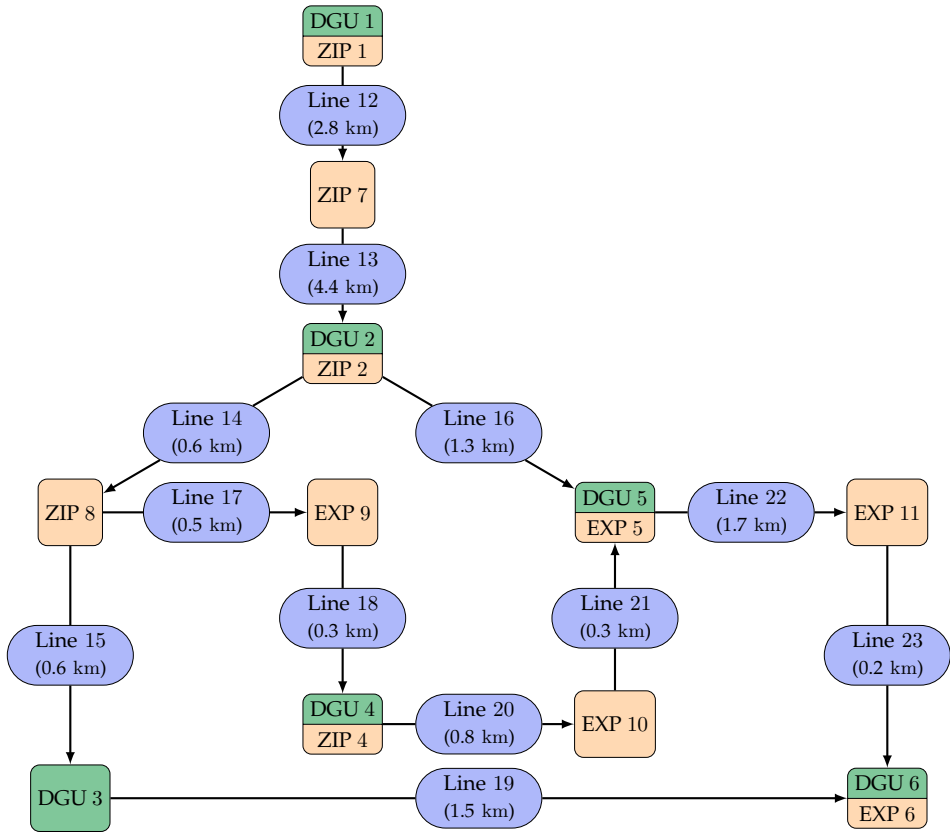


Figure 5.1: Digraph representation of Feeder 1 of the medium-voltage CIGRE AC distribution benchmark network [Strunz et al., 2014, Figure 6.5] comprising ZIP and exponential loads; DGUs are added at nodes $i \in \mathcal{D} = \{1, 2, 3, 4, 5, 6\}$.

in the dq frame rotating with some frequency $\omega_0 > 0$. Consequently, in steady state, periodic orbits are transformed into constant, two-dimensional equilibrium vectors, which simplifies the control design and analysis in AC power systems (for a comprehensive introduction into the topic of modeling electrical three-phase systems in the dq frame see, e.g., Schiffer et al. [2016], Baimel et al. [2017], and Levron et al. [2018]). In the remainder of this chapter, all three-phase voltage and currents are represented in dq coordinates resulting from the orthogonal, power-invariant version of the dq transformation (see, e.g., Schiffer et al. [2016, Equation (2.1)]). This version of the dq transformation preserves the proper relations between power, voltage, and current, and is thus desirable in a power system context [Paap, 2000]. Furthermore, under normal grid conditions, the following properties hold:

Property 5.1 (Voltage amplitudes and reference frequency)

The amplitude $V(t)$ of any instantaneous, complex dq voltage vector $\mathbf{V}^{\text{dq}}(t) \in \mathbb{R}^2$ is positive, i.e.

$$V(t) = \sqrt{V^{\text{d}}(t)^2 + V^{\text{q}}(t)^2} \geq 0, \quad \forall t \geq 0. \quad (5.2)$$

In steady state, the amplitude \bar{V} equals the phase-to-phase root-mean-square (RMS) voltage. Any nominal phase-to-phase RMS voltage is denoted by $V_0 > 0$ (e.g., $V_0 = 20$ kV). The reference frequency is strictly positive $\omega_0 > 0$.

In the following, the models of the DGUs and loads on the nodes \mathcal{V} and the power lines on the edges \mathcal{E} of the AC power system digraph are presented in dq coordinates.

5.1.2 Subsystems on Nodes

DGUs The circuit diagram of a DGU at any node $i \in \mathcal{D}$ in the AC power system is shown in the left dashed frame of Figure 5.2. The DGU comprises a DC voltage source, a voltage-source inverter (VSI), and a series RLC filter with parameters $R_i, L_i, C_i > 0$. The DC voltage source represents a RES (e.g., a wind power plant), a storage device or a combination thereof. The losses in the VSI and filter are lumped together in R_i . The VSI is modeled by a time-averaged model commonly employed for control design (see for example Chiniforoosh et al. [2010] and Schiffer et al. [2016]).³⁷ The DC source together with the averaged VSI model is assumed to form an ideal voltage source $\mathbf{V}_{S,i}^{\text{dq}}$ that supplies sufficient power at all times.³⁸

The current $I_{N,i}^{\text{dq}}$ is the net-current injected into the AC power system which equals the accumulated incoming and outgoing line currents. Furthermore, each DGU may supply a local load described by a voltage-dependent current sink $I_{L,i}^{\text{dq}}(\mathbf{V}_i^{\text{dq}})$.

By applying KCL and KVL to the components in dq coordinates (see Schiffer et al. [2016] and Baimel et al. [2017]), the dynamics for each DGU $i \in \mathcal{D}$ follow as

$$\begin{aligned} L_i \dot{I}_i^{\text{d}} &= \omega_0 L_i I_i^{\text{q}} - R_i I_i^{\text{d}} - V_i^{\text{d}} + V_{S,i}^{\text{d}}, \\ L_i \dot{I}_i^{\text{q}} &= -\omega_0 L_i I_i^{\text{d}} - R_i I_i^{\text{q}} - V_i^{\text{q}} + V_{S,i}^{\text{q}}, \\ C_i \dot{V}_i^{\text{d}} &= I_i^{\text{d}} + \omega_0 C_i V_i^{\text{q}} - I_{L,i}^{\text{d}}(\mathbf{V}_i^{\text{dq}}) - I_{N,i}^{\text{d}}, \\ C_i \dot{V}_i^{\text{q}} &= I_i^{\text{q}} - \omega_0 C_i V_i^{\text{d}} - I_{L,i}^{\text{q}}(\mathbf{V}_i^{\text{dq}}) - I_{N,i}^{\text{q}}, \end{aligned} \quad (5.3a)$$

³⁷ The average model is motivated by the fact that the switching frequencies of the inverters are typically very high (2 kHz-20 kHz) compared to the other system dynamics and sufficiently suppressed by the RLC filter.

³⁸ Implicitly or explicitly, the ideal voltage source assumption is commonly made in the literature without any further argument (see, e.g., the review in Section 2.1.1 and the works of Nahata and Ferrari-Trecate [2019], Watson et al. [2019], Ojo et al. [2021], and Watson et al. [2021] which were published in parallel to this thesis). In the discussion in Section 5.5, its practical implications will be illuminated.

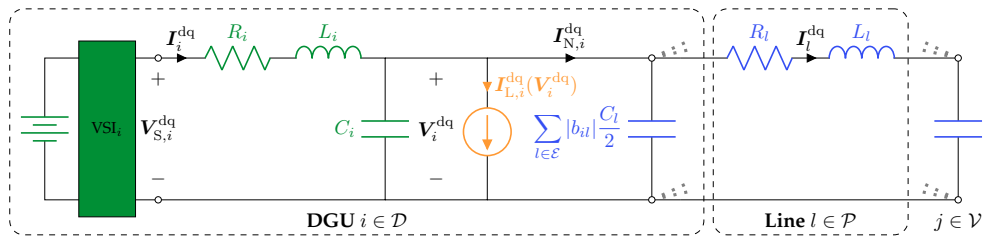


Figure 5.2: Circuit diagram of a DGU $i \in \mathcal{D}$ comprising a DC voltage source, a VSI with control input $V_{S,i}^{dq}$, and a series RLC filter (green) connected to Π -model power lines (blue) and a local AC load represented by a voltage-dependent current sink $I_{L,i}^{dq}(V_i^{dq})$ (orange). The line capacitances are considered to be part of the respective subsystems at the nodes.

with $I_i^{dq}, V_i^{dq}, V_{S,i}^{dq}, I_{N,i}^{dq} \in \mathbb{R}^2$, $I_{L,i}^{dq} : \mathbb{R}^2 \rightarrow \mathbb{R}^2$, and parameters $R_i, L_i, C_i > 0$. Similar to the DC case, the following assumption is necessary to write (5.3) in ISO-PHS form.

Assumption 5.2 (Monotonicity of AC load current functions)

The load current function $I_{L,i}^{dq}(V_i^{dq})$ is monotone and satisfies $I_{L,i}^{dq}(\mathbf{0}_2) = \mathbf{0}_2$.

Remark 5.1. In Section 5.2.2, conditions on the load parameters will be established such that Assumption 5.2 holds. It will be shown that these parameter specifications also ensure the load model is EIP.

Given Assumption 5.2, the DGU model (5.3) can be written as ISO-PHS of the form (3.9) with state and co-state vectors

$$\mathbf{x}_i = \begin{bmatrix} L_i I_i^d \\ L_i I_i^q \\ C_i V_i^d \\ C_i V_i^q \end{bmatrix}, \quad \frac{\partial H_i}{\partial \mathbf{x}_i}(\mathbf{x}_i) = \begin{bmatrix} I_i^d \\ I_i^q \\ V_i^d \\ V_i^q \end{bmatrix}, \quad (5.3b)$$

control port pair

$$\mathbf{u}_i = V_{S,i}^{dq}, \quad \mathbf{y}_i = I_i^{dq}, \quad (5.3c)$$

uncontrolled interaction (coupling) port pair

$$\mathbf{d}_i = -I_{N,i}^{dq} = \sum_{l \in \mathcal{E}} b_{il} I_l^{dq}, \quad \mathbf{z}_i = V_i^{dq}, \quad (5.3d)$$

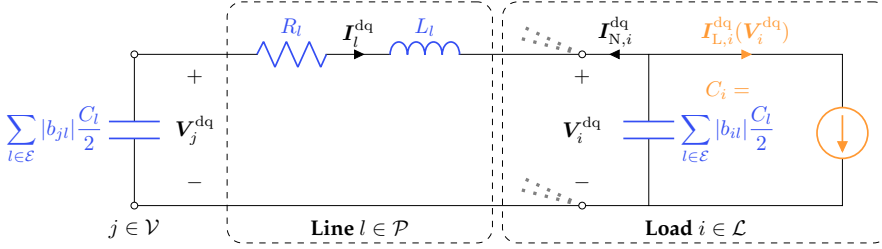


Figure 5.3: Circuit diagram of a load node $i \in \mathcal{L}$ comprising a nonlinear static AC ZIP or exponential load represented by a voltage-dependent current sink $I_{L,i}^{\text{dq}}(\mathbf{V}_i^{\text{dq}})$ (orange) connected to Π -model power lines (blue). The capacitance C_i is the sum of the parallel capacitances of the lines connecting to the load node.

matrices

$$\mathbf{J}_i = \begin{bmatrix} 0 & \omega_0 L_i & -1 & 0 \\ -\omega_0 L_i & 0 & 0 & -1 \\ 1 & 0 & 0 & \omega_0 C_i \\ 0 & 1 & -\omega_0 C_i & 0 \end{bmatrix}, \quad \mathbf{G}_i = \begin{bmatrix} 1 & 0 \\ 0 & 1 \\ 0 & 0 \\ 0 & 0 \end{bmatrix}, \quad \mathbf{K}_i = \begin{bmatrix} 0 & 0 \\ 0 & 0 \\ 1 & 0 \\ 0 & 1 \end{bmatrix}, \quad (5.3e)$$

$$\mathbf{R}_i = \text{diag}(R_i, R_i, 0, 0), \quad \mathbf{Q}_i = \text{diag}\left(\frac{1}{L_i}, \frac{1}{L_i}, \frac{1}{C_i}, \frac{1}{C_i}\right),$$

and nonlinear damping function

$$\mathcal{R}_i\left(\frac{\partial H_i}{\partial \mathbf{x}_i}(\mathbf{x}_i)\right) = \begin{bmatrix} 0 \\ 0 \\ I_{L,i}^{\text{d}}(\mathbf{V}_i^{\text{dq}}) \\ I_{L,i}^{\text{q}}(\mathbf{V}_i^{\text{dq}}) \end{bmatrix}. \quad (5.3f)$$

Remark 5.2. In this thesis, the specific current-voltage relation $I_{L,i}^{\text{dq}}(\mathbf{V}_i^{\text{dq}})$ of a local load is either given by (5.9) or (5.10). In case a DGU does not supply a local load, $I_{L,i}^{\text{dq}}(\mathbf{V}_i^{\text{dq}}) = \mathbf{0}_2$ and $\mathcal{R}_i\left(\frac{\partial H_i}{\partial \mathbf{x}_i}(\mathbf{x}_i)\right) = \mathbf{0}_4$.

Load nodes The circuit diagram of an AC load node $i \in \mathcal{L}$ along with connecting power lines is shown in Figure 5.3. The load is modeled as a voltage-dependent current sink representing a nonlinear static AC load. By applying KCL to the components in dq coordinates (see Schiffer et al. [2016] and Baimel et al. [2017]), the dynamic equation for each load node $i \in \mathcal{L}$ follows as

$$\begin{aligned} C_i \dot{V}_i^{\text{d}} &= -I_{L,i}^{\text{d}}(\mathbf{V}_i^{\text{dq}}) + \omega_0 C_i V_i^{\text{q}} - I_{N,i}^{\text{d}}, \\ C_i \dot{V}_i^{\text{q}} &= -I_{L,i}^{\text{q}}(\mathbf{V}_i^{\text{dq}}) - \omega_0 C_i V_i^{\text{d}} - I_{N,i}^{\text{q}}, \end{aligned} \quad (5.4a)$$

with $\mathbf{V}_i^{\text{dq}}, \mathbf{I}_{N,i}^{\text{dq}} \in \mathbb{R}^2$, $\mathbf{I}_{L,i}^{\text{dq}} : \mathbb{R}^2 \rightarrow \mathbb{R}^2$, and capacitance $C_i > 0$. Under Assumption 5.2, the load node model (5.4) can be written as ISO-PHS of the form (3.9) with state and co-state

$$\mathbf{x}_i = \begin{bmatrix} C_i V_i^{\text{d}} \\ C_i V_i^{\text{q}} \end{bmatrix}, \quad \frac{\partial H_i}{\partial \mathbf{x}_i}(\mathbf{x}_i) = \begin{bmatrix} V_i^{\text{d}} \\ V_i^{\text{q}} \end{bmatrix}, \quad (5.4b)$$

uncontrolled interaction (coupling) port pair

$$\mathbf{d}_i = -\mathbf{I}_{N,i}^{\text{dq}} = \sum_{l \in \mathcal{E}} b_{il} \mathbf{I}_l^{\text{dq}}, \quad \mathbf{z}_i = \mathbf{V}_i^{\text{dq}}, \quad (5.4c)$$

matrices

$$\mathbf{J}_i = \begin{bmatrix} 0 & \omega_0 C_i \\ -\omega_0 C_i & 0 \end{bmatrix}, \quad \mathbf{R}_i = \mathbf{0}_{2 \times 2}, \quad \mathbf{G}_i = \begin{bmatrix} 0 \\ 0 \end{bmatrix}, \quad \mathbf{K}_i = \begin{bmatrix} 1 & 0 \\ 0 & 1 \end{bmatrix}, \quad \mathbf{Q}_i = \begin{bmatrix} \frac{1}{C_i} & 0 \\ 0 & \frac{1}{C_i} \end{bmatrix}, \quad (5.4d)$$

and nonlinear damping function

$$\mathcal{R}_i \left(\frac{\partial H_i}{\partial \mathbf{x}_i}(\mathbf{x}_i) \right) = \mathbf{I}_{L,i}^{\text{dq}}(\mathbf{V}_i^{\text{dq}}). \quad (5.4e)$$

The nonlinear damping function (5.4e) is specified by the nonlinear, static current-voltage relation of the respective AC load models. In this thesis, the prevalent nonlinear, static *ZIP* and *exponential* load models are considered (see Appendix B.1). However, the active and reactive power representations (B.3), (B.4), and (B.5) found in the literature do not coincide with the first-principles modeling of a voltage-dependent current sink as in (5.4e). Furthermore, in contrast to the DC case (see the explanations around (4.2f) and (4.2g)), a simple division by the node voltage \mathbf{V}_i^{dq} is not possible as it is a two-dimensional vector. The following lemma outlines how to generally obtain current-voltage relations of the form $\mathbf{I}_L^{\text{dq}}(\mathbf{V}^{\text{dq}})$ from the active and reactive power representations $P_L(V)$ and $Q_L(V)$ of generally nonlinear, static AC loads.

Lemma 5.1 (Current-voltage relations of nonlinear static AC loads)

Consider a balanced, nonlinear, static three-phase AC load described by voltage-dependent active and reactive power equations $P_L(V)$ and $Q_L(V)$, respectively. Such a load can equivalently be represented by the dq current-voltage relation

$$\mathbf{I}_L^{\text{dq}}(\mathbf{V}^{\text{dq}}) = \frac{1}{V^2} \begin{bmatrix} P_L(V) & Q_L(V) \\ -Q_L(V) & P_L(V) \end{bmatrix} \begin{bmatrix} V^{\text{d}} \\ V^{\text{q}} \end{bmatrix}, \quad (5.5)$$

where $V \geq 0$ is the amplitude (Euclidean norm) of the instantaneous dq load voltage vector $\mathbf{V}^{\text{dq}} \in \mathbb{R}^2$ (see (5.2)).

Proof:

Let the instantaneous complex power of a load S_L be expressed in terms of the dq voltage V^{dq} over the load and the dq current I_L^{dq} flowing into the load (see Schiffer et al. [2016, Definition 2.11] and van Cutsem and Vournas [1998, p. 57])

$$S_L = P_L + jQ_L = (V^d I_L^d + V^q I_L^q) + j(V^q I_L^d - V^d I_L^q). \quad (5.6)$$

Equating the real and imaginary parts of (5.6) yields the linear system of equations

$$\begin{bmatrix} P_L \\ Q_L \end{bmatrix} = \begin{bmatrix} V^d & V^q \\ V^q & -V^d \end{bmatrix} \begin{bmatrix} I_L^d \\ I_L^q \end{bmatrix}. \quad (5.7)$$

Solving (5.7) for I_L^{dq} gives

$$I_L^d(V^{dq}) = \frac{V^d P_L(V) + V^q Q_L(V)}{(V^d)^2 + (V^q)^2}, \quad (5.8a)$$

$$I_L^q(V^{dq}) = \frac{V^q P_L(V) - V^d Q_L(V)}{(V^d)^2 + (V^q)^2}, \quad (5.8b)$$

which is equivalent to (5.5). \square

With Lemma 5.1, the current-voltage relations for ZIP and exponential AC loads can be calculated from the active and reactive power representations (B.3), (B.4), and (B.5). In particular, the ZIP load current relation is given by

$$I_{L,i}^{dq}(V_i^{dq}) = \begin{cases} \begin{bmatrix} \frac{P_{P,i} V_i^d + P_{Q,i} V_i^q}{V_i^2} + \frac{I_{P,i} V_i^d + I_{Q,i} V_i^q}{V_i} + Y_{P,i} V_i^d + Y_{Q,i} V_i^q \\ \frac{P_{P,i} V_i^q - P_{Q,i} V_i^d}{V_i^2} + \frac{I_{P,i} V_i^q - I_{Q,i} V_i^d}{V_i} + Y_{P,i} V_i^q - Y_{Q,i} V_i^d \end{bmatrix}, & V_i \geq 0.7 V_0, \\ \begin{bmatrix} \tilde{Y}_{P,i} V_i^d + \tilde{Y}_{Q,i} V_i^q \\ \tilde{Y}_{P,i} V_i^q - \tilde{Y}_{Q,i} V_i^d \end{bmatrix}, & V_i < 0.7 V_0, \end{cases} \quad (5.9a)$$

with ZIP parameters $Y_{P,i}, Y_{Q,i}, I_{P,i}, I_{Q,i}, P_{P,i}, P_{Q,i} \geq 0$, $\tilde{Y}_{P,i} = Y_{P,i} + \frac{I_{P,i}}{0.7 V_0} + \frac{P_{P,i}}{(0.7 V_0)^2}$, and $\tilde{Y}_{Q,i} = Y_{Q,i} + \frac{I_{Q,i}}{0.7 V_0} + \frac{P_{Q,i}}{(0.7 V_0)^2}$. The exponential load current relation is given by

$$I_{L,i}^{dq}(V_i^{dq}) = \begin{cases} \begin{bmatrix} \frac{P_{0,i} V_i^{n_{P,i}-2}}{V_0^{n_{Q,i}}} V_i^d + Q_{0,i} \frac{V_i^{n_{Q,i}-2}}{V_0^{n_{Q,i}}} V_i^q \\ \frac{P_{0,i} V_i^{n_{P,i}-2}}{V_0^{n_{Q,i}}} V_i^q - Q_{0,i} \frac{V_i^{n_{Q,i}-2}}{V_0^{n_{Q,i}}} V_i^d \end{bmatrix}, & V_i \geq 0.7 V_0, \\ \begin{bmatrix} \tilde{Y}_{P,i} V_i^d + \tilde{Y}_{Q,i} V_i^q \\ \tilde{Y}_{P,i} V_i^q - \tilde{Y}_{Q,i} V_i^d \end{bmatrix}, & V_i < 0.7 V_0, \end{cases} \quad (5.10a)$$

with nominal active and reactive power consumptions $P_{0,i}, Q_{0,i} \geq 0$, voltage indices $n_{P,i}, n_{Q,i} \geq 0$, and admittances $\tilde{Y}_{P,i} = \frac{P_{0,i} 0.7^{n_{P,i}}}{(0.7 V_0)^2}$, $\tilde{Y}_{Q,i} = \frac{Q_{0,i} 0.7^{n_{Q,i}}}{(0.7 V_0)^2}$.

5.1.3 Subsystems on Edges

Power lines The model of an AC power line at any edge $l \in \mathcal{P}$ is given by the Π -equivalent model of a transmission line [Kundur, 1994, pp. 201–207] with $C_l, R_l, L_l > 0$ as illustrated in Figures 5.2 and 5.3. The capacitances on both sides of the line are considered to be included in the equivalent capacitance C_i of the respective node subsystem $i \in \mathcal{V}$. This avoids dependent storages (i.e. parallel capacitances in this case) and thus dependent states. By applying KVL to the components in dq coordinates (see Schiffer et al. [2016] and Baimel et al. [2017]), the dynamic equation of each power line $l \in \mathcal{E}$ follows as

$$\begin{aligned} L_l \dot{I}_l^d &= \omega_0 L_l I_l^q - R_l I_l^d - \sum_{i \in \mathcal{V}} b_{il} V_i^d, \\ L_l \dot{I}_l^q &= -\omega_0 L_l I_l^d - R_l I_l^q - \sum_{i \in \mathcal{V}} b_{il} V_i^q, \end{aligned} \quad (5.11a)$$

with $I_l^{\text{dq}}, V_i^{\text{dq}} \in \mathbb{R}^2$, and parameters $R_l, L_l > 0$. Equation (5.11a) may be written as linear ISO-PHS of the form (3.9) with state and co-state vectors

$$\mathbf{x}_l = \begin{bmatrix} L_l I_l^d \\ L_l I_l^q \end{bmatrix}, \quad \frac{\partial H_l}{\partial \mathbf{x}_l}(\mathbf{x}_l) = \begin{bmatrix} I_l^d \\ I_l^q \end{bmatrix}, \quad (5.11b)$$

uncontrolled interaction (coupling) port pair

$$\mathbf{d}_l = - \sum_{i \in \mathcal{V}} b_{il} \mathbf{V}_i^{\text{dq}}, \quad \mathbf{z}_l = \mathbf{I}_l^{\text{dq}}, \quad (5.11c)$$

and matrices

$$\mathbf{J}_l = \begin{bmatrix} 0 & \omega_0 L_l \\ -\omega_0 L_l & 0 \end{bmatrix}, \quad \mathbf{R}_l = \begin{bmatrix} R_l & 0 \\ 0 & R_l \end{bmatrix}, \quad \mathbf{G}_l = \mathbf{0}_2, \quad \mathbf{K}_l = \begin{bmatrix} 1 & 0 \\ 0 & 1 \end{bmatrix}, \quad \mathbf{Q}_l = \begin{bmatrix} \frac{1}{L_l} & 0 \\ 0 & \frac{1}{L_l} \end{bmatrix}. \quad (5.11d)$$

Note that (5.11) has no control port $(\mathbf{u}_l, \mathbf{y}_l)$.

Remark 5.3. *The Π -equivalent model of a transmission line with lumped parameters is a simplified version of a more detailed distributed parameter line model, which can be obtained by connecting an arbitrary number of Π -model elements in series. As the number of used Π -model elements tends to infinity, this line model tends to the telegrapher equations (see Watson [2021, p. 119] for more details). For a clear presentation, the following elaborations are performed based on the the lumped parameter Π -model. However, the statements and results straightforwardly extended to the distributed line model.*

5.1.4 Interconnection Structure

The interconnection of the DGU and load subsystems on the nodes $i \in \mathcal{V}$ with the power line subsystems on the edges $l \in \mathcal{E}$ is clearly defined by the interaction (coupling) ports

(5.3d), (5.4c), (5.11c) arising from their respective PHS representations. In particular, it holds that

$$\mathbf{d}_i = \sum_{l \in \mathcal{E}} b_{il} \mathbf{I}_l^{\text{dq}} = \sum_{l \in \mathcal{E}} b_{il} \mathbf{z}_l, \quad (5.12a)$$

$$\mathbf{d}_l = - \sum_{i \in \mathcal{V}} b_{il} \mathbf{V}_i^{\text{dq}} = - \sum_{i \in \mathcal{V}} b_{il} \mathbf{z}_i, \quad (5.12b)$$

and (cf. (3.1e) with $m = 2$)

$$\begin{bmatrix} \mathbf{d}_{\mathcal{V}} \\ \mathbf{d}_{\mathcal{E}} \end{bmatrix} = \begin{bmatrix} \mathbf{0}_{|\mathcal{V}| \times |\mathcal{V}|} & \mathbf{B} \\ -\mathbf{B}^{\top} & \mathbf{0}_{|\mathcal{E}| \times |\mathcal{E}|} \end{bmatrix} \otimes \mathbf{I}_{2 \times 2} \begin{bmatrix} \mathbf{z}_{\mathcal{V}} \\ \mathbf{z}_{\mathcal{E}} \end{bmatrix} =: \mathbf{M} \begin{bmatrix} \mathbf{z}_{\mathcal{V}} \\ \mathbf{z}_{\mathcal{E}} \end{bmatrix} \quad (5.13)$$

with $(\cdot)_{\mathcal{V}} = \text{stack}((\cdot)_i)_{i \in \mathcal{V}}$ and $(\cdot)_{\mathcal{E}} = \text{stack}((\cdot)_l)_{l \in \mathcal{E}}$ denoting the respective, stacked vectors of the subsystems.

5.2 Asymptotic Stability Conditions and Control Problems

With the AC power system formalized as a digraph and its model established, research questions (Q1.1) and (Q1.2) can now formally be addressed. Firstly, in Section 5.2.1, decentralized asymptotic stability conditions are derived by application of Theorem 3.1 and Corollary 3.1. Subsequently, in Section 5.2.2, parameter requirements for the unactuated power line and load subsystems are established such that the derived, decentralized stability conditions are satisfied. Lastly, in Section 5.2.3, the remaining control problems for the actuated DGU subsystems are formulated. Their solution in Section 5.3 will provide answers to research question (Q1.2).

5.2.1 Decentralized Asymptotic Stability Conditions

In order to develop decentralized stability conditions that capture the system frequency, voltages, and currents, firstly recall that a variable

$$\mathbf{x}^{\text{dq}}(t) = \begin{bmatrix} x^{\text{d}}(t) \\ x^{\text{q}}(t) \end{bmatrix} \in \mathcal{X}^{\text{dq}} \subseteq \mathbb{R}^2 \quad (5.14)$$

in the dq frame rotating at frequency ω_0 can be considered a Cartesian representation of a complex vector with polar representation [Schiffer et al., 2016]

$$A(t) \angle \theta(t) \text{ with } \begin{cases} A(t) = \sqrt{(x^{\text{d}}(t))^2 + (x^{\text{q}}(t))^2} \\ \theta(t) = \arctan\left(\frac{x^{\text{q}}(t)}{x^{\text{d}}(t)}\right) \end{cases}, \quad (5.15)$$

often referred to as phasor [Machowski et al., 2008, p. 60]. From (5.15), it is evident that an asymptotically stable equilibrium $\bar{x}^{\text{dq}} \in \bar{\mathcal{X}}^{\text{dq}} \subset \mathbb{R}^2$ implies

$$\lim_{t \rightarrow \infty} A(t) = \text{const.}, \quad (5.16)$$

$$\lim_{t \rightarrow \infty} \theta(t) = \text{const.} \quad (5.17)$$

Thus, if the various nodal dq frames are synchronized to the desired system frequency ω_0 , asymptotic stability of the dq node voltages $\bar{V}_i^{\text{dq}}, i \in \mathcal{V}$, and the dq filter and line currents $\bar{I}_k^{\text{dq}}, k \in \mathcal{V} \cup \mathcal{E}$ also guarantees an asymptotically stable equilibrium $\bar{\omega}_0 = \omega_0$ for the system frequency. Technologies for achieving such synchronization via internal oscillators at each VSI and infrequent communication, e.g. via GPS, are available (see, e.g., Etemadi et al. [2012a], Etemadi et al. [2012b], IEEE 1588 [2008], and IEEE 1588 [2017]).³⁹ This motivates the following assumption, whose practical implications are discussed in detail in Section 5.5.

Assumption 5.3 (Synchronized dq frames)

The controller clocks and thus the dq reference frames at all nodes $i \in \mathcal{V}$ are synchronized to the desired system frequency ω_0 via internal oscillators at each VSI and infrequent GPS communication.

Remark 5.4. *Note that the dq reference frames for load nodes $i \in \mathcal{L}$ and power lines $l \in \mathcal{P}$ are only used as means to facilitate the analysis of the balanced, three-phase AC signals. As loads and power lines are unactuated, there is no need for synchronization. Their dq frames are simply set to rotate at the desired system frequency ω_0 .*

Under Assumption 5.3, research question (Q1.1) reduces to finding decentralized conditions that ensure asymptotic stability of any feasible equilibrium comprising the dq voltages and currents.

Next, note that the AC power system model outlined in Section 5.1 is similar to that of an autonomous, networked system given in Definition 3.1. So far, however, the control ports $(\mathbf{u}_i, \mathbf{y}_i)$ of the DGUs at nodes $i \in \mathcal{D}$ are open, i.e., the DGU models are of the form (3.2). In order to conduct an equilibrium stability analysis, it is thus assumed that each DGU is in closed loop with some controller (see Remark 3.2).

Then, by direct application of Theorem 3.1 and Corollary 3.1 to the now autonomous AC power system model, decentralized, analytical conditions can be obtained, which,

³⁹ Etemadi et al. [2012a] and Etemadi et al. [2012b] show that open-loop frequency control with (low-cost) internal oscillators of an accuracy between 20 ps–2 μ s and infrequent GPS synchronization (at 1 s intervals) of the oscillators with an accuracy of 1 μ s can keep frequencies well within permissible limits of standards and grid codes.

if satisfied, ensure asymptotic stability of any feasible AC power system equilibrium $\bar{x}_{AC} = \text{stack}(\bar{x}_k)_{k \in \mathcal{V} \cup \mathcal{E}}$. The vectors \bar{x}_k are the respective equilibrium state vectors of the subsystems that are proportional to the steady-state voltages and currents of the AC power system (cf. (5.3b), (5.4b), (5.11b)).⁴⁰

Theorem 5.1 (Decentralized, asymptotic stability conditions for AC power systems)

Consider an autonomous AC power system as described in Section 5.1 with some controller u_i at each DGU $i \in \mathcal{D}$. Any feasible equilibrium $\bar{x}_{AC} = \text{stack}(\bar{x}_k)_{k \in \mathcal{V} \cup \mathcal{E}}$ of such an autonomous AC power system is asymptotically stable, if the following two conditions hold:

(AC 1) each subsystem at a node $i \in \mathcal{V}$ is

- strictly EIP w.r.t. the supply rate $(d_i - \bar{d}_i)^\top (z_i - \bar{z}_i)$ and a continuously differentiable, positive definite storage function $S_i(x_i, \bar{x}_i)$, or
- EIP w.r.t. the supply rate $(d_i - \bar{d}_i)^\top (z_i - \bar{z}_i)$ and a continuously differentiable, positive definite storage function $S_i(x_i, \bar{x}_i)$, and such such that no solution other than $x_i(t) = \bar{x}_i$ can stay in $\mathbb{E}_i = \{x_i \in \mathcal{X}_i \subseteq \mathbb{R}^{n_i} \mid \dot{S}_i(x_i, \bar{x}_i) = 0, d_i = \bar{d}_i\}$ for all time.

(AC 2) each subsystem at an edge $l \in \mathcal{E}$ is

- strictly EIP w.r.t. the supply rate $(d_l - \bar{d}_l)^\top (z_l - \bar{z}_l)$ and a continuously differentiable, positive definite storage function $S_l(x_l, \bar{x}_l)$, or
- OSEIP w.r.t. the supply rate $(d_l - \bar{d}_l)^\top (z_l - \bar{z}_l)$ and a continuously differentiable, positive definite storage function $S_l(x_l, \bar{x}_l)$, and either EIO or such that no solution other than $x_l(t) = \bar{x}_l$ can stay in $\mathbb{E}_l = \{x_l \in \mathcal{X}_l \subseteq \mathbb{R}^{n_l} \mid \dot{S}_l(x_l, \bar{x}_l) = 0, d_l = \bar{d}_l\}$ for all time.

Proof:

The proof follows directly by application of Theorem 3.1 and Corollary 3.1 to the AC power system model established in Section 4.1 with some controller u_i at each DGU $i \in \mathcal{D}$. \square

Under Assumption 5.3, i.e., synchronized dq frames, the conditions (AC 1) and (AC 2) of Theorem 5.1 answer research question (Q1.1). Next, it has to be ensured that the DGU and load subsystems fulfill (AC 1) and the power line subsystems fulfill (AC 2).

⁴⁰ Note that \bar{x}_k for $k \in \mathcal{D}$ possibly implies a slight abuse of notation as in the case of dynamic DGU controllers the original state vector x_k from (5.3b) is augmented by additional controller states.

5.2.2 Properties of the Unactuated Systems

For the unactuated subsystems without control ports, i.e, load nodes $i \in \mathcal{L}$ (see (5.4)) and power lines $l \in \mathcal{P}$ (see (5.11)), requirements on the model parameters have to be established such that condition (AC 1) and (AC 2), respectively, are satisfied.

Load Nodes

Under Assumption 5.2, each load node $i \in \mathcal{L}$ can be represented as an ISO-PHS of the form (3.9) with $G(\mathbf{x}) = \mathbf{G} = \mathbf{0}_2$ (see (5.4d)). According to Lemma 3.1, the load node model (5.4) is thus EIP w.r.t. the supply rate $(\mathbf{d}_i - \bar{\mathbf{d}}_i)^\top (\mathbf{z}_i - \bar{\mathbf{z}}_i)$ and the shifted Hamiltonian as continuously differentiable, positive definite storage function $S_i(\mathbf{x}_i, \bar{\mathbf{x}}_i) = \frac{1}{2} \|\mathbf{x}_i - \bar{\mathbf{x}}_i\|_{\mathbf{Q}_i}^2$. So far, however, it has not been investigated when Assumption 5.2 holds.

In the following proposition, necessary and sufficient conditions are provided that ensure each load node $i \in \mathcal{L}$ fulfills Assumption 5.2 and condition (AC 1). Furthermore, in the proof, it will be shown that ensuring EIP is in fact equivalent to fulfilling the monotonicity property from Assumption 5.2.

Proposition 5.1 (EIP and confined dynamics behavior of ZIP and exponential AC loads)

Consider a load node $i \in \mathcal{L}$ described by (5.4). If and only if

- for ZIP loads with (5.9), it holds for all $V_i \geq 0.7 V_0$ that

$$Y_{P,i}^2 V_i^4 + Y_{P,i} I_{P,i} V_i^3 \geq \frac{1}{4} I_{Q,i} V_i^2 + (I_{P,i} P_{P,i} + I_{Q,i} P_{Q,i}) V_i + (P_{P,i}^2 + P_{Q,i}^2), \quad (5.18)$$

- for exponential loads with (5.10), it holds for all $V_i \geq 0.7 V_0$ that

$$4 (n_{P,i} - 1) P_{0,i}^2 \left(\frac{V_i}{V_0} \right)^{2n_{P,i}} \geq (n_{Q,i} - 2)^2 Q_{0,i}^2 \left(\frac{V_i}{V_0} \right)^{2n_{Q,i}}, \quad (5.19)$$

then Assumption 5.2 is fulfilled and (5.4a) is EIP w.r.t. the supply rate $(\mathbf{d}_i - \bar{\mathbf{d}}_i)^\top (\mathbf{z}_i - \bar{\mathbf{z}}_i)$ and the continuously differentiable, positive definite storage function

$$S_i(\mathbf{x}_i, \bar{\mathbf{x}}_i) = \frac{1}{2} \|\mathbf{x}_i - \bar{\mathbf{x}}_i\|_{\mathbf{Q}_i}^2 \quad (5.20)$$

for any (feasible) equilibrium pair $(\bar{\mathbf{d}}_i, \bar{\mathbf{z}}_i)$ and associated equilibrium state vector

$$\bar{\mathbf{x}}_i = \mathbf{C}_i \bar{\mathbf{V}}_i^{\text{dq}}. \quad (5.21)$$

Furthermore, no solution other than $\mathbf{x}_i(t) = \bar{\mathbf{x}}_i$ as in (5.21) can stay in $\mathbb{E}_i = \{\mathbf{x}_i \in \mathcal{X}_i \subseteq \mathbb{R}^2 \mid \dot{S}_i(\mathbf{x}_i, \bar{\mathbf{x}}_i) = 0, \mathbf{d}_i = \bar{\mathbf{d}}_i\}$ for all time.

Proof:

In order to show that the load model (5.4) is EIP w.r.t. the supply rate $(\mathbf{d}_i - \bar{\mathbf{d}}_i)^\top (\mathbf{z}_i - \bar{\mathbf{z}}_i)$ and the continuously differentiable, positive definite storage function $S_i(\mathbf{x}_i, \bar{\mathbf{x}}_i)$ in (5.20), let \mathbf{d}_i be fixed to an arbitrary equilibrium value $\bar{\mathbf{d}}_i$ with associated equilibrium values $\bar{\mathbf{z}}_i = \bar{\mathbf{V}}_i^{\text{dq}}$ and $\bar{\mathbf{x}}_i = C_i \bar{\mathbf{V}}_i^{\text{dq}}$ (cf. (5.4b), (5.4c)) for the interaction output and state, respectively. Since $\bar{\mathbf{x}}_i$ satisfies $\mathbf{J}_i \frac{\partial H_i}{\partial \mathbf{x}_i}(\bar{\mathbf{x}}_i) - \mathcal{R}_i \left(\frac{\partial H_i}{\partial \mathbf{x}_i}(\bar{\mathbf{x}}_i) \right) + \bar{\mathbf{d}}_i = 0$, the load model (5.4) can equivalently be written as

$$\dot{\mathbf{x}}_i = \mathbf{J}_i \left(\frac{\partial H_i}{\partial \mathbf{x}_i}(\mathbf{x}_i) - \frac{\partial H_i}{\partial \mathbf{x}_i}(\bar{\mathbf{x}}_i) \right) - \left[\mathcal{R}_i \left(\frac{\partial H_i}{\partial \mathbf{x}_i}(\mathbf{x}_i) \right) - \mathcal{R}_i \left(\frac{\partial H_i}{\partial \mathbf{x}_i}(\bar{\mathbf{x}}_i) \right) \right] + \mathbf{K}_i(\mathbf{d}_i - \bar{\mathbf{d}}_i). \quad (5.22)$$

For the time derivative of $S_i(\mathbf{x}_i, \bar{\mathbf{x}}_i)$ in (5.20), it holds that

$$\begin{aligned} \dot{S}_i(\mathbf{x}_i, \bar{\mathbf{x}}_i) &= - \underbrace{\left(\frac{\partial H_i}{\partial \mathbf{x}_i}(\mathbf{x}_i) - \frac{\partial H_i}{\partial \mathbf{x}_i}(\bar{\mathbf{x}}_i) \right)^\top \left[\mathcal{R}_i \left(\frac{\partial H_i}{\partial \mathbf{x}_i}(\mathbf{x}_i) \right) - \mathcal{R}_i \left(\frac{\partial H_i}{\partial \mathbf{x}_i}(\bar{\mathbf{x}}_i) \right) \right]}_{\psi_i(\mathbf{x}_i, \bar{\mathbf{x}}_i)} \\ &\quad + \underbrace{\left(\frac{\partial H_i}{\partial \mathbf{x}_i}(\mathbf{x}_i) - \frac{\partial H_i}{\partial \mathbf{x}_i}(\bar{\mathbf{x}}_i) \right)^\top}_{(\mathbf{z}_i - \bar{\mathbf{z}}_i)^\top} \mathbf{K}_i(\mathbf{d}_i - \bar{\mathbf{d}}_i). \end{aligned} \quad (5.23)$$

Following Definition 3.2, the load model (5.4) is EIP, if and only if

$$\psi_i(\mathbf{x}_i, \bar{\mathbf{x}}_i) \stackrel{(5.4)}{=} \left(\mathbf{V}_i^{\text{dq}} - \bar{\mathbf{V}}_i^{\text{dq}} \right)^\top \left(\mathbf{I}_{L,i}^{\text{dq}}(\mathbf{V}_i^{\text{dq}}) - \mathbf{I}_{L,i}^{\text{dq}}(\bar{\mathbf{V}}_i^{\text{dq}}) \right) \geq 0. \quad (5.24)$$

Note that according to Rockafellar and Wets [1998, Definition 12.1], (5.24) is the definition of a monotone, differentiable mapping $\mathbf{I}_{L,i}^{\text{dq}} : \mathbb{R}^2 \rightarrow \mathbb{R}^2$. Thus, (5.24) is fulfilled, if and only if the load current function $\mathbf{I}_{L,i}^{\text{dq}}(\mathbf{V}_i^{\text{dq}})$ is monotone. Additionally, $\mathbf{I}_{L,i}^{\text{dq}}(\mathbf{0}_2) = \mathbf{0}_2$ holds (see (5.9) and (5.10)). Thus, fulfilling Assumption 4.1 and ensuring EIP are equivalent.

Next, monotonicity conditions for $\mathbf{I}_{L,i}^{\text{dq}}(\mathbf{V}_i^{\text{dq}})$ are derived. Following Rockafellar and Wets [1998, Proposition 12.3], $\mathbf{I}_{L,i}^{\text{dq}}(\mathbf{V}_i^{\text{dq}})$ is monotone, if and only if its Jacobian

$$\nabla \mathbf{I}_{L,i}^{\text{dq}}(\mathbf{V}_i^{\text{dq}}) = \frac{\partial \mathbf{I}_{L,i}^{\text{dq}}(\mathbf{V}_i^{\text{dq}})}{\partial \mathbf{V}_i^{\text{dq}}} = \begin{bmatrix} \mathbf{I}_{L,i}^{\text{d}} & \mathbf{I}_{L,i}^{\text{d}} \\ \frac{\partial \mathbf{V}_i^{\text{d}}}{\partial \mathbf{V}_i^{\text{dq}}} & \frac{\partial \mathbf{V}_i^{\text{q}}}{\partial \mathbf{V}_i^{\text{dq}}} \\ \mathbf{I}_{L,i}^{\text{q}} & \mathbf{I}_{L,i}^{\text{q}} \\ \frac{\partial \mathbf{V}_i^{\text{d}}}{\partial \mathbf{V}_i^{\text{q}}} & \frac{\partial \mathbf{V}_i^{\text{q}}}{\partial \mathbf{V}_i^{\text{q}}} \end{bmatrix} \quad (5.25)$$

is positive semidefinite. Furthermore, since the Jacobian is a real-valued, quadratic matrix $\nabla \mathbf{I}_{L,i}^{\text{dq}}(\mathbf{V}_i^{\text{dq}}) \in \mathbb{R}^{2 \times 2}$, its definiteness properties are simply those of its symmetric part (see Rockafellar and Wets [1998, p. 534])

$$\frac{\nabla \mathbf{I}_{L,i}^{\text{dq}}(\mathbf{V}_i^{\text{dq}}) + \left(\nabla \mathbf{I}_{L,i}^{\text{dq}}(\mathbf{V}_i^{\text{dq}}) \right)^\top}{2} := \begin{bmatrix} a & b \\ b & c \end{bmatrix} \quad (5.26)$$

Note that the dependence of the amplitude V_i on the elements in V_i^{dq} (see (5.2)) must be taken into account when calculating the partial derivatives in (5.25) and (5.26), respectively.

For the ZIP current-voltage function (5.9) at voltage amplitudes $V_i \geq 0.7V_0$, (5.26) results in

$$a = Y_{P,i} + \frac{I_{P,i}(V_i^{\text{q}})^2 - I_{Q,i}V_i^{\text{d}}V_i^{\text{q}}}{V_i^3} - \frac{P_{P,i}\left((V_i^{\text{d}})^2 - (V_i^{\text{q}})^2\right) + 2P_{P,i}V_i^{\text{d}}V_i^{\text{q}}}{V_i^4}, \quad (5.27a)$$

$$b = \frac{I_{Q,i}\left((V_i^{\text{d}})^2 - (V_i^{\text{q}})^2\right) - 2I_{P,i}V_i^{\text{d}}V_i^{\text{q}}}{2V_i^3} + \frac{P_{Q,i}\left((V_i^{\text{d}})^2 - (V_i^{\text{q}})^2\right) - P_{P,i}V_i^{\text{d}}V_i^{\text{q}}}{V_i^4}, \quad (5.27b)$$

$$c = Y_{P,i} + \frac{I_{P,i}(V_i^{\text{q}})^2 + I_{Q,i}V_i^{\text{d}}V_i^{\text{q}}}{V_i^3} + \frac{P_{P,i}\left((V_i^{\text{d}})^2 - (V_i^{\text{q}})^2\right) + 2P_{P,i}V_i^{\text{d}}V_i^{\text{q}}}{V_i^4}. \quad (5.27c)$$

Then, using computer algebra software, the eigenvalues of (5.26) with (5.27) can be computed as

$$\begin{aligned} \lambda_{1,2} &= Y_{P,i} + \frac{I_{P,i}}{2V_i} \\ &\pm \frac{1}{V_i^2} \left[\frac{1}{4} (I_{P,i}^2 + I_{Q,i}^2) V_i^2 + (I_{P,i}P_{P,i} + I_{Q,i}P_{Q,i}) V_i + P_{P,i}^2 + P_{Q,i}^2 \right]^{\frac{1}{2}}. \end{aligned} \quad (5.28)$$

Finally, it is evaluated when the eigenvalues (5.28) are non-negative to infer positive semidefiniteness of the symmetric part of the Jacobian, i.e., (5.26) with (5.27). As (5.28) are eigenvalues of a real-valued, symmetric matrix, their values are always real [Rugh, 1996, p. 8]. Consequently, λ_2 , where the square-root term is subtracted, is critical for investigating the non-negativity of the eigenvalues (5.28). Multiplication with V_i^2 yields the inequality

$$Y_{P,i}V_i^2 + \frac{1}{2}I_{P,i}V_i \geq \left[\frac{1}{4} (I_{P,i}^2 + I_{Q,i}^2) V_i^2 + (I_{P,i}P_{P,i} + I_{Q,i}P_{Q,i}) V_i + P_{P,i}^2 + P_{Q,i}^2 \right]^{\frac{1}{2}}. \quad (5.29)$$

Since $Y_{P,i}, I_{P,i}, P_{P,i}, Y_{Q,i}, I_{Q,i}, P_{Q,i} \geq 0$ per definition, both sides in (5.29) are positive. Squaring them results in

$$\begin{aligned} Y_{P,i}^2V_i^4 + Y_{P,i}I_{P,i}V_i^3 + \frac{1}{4}I_{P,i}^2V_i^2 \\ \geq \frac{1}{4} (I_{P,i}^2 + I_{Q,i}^2) V_i^2 + (I_{P,i}P_{P,i} + I_{Q,i}P_{Q,i}) V_i + P_{P,i}^2 + P_{Q,i}^2, \end{aligned} \quad (5.30)$$

which after rearranging is equivalent to (5.18).

For the exponential current-voltage function (5.10) at voltage amplitudes $V_i \geq 0.7 V_0$, the procedure is similar. The symmetric part of the Jacobian (5.26) is given by

$$a = \frac{P_{0,i} \left[(n_{P,i} - 1) (V_i^d)^2 + (V_i^q)^2 \right]}{V_0^{n_{P,i}} V_i^{4-n_{P,i}}} + \frac{(n_{Q,i} - 2) Q_{0,i} V_i^d V_i^q}{V_0^{n_{Q,i}} V_i^{4-n_{Q,i}}}, \quad (5.31a)$$

$$b = \frac{(n_{P,i} - 2) P_{0,i} V_i^d V_i^q}{V_0^{n_{P,i}} V_i^{4-n_{P,i}}} - \frac{(n_{Q,i} - 2) Q_{0,i} \left((V_i^d)^2 - (V_i^q)^2 \right)}{2 V_0^{n_{Q,i}} V_i^{4-n_{Q,i}}}, \quad (5.31b)$$

$$c = \frac{P_{0,i} \left[(n_{P,i} - 1) (V_i^d)^2 + (V_i^q)^2 \right]}{V_0^{n_{P,i}} V_i^{4-n_{P,i}}} - \frac{(n_{Q,i} - 2) Q_{0,i} V_i^d V_i^q}{V_0^{n_{Q,i}} V_i^{4-n_{Q,i}}}, \quad (5.31c)$$

with eigenvalues

$$\lambda_{1,2} = \frac{1}{2V_i^2} \left(n_{P,i} P_{0,i} \left(\frac{V_i}{V_0} \right)^{n_{P,i}} \pm \left[(n_{P,i} - 2)^2 P_{0,i}^2 \left(\frac{V_i}{V_0} \right)^{2n_{P,i}} + (n_{Q,i} - 2)^2 Q_{0,i}^2 \left(\frac{V_i}{V_0} \right)^{2n_{Q,i}} \right]^{\frac{1}{2}} \right). \quad (5.32)$$

The critical eigenvalue λ_2 (see (5.32)) is positive under

$$n_{P,i} P_{0,i} \left(\frac{V_i}{V_0} \right)^{n_{P,i}} \geq \left[(n_{P,i} - 2)^2 P_{0,i}^2 \left(\frac{V_i}{V_0} \right)^{2n_{P,i}} + (n_{Q,i} - 2)^2 Q_{0,i}^2 \left(\frac{V_i}{V_0} \right)^{2n_{Q,i}} \right]^{\frac{1}{2}}. \quad (5.33)$$

Since both sides in (5.33) are positive, squaring them results in

$$n_{P,i} P_{0,i} \left(\frac{V_i}{V_0} \right)^{2n_{P,i}} \geq (n_{P,i} - 2)^2 P_{0,i}^2 \left(\frac{V_i}{V_0} \right)^{2n_{P,i}} + (n_{Q,i} - 2)^2 Q_{0,i}^2 \left(\frac{V_i}{V_0} \right)^{2n_{Q,i}}, \quad (5.34)$$

which after rearranging is equivalent to (5.19).

For $V_i < 0.7 V_0$, the procedure for both ZIP and exponential loads is as before. The symmetric part of the Jacobian is given by (5.26) with

$$a = \tilde{Y}_{P,i}, \quad b = 0, \quad c = \tilde{Y}_{P,i}. \quad (5.35a)$$

Since $\tilde{Y}_{P,i} \geq 0$ per definition (see (5.9) and (5.10)), monotonicity and thus EIP follow directly.

Lastly, it is proved that conditions (5.18) and (5.19), respectively, also imply that no solution other than \bar{x}_i as in (5.21) can stay in $\mathbb{E}_i = \{x_i \in \mathcal{X}_i \subseteq \mathbb{R}^2 \mid \dot{S}_i(x_i, \bar{x}_i) = 0, \mathbf{d}_i = \bar{\mathbf{d}}_i\}$ for all time. From (5.23), it follows that set \mathbb{E}_i is characterized by $\psi_i(x_i, \bar{x}_i) = 0$, which either directly implies $\mathbf{V}_i^{\text{dq}} \equiv \bar{\mathbf{V}}_i^{\text{dq}}$ or $\mathbf{I}_{L,i}^{\text{dq}}(\mathbf{V}_i^{\text{dq}}) - \mathbf{I}_{L,i}^{\text{dq}}(\bar{\mathbf{V}}_i^{\text{dq}}) = \mathbf{0}_2$. For the latter, consider the evolution of a solution of (5.22) starting in \mathbb{E}_i . Confine the dynamics (5.22) to \mathbb{E}_i

for any future time by inserting $\mathcal{R}_i \left(\frac{\partial H_i}{\partial \mathbf{x}_i}(\mathbf{x}_i) \right) - \mathcal{R}_i \left(\frac{\partial H_i}{\partial \mathbf{x}_i}(\bar{\mathbf{x}}_i) \right) = \mathbf{0}_2$ and $\mathbf{d}_i = \bar{\mathbf{d}}_i$. This yields the set of equations

$$\begin{aligned} 0 &= \omega_0 C_i (V_i^q - \bar{V}_i^q), \\ 0 &= -\omega_0 C_i (V_i^d - \bar{V}_i^d), \end{aligned} \quad (5.36)$$

whose unique solution is $V_i^d \equiv \bar{V}_i^d$, $V_i^q \equiv \bar{V}_i^q$ implying $\mathbf{x}_i \equiv \bar{\mathbf{x}}_i$. Thus, no solution other than $\bar{\mathbf{x}}_i$ as in (5.21) can stay in \mathbb{E}_i for all time. \square

Remark 5.5. The ZIP load condition (5.18) is most restrictive on the ratio between its parameters at the lower voltage bound $V_i = 0.7V_0$. Thus, to ensure that some load node $i \in \mathcal{L}$ fulfills (AC 1) for all voltages $V_i \geq 0$, the inequality

$$\begin{aligned} Y_{P,i}^2(0.7V_0)^4 + Y_{P,i}I_{P,i}(0.7V_0)^3 &\geq \frac{1}{4}I_{Q,i}(0.7V_0)^2 + (I_{P,i}P_{P,i} + I_{Q,i}P_{Q,i})0.7V_0 \\ &+ (P_{P,i}^2 + P_{Q,i}^2) \end{aligned} \quad (5.37)$$

has to be fulfilled. In contrast, the exponential load condition (5.19) does not allow for a conservative worst-case approximation. Instead, the validity of (5.19) has to be checked for voltage amplitudes V_i within some set that covers all voltage amplitudes that might reasonably occur during operation.

Remark 5.6. From (5.18), (5.37), and (5.19), it can be seen that a purely reactive power consumption violates the load conditions. Furthermore, as with the DC case (see Remark 4.4), it can be seen that a too dominant constant power load behavior also violates the derived conditions.

Remark 5.7. Note that if (5.18) and (5.19), respectively, hold strictly and additionally $\tilde{Y}_{P,i} > 0$, the load current function $\mathbf{I}_{L,i}^{\text{dq}}(\mathbf{V}_i^{\text{dq}})$ is strictly monotone and the load model is strictly EIP.

Power Lines

The AC power line models (5.11) can be represented as linear ISO-PHS models with constant matrices and positive definite dissipation matrix $\mathbf{R}_l \succ 0$ (see (5.11d)). According to Lemma 3.1, the power line models (5.11) are thus strictly EIP w.r.t. the supply rate $(\mathbf{d}_l - \bar{\mathbf{d}}_l)^\top (z_l - \bar{z}_l)$ and the shifted Hamiltonian as continuously differentiable, positive definite storage function $S_l(\mathbf{x}_l, \bar{\mathbf{x}}_l) = \frac{1}{2} \|\mathbf{x}_l - \bar{\mathbf{x}}_l\|_{\mathbf{Q}_l}^2$. Consequently, they satisfy condition (AC 2) for all model parameters.

5.2.3 Control Problems

For the actuated DGU subsystems $i \in \mathcal{D}$, decentralized controllers for the VSIs are to be designed such that the closed-loop systems satisfy condition (AC 1). Furthermore, the respective closed-loop equilibrium state vectors $\hat{\mathbf{x}}_i$, $i \in \mathcal{D}$, should be such that desired node voltages $\bar{\mathbf{V}}_i^{\text{dq}} = \mathbf{V}_i^{\text{dq}*} \in \mathbb{R}^2$ and current injections $\bar{\mathbf{I}}_i^{\text{dq}} = \mathbf{I}_i^{\text{dq}*} \in \mathbb{R}^2$ are established in steady state (see research question (Q1.2)).

In particular, recall from Section 2.1 that the operating modes of VSIs can be separated into grid-forming voltage control and grid-feeding current control (see also Rocabert et al. [2012]). Consequently, following the notation used for the DC case (see Section 4.2.3), the set of DGUs with VSIs stabilizing voltage setpoints $\mathbf{V}_i^{\text{dq}*}$ is denoted by $\mathcal{D}_{\text{form}}$. Conversely, the set of DGUs with VSIs stabilizing the injected currents to setpoints \mathbf{I}_i^* is denoted by $\mathcal{D}_{\text{feed}}$.

In order to achieve decentralized stabilization in AC power systems as per Definition 2.3 and provide answers to research question (Q1.2), the following control problem is left to be addressed:

Problem 5.1 (Decentralized voltage and current control)

Consider DGUs $i \in \mathcal{D}$ described in open loop by (5.3). For the VSI in each DGU $i \in \mathcal{D}$, design decentralized controllers of the form

$$\dot{\mathbf{x}}_{c,i} = \mathbf{f}_{c,i}(\mathbf{x}_i, \mathbf{x}_{c,i}), \quad \mathbf{u}_i = \mathbf{V}_{S,i}^{\text{dq}} = \hat{\mathbf{u}}_i(\mathbf{x}_i, \mathbf{x}_{c,i}) \quad (5.38)$$

with controller states $\mathbf{x}_{c,i} \in \mathbb{R}^2$ such that the resulting closed-loop system fulfills (AC 1). Furthermore, the respective closed-loop equilibrium state vector $\hat{\mathbf{x}}_i = [\hat{\mathbf{x}}_i^\top, \hat{\mathbf{x}}_{c,i}^\top]^\top$ shall fulfill the following characteristics:

- (a) For each grid-feeding DGU $i \in \mathcal{D}_{\text{feed}}$, $\bar{\mathbf{I}}_i^{\text{dq}} = \mathbf{I}_i^{\text{dq}*} \in \mathbb{R}^2$ in $\hat{\mathbf{x}}_i$.
- (b) For each grid-forming DGU $i \in \mathcal{D}_{\text{form}}$, $\bar{\mathbf{V}}_i^{\text{dq}} = \mathbf{V}_i^{\text{dq}*} \in \mathbb{R}^2$ in $\hat{\mathbf{x}}_i$.

Remark 5.8. In line with the hierarchical control structure discussed in Section 2.1.2, the setpoints $\mathbf{V}_i^{\text{dq}*}$ and $\mathbf{I}_i^{\text{dq}*}$ are assumed to be known and specified by a higher-level control ensuring that these setpoints constitute feasible AC power system equilibria $\bar{\mathbf{x}}_{\text{AC}}$ within the operational constraints.

5.3 Passivity-Based Control Design

In this section, Problem 5.1 is addressed. In Sections 5.3.1 and 5.3.2, current and voltage controllers are designed for the VSIs such that the closed-loop DGU models fulfill the requirements in Problem 5.1. To showcase the unifying nature of the derived decentralized stability conditions, Section 5.3.3 demonstrates by example of the voltage controller proposed by Nahata and Ferrari-Trecate [2019] that decentralized, passivity-based controllers which are available in the literature are compatible with condition (AC 1).

5.3.1 Current Controller

The goal of current controllers in grid-feeding DGUs $i \in \mathcal{D}_{\text{feed}}$ is to asymptotically stabilize closed-loop DGU equilibria $\bar{\mathbf{x}}_i = [L_i I_i^{\text{dq}*}, L_i I_i^{\text{q}*}, C_i \bar{V}_i^{\text{d}}, C_i \bar{V}_i^{\text{q}}, \bar{\mathbf{x}}_{\text{c},i}^\top]^\top$ containing some desired VSI output current $I_i^{\text{dq}*}$ (see Problem 5.1 (a)). As in the DC case (see Section 4.3.1), $I_i^{\text{dq}} = \mathbf{y}_i$ is the natural passive control output of the open-loop DGU model (see (5.3c)). Thus, a standard PI controller working on $\mathbf{y}_i^* - \mathbf{y}_i = I_i^{\text{dq}*} - I_i^{\text{dq}}$ can stabilize any equilibrium value $\bar{\mathbf{x}}_i$ while preserving EIP of the closed-loop system with respect to the supply rate $(\mathbf{d}_i - \bar{\mathbf{d}}_i)^\top (\mathbf{z}_i - \bar{\mathbf{z}}_i)$ (cf. Jayawardhana et al. [2007]). In the present case of grid-feeding DGUs $i \in \mathcal{D}_{\text{feed}}$, it can be shown that a standard PI current controller also suffices to ensure the additional confined dynamics requirement posed by (AC 1).

Proposition 5.2 (Current controller for grid-feeding DGUs)

Consider a grid-feeding DGU $i \in \mathcal{D}_{\text{feed}}$ described in open loop by (5.3). Assume the local ZIP or exponential load (5.3f) fulfills the conditions of Proposition 5.1. Assign the control input $\mathbf{u}_i = \mathbf{V}_{\text{S},i}^{\text{dq}}$ with the PI controller

$$\begin{bmatrix} Q_{1,i}^{\text{d}} & 0 \\ 0 & Q_{1,i}^{\text{q}} \end{bmatrix} \dot{\mathbf{r}}_i = - \left(\mathbf{I}_i^{\text{dq}} - \mathbf{I}_i^{\text{dq}*} \right), \quad (5.39a)$$

$$\mathbf{u}_i = \begin{bmatrix} k_{\text{P},i}^{\text{d}} & 0 \\ 0 & k_{\text{P},i}^{\text{q}} \end{bmatrix} \left(\mathbf{I}_i^{\text{dq}} - \mathbf{I}_i^{\text{dq}*} \right) + \mathbf{r}_i + \begin{bmatrix} -\omega_0 L_i I_i^{\text{q}} \\ \omega_0 L_i I_i^{\text{d}} \end{bmatrix}, \quad (5.39b)$$

where $\mathbf{I}_i^{\text{dq}*} \in \mathbb{R}^2$ is a desired dq current setpoint and $k_{\text{P},i}^{\text{d}}, k_{\text{P},i}^{\text{q}}, Q_{1,i}^{\text{d}}, Q_{1,i}^{\text{q}} > 0$ are control parameters. Then, the closed-loop DGU system can be written as

$$\frac{d}{dt} \underbrace{\begin{bmatrix} L_i I_i^d \\ L_i I_i^q \\ C_i V_i^d \\ C_i V_i^q \\ Q_{I,i}^d r_i^d \\ Q_{I,i}^q r_i^q \end{bmatrix}}_{\hat{\mathbf{x}}_i} = \underbrace{\begin{bmatrix} -R_i I_i^d - V_i^d - k_{P,i}^d (I_i^d - I_i^{d*}) + r_i^d \\ -R_i I_i^q - V_i^q - k_{P,i}^q (I_i^q - I_i^{q*}) + r_i^q \\ I_i^d + \omega_0 C_i V_i^q - I_{L,i}^d (V_i^{dq}) \\ I_i^q - \omega_0 C_i V_i^d - I_{L,i}^q (V_i^{dq}) \\ -(I_i^d - I_i^{d*}) \\ -(I_i^q - I_i^{q*}) \end{bmatrix}}_{f_i(\hat{\mathbf{x}}_i)} + \underbrace{\begin{bmatrix} 0 & 0 \\ 0 & 0 \\ 1 & 0 \\ 0 & 1 \\ 0 & 0 \\ 0 & 0 \end{bmatrix}}_{\mathbf{K}_i} \mathbf{d}_i, \quad (5.40a)$$

$$\mathbf{z}_i = \mathbf{V}_i^{dq}. \quad (5.40b)$$

Moreover, (5.40) is EIP w.r.t. the supply rate $(\mathbf{d}_i - \bar{\mathbf{d}}_i)^\top (\mathbf{z}_i - \bar{\mathbf{z}}_i)$ and the continuously differentiable, positive definite storage function

$$\hat{S}_i(\hat{\mathbf{x}}_i, \bar{\mathbf{x}}_i) = \frac{1}{2} \|\hat{\mathbf{x}}_i - \bar{\mathbf{x}}_i\|_{\hat{\mathbf{Q}}_i}^2, \quad (5.41a)$$

$$\hat{\mathbf{Q}}_i = \text{diag} \left(\frac{1}{L_i}, \frac{1}{L_i}, \frac{1}{C_i}, \frac{1}{C_i}, \frac{1}{Q_{I,i}^d}, \frac{1}{Q_{I,i}^q} \right) \quad (5.41b)$$

for any (feasible) equilibrium pair $(\bar{\mathbf{d}}_i, \mathbf{z}_i)$ and associated equilibrium state vector

$$\bar{\mathbf{x}}_i = \left[L_i I_i^{d*}, L_i I_i^{q*}, C_i \bar{V}_i^d, C_i \bar{V}_i^q, Q_{I,i}^d \bar{r}_i^d, Q_{I,i}^q \bar{r}_i^q \right]^\top. \quad (5.42)$$

Furthermore, no solution other than $\hat{\mathbf{x}}_i = \bar{\mathbf{x}}_i$ as in (5.42) can stay in $\mathbb{E}_i = \{\hat{\mathbf{x}}_i \in \hat{\mathcal{X}}_i \subseteq \mathbb{R}^6 \mid \hat{S}_i(\hat{\mathbf{x}}_i, \bar{\mathbf{x}}_i) = 0, \mathbf{d}_i = \bar{\mathbf{d}}_i\}$ for all time.

Proof:

Writing the closed-loop DGU model as in (5.40) directly follows by inserting the PI controller (5.39) into the open-loop DGU model (5.3). The remaining proof is largely identical to that of Proposition 4.2. Substitute the variables, vectors, and matrices with the respective ones from (5.3) and (5.40).

In particular, the dissipation rate is given by

$$\begin{aligned} \hat{\psi}_i(\hat{\mathbf{x}}_i, \bar{\mathbf{x}}_i) &= (R_i + k_{P,i}^d) (I_i^d - I_i^{d*})^2 + (R_i + k_{P,i}^q) (I_i^q - I_i^{q*})^2 \\ &\quad + \left(\mathbf{V}_i^{dq} - \bar{\mathbf{V}}_i^{dq} \right)^\top \left(\mathbf{I}_{L,i}^{dq} (\mathbf{V}_i^{dq}) - \mathbf{I}_{L,i}^{dq} (\bar{\mathbf{V}}_i^{dq}) \right) \end{aligned} \quad (5.43)$$

and positive semidefinite under the load conditions of Proposition 5.1 ($R_i, k_{P,i}^d, k_{P,i}^q > 0$ per definition). Furthermore, set \mathbb{E}_i is characterized by

$$\hat{\psi}_i(\hat{\mathbf{x}}_i, \bar{\mathbf{x}}_i) \equiv 0 \stackrel{(5.43)}{\implies} \mathbf{I}_i^{dq} \equiv \mathbf{I}_i^{dq*}. \quad (5.44)$$

The shifted dynamics of (5.40) confined to \mathbb{E}_i are given by

$$\begin{aligned}
0 &= r_i^d - \bar{r}_i^d - (V_i^d - \bar{V}_i^d), \\
0 &= r_i^q - \bar{r}_i^q - (V_i^q - \bar{V}_i^q), \\
C_i \dot{V}_i^d &= \omega_0 C_i (V_i^q - \bar{V}_i^q) - \left(I_{L,i}^d(\mathbf{V}_i^{\text{dq}}) - I_{L,i}^d(\bar{\mathbf{V}}_i^{\text{dq}}) \right), \\
C_i \dot{V}_i^q &= -\omega_0 C_i (V_i^d - \bar{V}_i^d) - \left(I_{L,i}^q(\mathbf{V}_i^{\text{dq}}) - I_{L,i}^q(\bar{\mathbf{V}}_i^{\text{dq}}) \right), \\
Q_{L,i}^d \dot{r}_i^d &= 0, \\
Q_{L,i}^q \dot{r}_i^q &= 0,
\end{aligned} \tag{5.45}$$

whose unique solution is $\mathbf{V}_i^{\text{dq}} \equiv \bar{\mathbf{V}}_i^{\text{dq}}$, $\mathbf{r}_i \equiv \bar{\mathbf{r}}_i$. \square

Remark 5.9. *The last term in (5.39b) is added to decouple the dynamics of the d and q component of \mathbf{I}_i^{dq} (compare (5.40) with (5.3a)). While the results of Proposition 5.2 hold without such a decoupling, the decoupling is commonly done in practice when designing dq current controllers to improve control performance.*

Similar to the DC current controller, the statements of Proposition 5.2 still hold when a grid-feeding DGU $i \in \mathcal{D}_{\text{feed}}$ does not supply a local load, i.e., $\mathbf{I}_{L,i}^{\text{dq}}(\mathbf{V}_i^{\text{dq}}) = \mathbf{0}_2$ (see Remark 5.2). The following corollary summarizes this insight.

Corollary 5.1 (Current control of grid-feeding DGUs without local loads)

Consider a grid-feeding DGU $i \in \mathcal{D}_{\text{feed}}$ that does not supply a local load, i.e., its open-loop model is given by (5.3) with $\mathbf{I}_{L,i}^{\text{dq}}(\mathbf{V}_i^{\text{dq}}) = \mathbf{0}_2$. Assign the control input with the PI controller as in Proposition 5.2. Then the closed-loop DGU system is given by (5.40) with $\mathbf{I}_{L,i}^{\text{dq}}(\mathbf{V}_i^{\text{dq}}) = \mathbf{0}_2$. Moreover, all statements from Proposition 5.2 regarding the EIP properties of the closed loop and its dynamics confined to set \mathbb{E}_i hold.

Proof:

The proof is identical to that of Proposition 5.2 except with $\mathbf{I}_{L,i}^{\text{dq}}(\mathbf{V}_i^{\text{dq}}) = \mathbf{I}_{L,i}^{\text{dq}}(\bar{\mathbf{V}}_i^{\text{dq}}) = \mathbf{0}_2$ in the respective equations. \square

5.3.2 Voltage Controller

The goal of voltage controllers in grid-forming DGUs $i \in \mathcal{D}_{\text{form}}$ is to asymptotically stabilize DGU equilibria $\bar{\mathbf{x}}_i = [L_i \bar{I}_i^d, L_i \bar{I}_i^q, C_i V_i^{\text{d}*}, C_i V_i^{\text{q}*}, \bar{\mathbf{x}}_{c,i}^\top]^\top$ containing some desired node voltage $V_i^{\text{dq}*}$ (see Problem 5.1 (b)). However, the node voltage is the passive interaction output $\mathbf{z}_i = \mathbf{V}_i^{\text{dq}}$ (see (5.3d)) whose corresponding input \mathbf{d}_i is not accessible

as control input. Thus, a similar control design as in the DC case is used which combines algebraic IDA-PBC from Ortega and García-Canseco [2004] and integral action from Donaire and Junco [2009].

Proposition 5.3 (Voltage controller for grid-forming DGUs)

Consider a grid-forming DGU $i \in \mathcal{D}_{\text{form}}$ described in open loop by (5.3). Assume the local ZIP or exponential load (5.3f) fulfills the conditions of Proposition 5.1. Assign the control input $\mathbf{u}_i = \mathbf{V}_{S,i}^{\text{dq}}$ as

$$\begin{bmatrix} Q_{1,i}^{\text{d}} & 0 \\ 0 & Q_{1,i}^{\text{q}} \end{bmatrix} \dot{\mathbf{r}}_i = \mathbf{V}_i^{\text{dq}} - \mathbf{V}_i^{\text{dq}*}, \quad (5.46a)$$

$$\begin{aligned} \mathbf{u}_i = & \begin{bmatrix} (1 - \hat{R}_i^{\text{d}} \omega_0 C_i) V_i^{\text{q}*} \\ (1 + \hat{R}_i^{\text{q}} \omega_0 C_i) V_i^{\text{d}*} \end{bmatrix} + \begin{bmatrix} (R_i - \hat{R}_i^{\text{d}} - \omega_0 L_i) I_i^{\text{d}} \\ (R_i - \hat{R}_i^{\text{q}} + \omega_0 L_i) I_i^{\text{q}} \end{bmatrix} \\ & - \begin{bmatrix} \hat{R}_i^{\text{d}} & 0 \\ 0 & \hat{R}_i^{\text{q}} \end{bmatrix} \mathbf{r}_i + \begin{bmatrix} \frac{L_i}{Q_{1,i}^{\text{d}}} & 0 \\ 0 & \frac{L_i}{Q_{1,i}^{\text{q}}} \end{bmatrix} (\mathbf{V}_i^{\text{dq}*} - \mathbf{V}_i^{\text{dq}}), \end{aligned} \quad (5.46b)$$

where $\mathbf{V}_i^{\text{dq}*} \in \mathbb{R}^2$ is a desired dq voltage setpoint and $\hat{R}_i^{\text{d}}, \hat{R}_i^{\text{q}}, Q_{1,i}^{\text{d}}, Q_{1,i}^{\text{q}} > 0$ are control parameters. Then, with the change of coordinates from \mathbf{I}_i^{dq} to

$$\boldsymbol{\chi}_i := \mathbf{I}_i^{\text{dq}} + \mathbf{r}_i + \begin{bmatrix} \omega_0 C_i V_i^{\text{q}*} \\ -\omega_0 C_i V_i^{\text{d}*} \end{bmatrix}, \quad (5.47)$$

the closed-loop DGU system can be written as

$$\frac{\text{d}}{\text{d}t} \underbrace{\begin{bmatrix} L_i \chi_i^{\text{d}} \\ L_i \chi_i^{\text{q}} \\ C_i V_i^{\text{d}} \\ C_i V_i^{\text{q}} \\ Q_{1,i}^{\text{d}} r_i^{\text{d}} \\ Q_{1,i}^{\text{q}} r_i^{\text{q}} \end{bmatrix}}_{\hat{\mathbf{x}}_i} = \underbrace{\begin{bmatrix} -\hat{R}_i^{\text{d}} \chi_i^{\text{d}} - (V_i^{\text{d}} - V_i^{\text{d}*}) \\ -\hat{R}_i^{\text{q}} \chi_i^{\text{q}} - (V_i^{\text{q}} - V_i^{\text{q}*}) \\ \chi_i^{\text{d}} + \omega_0 C_i (V_i^{\text{q}} - V_i^{\text{q}*}) - r_i^{\text{d}} - I_{L,i}^{\text{d}}(\mathbf{V}_i^{\text{dq}}) \\ \chi_i^{\text{q}} - \omega_0 C_i (V_i^{\text{d}} - V_i^{\text{d}*}) - r_i^{\text{q}} - I_{L,i}^{\text{q}}(\mathbf{V}_i^{\text{dq}}) \\ (V_i^{\text{d}} - V_i^{\text{d}*}) \\ (V_i^{\text{q}} - V_i^{\text{q}*}) \end{bmatrix}}_{\hat{\mathbf{f}}_i(\hat{\mathbf{x}}_i)} + \underbrace{\begin{bmatrix} 0 & 0 \\ 0 & 0 \\ 1 & 0 \\ 0 & 1 \\ 0 & 0 \\ 0 & 0 \end{bmatrix}}_{\hat{\mathbf{K}}_i} \mathbf{d}_i, \quad (5.48a)$$

$$\mathbf{z}_i - \bar{\mathbf{z}} = \mathbf{V}_i^{\text{dq}} - \mathbf{V}_i^{\text{dq}*}. \quad (5.48b)$$

Moreover, (5.48) is EIP w.r.t. the supply rate $(\mathbf{d}_i - \bar{\mathbf{d}}_i)^\top (\mathbf{z}_i - \bar{\mathbf{z}}_i)$ and the continuously differentiable, positive definite storage function

$$\hat{S}_i(\hat{\mathbf{x}}_i, \bar{\hat{\mathbf{x}}}_i) = \frac{1}{2} \|\hat{\mathbf{x}}_i - \bar{\hat{\mathbf{x}}}_i\|_{\hat{\mathbf{Q}}_i}^2, \quad (5.49a)$$

$$\hat{\mathbf{Q}}_i = \text{diag} \left(\frac{1}{L_i}, \frac{1}{L_i}, \frac{1}{C_i}, \frac{1}{C_i}, \frac{1}{Q_{1,i}^{\text{d}}}, \frac{1}{Q_{1,i}^{\text{q}}} \right) \quad (5.49b)$$

for any (feasible) equilibrium pair $(\bar{\mathbf{d}}_i, \bar{\mathbf{z}}_i)$ and associated equilibrium state

$$\hat{\mathbf{x}}_i = \left[L_i \bar{\chi}_i^d, L_i \bar{\chi}_i^q, C_i V_i^{d*}, C_i V_i^{q*}, Q_{L,i}^d \bar{r}_i^d, Q_{L,i}^q \bar{r}_i^q \right]^\top. \quad (5.50)$$

Furthermore, no solution other than $\hat{\mathbf{x}}_i = \bar{\mathbf{x}}_i$ as in (5.50) can stay in $\mathbb{E}_i = \{\hat{\mathbf{x}}_i \in \hat{\mathcal{X}}_i \subseteq \mathbb{R}^6 \mid \hat{S}_i(\hat{\mathbf{x}}_i, \bar{\mathbf{x}}_i) = 0, \mathbf{d}_i = \bar{\mathbf{d}}_i\}$ for all time.

Proof:

Firstly, it is illustrated how to assign desired closed-loop dynamics (5.48) according to IDA-PBC and systematically derive the coordinate transformation (5.47). Following the IDA-PBC design methodology from Ortega and García-Canseco [2004], the directly actuated current dynamics (see (5.3a)) are assigned a desired damping $\hat{R}_i^d, \hat{R}_i^q > 0$ and the Hamiltonian is shifted such that it contains the terms $C_i(V_i^d - V_i^{d*})$ and $C_i(V_i^q - V_i^{q*})$ implying a minimum at the desired voltage setpoint \mathbf{V}_i^{dq*} . Additionally, the current dynamics are assigned a decoupled structure by removing the terms containing $\omega_0 L_i$.

Next, following Donaire and Junco [2009], two integrator states (5.46a) are added to guarantee zero steady-state voltage errors. Subsequently, by introducing a new coordinate vector $\chi_i = [\chi_i^d, \chi_i^q]^\top$, the resulting DGU dynamics in closed-loop (cf. (5.48a)) can be written in the form of an ISO-PHS (3.9)

$$\frac{d}{dt} \begin{bmatrix} L_i \chi_i^d \\ L_i \chi_i^q \\ C_i V_i^d \\ C_i V_i^q \\ Q_{L,i}^d r_i^d \\ Q_{L,i}^q r_i^q \end{bmatrix} = \begin{bmatrix} -\hat{R}_i^d & 0 & -1 & 0 & 0 & 0 \\ 0 & -\hat{R}_i^q & 0 & -1 & 0 & 0 \\ 1 & 0 & 0 & \omega_0 C_i & -1 & 0 \\ 0 & 1 & -\omega_0 C_i & 0 & 0 & -1 \\ 0 & 0 & 1 & 0 & 0 & 0 \\ 0 & 0 & 0 & 1 & 0 & 0 \end{bmatrix} \begin{bmatrix} \chi_i^d \\ \chi_i^q \\ V_i^d - V_i^{d*} \\ V_i^q - V_i^{q*} \\ r_i^d \\ r_i^q \end{bmatrix} - \begin{bmatrix} 0 \\ 0 \\ I_{L,i}^d(\mathbf{V}_i^{dq}) \\ I_{L,i}^q(\mathbf{V}_i^{dq}) \\ 0 \\ 0 \end{bmatrix} + \begin{bmatrix} 0 \\ 0 \\ 1 \\ 1 \\ 0 \\ 0 \end{bmatrix} \mathbf{d}_i. \quad (5.51)$$

The specific coordinate transformation (5.47) is found by matching the voltage dynamics, which are not directly actuated, in closed loop (5.48a) (see also (5.51)) and open loop (5.3a). This yields

$$\chi_i + \begin{bmatrix} 0 & \omega_0 C_i \\ -\omega_0 C_i & 0 \end{bmatrix} (\mathbf{V}_i^{dq} - \mathbf{V}_i^{dq*}) - \mathbf{r}_i - \mathbf{I}_{L,i}^{dq}(\mathbf{V}_i^{dq}) + \mathbf{d}_i = \mathbf{I}_i^{dq} + \begin{bmatrix} 0 & \omega_0 C_i \\ -\omega_0 C_i & 0 \end{bmatrix} \mathbf{V}_i^{dq} - \mathbf{I}_{L,i}^{dq}(\mathbf{V}_i^{dq}) + \mathbf{d}_i \quad (5.52)$$

$$\Leftrightarrow \chi_i = \mathbf{I}_i^{dq} + \mathbf{r}_i + \begin{bmatrix} \omega_0 C_i V_i^{q*} \\ -\omega_0 C_i V_i^{d*} \end{bmatrix} \quad (5.53)$$

as in (5.47). In order to derive the controller (5.46b), compute $L_i \dot{\chi}_i$ to get

$$\begin{aligned} L_i \dot{\chi}_i &\stackrel{(5.47)}{=} L_i \dot{\mathbf{I}}_i^{dq} + L_i \dot{\mathbf{r}}_i \\ &\stackrel{(5.3a)}{=} \stackrel{(5.46a)}{=} \begin{bmatrix} -R_i + \omega_0 L_i I_i^q \\ -R_i - \omega_0 L_i I_i^d \end{bmatrix} - \mathbf{V}_i^{dq} + \mathbf{u}_i + \begin{bmatrix} \frac{L_i}{Q_{L,i}^d} & 0 \\ 0 & \frac{L_i}{Q_{L,i}^q} \end{bmatrix} (\mathbf{V}_i^{dq} - \mathbf{V}_i^{dq*}). \end{aligned} \quad (5.54)$$

By matching (5.54) with the assigned $L_i \chi_i$ dynamics in (5.48a) (see also (5.51)), i.e.,

$$\begin{aligned} \begin{bmatrix} -\hat{R}_i^d \chi_i^d \\ -\hat{R}_i^q \chi_i^q \end{bmatrix} - (\mathbf{V}_i^{\text{dq}} - \mathbf{V}_i^{\text{dq}*}) &\stackrel{(5.47)}{=} \begin{bmatrix} -\hat{R}_i^d (I_i^d + r_i^d + \omega_0 C_i V_i^{\text{dq}*}) \\ -\hat{R}_i^q (I_i^q + r_i^q - \omega_0 C_i V_i^{\text{dq}*}) \end{bmatrix} - (\mathbf{V}_i^{\text{dq}} - \mathbf{V}_i^{\text{dq}*}) \\ &= \begin{bmatrix} -R_i + \omega_0 L_i I_i^q \\ -R_i - \omega_0 L_i I_i^d \end{bmatrix} - \mathbf{V}_i^{\text{dq}} + \mathbf{u}_i + \begin{bmatrix} \frac{L_i}{Q_{1,i}^d} & 0 \\ 0 & \frac{L_i}{Q_{1,i}^q} \end{bmatrix} (\mathbf{V}_i^{\text{dq}} - \mathbf{V}_i^{\text{dq}*}), \end{aligned} \quad (5.55)$$

and rearranging, the control law (5.46b) is obtained.

The remaining proof is largely identical to that of Proposition 4.3. Simply substitute the variables, vectors, and matrices with the respective ones from (5.3) and (5.48). In particular, the dissipation rate is given by

$$\begin{aligned} \hat{\psi}_i(\hat{\mathbf{x}}_i, \bar{\mathbf{x}}_i) &= \hat{R}_i^d (\chi_i^d - \bar{\chi}_i^d)^2 + \hat{R}_i^q (\chi_i^q - \bar{\chi}_i^q)^2 \\ &\quad + (\mathbf{V}_i^{\text{dq}} - \bar{\mathbf{V}}_i^{\text{dq}})^\top \left(\mathbf{I}_{L,i}^{\text{dq}} (\mathbf{V}_i^{\text{dq}}) - \mathbf{I}_{L,i}^{\text{dq}} (\bar{\mathbf{V}}_i^{\text{dq}}) \right) \end{aligned} \quad (5.56)$$

and positive semidefinite under the load conditions of Proposition 5.1 ($\hat{R}_i^d, \hat{R}_i^q > 0$ per definition). Furthermore, set \mathbb{E}_i is characterized by

$$\hat{\psi}_i(\hat{\mathbf{x}}_i, \bar{\mathbf{x}}_i) \equiv 0 \stackrel{(5.56)}{\implies} \chi_i \equiv \bar{\chi}_i. \quad (5.57)$$

The shifted dynamics of (5.48) confined to \mathbb{E}_i are given by

$$\begin{aligned} 0 &= - (V_i^d - V_i^{\text{dq}*}), \\ 0 &= - (V_i^q - V_i^{\text{dq}*}), \\ C_i \dot{V}_i^d &= \omega_0 C_i (V_i^q - V_i^{\text{dq}*}) - (r_i^d - \bar{r}_i^d) - \left(I_{L,i}^d (\mathbf{V}_i^{\text{dq}}) - I_{L,i}^d (\mathbf{V}_i^{\text{dq}*}) \right), \\ C_i \dot{V}_i^q &= -\omega_0 C_i (V_i^d - V_i^{\text{dq}*}) - (r_i^q - \bar{r}_i^q) - \left(I_{L,i}^q (\mathbf{V}_i^{\text{dq}}) - I_{L,i}^q (\mathbf{V}_i^{\text{dq}*}) \right), \\ Q_{1,i}^d \dot{r}_i^d &= V d_i - V_i^{\text{dq}*}, \\ Q_{1,i}^q \dot{r}_i^q &= V_i^q - V_i^{\text{dq}*}, \end{aligned} \quad (5.58)$$

whose unique solution is $\mathbf{V}_i^{\text{dq}} \equiv \mathbf{V}_i^{\text{dq}*}$, $\mathbf{r}_i \equiv \bar{\mathbf{r}}_i$. \square

Remark 5.10. Note that the controller (5.46) is composed of a setpoint feedforward proportional to $\mathbf{V}_i^{\text{dq}*}$, a static state feedback proportional to \mathbf{I}_i^{dq} for damping assignment and decoupling, and a PI term acting on the control error $\mathbf{V}_i^{\text{dq}*} - \mathbf{V}_i^{\text{dq}}$ to ensure zero steady-state errors under parameter uncertainties and unknown, steady-state interaction inputs $\bar{\mathbf{d}}_i = -\bar{\mathbf{I}}_{N,i}^{\text{dq}}$. All these building blocks are available as industrial standard, off-the-shelf control functions.

Similar to the AC voltage controller, the statements of Proposition 5.3 still hold when a grid-forming DGU $i \in \mathcal{D}_{\text{form}}$ does not supply a local load, i.e., $\mathbf{I}_{L,i}^{\text{dq}} (\mathbf{V}_i^{\text{dq}}) = \mathbf{0}_2$ (see Remark 5.2). The following corollary summarizes this insight.

Corollary 5.2 (Voltage control of grid-forming DGUs without local loads)

Consider a grid-forming DGU $i \in \mathcal{D}_{\text{form}}$ that does not supply a local load, i.e., its open-loop model is given by (5.3) with $\mathbf{I}_{L,i}^{\text{dq}}(\mathbf{V}_i^{\text{dq}}) = \mathbf{0}_2$. Assign the control input and coordinate transformation as in Proposition 5.2. Then the closed-loop DGU system is given by (5.48) with $\mathbf{I}_{L,i}^{\text{dq}}(\mathbf{V}_i^{\text{dq}}) = \mathbf{0}_2$. Moreover, all statements from Proposition 5.3 regarding the EIP properties of the closed-loop and its dynamics confined to set \mathbb{E}_i hold.

Proof:

The proof is identical to that of Proposition 5.3 except with $\mathbf{I}_{L,i}^{\text{dq}}(\mathbf{V}_i^{\text{dq}}) = \mathbf{I}_{L,i}^{\text{dq}}(\bar{\mathbf{V}}_i^{\text{dq}}) = \mathbf{0}_2$ in the respective equations. \square

5.3.3 Voltage Controller of Nahata and Ferrari-Trecate [2019]

In this section, it is shown by example of the voltage controller proposed by Nahata and Ferrari-Trecate [2019] that decentralized controllers in the literature are readily compatible with the decentralized stability conditions of Theorem 5.1.

As with their DC version (see Section 4.3.3), Nahata and Ferrari-Trecate [2019] model DGUs with the permuted version of the co-state vector $\frac{\partial H_i}{\partial \mathbf{x}_i}(\mathbf{x}_i)$ (5.3b) as actual state vector, i.e., $\mathbf{x}_i = [V_i^{\text{d}}, V_i^{\text{q}}, I_i^{\text{d}}, I_i^{\text{q}}]^{\top}$. To allow for a transparent cross-referencing, this model perspective is used in the following proposition.⁴¹

Proposition 5.4 (Voltage controller of Nahata and Ferrari-Trecate [2019])

Consider a grid-forming DGU $i \in \mathcal{D}_{\text{form}}$ described in open loop by (5.3). Assume the local ZIP or exponential load (5.3f) fulfills the conditions of Proposition 5.1. Assign the control input $\mathbf{u}_i = \mathbf{V}_{S,i}^{\text{dq}}$ according to Nahata and Ferrari-Trecate [2019] as

$$\dot{\mathbf{r}}_i = - \left(\mathbf{V}_i^{\text{dq}} - \mathbf{V}_i^{\text{dq}*} \right), \quad (5.59\text{a})$$

$$\mathbf{u}_i = \mathbf{K}_{11,i} \mathbf{V}_i^{\text{dq}} + \mathbf{K}_{12,i} \mathbf{I}_i^{\text{dq}} + \mathbf{K}_{13,i} \mathbf{r}_i, \quad (5.59\text{b})$$

⁴¹ Note that in the following elaborations, reference is made to the PhD thesis by Nahata [2021] since major parts of the proofs and information is missing in the abbreviated conference version Nahata and Ferrari-Trecate [2019].

with dq voltage setpoint $V_i^{\text{dq}*} \in \mathbb{R}^2$ and control parameter matrices $\mathbf{K}_{11,i}$, $\mathbf{K}_{12,i}$, $\mathbf{K}_{13,i} \in \mathbb{R}^{2 \times 2}$. Then, the closed-loop DGU system can be written as

$$\frac{d}{dt} \underbrace{\begin{bmatrix} V_i^{\text{dq}} \\ I_i^{\text{dq}} \\ r_i \end{bmatrix}}_{\hat{x}_i} = \underbrace{\begin{bmatrix} F_{11,i} V_i^{\text{dq}} + F_{12,i} I_i^{\text{dq}} - \frac{1}{C_i} I_{L,i}^{\text{dq}} (V_i^{\text{dq}}) \\ F_{21,i} V_i^{\text{dq}} + F_{22,i} I_i^{\text{dq}} + F_{23,i} r_i \\ - (V_i^{\text{dq}} - V_i^{\text{dq}*}) \end{bmatrix}}_{\hat{f}_i(\hat{x}_i)} + \underbrace{\begin{bmatrix} \frac{1}{C_i} I_2 \\ \mathbf{0}_{2 \times 2} \\ \mathbf{0}_{2 \times 2} \end{bmatrix}}_{\hat{K}_i} d_i, \quad (5.60a)$$

$$z_i = V_i^{\text{dq}}, \quad (5.60b)$$

with matrices

$$F_{11,i} = \begin{bmatrix} 0 & \omega_0 \\ -\omega_0 & 0 \end{bmatrix}, F_{12,i} = \frac{1}{C_i} I_2, \quad (5.60c)$$

$$F_{21,i} = -\frac{1}{L_i} (I_2 - \mathbf{K}_{11,i}), F_{22,i} = \begin{bmatrix} -\frac{R_i}{L_i} & \omega_0 \\ -\omega_0 & -\frac{R_i}{L_i} \end{bmatrix} + \frac{1}{L_i} \mathbf{K}_{12,i}, F_{23,i} = \frac{1}{L_i} \mathbf{K}_{13,i}. \quad (5.60d)$$

If the control parameter matrices satisfy

$$\mathbf{K}_{11,i} = L_i \mathbf{X}_i^{-1} + I_2, \quad (5.61a)$$

$$\mathbf{K}_{12,i} = \begin{bmatrix} R_i & -\omega_0 L_i \\ \omega_0 L_i & R_i \end{bmatrix} - \mathbf{K}_{13,i} (\mathbf{Z}_i^{-1} + \mathbf{X}_i), \quad (5.61b)$$

$$-\mathbf{K}_{13,i} (\mathbf{Z}_i^{-1} \mathbf{X}_i^{-1}) - (\mathbf{Z}_i^{-1} \mathbf{X}_i^{-1})^\top \mathbf{K}_{13,i}^\top \prec 0, \quad (5.61c)$$

with $\mathbf{X}_i, \mathbf{Z}_i \in \mathbb{R}^{2 \times 2}$, $\mathbf{X}_i, \mathbf{Z}_i \succ 0$, then (5.60) is EIP w.r.t. the supply rate $(d_i - \bar{d}_i)^\top (z_i - \bar{z}_i)$ and the continuously differentiable, positive definite storage function

$$\hat{S}_i(\hat{x}_i, \bar{x}_i) = \frac{1}{2} \|\hat{x}_i - \bar{x}_i\|_{\hat{Q}_i}^2, \quad (5.62a)$$

$$\hat{Q}_i = \begin{bmatrix} C_i I_2 & \mathbf{0}_{2 \times 2} & \mathbf{0}_{2 \times 2} \\ \mathbf{0}_{2 \times 2} & \mathbf{X}_i + \mathbf{X}_i \mathbf{Z}_i \mathbf{X}_i & \mathbf{X}_i \mathbf{Z}_i \\ \mathbf{0}_{2 \times 2} & -\mathbf{Z}_i \mathbf{X}_i & \mathbf{Z}_i \end{bmatrix}, \quad (5.62b)$$

for any (feasible) equilibrium pair (\bar{d}_i, \bar{z}_i) and associated equilibrium state

$$\bar{x}_i = [\bar{I}_i^d, \bar{I}_i^q, V_i^{\text{dq}*}, V_i^{\text{dq}*}, \bar{r}_i^d, \bar{r}_i^q]^\top. \quad (5.63)$$

Furthermore, no solution other than $\hat{x}_i = \bar{x}_i$ as in (5.50) can stay in $\mathbb{E}_i = \{\hat{x}_i \in \hat{\mathcal{X}}_i \subseteq \mathbb{R}^6 \mid \hat{S}_i(\hat{x}_i, \bar{x}_i) = 0, d_i = \bar{d}_i\}$ for all time.

Proof:

Writing the closed-loop DGU model as in (5.60) directly follows by inserting the state-feedback controller (5.59) into the open-loop DGU model (5.3) and rewriting with states

as in Nahata and Ferrari-Trecate [2019] (cf. Nahata [2021, Equations (4.17)–(4.20)]).

In order to show that (5.60) is EIP w.r.t. the supply rate $(\mathbf{d}_i - \bar{\mathbf{d}}_i)^\top (\mathbf{z}_i - \bar{\mathbf{z}}_i)$ and the continuously differentiable, positive definite storage function (5.62), the same reasoning as in the proof of Proposition 4.4 is used. In particular, the closed-loop DGU model (5.60) can equivalently be written as

$$\dot{\hat{\mathbf{x}}}_i = \hat{\mathbf{f}}_i(\hat{\mathbf{x}}_i) - \hat{\mathbf{f}}_i(\bar{\mathbf{x}}_i) + \hat{\mathbf{K}}_i(\mathbf{d}_i - \bar{\mathbf{d}}_i) \quad (5.64a)$$

$$\begin{aligned} & \stackrel{(5.60)}{=} \left[\begin{array}{l} \mathbf{F}_{11,i} (\mathbf{V}_i^{\text{dq}} - \mathbf{V}_i^{\text{dq}*}) + \mathbf{F}_{12,i} (\mathbf{I}_i^{\text{dq}} - \bar{\mathbf{I}}_i^{\text{dq}}) - \frac{1}{C_i} (\mathbf{I}_{L,i}^{\text{dq}} (\mathbf{V}_i^{\text{dq}}) - \mathbf{I}_{L,i}^{\text{dq}} (\mathbf{V}_i^{\text{dq}*})) \\ \mathbf{F}_{21,i} (\mathbf{V}_i^{\text{dq}} - \mathbf{V}_i^{\text{dq}*}) + \mathbf{F}_{22,i} (\mathbf{I}_i^{\text{dq}} - \bar{\mathbf{I}}_i^{\text{dq}}) + \mathbf{F}_{23,i} (\mathbf{r}_i - \bar{\mathbf{r}}_i) \\ - (\mathbf{V}_i^{\text{dq}} - \mathbf{V}_i^{\text{dq}*}) \end{array} \right] \\ & + \left[\frac{1}{C_i} \mathbf{I}_2 \quad \mathbf{0}_{2 \times 2} \quad \mathbf{0}_{2 \times 2} \right]^\top (\mathbf{d}_i - \bar{\mathbf{d}}_i) \end{aligned} \quad (5.64b)$$

$$\mathbf{z}_i - \bar{\mathbf{z}}_i = \mathbf{V}_i^{\text{dq}} - \mathbf{V}_i^{\text{dq}*} \quad (5.64c)$$

For the time derivative of $\hat{S}_i(\hat{\mathbf{x}}_i, \bar{\mathbf{x}}_i)$ in (5.62), it holds that

$$\dot{\hat{S}}_i(\hat{\mathbf{x}}_i, \bar{\mathbf{x}}_i) = \underbrace{(\hat{\mathbf{x}}_i - \bar{\mathbf{x}}_i)^\top \hat{\mathbf{Q}}_i (\hat{\mathbf{f}}_i(\hat{\mathbf{x}}_i) - \hat{\mathbf{f}}_i(\bar{\mathbf{x}}_i))}_{-\hat{\psi}_i(\hat{\mathbf{x}}_i, \bar{\mathbf{x}}_i)} + \underbrace{(\hat{\mathbf{x}}_i - \bar{\mathbf{x}}_i)^\top \hat{\mathbf{Q}}_i \hat{\mathbf{K}}_i}_{(\mathbf{z}_i - \bar{\mathbf{z}}_i)} (\mathbf{d}_i - \bar{\mathbf{d}}_i). \quad (5.65)$$

With (5.60), (5.62), and (5.63), the dissipation rate can be written as (cf. Nahata [2021, Equations (4.17), (4.27)])

$$\begin{aligned} \hat{\psi}_i(\hat{\mathbf{x}}_i, \bar{\mathbf{x}}_i) &= -(\hat{\mathbf{x}}_i - \bar{\mathbf{x}}_i)^\top \left(\mathbf{F}_i^\top \hat{\mathbf{Q}}_i + \hat{\mathbf{Q}}_i \mathbf{F}_i \right) (\hat{\mathbf{x}}_i - \bar{\mathbf{x}}_i) \\ &+ \left(\mathbf{V}_i^{\text{dq}} - \bar{\mathbf{V}}_i^{\text{dq}} \right)^\top \left(\mathbf{I}_{L,i}^{\text{dq}} (\mathbf{V}_i^{\text{dq}}) - \mathbf{I}_{L,i}^{\text{dq}} (\bar{\mathbf{V}}_i^{\text{dq}}) \right) \end{aligned} \quad (5.66a)$$

with

$$\mathbf{F}_i = \begin{bmatrix} \mathbf{F}_{11,i} & \mathbf{F}_{12,i} & \mathbf{0}_{2 \times 2} \\ \mathbf{F}_{21,i} & \mathbf{F}_{22,i} & \mathbf{F}_{23,i} \\ -\mathbf{I}_2 & \mathbf{0}_{2 \times 2} & \mathbf{0}_{2 \times 2} \end{bmatrix}. \quad (5.66b)$$

If the control parameter matrices contained in \mathbf{F}_i satisfy (5.61) (see the proof of Theorem 4.3.1 in Nahata [2021]) and the load conditions of Proposition 5.1 hold, it follows that $\hat{\psi}_i(\hat{\mathbf{x}}_i, \bar{\mathbf{x}}_i) \geq 0$. Thus, according to Definition 3.2, the closed-loop DGU model (5.60) is EIP w.r.t. the supply rate $(\mathbf{d}_i - \bar{\mathbf{d}}_i)^\top (\mathbf{z}_i - \bar{\mathbf{z}}_i)$ and the continuously differentiable, positive definite storage function (5.62).

Lastly, it is proved that no solution other than $\bar{\mathbf{x}}_i$ as in (5.50) can stay in $\mathbb{E}_i = \{\hat{\mathbf{x}}_i \in \hat{\mathcal{X}}_i \subseteq \mathbb{R}^6 \mid \dot{\hat{S}}_i(\hat{\mathbf{x}}_i, \bar{\mathbf{x}}_i) = 0, \mathbf{d}_i = \bar{\mathbf{d}}_i\}$ for all time. From (5.65), it follows that set \mathbb{E}_i is characterized by $\hat{\psi}_i(\hat{\mathbf{x}}_i, \bar{\mathbf{x}}_i) \equiv 0$. Following Nahata [2021, Equations (4.58)–(4.68)], it can be shown that $\hat{\psi}_i(\hat{\mathbf{x}}_i, \bar{\mathbf{x}}_i) \equiv 0$ implies

$$\mathbf{V}_i^{\text{dq}} \equiv \mathbf{V}_i^{\text{dq}*}. \quad (5.67)$$

Under (5.67), the evolution of a solution of the shifted dynamics (5.64b) confined to \mathbb{E}_i is given by

$$\mathbf{0}_2 = \mathbf{F}_{12,i} \left(\mathbf{I}_i^{\text{dq}} - \bar{\mathbf{I}}_i^{\text{dq}} \right), \quad (5.68a)$$

$$\dot{\mathbf{I}}_i^{\text{dq}} = \mathbf{F}_{22,i} \left(\mathbf{I}_i^{\text{dq}} - \bar{\mathbf{I}}_i^{\text{dq}} \right) + \mathbf{F}_{23,i} (\mathbf{r}_i - \bar{\mathbf{r}}_i), \quad (5.68b)$$

$$\dot{\mathbf{r}}_i = \mathbf{0}_2, \quad (5.68c)$$

whose unique solution is $\mathbf{I}_i^{\text{dq}} \equiv \bar{\mathbf{I}}_i^{\text{dq}}$, $\mathbf{r}_i \equiv \bar{\mathbf{r}}_i$. Thus, no solution other than $\bar{\mathbf{x}}_i$ as in (5.63) can stay in \mathbb{E}_i for all time. \square

Remark 5.11. Note that compared to the voltage controller (5.46) in Proposition 5.3, the voltage control law (5.59) by Nahata and Ferrari-Trecate [2019] is more restrictive on the choice of control parameters that are required to fulfill condition (AC 1). While the controller (5.46) only requires positive control parameters $\hat{R}_i^{\text{d}}, \hat{R}_i^{\text{q}}, Q_{1,i}^{\text{d}}, Q_{1,i}^{\text{q}} > 0$, the control parameters of (5.59) must fulfill the three equations given by (5.61), one of which is a linear matrix inequality. On the other hand, the voltage controller (5.59) of Nahata and Ferrari-Trecate [2019] comprises individual gains for the voltage \mathbf{V}_i^{dq} , the current \mathbf{I}_i^{dq} , and the integral voltage error \mathbf{r}_i together with cross-coupling terms, while the voltage controller (5.46) only has four control parameters for the six terms containing \mathbf{V}_i^{dq} , \mathbf{I}_i^{dq} , and \mathbf{r}_i .

5.4 Simulation

This section demonstrates the validity of the presented unifying stabilization framework via two simulative case studies. In particular, the stability properties of ZIP and exponential loads under the conditions of Proposition 5.1 as well as the stabilizing properties, plug-and-play capabilities, and disturbance rejection behavior of the voltage and current controllers from Propositions 5.2 and 5.3 are shown. The simulated scenarios and most of the general setup are identical to the DC case presented in Chapter 4, Section 4.4. However, as the DC case required some adaptations, all necessary information for the following simulation studies, even if redundant, is given in this section to ensure a consistent and clear presentation.

The first scenario in Section 5.4.2 focuses on plug-and-play operations of DGUs and flexible, time-varying system configurations. The second scenario in Section 5.4.3 investigates whether different setpoints for the controlled dq node voltages and VSI output currents can be asymptotically stabilized and disturbances arising from load variations be rejected. In order to highlight the unifying nature of the presented, EIP-based stabilization framework, both scenarios are complemented with a DGU controlled by the voltage controller of Nahata and Ferrari-Trecate [2019] (see Proposition 5.4). Additionally, both scenarios are simulated with an uncertainty on the DGU filter parameters

to evaluate the disturbance rejection capabilities of the controllers against parameter uncertainties.

5.4.1 General Simulation Setup

For the simulations, an AC power system based on Feeder 1 of the CIGRE medium-voltage AC benchmark network from Strunz et al. [2014, Figure 6.5] and Farrokhhabadi et al. [2018, pp. 42ff] is implemented in MATLAB/SIMULINK using SIMSCAPE components. The CIGRE network operates at $V_0 = 20$ kV, $f_0 = 50$ Hz, and comprises 11 nodes. In its original form, the CIGRE network reflects a classical AC distribution system structure in which the medium-voltage feeder only comprises loads and is fed by a 110 kV high-voltage transmission network via a transformer at node 1.

Thus, in order to assess the control schemes proposed in this chapter and operational scenarios arising with the pervasive integration of RESs, the network is modified in two ways as illustrated in Figure 5.1:

- The connection to the 110 kV transmission network at node 1 is resolved. Instead, DGUs are added at nodes $i \in \mathcal{D} = \{1, 2, 3, 4, 5, 6\}$ with the proposed current controller (5.39) at DGUs $i \in \mathcal{D}_{\text{feed}} = \{3, 5, 6\}$, the proposed voltage controller (5.46) at DGUs $i \in \mathcal{D}_{\text{PBC}} = \{2, 4\}$, and the voltage controller (5.59) from Nahata and Ferrari-Trecate [2019] at DGU $i \in \mathcal{D}_{\text{N19}} = \{1\}$.
- Instead of only exponential loads as in Farrokhhabadi et al. [2018, pp. 42ff], ZIP loads are connected at nodes $i \in \mathcal{L}_{\text{ZIP}} = \{1, 2, 4, 7, 8\}$, while exponential loads remain at nodes $i \in \mathcal{L}_{\text{EXP}} = \{5, 6, 9, 10, 11\}$.

The network, DGU, and electrical line parameters used in the simulations are summarized in Table 5.1. They are in line with typical values (see, e.g., Strunz et al. [2014], Rivero et al. [2015], and Watson et al. [2021]). In both simulations, the RLC filters of all DGUs are parameterized identically with nominal values as in Table 5.1. These nominal values are used in all DGU controllers (5.39), (5.46), and (5.59), while the actual implemented filter parameters have a +10% offset to evaluate the disturbance rejection capabilities of the controllers against parameter uncertainties. The resulting effective cut-off frequency of the RLC filters is thus $f_{\text{cut}} = \frac{1}{\sqrt{L_i C_i}} = 682$ Hz.

The line parameters in Table 5.1 follow from Strunz et al. [2014, Table 6.12] by using the relations in Strunz et al. [2014, Equations (18),(19)] and solving for the positive-sequence components. Note that as only balanced AC power systems are considered in this thesis (see Assumption 5.1), the lines have only positive-sequence and no zero-sequence components.

The parameters of the controllers are summarized in Table 5.1. The structures of the gain matrices for the controller (5.59) of Nahata and Ferrari-Trecate [2019] are chosen according to the elaborations around Nahata [2021, p. 58] where $\mathbf{X}_i = \mathbf{Z}_i = \mathbf{I}_2$. However, to allow for tuning and a better control performance, two parameters $a, b > 0$

are introduced such that $\mathbf{X}_i^{-1} = a\mathbf{I}_2$, $\mathbf{Z}_i = \mathbf{I}_2$, and $\mathbf{K}_{13,i} = b\mathbf{I}_2$. Note that for any $a, b > 0$ the obtained gain matrices satisfy (5.61).

The DGU references used in the controllers are set as in Table 5.2 to yield reasonable network situations.

The load parameters are given in Tables 5.3 and 5.4. The exponential load parameters are taken from Farrokhhabadi et al. [2018, pp. 42,45]. The ZIP load parameters follow from the exponential load parameters in Farrokhhabadi et al. [2018, pp. 42,45] via the equivalence transformations in Farrokhhabadi et al. [2018, Equations (38),(41)] with $Z^p = Z^q = \frac{5}{14}$, $I^p = I^q = \frac{1}{14}$, $P^p = P^q = \frac{1}{14}$. The parameters of each ZIP load satisfy the condition (5.18) in Proposition 5.1 for all voltage amplitudes $V_i \geq 0$. This means that condition (5.37) from Remark 5.5 is fulfilled. As discussed in Remark 5.5, the exponential load condition (5.19) does not allow for a conservative worst-case approximation. Instead, the validity of (5.19) for the parameters of each exponential load is checked for voltage amplitudes within a range of $V_i \in [0.7 V_0; 2 V_0]$, which securely covers all voltage amplitudes that might reasonably occur during operation.

Table 5.1: Simulation parameters for the AC power system simulation

Network	$V_0 = 20 \text{ kV}, f_0 = 50 \text{ Hz}$
DGU filters (5.3)	$R_i = 0.1 \Omega, L_i = 1.8 \text{ mH}, C_i = 25 \mu\text{F}$
Electrical lines (5.11)	$R_l = 0.343 \Omega/\text{km}, L_l = 0.875 \text{ mH}/\text{km},$ $C_l = 151.2 \text{ nF}/\text{km}$ length $\in [0.24; 4.42] \text{ km}$ (see Figure 5.1)
Current controller (5.39), $i \in \mathcal{D}_{\text{feed}}$	$k_{\text{P},i}^{\text{d}} = k_{\text{P},i}^{\text{q}} = 0.1, Q_{\text{I},i}^{\text{d}} = Q_{\text{I},i}^{\text{q}} = \frac{1}{15}$
Voltage controller (5.46), $i \in \mathcal{D}_{\text{PBC}}$	$\hat{R}_i^{\text{d}} = \hat{R}_i^{\text{q}} = 0.4, Q_{\text{I},i}^{\text{d}} = Q_{\text{I},i}^{\text{q}} = \frac{1}{200}$
Voltage controller (5.59), $i \in \mathcal{D}_{\text{N19}}$	$\mathbf{K}_{11,i} = (aL_i + 1)\mathbf{I}_{2 \times 2},$ $\mathbf{K}_{12,i} = \begin{bmatrix} R_i & -\omega_0 L_i \\ \omega_0 L_i & R_i \end{bmatrix} - \mathbf{K}_{13,i} \left(\frac{1}{a} + 1\right),$ $\mathbf{K}_{13,i} = b\mathbf{I}_{2 \times 2}, a = b = 1000$

Table 5.2: Voltage and current setpoints of the DGUs. For Scenario A in Section 5.4.2, only the base values are used. For Scenario B in Section 5.4.3 featuring load and setpoint changes, the values vary at the indicated times.

DGU	i	1 (blue)	2 (red)	3 (yellow)	4 (purple)	5 (turquoise)	6 (black)
base	V_i^{d*} (kV)	21	20.998	–	20.996	–	–
$t = 15$ s	V_i^{d*} (kV)	21.05	21.048	–	21.046	–	–
base	V_i^{q*} (V)	1000	998	–	996	–	–
$t = 20$ s	V_i^{q*} (V)	950	948	–	946	–	–
base	I_i^{d*} (A)	–	–	-3	–	-5	-6
$t = 25$ s	I_i^{d*} (A)	–	–	-2	–	-4	-5
base	I_i^{q*} (A)	–	–	160	–	161	162
$t = 30$ s	I_i^{q*} (A)	–	–	161	–	162	163

Table 5.3: ZIP load parameters. For Scenario A in Section 5.4.2, only the base values are used. For Scenario B in Section 5.4.3 featuring load and setpoint changes, the values vary at the indicated times.

	i		1	2	4	7	8
base	$Y_{P,i} = Y_{Q,i}$	(μ S)	75	97.5	51.96	51.96	58.48
$t = 1$ s	$Y_{P,i} = Y_{Q,i}$	(μ S)	112.5	146.25	77.95	77.95	87.72
base	$I_{P,i} = I_{Q,i}$	(A)	0.3	0.39	0.208	0.208	0.234
$t = 1$ s	$I_{P,i} = I_{Q,i}$	(A)	0.45	0.585	0.312	0.312	0.351
base	$P_{P,i} = P_{Q,i}$	(kW, kVar)	6	7.8	4.157	4.157	4.679
$t = 1$ s	$P_{P,i} = P_{Q,i}$	(kW, kVar)	9	11.7	6.235	6.235	7.018

Table 5.4: Exponential load parameters. For Scenario A in Section 5.4.2, only the base values are used. For Scenario B in Section 5.4.3 featuring load and setpoint changes, the base values are ramped up from $t = 5$ s to the final value at $t = 10$ s.

	i		5	6	9	10	11
base	$P_{0,i} = Q_{0,i}$	(kW, kVar)	90.5	46.8	50.9	72.8	80
$t = 10$ s	$P_{0,i} = Q_{0,i}$	(kW, kVar)	135.75	70.2	76.35	109.2	120
base	$n_{P,i} = n_{Q,i}$		1.5	1.5	1.5	1.5	1.5
$t = 10$ s	$n_{P,i} = n_{Q,i}$		1.5	1.5	1.5	1.5	1.5

5.4.2 Scenario A: Plug-and-Play

This scenario features disconnecting and connecting DGUs and power lines in order to validate the decentralized nature of the stability conditions (AC 1) and (AC 2). At the indicated times, the following events occur (see Figure 5.1 for the network):

- $t = 5$ s: DGU 4 disconnects.
- $t = 10$ s: Power lines 17 and 19 disconnect.
- $t = 15$ s: DGU 4 reconnects.
- $t = 20$ s: DGU 5 disconnects.
- $t = 25$ s: Power lines 17 and 19 reconnect.
- $t = 30$ s: DGU 5 reconnects.

During the complete scenario, the DGU setpoints as well as the load parameters remain at the base values provided in Tables 5.2, 5.3, and 5.4.

The results of the simulation are given in Figures 5.4–5.6. The colored lines represent the dq node voltages V_i^{dq} and filter currents I_i^{dq} of the voltage- and current-controlled DGUs $i \in \mathcal{D} = \{1, 2, 3, 4, 5, 6\}$ with colors as per Table 5.2. Additionally, all uncontrolled dq node voltages as well as all uncontrolled dq filter, load, and line currents are given in grey. The deviations of controlled node voltages V_i^{dq} , $i \in \{1, 2, 4\}$, and controlled filter currents I_i^{dq} , $i \in \{3, 5, 6\}$, from their setpoints in Table 5.2 are given with respect to the nominal voltage $V_0 = 20$ kV and the average amplitude of the current setpoints $I_0 = 161.07$ A, respectively.

The maximum voltage errors at the voltage-controlled DGU nodes $i \in \mathcal{D} = \{1, 2, 4\}$ remain within a 0.22 % (44 V) band for the d component and a 0.33 % (66 V) band for the q component. At the latest 70 ms after an event, the controlled dq node voltages settle to within a 0.005 % (1 V) band around their desired setpoints. The uncontrolled node voltages show similar deviation magnitudes and converge similarly fast to their corresponding steady-state values. Overall, the voltages thus stay well within the 4 % voltage band around the nominal voltage which is prescribed in the AC power system standard EN 50160 for fast voltage transients in medium-voltage networks. Note that between $t = 5$ s – 15 s, the voltage at node 4 (purple line) is not controlled since DGU 4 is disconnected. Consequently, during that period, the voltage error is set to zero.

The maximum current error for the d component at the current-controlled DGU nodes $i \in \mathcal{D} = \{3, 5, 6\}$ remains within a 4.25 % (6.85 A) band. The error for the q component remains within a 6.8 % (10.95 A) band except for the overshoot at $t = 30$ s of approximately 12.7 % (20.5 A) which lasts for around 6 ms. At the latest 0.6 s after an event, the controlled dq filter currents settle to within a 0.06 % (0.1 A) band around their desired setpoints. The uncontrolled filter, load, and line currents converge similarly fast to their corresponding steady-state values (see Figures 5.5 and 5.6). Note that between

$t = 5 \text{ s} - 15 \text{ s}$ and $t = 20 \text{ s} - 30 \text{ s}$, DGU 4 and DGU 5, respectively, are disconnected and their filter currents as well as the current error for DGU 5 are set to zero.

The reason for the peak in I_i^{d} at $t = 30 \text{ s}$ are compensation currents that flow for a very short time into the filter capacitance when DGU 4 is reconnected. For the simulations, the reconnection of DGUs is tuned with a simple heuristic in which the voltage over the filter capacitance is firstly controlled close to the present node voltage before the respective DGU is connected. For a practical implementation, more elaborated schemes can be used, which are, however, outside the scope of this thesis.

Another interesting observation related to the filter capacitances can be made by considering the $I_i^{\text{q}}, I_{L,i}^{\text{q}}$ plot in Figure 5.5. In particular, note that the upper current lines between $150 \text{ A} - 250 \text{ A}$ all represent filter currents I_i^{q} of DGUs $i \in \mathcal{D} = \{1, 2, 3, 4, 5, 6\}$. The reason for their different order of magnitude compared to the load currents $I_{L,i}^{\text{q}}$ and the line currents I_l^{q} in Figure 5.6 is the high reactive power demand of the filter capacitances. Figure 5.7 illustrates this fact by plotting the injected net-current $I_{N,i}^{\text{dq}}$ after the filter capacitance instead of I_i^{dq} together with the load currents $I_{L,i}^{\text{dq}}$.

In summary, the results confirm the statements of Theorem 5.1 and demonstrate that all node voltages and currents and thus all states of the system (see (5.3b), (5.4b), (5.11b)) can be asymptotically stabilized throughout the complete scenario despite flexible system configurations with plug-and-play operations and topology changes. Furthermore, the integral parts of the proposed controllers ensure zero steady-state errors in the presence of parameter uncertainties which naturally occur in practice.

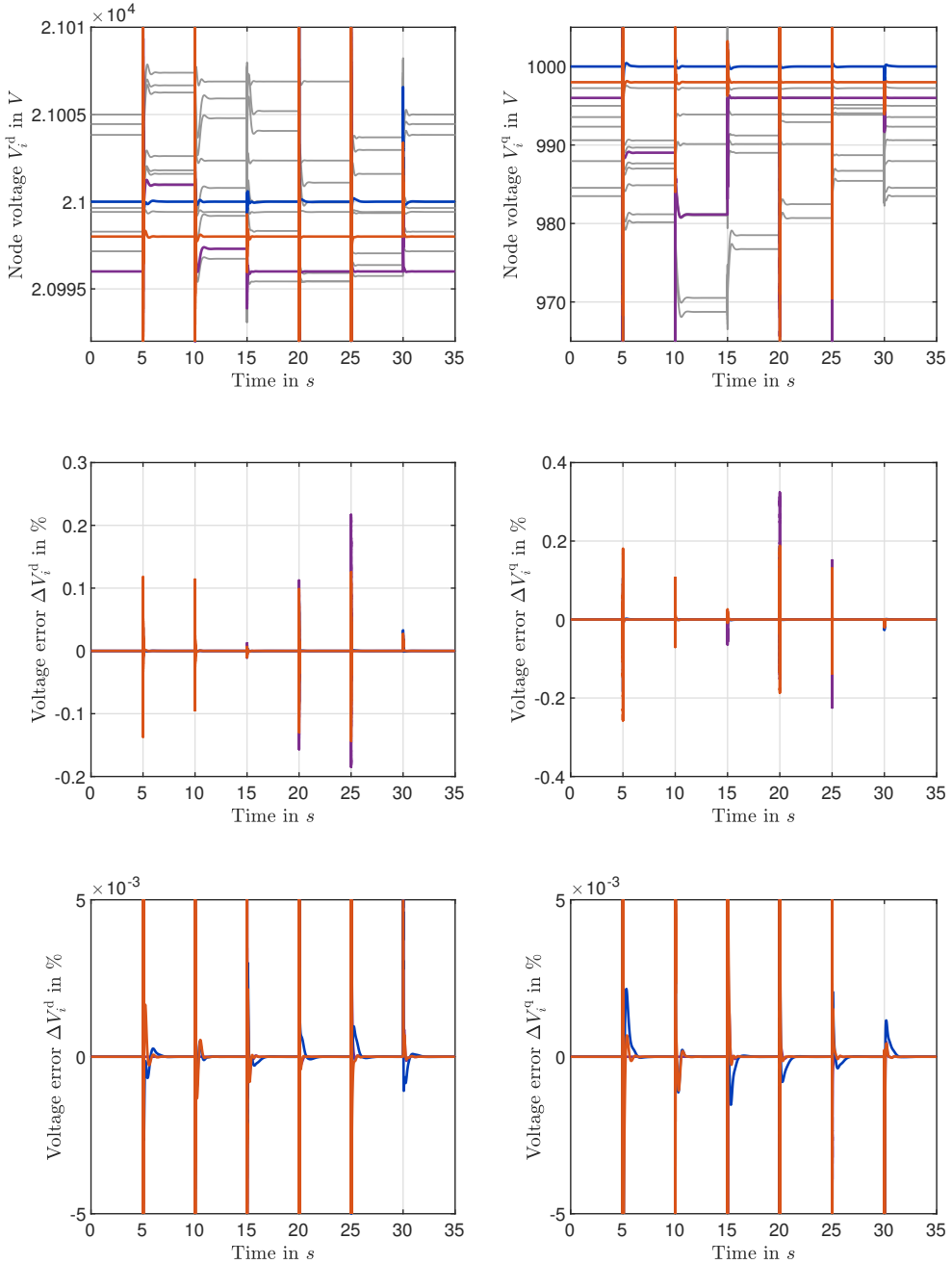


Figure 5.4: Scenario A: node voltages V_i^{dq} with uncontrolled nodes in grey. The colors of the voltage-controlled DGU nodes $i \in \{1, 2, 4\}$ and their setpoints are given in Table 5.2. The voltage deviations ΔV_i^{dq} from the setpoints are given in % w.r.t. the nominal voltage $V_0 = 20 \text{ kV}$ and provided in full view and a zoomed perspective.

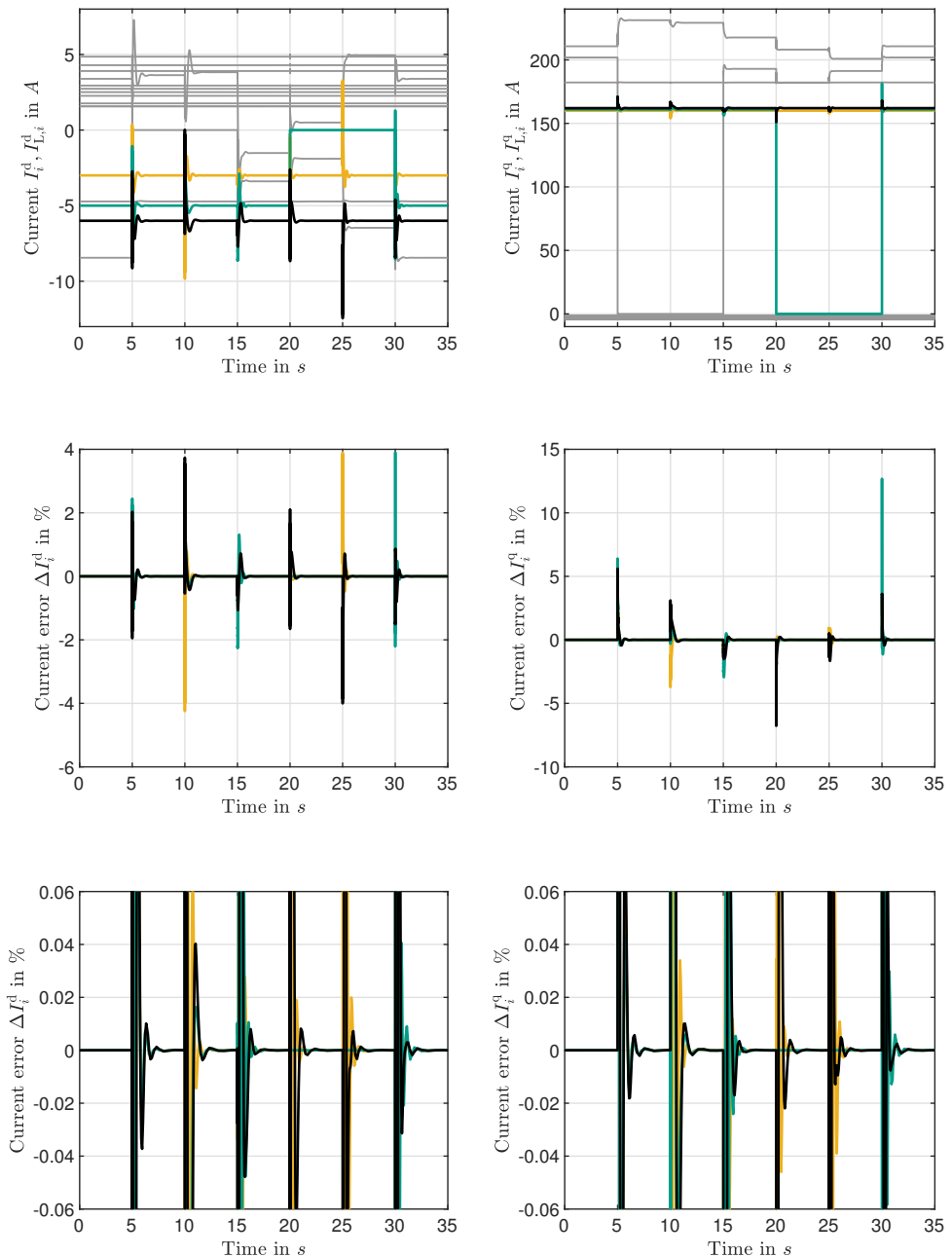


Figure 5.5: Scenario A: filter currents I_i^{dq} and load currents $I_{L,i}^{\text{dq}}$ with uncontrolled currents in grey. The colors of the current-controlled DGU nodes $i \in \{3, 5, 6\}$ and their setpoints are given in Table 5.2. The current deviations ΔI_i^{dq} from the setpoints are given in % w.r.t. the average amplitude of the current setpoints $I_0 = 161.07$ A and provided in full view and a zoomed perspective.

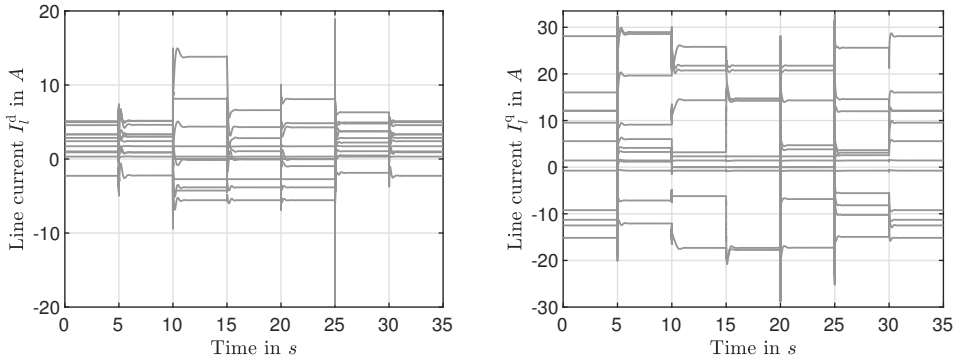


Figure 5.6: Scenario A: line currents $I_l^{\text{dq}}, l \in \mathcal{P} = \{12, \dots, 23\}$.

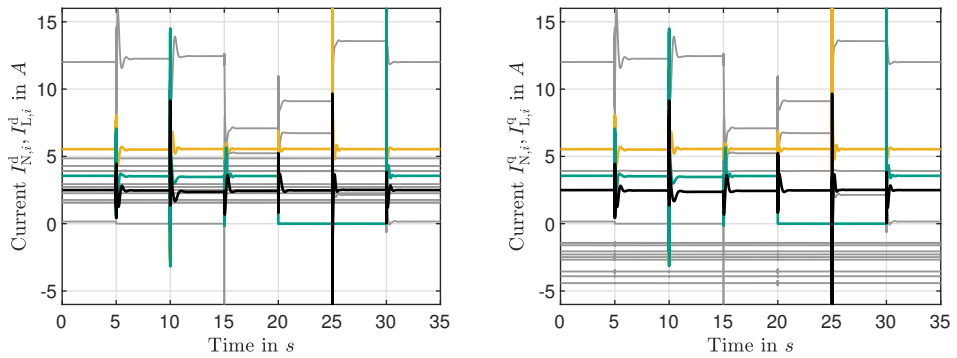


Figure 5.7: Scenario A: injected net-currents $I_{N,i}^{\text{dq}}$ of the DGUs and load currents $I_{L,i}^{\text{dq}}$ with uncontrolled currents in grey. The colors of the current-controlled DGU nodes $i \in \{3, 5, 6\}$ are given in Table 5.2.

5.4.3 Scenario B: Setpoint and Load Changes

This scenario features changes in the dq voltage and current setpoints of the DGU controllers to investigate whether the asymptotic stability guarantee given by Theorem 5.1 is indeed independent of the specific equilibrium values. In addition to parameter uncertainties, load variations in form of step changes and ramps are simulated to further evaluate the disturbance rejection capabilities of the proposed controllers. At the indicated times, the following events occur (see Figure 5.1 for the network):

- $t = 1$ s: All ZIP loads $i \in \mathcal{L}_{\text{ZIP}} = \{1, 2, 4, 7, 8\}$ increase their demand by 50 %.
- $t = 5$ s – 10 s: All exponential loads $i \in \mathcal{L}_{\text{EXP}} = \{5, 6, 9, 10, 11\}$ ramp up their demand by 50 %.
- $t = 15$ s: All voltage setpoints $V_i^{\text{d}*}, i \in \mathcal{D} = \{1, 2, 4\}$ are increased by 50 V.
- $t = 20$ s: All voltage setpoints $V_i^{\text{q}*}, i \in \mathcal{D} = \{1, 2, 4\}$ are decreased by 50 V.
- $t = 25$ s: All current setpoints $I_i^{\text{d}*}, i \in \mathcal{D} = \{3, 5, 6\}$ are increased by 1 A.
- $t = 30$ s: All current setpoints $I_i^{\text{q}*}, i \in \mathcal{D} = \{3, 5, 6\}$ are increased by 1 A.

The DGU setpoints as well as the load parameters before and after the changes are summarized in Tables 5.2, 5.3, and 5.4.

The results of the simulation are given in Figures 5.8–5.10. The colored lines represent the dq node voltages V_i^{dq} and filter currents I_i^{dq} of the voltage- and current-controlled DGUs $i \in \mathcal{D} = \{1, 2, 3, 4, 5, 6\}$ with colors as per Table 5.2. Additionally, all uncontrolled dq node voltages as well as all uncontrolled dq filter, load, and line currents are given in grey. The deviations of controlled node voltages $V_i^{\text{dq}}, i \in \{1, 2, 4\}$, and controlled filter currents $I_i^{\text{dq}}, i \in \{3, 5, 6\}$, from their setpoints in Table 5.2 are given with respect to the nominal voltage $V_0 = 20$ kV and the average amplitude of the current setpoints $I_0 = 161.56$ A, respectively.

The maximum voltage errors at the voltage-controlled DGU nodes $i \in \mathcal{D} = \{1, 2, 4\}$ remain within a 0.25 % (50 V) band around their setpoints for both the d and q component. At the latest 0.8 s after an event, the controlled dq node voltages settle to within a 0.005 % (1 V) band around their desired setpoints. The uncontrolled node voltages show similar deviation magnitudes and converge similarly fast to their corresponding steady-state values. During the load ramps between $t = 5$ s – 10 s, the maximum voltage errors remain below 0.0001 % (0.02 V). As in Scenario A, the voltages throughout Scenario B stay well within the prescribed 4 % voltage band around the nominal voltage.

The maximum current errors at the current-controlled DGU nodes $i \in \mathcal{D} = \{3, 5, 6\}$ remain within a 17.4 % (28.1 A) band for both the d and q component. At the latest 1.2 s after an event, the controlled dq filter currents settle to within a 0.06 % (0.1 A) band around their desired setpoints. The uncontrolled filter, load, and line currents converge similarly fast to their corresponding steady-state values (see Figures 5.9 and

5.10). During the load ramps between $t = 5 \text{ s} - 10 \text{ s}$, the maximum current errors remain below 0.037% (0.06 A).

In summary, the results confirm the statements of Theorem 5.1 and demonstrate that the asymptotically stabilizing properties of the controllers (5.39), (5.46), and (5.59) are indeed independent of the specific dq voltage and current setpoints. Furthermore, although not a specific focus of the controller designs, constant disturbances arising from unknown load demands and parameter uncertainties can be fully rejected by the integral parts of the controllers. Additionally, the integrators are sufficiently fast to reject the time-varying disturbances caused by the load ramps to negligible values.

This concludes the presentation and validation of the unifying stabilization framework for AC power systems. In the next section, the presented model, decentralized stability conditions, and controller designs are discussed with respect to the main research questions (Q1.1) and (Q1.2). Additionally, the results from this chapter are compared to those of the passivity-based works that have been published in parallel to this thesis (see Section 2.4.1).

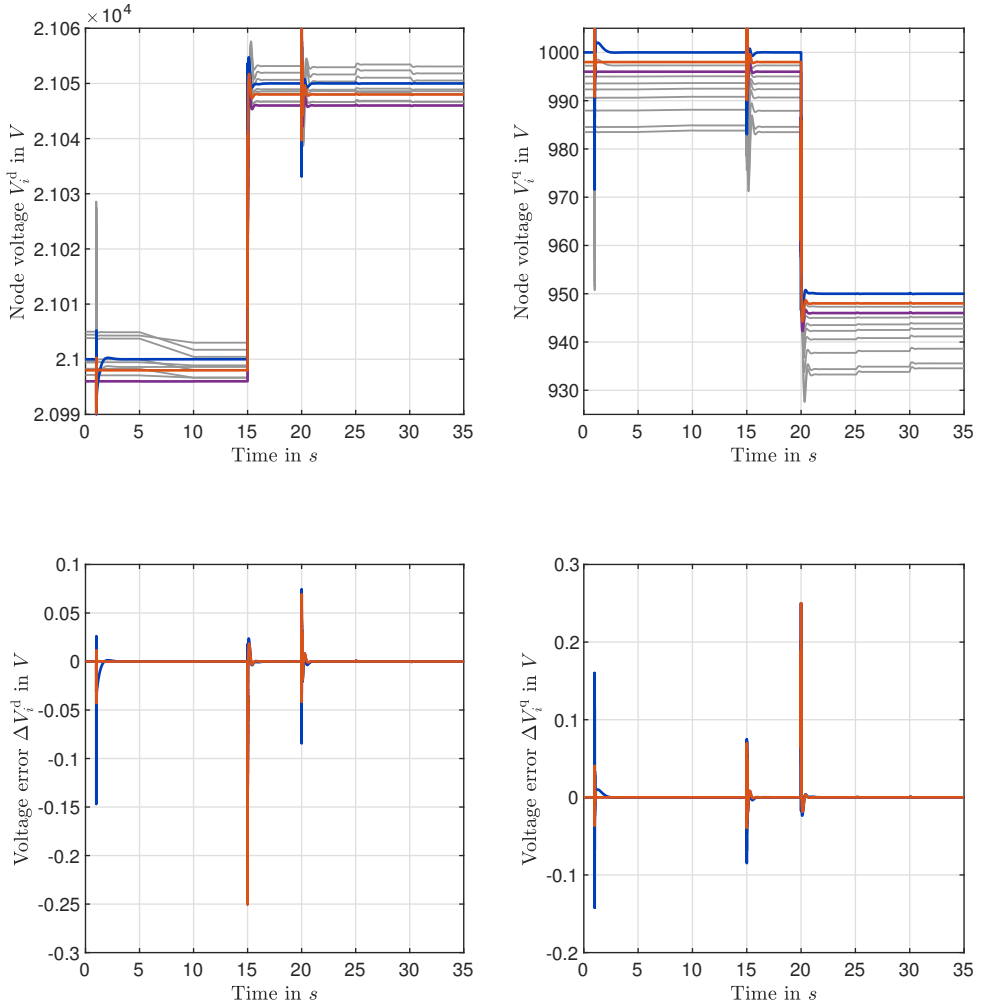


Figure 5.8: Scenario B: node voltages V_i^{dq} with uncontrolled nodes in grey. The colors of the voltage-controlled DGU nodes $i \in \{1, 2, 4\}$ and their setpoints are given in Table 5.2. The voltage deviations ΔV_i^{dq} from the setpoints are given in % w.r.t. the nominal voltage $V_0 = 20$ kV.

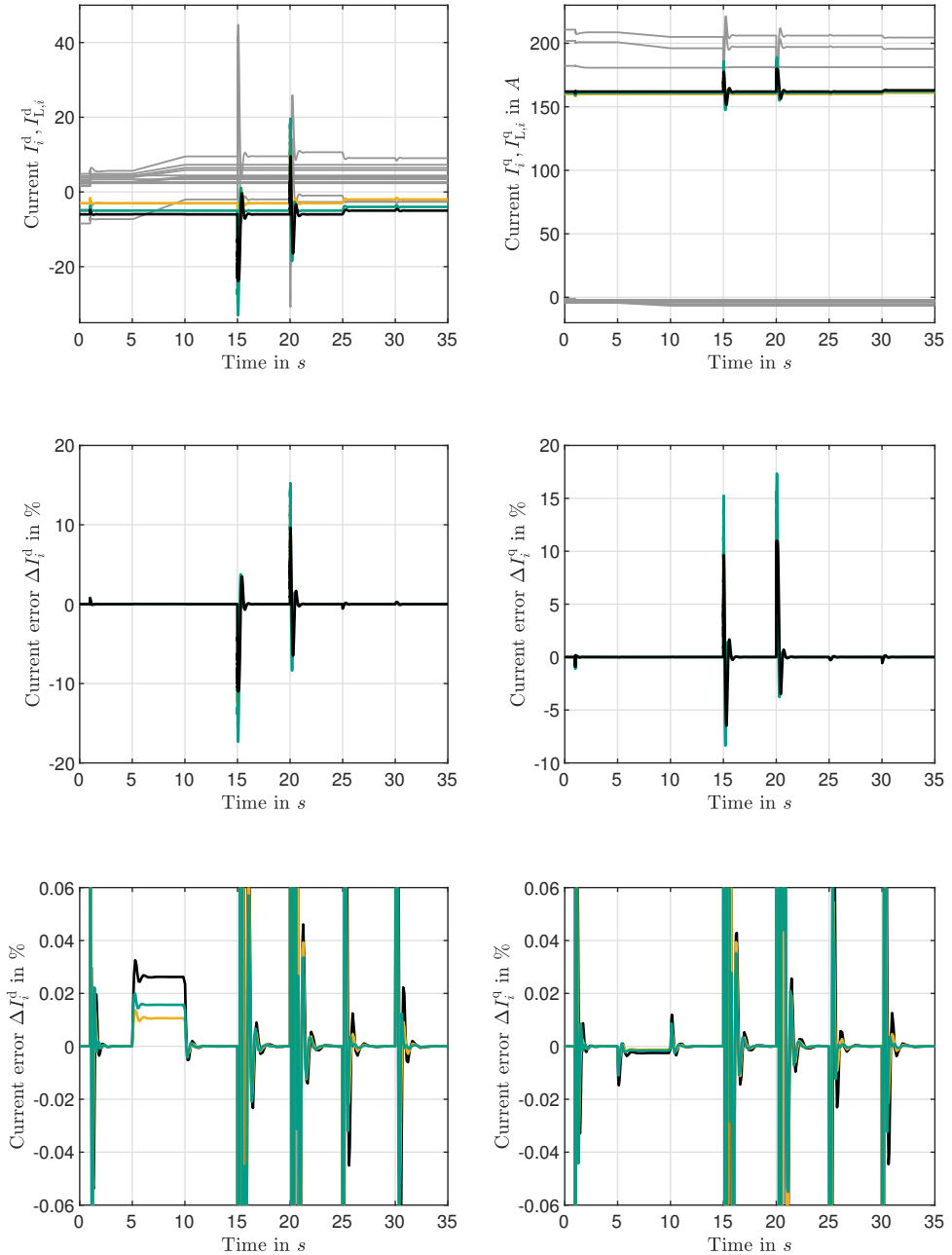


Figure 5.9: Scenario B: filter currents I_i^{dq} and load currents $I_{L,i}^{dq}$ with uncontrolled currents in grey. The colors of the current-controlled DGU nodes $i \in \{3, 5, 6\}$ and their setpoints are given in Table 5.2. The current deviations ΔI_i^{dq} from the setpoints are given in % w.r.t. the average amplitude of the current setpoints $I_0 = 161.56$ A and provided in full view and a zoomed perspective.

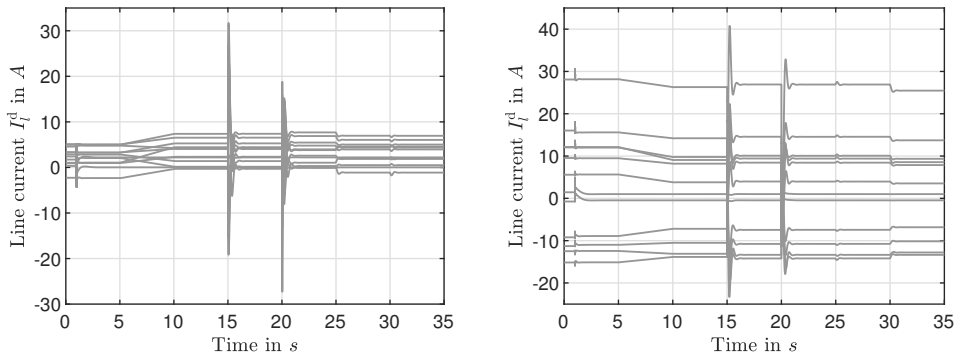


Figure 5.10: Scenario B: line currents I_l^{dq} , $l \in \mathcal{P} = \{12, \dots, 23\}$.

5.5 Discussion

Theorem 5.1 and Propositions 5.1, 5.2, 5.3 are the main results of this chapter. Together, these results establish a cross-technology framework for the decentralized stabilization of the system frequency, voltages, and currents in AC power systems.

Remarkably, despite the technical differences between DC and AC power systems, the findings of this chapter share many similarities with the DC results in Chapter 4:

- Similar to Theorem 4.1 answering (Q1.1), Theorem 5.1 answers research question (Q2.1) and provides two sufficient conditions (AC 1) and (AC 2) that establish model- and technology-independent system and control design requirements for the decentralized stabilization in flexible AC power system configurations. In fact, these conditions are identical to (DC 1) and (DC 2) in Theorem 4.1. Other subsystem models (e.g., for more detailed line models (see Remark 5.3), different loads, more detailed inverter models, different inverter topologies and technologies with output filters different than RLC, or altogether new units such as FACTSs or synchronous generators) can readily be integrated into the presented AC power system model. Then, following the steps taken in this chapter, parameter requirements and/or appropriate controllers can be developed to ensure (AC 1) and (AC 2) are satisfied.
- Propositions 5.1, 5.2 and 5.3 follow the same principle steps and controller designs as Propositions 4.1, 4.2 and 4.3. Similar to the DC case, these propositions ensure via parameter requirements and controllers that the conditions of Theorem 5.1 are met for the AC power system described in Section 5.1. The passivity-based current and voltage controllers in particular provide an explicit answer to research question (Q1.2). However, due to the technology-independent nature of the decentralized stabilization conditions, research question (Q1.2) allows for a variety of decentralized control solutions as illustrated by example of the voltage controller from Nahata and Ferrari-Trecate [2019] in Proposition 5.4.
- Similar to the DC results, the controllers required to enforce conditions (AC 1) and (AC 2) use standard control functions such as a PI term, a state feedback, and a setpoint feedforward (see (5.39), (5.46), Remark 5.10, and (5.59)). Furthermore, it should be highlighted that the controllers proposed in this thesis follow a single-loop design. In recent years, such single-loop designs have emerged as promising alternatives to the traditional double-loop designs with inner current and outer voltage control loops as they are easier to implement and show better stability properties (see Watson et al. [2021] and the references therein). Lastly, note that each of the control inputs $\mathbf{u}_i = \mathbf{V}_{S,i}^{\text{dq}}$ is again a function of the duty cycle δ_i of the VSI and the DC voltage $V_{\text{DC},i}$ supplied by the DC voltage source, i.e., a RES, a storage device, or a combination thereof (see Section 5.1.2). For a practical implementation of any control law \mathbf{u}_i , the duty cycle δ_i can be obtained from \mathbf{u}_i .

- Analogously to the DC case, it is crucial for a proper functioning of the AC controllers and a stabilization-coordination hierarchy as proposed in Section 2.1.2 that the combination of DC voltage source and VSI approximately behaves like an ideal voltage source $V_{S,i}^{dq}$ (see Section 5.1.2). Consequently, this entails the same practical requirements as discussed in Section 4.5, viz. sufficient short-term energy buffer via battery storage, supercapacitors, headroom on generation, or a combination thereof, sufficient peak power capability, and a sufficiently fast coordination layer that can reschedule setpoints within several seconds to a few minutes.⁴² For example, for the 20 kV CIGRE AC power system from Section 5.4 with an overall demand of approximately 787.4 kW and 787.4 kVar, a 50 % demand increase of all loads equals 393.7 kW and 393.7 kVar. Depending on the communication rate with the coordination layer and assuming no headroom for the DGU generation, stored energy of 98.4 kW h/98.4 kVar h for a 15 min communication interval, 6.56 kW h/6.56 kVar h for a 1 min interval, and 1.1 kW h/1.1 kVar h for a 10 s interval must be available. Furthermore, for both scenarios from Section 5.4, the maximum power peaks are in the range of 800 kW and 1000 kVar, respectively. Practical experience indicates that integrated energy storage architectures combining batteries and supercapacitors are promising solutions for providing both, fast, high-power transients as well as sufficient short-term energy storage [Matevosyan et al., 2019; Rocabert et al., 2019].

However, in addition to the DC power system results, the findings in this chapter are based on two further assumptions, which account for the technical characteristics of AC power systems: firstly, Assumption 5.1 restricts the investigation to balanced three-phase signals such that two-dimensional dq coordinates can be used for modeling AC power systems. Secondly, Assumption 5.3 requires the local controller clocks and dq frames to be synchronized to the desired system frequency ω_0 .

The balanced assumption is motivated by the fact that AC power systems are typically designed to be balanced to ensure an efficient and reliable power supply and minimize the losses during transmission and distribution (see, e.g., Glover et al. [2012, p. 74–75] and Gómez-Expósito et al. [2018, pp.280–281]). Thus, it is common practice to assume balanced operating conditions (see, e.g., Etemadi et al. [2012a], Rivero et al. [2015], Schiffer et al. [2016], and Baimel et al. [2017]). Furthermore, in case of unbalanced conditions, the unbalanced three-phase system can be decomposed via the method of symmetrical components into three balanced systems exhibiting a positive, negative, and zero sequence (see Glover et al. [2012, p. 419ff], Akagi et al. [2007, p. 34], Gómez-Expósito et al. [2018, p. 281–282], and Paap [2000]). Subsequently, elaborating on the ideas in Ojo and Schiffer [2017], each of the (balanced) sequences can be represented again in dq or $dq0$ coordinates, respectively. Consequently, results obtained for balanced systems, such as the ones presented in this chapter, can in principle be extended to the unbalanced case.

⁴² In the last years, first coordination schemes that operate on such smaller time-scales have been developed (see for example Milano et al. [2018], Dörfler et al. [2019], and the references therein).

The assumption of synchronized local controller clocks (see Assumption 5.3) has seen increasing use in the last decade (see, e.g., the review in Section 2.1.1 as well as Babazadeh and Karimi [2013], Nahata and Ferrari-Trecate [2019], and Watson et al. [2021]). It is motivated by well-established technological results that allow to achieve practically negligible synchronization errors via an open-loop frequency control based on internal oscillators at each VSI and infrequent communication solutions. The Precision Time Protocol IEEE standard [IEEE 1588, 2008] and its use in power system applications [IEEE 1588, 2017], for example, provide solutions based on GPS and Ethernet that achieve a clock accuracy of 100 ns – $1\text{ }\mu\text{s}$ via infrequent updates in time intervals of 10 ms – 1 s (see also Tucci and Ferrari-Trecate [2020]). Etemadi et al. [2012a] provide a good review for (low-cost) crystal oscillators that achieve a high accuracy with drifts of 20 ps – $2\text{ }\mu\text{s}$ per year. A highly reliable synchronization of these local oscillators can be achieved via a common timing signal such as the GPS radio clock (accuracy $1\text{ }\mu\text{s}$) that is communicated infrequently at time intervals of 1 s and more. In Etemadi et al. [2012b], the same authors validate their prior statements by extensive lab studies and show that low-cost, local crystal oscillators together with infrequent GPS synchronization can keep the system frequency well within permissible limits of practical standards and grid codes.

Overall, the results of this chapter illustrate that a similar passivity-based approach can be used to establish decentralized, cross-technology stabilization frameworks in both DC and AC power systems. Moreover, the results obtained by such a passivity-based approach show similarities across the different domains. Most notably, the decentralized asymptotic stability conditions in Theorem 4.1 and Theorem 5.1, which form the core of the stabilization frameworks, are identical. In addition to creating a large, technology-neutral solution space to the decentralized stabilization problems in DC or AC power systems, these conditions thus also establish a common system-theoretical basis that ensures interoperability of decentralized stabilization solutions in hybrid DC/AC settings, i.e., across domain borders.

5.5.1 Comparison with Parallel Works

As outlined in Section 2.4, during the time of this thesis, several other research groups have explored independently from each other the possibilities of using passivity techniques to provide decentralized stability conditions and controller designs for AC power systems.

Similar to the results of this chapter, all these work consider balanced three-phase signals and model AC power systems in dq coordinates. Moreover, in contrast to the DC case, the lack of an analytical framework with conditions that ensure decentralized stabilization in AC power systems under “heterogeneous generation technologies across physics, control, and overlapping timescales” [Dörfler and Groß, 2023] has been addressed in the works of Spanias and Lestas [2019], Spanias et al. [2020], and Watson et al. [2021].

Spanias and Lestas [2019] and Spanias et al. [2020] view AC power systems as negative feedback, i.e., skew-symmetric, interconnection and establish decentralized conditions based on strict passivity properties of the node dynamics such that the overall system equilibrium is asymptotically stable. While the general idea of establishing technology-independent, decentralized stability conditions via passivity properties is similar to Theorem 4.1, the conditions from Spanias and Lestas [2019] and Spanias et al. [2020] require more restrictive, strict passivity properties. As shown within this chapter, this requirement cannot always be fulfilled.

Nevertheless, the decentralized, passivity-based stability conditions of Spanias and Lestas [2019] can be applied to certain systems as illustrated by Watson et al. [2019]. The authors compare control performances and conduct a numerical passivity analysis for linearized closed-loop DGUs that use several existing control schemes for frequency/active power regulation of grid-forming inverters such as frequency droop, angle droop, and matching control. While their results are numerical, require a linearization, and are restricted to Z loads, their focus on the passivity properties of other established control schemes represents an interesting starting point for further assessing the unifying character of the results of this chapter in future research.

Watson et al. [2021] establish less restrictive conditions than Spanias and Lestas [2019] and Spanias et al. [2020], which ensure asymptotic stability of the AC power system equilibrium under shifted OSP properties of the closed-loop DGU nodes. Subsequently, they propose two decentralized grid-forming voltage controllers to achieve OSP. Their first controller is based on full state-feedback design. Their second controller results from a mixed H_∞ /passivity design that additionally provides desired closed-loop performance guarantees (small control inputs, fast convergence, limited inverter coupling) via H_∞ constraints. Similar to the results of this chapter, frequency control is assumed to be conducted in open loop via internal oscillators and infrequent synchronization. The considered network model comprises detailed, dynamic distributed power line models as discussed in Remark 5.3. Loads are however not considered in detail. Instead, the authors refer to the preliminary version of the load analysis of Proposition 5.1 which is provided in Strehle et al. [2020a]. Considering that the shifted OSP properties are still more conservative than condition (AC 1) and thus compatible with it, the controllers proposed by Watson et al. [2021] present promising alternatives to the controllers designed in this chapter. Particularly in some demanding real-world settings the closed-loop performance guarantees might warrant the additional cost of a mixed H_∞ /passivity design.

In contrast to the above works that develop or use decentralized, asymptotic stability conditions, Nahata and Ferrari-Trecate [2019] and Ojo et al. [2021] focus on developing decentralized, passivity-based voltage controllers for grid-forming inverters. Similar to the parallel DC works discussed in Section 4.5.1, the passivity properties of the subsystem models are then merely used to facilitate the stability statement.

The results of Nahata and Ferrari-Trecate [2019] in particular are a direct extension of their decentralized DC voltage control design from Nahata et al. [2020] to AC power systems. That is, they use the same decentralized, state-feedback controller structure than in the DC case (compare (4.41) and (5.59)) to ensure that the closed-loop DGU is passive. As illustrated in this chapter, the so-obtained closed-loop DGU properties are readily compatible with the condition (AC 1) from Theorem 5.1. Furthermore, similar to the results of this chapter and Watson et al. [2021], frequency control is assumed to be conducted in open loop via internal oscillators and infrequent synchronization.

Ojo et al. [2021] propose a decentralized frequency and voltage control scheme for grid-forming inverters. Via a numerical analysis, the authors demonstrate that the linearized, closed-loop DGU model can be made strictly passive by an appropriate choice of the controllers gains. While the linearization and purely numerical passivity analysis present a limitation on the stability statement, the proposed control design opens up several possible directions of complementing the results from this chapter. The dedicated frequency feedback loop based on angle droop and its passivity-based interpretation in particular provide a promising starting point for developing frequency controllers under the roof of the conditions of Theorem 5.1. Additionally, including the DC voltage in the voltage control loop as done by Ojo et al. [2021] seems to provide a simple means to improve the performance of the voltage controller in Proposition 5.3, if this should be needed in some practical applications.

Lastly, the results of this chapter extend the existing body of research by a detailed load modeling with accompanying EIP analysis (see Section 5.1.2 and Proposition 5.1).⁴³ Furthermore, in contrast to the above-discussed works, the problem of current control in grid-feeding DGUs is considered explicitly (see Proposition 5.2).

5.6 Summary and Contributions

In the wake of the sustainable energy transition, future power system operation is in need of novel methods that ensure stabilization in the face of large numbers of interacting units with a wide variety of deployed technologies and control strategies. This chapter provides a passivity-based framework for AC power system stabilization that makes large numbers of units manageable by means of decentralized methods and ensures interoperability across different AC power system technologies and control strategies. Together with the findings of Spanias and Lestas [2019], Spanias et al. [2020], and Watson et al. [2021], the results of this chapter are among the first to provide such decentralized, cross-technology stabilization frameworks in AC power systems. In particular, while the conditions of Theorem 5.1 are not the sole result in this area, they to date provide the least restrictive, technology-independent framework for the

⁴³ All the above-referenced works do not consider loads in detail and at most treat linear load models (ZI or RL).

decentralized stabilization in AC power systems. In summary, the main contributions of this chapter are:

- a generalized networked system model for AC power systems which combines graph theory with PHS modeling (Section 5.1);
- decentralized, EIP-based conditions that provide model- and technology-independent system and control design requirements for ensuring asymptotic stability of any feasible AC power system equilibrium (Theorem 5.1);
- parameter specifications and decentralized converter controllers that ensure the EIP-based asymptotic stability conditions are met and desired voltage and current setpoints are asymptotically stabilized (Propositions 5.1, 5.2, and 5.3).

Together, these contributions answer the research questions (Q1.1) and (Q1.2) formulated in Section 2.1.2. Simulation studies based on a CIGRE benchmark network demonstrate the functionality of the developed decentralized stabilization framework and illustrate its unifying nature.

In addition to these main findings, the results of this chapter highlight that a passivity-based framework can not only serve as a unifying concept for ensuring decentralized stabilization across different technologies and control strategies within a specific energy system, but also across energy system domains (in this case DC and AC power systems). To further explore this domain-unifying aspect, the development of a decentralized, cross-technology framework for the decentralized stabilization of the hydraulics in DHNs shall initially be approached with the same passivity-based methods as before.

6 Passivity-Based Decentralized Stabilization in District Heating Networks

So far, passivity-based, cross-technology frameworks for the decentralized stabilization in electrical DC and AC power systems have been developed. It has been observed that the graph-based description of a networked system, PHS modeling, and the EIP-based asymptotic stability theorem from Chapter 3 can provide unifying, model- and technology-independent requirements that ensure decentralized stabilization across different electrical energy systems. Motivated by the unifying nature of these results, this chapter approaches the goal of establishing a decentralized, cross-technology framework for the decentralized stabilization of pressures and volume flow rates in DHNs along the same lines as Chapters 4 and 5. In addition to profiting from a transfer of knowledge, this procedure allows to further assess the domain-unifying features of a passivity-based, decentralized stabilization framework.

Thus, Section 6.1 starts with developing a hydraulic DHN model that combines a graph-based, networked system representation along the lines of Definition 3.1 with generalized, ISO-PHS models of the subsystems at the nodes and edges of the DHN digraph. In contrast to DC and AC power systems, this modeling part is more extensive and constitutes to answering its own research question, viz. (Q3.1). This is due to the fact that the literature on system and control design models for DHN hydraulics is scattered, incomplete, and a lot of information can only be found in white papers, reports, etc. of manufacturers, suppliers, and operators.

Subsequently, Section 6.2 demonstrates how the passivity-based approach of Theorem 3.1 and Corollary 3.1 can be used to derive decentralized, cross-technology, asymptotic stability conditions that answer research question (Q3.2). After proving that the unactuated DHN subsystems inherently fulfill the derived conditions, the main control problems related to answering research question (Q3.3) are formulated.

In Section 6.3, the formulated control problems are addressed. To begin with, decentralized, passivity-based pressure and volume flow rate controllers are developed for the main actuators, i.e., pumps and valves. Then, the actuated subsystems containing the controlled pumps and valves are shown to fulfill the requirements formulated in the control problems in Section 6.2.

Afterwards, Section 6.4 presents simulation scenarios to validate the findings.

Sections 6.5 and 6.6 conclude this chapter with a discussion and summary of the main contributions. In particular, the main results are compared to the passivity-based works

published in parallel to this thesis (see Section 2.4).⁴⁴

6.1 Modeling

In this section, the model of the considered DHN is established along the lines of Definition 3.1. Firstly, in Section 6.1.1, the DHN setup is outlined and formally described as a digraph. Subsequently, in Section 6.1.2, the main hydraulic actuators *pumps* and *valves*, which are responsible for pressure and volume flow rate control in DHNs, are modeled. Their models serve as building blocks for the actual models of the subsystem on the edges and nodes of the DHN digraph in Sections 6.1.3 and 6.1.4. To provide a clear presentation for the subsequent stability analysis and control design, the ISO-PHS representations of the subsystems are summarized in Section 6.1.5. Lastly, in Section 6.1.6, the interconnection structure of the subsystems is formalized via the incidence matrix of the DHN digraph.

6.1.1 System Setup

This chapter considers DHNs comprising DGUs, consumers, pipes, mixing connections (for temperature cascading), and pressure holding units that are connected in flexible, time-varying system configurations (see, e.g., Figure 6.1). Such DHNs can be described by a weakly connected digraph $\mathcal{G} = (\mathcal{V}, \mathcal{E})$ without self-loops as illustrated in Figure 6.2 with subsystems on the nodes \mathcal{V} and edges \mathcal{E} . The edges \mathcal{E} are partitioned into four sets: $\mathcal{D} = \{1, \dots, D\}$, $D \geq 1$, represents the DGUs, $\mathcal{L} = \{D + 1, \dots, D + L\}$, $L \geq 1$, the consumers (loads), $\mathcal{P} = \{D + L + 1, \dots, D + L + P\}$, $P \geq 2$, the pipes, and $\mathcal{M} = \{D + L + P + 1, \dots, D + L + P + M\}$, $M \geq 0$, the mixing connections. The nodes \mathcal{V} are composed of two sets: \mathcal{H} represents the pressure holding units and $\mathcal{C} = \mathcal{V} \setminus \mathcal{H}$ the capacitances arising from volume storage in the DGU circuits, consumer circuits, and pipes. The orientation of the edges represents the arbitrary reference direction of positive volume flow rates. Furthermore, the digraph \mathcal{G} is completely specified by its incidence matrix $\mathbf{B} \in \mathbb{R}^{|\mathcal{V}| \times |\mathcal{E}|}$ with elements b_{il} (cf. (1.1)).

Note that conversely to the power systems models in Sections 4.1 and 5.1, the main subsystems for DHNs are represented by edges.

⁴⁴ Preliminary results leading to the content of this chapter have been published in the conference papers [Strehle et al., 2021; Strehle et al., 2022a].

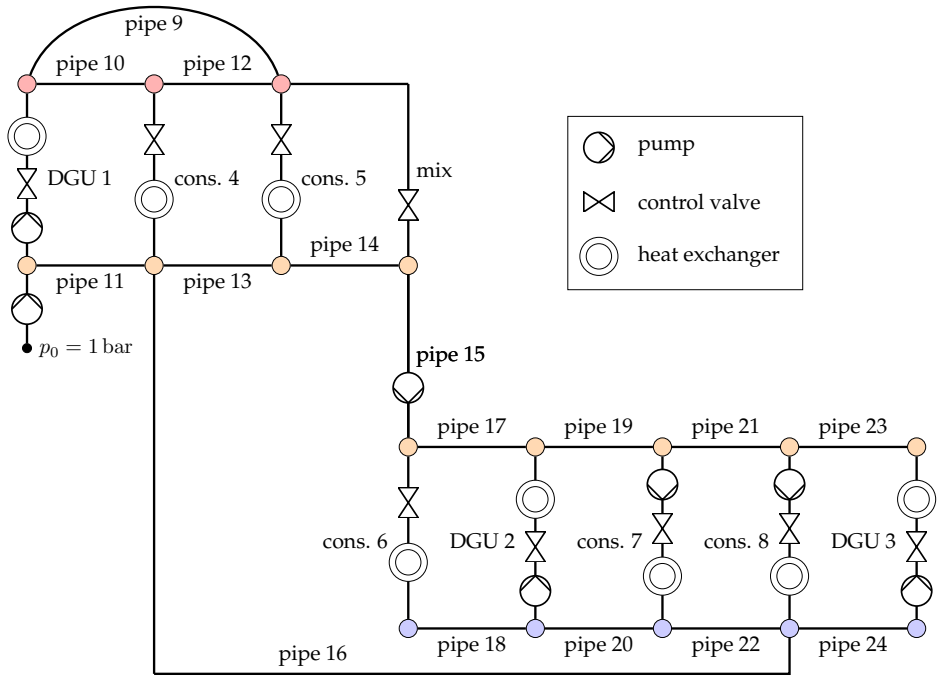


Figure 6.1: Hydraulic schematic of a DHN containing three DGUs, a pressure holding unit at the return side of DGU 1, five consumers, 16 pipes (pipe 15 with booster pump), and one mixing connection in a three-temperature layer topology indicated by the three different colors of the network nodes.

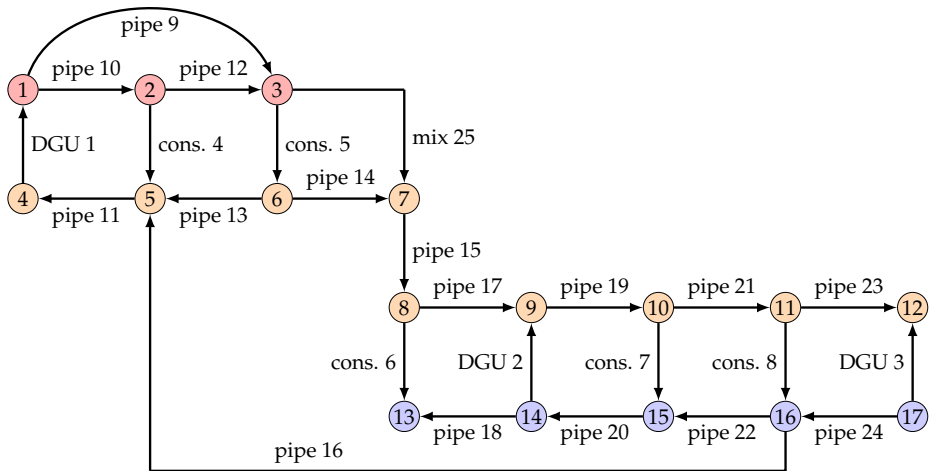


Figure 6.2: Digraph representation of the DHN from Figure 6.1 containing three DGUs $l \in \mathcal{D} = \{1, 2, 3\}$, five consumers $l \in \mathcal{L} = \{4, 5, 6, 7, 8\}$, 16 pipes $l \in \mathcal{P} = \{9, \dots, 24\}$ ($l \in \mathcal{P}_{\text{boost}} = \{15\}$ with booster pump), and one mixing connection $l \in \mathcal{M} = \{25\}$ in a three-temperature layer topology. The 17 nodes represent one pressure holding unit $i \in \mathcal{H} = \{4\}$ and 16 capacitances $i \in \mathcal{C} = \mathcal{V} \setminus \{4\}$.

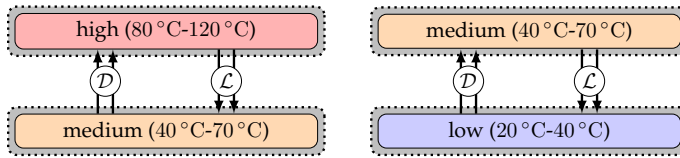


Figure 6.3: Illustration of a traditional 2nd or 3rd generation DHN with high-temperature supply and medium-temperature return (left) and a 4th generation DHN with medium-temperature supply and low-temperature return (right). Between the temperature layers may be any number of $D \geq 1$ DGU and $L \geq 1$ consumer edges. The two temperature layers coincide with the two hydraulic layers (dashed grey bubbles).

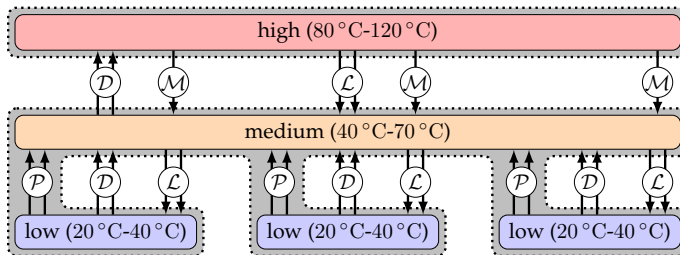


Figure 6.4: Illustration of a DHN with the three temperature layers high (red), medium (orange), low (blue), and the two hydraulic layers (dashed grey bubbles). Between the temperature layers may be any number of $D \geq 1$ DGU and $L \geq 1$ consumer edges. Between the high and medium layer may be any number of $M \geq 0$ mixing connections.

Temperature and Hydraulic Layers

As illustrated in Figures 6.1–6.4, DHNs may comprise different temperature layers. It is standard practice to distinguish between three temperature layers: *high temperature* (80 °C–120 °C), *medium temperature* (40 °C–70 °C), and *low temperature* (20 °C–40 °C) (see Lund et al. [2014], Hertle et al. [2015, pp. 33,59], Li et al. [2017, pp. 16–17], Nussbaumer et al. [2020, p. 44], Volkova et al. [2020], and Volkova et al. [2022]). The high- and medium-temperature layers form the supply and return of the dominating 2nd and 3rd generation DHNs, while the medium- and low-temperature layers form the supply and return of the emerging 4th generation DHNs (see Figure 6.3) [Lund et al., 2014]; [Li et al., 2017, pp. 16–17].

In future DHNs, the medium-temperature return of a 2nd or 3rd generation DHN may additionally serve as supply for (new) low-temperature DHN sections, yielding a three temperature layer topology as illustrated in Figures 6.2 and 6.4. Such low-temperature DHN sections allow to efficiently use the heat energy in a DHN (temperature cascading) and integrate renewable heat sources (e.g., waste heat, solar thermal, heat pumps) and new consumers (e.g., low-energy buildings) into existing DHNs [Hertle et al., 2015, pp. 33,59]; [Nussbaumer et al., 2020, p. 44]; [Köfing et al., 2017; Volkova et al., 2020, 2022]. However, due to the ongoing trend of decreasing DHN temperatures, particularly in summer, the medium-temperature might not be sufficiently high to cover the heat

demand of some low-temperature consumers. Thus, low-temperature DHN sections in a three layer topology typically have at least one mixing connection, i.e., an edge $i \in \mathcal{M}$, that allows to boost the temperature by mixing high with medium-temperature water (see node 7 in Figure 6.2) [Köfing et al., 2017; Volkova et al., 2020, 2022].

Furthermore, in a three-temperature layer topology, the low-temperature water is typically fed directly into the medium-temperature layer (see node 5 in Figure 6.2 and the set of pipe edges \mathcal{P} between low- and medium-temperature in Figure 6.4) [Köfing et al., 2017; Volkova et al., 2020, 2022]. This implies that despite possibly three temperature layers, there are exactly two hydraulic layers (see Figure 6.4). The number of hydraulic layers can be defined as follows:

Definition 6.1 (Hydraulic layers in a DHN)

A DHN has $n_h \geq 2$ hydraulic layers, where n_h is the number of weakly connected subgraphs $\mathcal{G}_1, \dots, \mathcal{G}_{n_h}$ obtained by removing all edges $l \in \mathcal{D} \cup \mathcal{L} \cup \mathcal{M}$, i.e., all DGUs, consumers, and mixing connections, from \mathcal{G} .

6.1.2 Hydraulic Actuators

With the DHN setup formalized as a digraph, the next step is to derive the mathematical models describing the hydraulic dynamics of the subsystems on the edges and nodes of the DHN digraph. As a preliminary step, this section first presents the models of the main actuators responsible for pressure and volume flow rate control, i.e., *pumps* and *valves*. These models serve as building blocks for the hydraulic models of the DGUs, consumers, pipes, and mixing connections on the edges \mathcal{E} (see Section 6.1.3) as well as the pressure holding units and capacitances on the nodes \mathcal{V} (see Section 6.1.4).

For the modeling, the following assumption is made which is valid under normal operating conditions [De Persis and Kallesøe, 2011; Chertkov and Novitsky, 2019].

Assumption 6.1 (Incompressible water)

The compressibility of water is neglected.

Furthermore, the following monotonicity properties hold for the pressure losses due to friction in pipes and valves [Boysen and Thorsen, 2003, Equations (7) and (12)]; [De Persis and Kallesøe, 2011]; [Nussbaumer et al., 2020, pp. 117–119].

Property 6.1 (Monotonicity of pressure losses inside pipes and valves)

Pressure losses inside pipes $\lambda(q) : \mathbb{R} \rightarrow \mathbb{R}$ and valves $\mu(q, s) : \mathbb{R} \times \mathbb{R}_{\geq 0} \rightarrow \mathbb{R}$ caused by volume flow rates $q \in \mathbb{R}$ are continuously differentiable, strictly increasing functions and satisfy $\lambda(0) = 0$ and $\mu(0, s) = 0$ for all valve stem positions $s \in \mathbb{R}_{\geq 0}$, respectively.

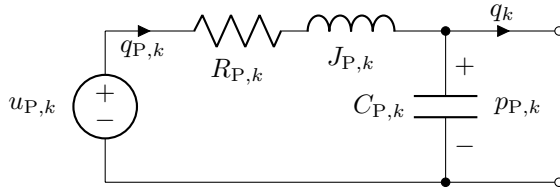
Pumps

Figure 6.5: Equivalent circuit of a linear, second-order approximation of pump dynamics (cf. Goppelt et al. [2018]).

Pumps are the essential actuated components in DHNs. They are used for controlling the absolute pressure at specific points (pressure holding) (see Wang et al. [2017a] and Nussbaumer et al. [2020, pp. 54–55]), for (differential) pressure and volume flow rate control in DGUs (see De Persis and Kallesøe [2011], De Persis et al. [2014], Wang et al. [2017a], Vandermeulen et al. [2018], and Gong et al. [2019]) for boosting the pressure in consumers and pipes (see De Persis and Kallesøe [2011], and Lund et al. [2014]), and for direct volume flow rate control in consumers (see Yan et al. [2013], Wang et al. [2017a], and Gong et al. [2019]).

In the prevalent literature (see, e.g., the above-referenced literature or the discussion in Section 2.3.2), pumps are considered as ideal pressure sources modeled by an ideal generalized DC voltage source in the equivalent circuit diagram. However, the dynamics of pumps, particularly the ones of centrifugal pumps that are widely used in DHNs [De Persis and Kallesøe, 2011; Scholten et al., 2017b], lie in the range of several hundred milliseconds (see, e.g., Goppelt et al. [2018, Figures 8 and 9]). Since this is a time scale comparable to that of the overall DHN hydraulics (see, e.g., Chertkov and Novitsky [2019] and Novitsky et al. [2020]), a more accurate control design and system analysis by means of dynamic pump models must be performed if increasing numbers of pumps are integrated into DHNs.

As a starting point for such an improved design and analysis, the complex arrangement of power electronics, speed-controlled AC motor, and pump hydraulics is approximated by a linear second-order system (see also Goppelt et al. [2018]). The linear second-order system can be represented by a linear RLC equivalent circuit as illustrated in Figure 6.5. The parameters $R_{P,k}, J_{P,k}, C_{P,k} > 0$ are pure black box parameters without

physical interpretation. This is due to the fact that in the RLC equivalent circuit, the speed control and AC motor dynamics are merged with the hydraulic pump dynamics comprising fluid mass inertia, pressure losses, and hydraulic capacitance due to fluid compressibility and fluid volume [Goppelt et al., 2018]. The control input $u_{P,k} \in \mathbb{R}$ can be interpreted as a pressure source originating from the rotational speed of the pump produced by an AC motor.⁴⁵ The pressure difference produced by the pump between its terminals is given by $p_{P,k} \in \mathbb{R}$. The volume flow rate through the pump is given by $q_k \in \mathbb{R}$, while $q_{P,k} \in \mathbb{R}$ is an auxiliary variable without physical interpretation.

By applying KVL and KCL to Figure 6.5, the pump dynamics can be obtained as

$$\begin{aligned} J_{P,k} \dot{q}_{P,k} &= -p_{P,k} - R_{P,k} q_{P,k} + u_{P,k}, \\ C_{P,k} \dot{p}_{P,k} &= q_{P,k} - q_k, \end{aligned} \quad (6.1)$$

with $q_{P,k}, p_{P,k}, q_k, u_{P,k} \in \mathbb{R}$, and parameters $R_{P,k}, J_{P,k}, C_{P,k} > 0$.

Remark 6.1. *In practice, the black-box parameters $R_{P,k}$, $J_{P,k}$, and $C_{P,k}$ can be identified from measurement data obtained by operating the respective pump in typical scenarios (see, e.g., Goppelt et al. [2018]). Alternatively, they can be fitted in simulations to match characteristic curves provided in data sheets.*

Control Valves

Besides pumps, valves are the main actuators in DHNs. Their main task is the regulation of volume flow rates [Li et al., 2017, p. 19,29]; [Wang et al., 2017b; Vandermeulen et al., 2018]; [Nussbaumer et al., 2020, pp. 143–145,151]. In order to establish a desired volume flow rate q_k^* , valves adjust their pressure drop $\mu_k(s_{v,k}, q_k)$ by varying their stem position between fully closed ($s_{v,k} = 0$) and fully open ($s_{v,k} = 1$). That is, they behave as variable, nonlinear flow resistors. In order to avoid volume surge behavior around their closing point, valves are designed such that the stem has a lower limit just above zero in normal operation [Nussbaumer et al., 2020, pp. 145]. Consequently, the following assumption can be made:

Assumption 6.2 (Valve design)

In normal operation, the valve stem position is never zero, i.e., $s_{v,k} \in (0, 1]$.

The nonlinear characteristic pressure drop equation of any valve is given by [Wang et al., 2017b, Equation (18)]; [Gong et al., 2019, Equation (5)]

$$\mu_k(s_{v,k}, q_k) = \frac{1}{(C_{v,k} f_{v,k}(s_{v,k}))^2} |q_k| q_k, \quad (6.2a)$$

⁴⁵ In practice, the actual control input of a pump system is a desired rotational speed, which enters into an automatic speed control of the AC motor driving the pump [KSB Aktiengesellschaft, 2006, pp. 28,51]; [Goppelt et al., 2018].

where $s_{v,k} \in (0, 1]$ is the stem position, $q_k \in \mathbb{R}$ the volume flow rate through the valve, $C_{v,k} > 0$ the flow capacity of the valve, and $f_{v,k}(s_{v,k})$ the valve characteristic⁴⁶ (see also the static orifice law in Boysen and Thorsen [2003, Equation (12)] or the definition of the k_v -value in Nussbaumer et al. [2020, p. 144]). By substituting

$$u_{v,k}(s_{v,k}) := \frac{1}{f_{v,k}(s_{v,k})^2}, \quad \tilde{\mu}_k(q_k) := \frac{1}{C_{v,k}^2} |q_k| q_k \quad (6.2b)$$

in (6.2a), the pressure drop can be written as

$$\mu_k(s_{v,k}, q_k) = u_{v,k}(s_{v,k}) \tilde{\mu}_k(q_k), \quad (6.3)$$

where $u_{v,k}(s_{v,k}) : (0, 1] \rightarrow \mathbb{R}_{>0}$ is a bijective mapping of the actual stem position $s_{v,l} \in (0, 1]$ to the virtual control input $u_{v,k} > 1$, and $\tilde{\mu}_k(q_k) : \mathbb{R} \rightarrow \mathbb{R}$ a continuously differentiable, strictly increasing function satisfying $\tilde{\mu}_k(0) = 0$. Note that (6.3) is affine in the virtual control input $u_{v,k}$.

Remark 6.2. *It might not be intuitively clear that $f(s_{v,k}) = s_{v,k}$ represents a linear valve characteristic $q_k = v_k \cdot s_{v,k}$ with some constant $v_k > 0$. However, when considering that valve characteristics are specified assuming a fixed pressure drop $\mu_k(s_{v,k}, q_k) = \bar{\mu}_k > 0$ [Nussbaumer et al., 2020, pp. 143–145, 151], (6.2a) can directly be rewritten as $q_k = v_k \cdot f_{v,k}(s_{v,k}) = v_k \cdot s_{v,k}$ with $v_k = C_{v,k} \sqrt{\bar{\mu}_k}$.*

Remark 6.3. *Since valves can only function as variable, nonlinear flow resistors, valve-based volume flow rate control requires sufficient differential pressure over the hydraulic circuit the valve is part of (see Assumption 6.3 in the sequel). In future DHNs with frequently changing hydraulic conditions, this motivates the addition of booster pumps in some consumer circuits or pipes (see Figures 6.7 and 6.11).*

6.1.3 Subsystems on Edges

In this section, the hydraulic models of the DGUs $l \in \mathcal{D}$, consumers $l \in \mathcal{L}$, pipes $l \in \mathcal{P}$, and mixing connections $l \in \mathcal{M}$ on the edges $\mathcal{E} = \mathcal{D} \cup \mathcal{L} \cup \mathcal{P} \cup \mathcal{M}$ of the DHN diagram are presented.

Pipe Model

The hydraulic schematic of a pipe at an edge $l \in \mathcal{P}$ is illustrated in Figure 6.6. The corresponding equivalent circuit is given in Figure 6.7. The pipe friction is modeled by a nonlinear, volume flow-dependent resistance $\lambda_l(q_l) : \mathbb{R} \rightarrow \mathbb{R}$ (see Property 6.1) and the

⁴⁶ The two most common valve types are equal percentage valves with characteristic $f_{v,k}(s_{v,k}) = \eta_k^{s_{v,k}-1}$ and rangeability $\eta_k > 0$ and linear valves with characteristic $f_{v,k}(s_{v,k}) = s_{v,k}$.

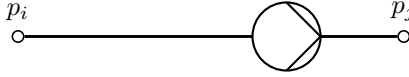


Figure 6.6: Hydraulic schematic of a pipe $l \in \mathcal{P}$ with optional booster pump.

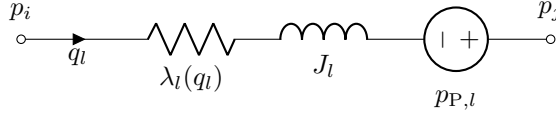


Figure 6.7: Equivalent circuit of a hydraulic pipe model $l \in \mathcal{P}$ with optional booster pump $p_{P,l}$; $i, j \in \mathcal{V}$, $i \neq j$

volume inertia by the linear inductance $J_l > 0$. Any kind of volume storage in a pipe is modeled by a capacitance C_i and C_j at the source and target node, respectively (see Section 6.1.4). Furthermore, it is taken into account that some pipes might have booster pumps in series. Such a pump is represented by the generalized voltage source in Figure 6.7 and modeled by (6.1). By applying KVL and KCL to Figure 6.7, the dynamics for each pipe $l \in \mathcal{P}$ follow as

$$J_l \dot{q}_l = p_{P,l} - \lambda_l(q_l) - \sum_{i \in \mathcal{V}} b_{il} p_i, \quad (6.4a)$$

$$J_{P,l} \dot{q}_{P,l} = -p_{P,l} - R_{P,l} q_{P,l} + u_{P,l}, \quad (6.4b)$$

$$C_{P,l} \dot{p}_{P,l} = q_{P,l} - q_l, \quad (6.4c)$$

with $p_i \geq 0$, $q_l, p_{P,l}, q_{P,l}, u_{P,l} \in \mathbb{R}$, parameters $J_l, R_{P,l}, J_{P,l}, C_{P,l} > 0$, elements of the incidence matrix b_{il} (see (1.1)), and continuously differentiable, strictly increasing function $\lambda_l : \mathbb{R} \rightarrow \mathbb{R}$, $\lambda_l(0) = 0$ (see Property 6.1).

Remark 6.4. Any pipe $l \in \mathcal{P} \setminus \mathcal{P}_{\text{boost}}$ without a booster pump can be modeled by (6.5) by fixing $u_{P,l} = p_{P,l} = 0$ and removing the part corresponding to the dynamics of $q_{P,l}$ and $p_{P,l}$.

DGU Model

From a hydraulic viewpoint, a DGU may comprise two main parts as illustrated in the hydraulic schematic in Figure 6.8 and the corresponding equivalent circuit in Figure 6.9: a circulation circuit (green) [Lamaison et al., 2017; Lennermo et al., 2019] and an optional pressure holding unit (black generalized voltage source) [Nussbaumer et al., 2020, pp. 54–55]. The circulation circuit in green is viewed as the actual edge $l \in \mathcal{D}$. It comprises a serial connection of a circulation pump, a control valve, pipes, and a heat exchanger. The circulation pump is represented by the green generalized voltage source in Figure 6.9 and modeled by (6.1). The control valve is modeled as a variable, nonlinear resistance $\tilde{\mu}_l(q_l) u_{v,l}(s_{v,l})$ with control input $u_{v,l}(s_{v,l})$ as in (6.2). All pipe segments including those

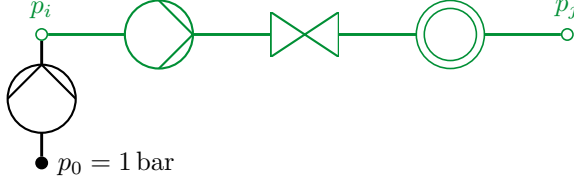


Figure 6.8: Hydraulic schematic of a DGU $l \in \mathcal{D}$ comprising a circulation pump, a control valve, pipes, and a heat exchanger (green). At the suction side of the circulation pump, a pressure holding unit is connected (black pump).

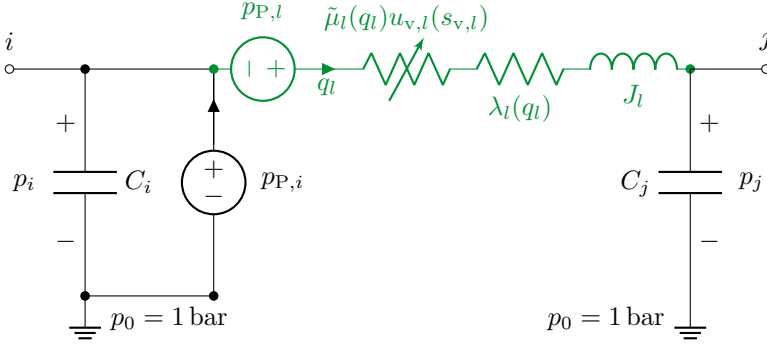


Figure 6.9: Equivalent circuit of the hydraulic DGU schematic from Figure 6.8. The DGU $l \in \mathcal{D}$ comprises a pressure holding unit (black voltage source) and a circulation circuit (green). Without loss of generality, the capacitance C_i may be lumped with the pressure holding unit (see Section 6.1.4); $i, j \in \mathcal{V}, i \neq j$.

of the heat exchanger are lumped into the nonlinear, volume flow-dependent resistance $\lambda_l(q_l) : \mathbb{R} \rightarrow \mathbb{R}$ (see Property 6.1) and the linear inductance $J_l > 0$, which represent the pipe friction and volume inertia, respectively. By applying KVL and KCL to the green part in Figure 6.9, the dynamics for each DGU $l \in \mathcal{D}$ follow as

$$J_l \dot{q}_l = p_{P,l} - \lambda_l(q_l) - \tilde{\mu}_l(q_l) u_{v,l}(s_{v,l}) - \sum_{i \in \mathcal{V}} b_{il} p_i, \quad (6.5a)$$

$$J_{P,l} \dot{q}_{P,l} = -p_{P,l} - R_{P,l} q_{P,l} + u_{P,l}, \quad (6.5b)$$

$$C_{P,l} \dot{p}_{P,l} = q_{P,l} - q_l, \quad (6.5c)$$

with $q_l, p_{P,l}, q_{P,l}, p_i \geq 0$, $u_{P,l} \in \mathbb{R}$, $u_{v,l} : (0, 1] \rightarrow [1, \infty)$, parameters $J_l, R_{P,l}, J_{P,l}, C_{P,l} > 0$, elements of the incidence matrix b_{il} (see (1.1)), and continuously differentiable, strictly increasing functions $\lambda_l : \mathbb{R} \rightarrow \mathbb{R}$, $\lambda_l(0) = 0$ (see Property 6.1) and $\tilde{\mu}_l : \mathbb{R} \rightarrow \mathbb{R}$, $\tilde{\mu}_l(0) = 0$ (see (6.2b)).

Remark 6.5. In case a given DGU comprises a pressure holding unit, it is represented by the black generalized voltage source $p_{P,l}$ shown in Figure 6.9. The capacitances C_i and C_j model any volume storage effect, e.g., due to hydraulic elasticity of the components in the DGU circulation

circuit, particularly of the heat exchanger [Stræde, 1995; Boysen and Thorsen, 2003]. To avoid dependent storages and thus dependent states, it is assumed that C_i is lumped with $C_{P,i}$ of the pressure holding (see Figure 6.5). Furthermore, to clearly describe the network interconnection among all the subsystems in the DHN via the incidence matrix as in (3.1e), the pressure holding unit and the capacitances are viewed as nodes of the DHN digraph. Their models are elaborated in Section 6.1.4.

Consumer Model

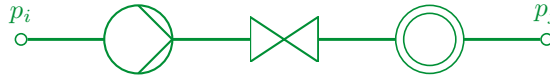


Figure 6.10: Hydraulic schematic of a consumer $l \in \mathcal{L}$ with optional pump.

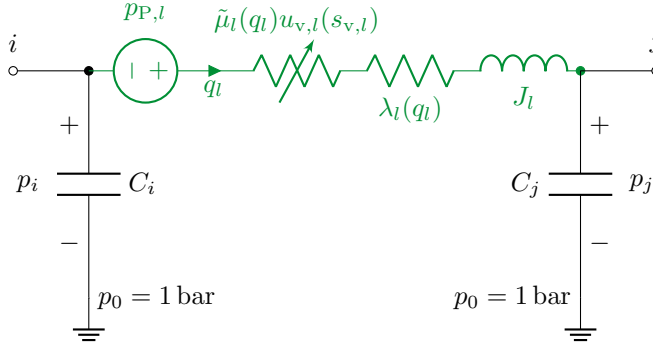


Figure 6.11: Equivalent circuit of the hydraulic model of a consumer $l \in \mathcal{L}$ with optional pump pp,l (green); $i, j \in \mathcal{V}, i \neq j$.

Most of nowadays consumers are connected indirectly to a DHN via heat exchangers in series with pipes and a control valve for volume flow rate control [Nussbaumer et al., 2020, pp. 87,143]. In future DHNs, however, additional pumps are expected to be included in some (up to all) consumer circuits as illustrated in Figure 6.10: either for pressure boosting to ensure a proper functioning of the control valves under unclear and changing hydraulic conditions (see Remark 6.3, De Persis and Kallesøe [2011], and Lund et al. [2014]) or in DHNs operated with DVSPs [Yan et al., 2013; Wang et al., 2017a; Gong et al., 2019]. Consequently, the hydraulic consumer circuit at an edge $l \in \mathcal{L}$ is modeled similarly to the hydraulic DGU circulation circuit (compare the green part in Figures 6.9 and 6.11). The only differences are on the working direction of the pump and the sign convention of the volume flow rate, which is reflected in the edge orientation in the DHN digraph (see Figure 6.2 and Nussbaumer et al. [2020, pp. 87,143]). Similar to the DGU model (see Remark 6.5), the capacitances C_i and C_j are considered to be part of the set of nodes \mathcal{V} . Furthermore, pressure holding units are typically not installed at

consumers. By applying KVL and KCL to Figure 6.11, the dynamics for each consumer $l \in \mathcal{L}$ follow as in (6.5).

Remark 6.6. Any consumer $l \in \mathcal{L}$ without a pump can be modeled by (6.5) by fixing $u_{P,l} = p_{P,l} = 0$ and removing the part corresponding to the dynamics of $q_{P,l}$ and $p_{P,l}$. Such consumers regulate their volume flow rate q_l through their respective control valve with control input $u_{v,l}$.

Mixing Connection Model

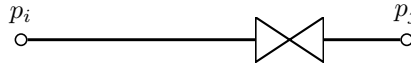


Figure 6.12: Hydraulic schematic of a mixing connection $l \in \mathcal{M}$.

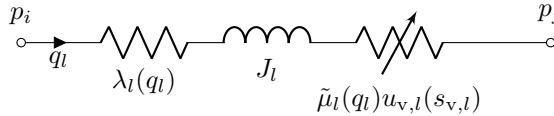


Figure 6.13: Equivalent circuit of the hydraulic model of a mixing connection $l \in \mathcal{M}$; $i, j \in \mathcal{V}$, $i \neq j$.

As outlined in Section 6.1.1, future DHNs may have a topology with three temperature layers. In order to guarantee sufficient heat supply of the low-temperature sections, the medium-temperature water is typically mixed with high-temperature water via a mixing connection before it is fed into the low-temperature section (see, e.g., node 7 in Figure 6.2) [Köfinger et al., 2017; Volkova et al., 2020, 2022]. The hydraulic schematic of a mixing connection at an edge $l \in \mathcal{M}$ is illustrated in Figure 6.12 and comprises a pipe in series with a control valve. The corresponding equivalent circuit is given in Figure 6.13. By applying KVL to Figure 6.13, the dynamic equation for each mixing connection $l \in \mathcal{M}$ follows as

$$J_l \dot{q}_l = -\lambda_l(q_l) - \tilde{\mu}_l(q_l)u_{v,l}(s_{v,l}) - \sum_{i \in \mathcal{V}} b_{il}p_i, \quad (6.6)$$

with $q_l, p_i \geq 0$, $u_{v,l} : (0, 1] \rightarrow [1, \infty)$, parameter $J_l > 0$, elements of the incidence matrix b_{il} (see (1.1)), and continuously differentiable, strictly increasing functions $\lambda_l : \mathbb{R} \rightarrow \mathbb{R}$, $\lambda_l(0) = 0$ (see Property 6.1) and $\tilde{\mu}_l : \mathbb{R} \rightarrow \mathbb{R}$, $\tilde{\mu}_l(0) = 0$ (see (6.2b)). Note that as with the pipe model, any kind of volume storage is modeled by a capacitance C_i and C_j at the source and target node, respectively (see Section 6.1.4).

6.1.4 Subsystems on Nodes

In this section, the hydraulic models of the pressure holding units \mathcal{H} and capacitors \mathcal{C} on the nodes $\mathcal{V} = \mathcal{H} \cup \mathcal{C}$ of the DHN diagram are presented.

Pressure Holding Model

Pressure holding units are realized technically in two ways: dynamic pressure holding with a pressure dictation pump, and static pressure holding with a closed vessel [Nussbaumer et al., 2020, pp. 54–56]. In both cases, pressure holding units are almost exclusively installed on the suction side of circulation pumps (pre-pressure control) (see Figure 6.9) and are instrumental in avoiding pipe bursts or damaging equipment, e.g., by cavitation in the circulation pumps [Sommer et al., 2019]; [Nussbaumer et al., 2020, pp. 54–55]; [Buffa et al., 2021, Figure 1].

Dynamic pressure holding is typically conducted in larger DGUs with powerful circulation pumps. It is realized by a pressure dictation pump located between a pressurized container and the DHN [Nussbaumer et al., 2020, pp. 54–55]; [Buffa et al., 2021, Figure 1]. As outlined in Section 6.1.2, the dynamics of any pump are approximated within this thesis by the linear second-order system (6.1). Thus, the case in which a dynamic pressure holding unit is installed at a DGU $l \in \mathcal{D}$ is equivalent to replacing the black generalized voltage source in Figure 6.9 by the RLC equivalent circuit in Figure 6.5. Note that in contrast to the circulation pump, which is coupled with the circulation circuit (green part in Figure 6.9), the black generalized voltage source already represents the entire pressure holding unit. That is, the dictation pump is assumed to be lumped together with the pressurized container.

The dynamics for each pressure holding unit $i \in \mathcal{H}$ are thus similar to (6.1) and given by

$$\begin{aligned} J_{P,i} \dot{q}_{P,i} &= -p_{P,i} - R_{P,i} q_{P,i} + u_{P,i}, \\ C_{P,i} \dot{p}_{P,i} &= q_{P,i} + \sum_{l \in \mathcal{E}} b_{il} q_l, \end{aligned} \quad (6.7)$$

with $p_{P,i} \geq 0$, $q_{P,i}, u_{P,i}, q_l \in \mathbb{R}$, parameters $R_{P,i}, J_{P,i}, C_{P,i} > 0$, and elements of the incidence matrix b_{il} (see (1.1)).

Static pressure holding is installed in smaller DGUs with compact circulation pumps. It is realized by directly adding a closed, pressurized vessel. From an equivalent circuit perspective, this can be understood as a preloaded capacitance. Thus, in case of static pressure holding, the black generalized voltage source in Figure 6.9 is replaced with a capacitance. To avoid dependent storages and thus dependent states, this capacitance is assumed to be lumped with C_i (see also the power line models in Sections 4.1.3 and 5.1.3). Consequently, the case of static pressure holding is not considered further in the following.

Remark 6.7. *The presented DHN model allows for pressure holding units to be installed at the suction side of each DGU $l \in \mathcal{D}$. In practice, however, it is typically sufficient to operate only one of them at any given time (see, e.g., Nussbaumer et al. [2020, p. 55], Buffa et al. [2021, Figure 1], and Figure 6.2). This is due to the fact that in a connected and closed hydraulic*

network, the pressure values at each node $i \in \mathcal{V}$ are uniquely determined by fixing one node pressure value and expressing all edge subsystems by means of differential pressure dynamics as done in Section 6.1.3 (see, e.g., Krug et al. [2021, Section 2.3]).

Capacitor Node Model

The capacitances C_i arising from volume storage in the DGU circuits, consumer circuits, and pipes are viewed as nodes $i \in \mathcal{C}$ of the DHN digraph. From KCL, the dynamic equation for each capacitor node $i \in \mathcal{C}$ follows as

$$C_i \dot{p}_i = \sum_{l \in \mathcal{E}} b_{il} q_l, \quad (6.8)$$

with $p_i \geq 0$, $q_l \in \mathbb{R}$, parameter $C_i > 0$, and elements of the incidence matrix b_{il} (see (1.1)).

6.1.5 Port-Hamiltonian System Representation

In this section, it is shown that the subsystem models from Sections 6.1.3 and 6.1.4 can be written as ISO-PHS models of the form (3.9). For the subsequent stability analysis and control designs, this gives a clear perspective on which input-output ports are accessible—or are convenient for control—and over which ports subsystems interact with each other. Furthermore, the passivity properties with respect to these ports and the Hamiltonian as a storage function are directly visible. In particular, since the Hamiltonians are quadratic functions, their shifted versions directly qualify as positive definite storage functions for proving EIP (see Lemma 3.1).

Pumps (6.1) and pressure holding units (6.7) The ISO-PHS model is given by (3.9) with state and co-state

$$\mathbf{x}_k = \begin{bmatrix} J_{P,k} q_{P,k} \\ C_{P,k} p_{P,k} \end{bmatrix}, \quad \frac{\partial H_k}{\partial \mathbf{x}_k}(\mathbf{x}_k) = \begin{bmatrix} q_{P,k} \\ p_{P,k} \end{bmatrix}, \quad (6.9a)$$

control port pair

$$u_k = u_{P,k}, \quad y_k = q_{P,k}, \quad (6.9b)$$

uncontrolled interaction (coupling) port pair

$$d_k = -q_k, \quad z_k = p_{P,k}, \quad (6.9c)$$

and matrices

$$\mathbf{J}_k = \begin{bmatrix} 0 & -1 \\ 1 & 0 \end{bmatrix}, \quad \mathbf{R}_k = \begin{bmatrix} R_{P,k} & 0 \\ 0 & 0 \end{bmatrix}, \quad \mathbf{G}_k = \begin{bmatrix} 1 \\ 0 \end{bmatrix}, \quad \mathbf{K}_k = \begin{bmatrix} 0 \\ 1 \end{bmatrix}, \quad (6.9d)$$

$$\mathbf{Q}_k = \text{diag} \left(\frac{1}{J_{P,k}}, \frac{1}{C_{P,k}} \right)$$

For pressure holding units (6.7) replace the index k with i .

Pipes (6.4) The ISO-PHS model is given by (3.9) with state and co-state

$$\mathbf{x}_l = \begin{bmatrix} J_l q_l \\ J_{P,l} q_{P,l} \\ C_{P,l} p_{P,l} \end{bmatrix}, \quad \frac{\partial H_l}{\partial \mathbf{x}_l}(\mathbf{x}_l) = \begin{bmatrix} q_l \\ q_{P,l} \\ p_{P,l} \end{bmatrix}, \quad (6.10a)$$

control port pair

$$u_l = u_{P,l}, \quad y_l = q_{P,l}, \quad (6.10b)$$

uncontrolled interaction (coupling) port pair

$$d_l = - \sum_{i \in \mathcal{V}} b_{il} p_i, \quad z_l = q_l, \quad (6.10c)$$

matrices

$$\mathbf{J}_l = \begin{bmatrix} 0 & 0 & 1 \\ 0 & 0 & -1 \\ -1 & 1 & 0 \end{bmatrix}, \quad \mathbf{R}_l = \begin{bmatrix} 0 & 0 & 0 \\ 0 & R_{P,l} & 0 \\ 0 & 0 & 0 \end{bmatrix}, \quad \mathbf{G}_l = \begin{bmatrix} 0 \\ 1 \\ 0 \end{bmatrix}, \quad \mathbf{K}_l = \begin{bmatrix} 1 \\ 0 \\ 0 \end{bmatrix}, \quad (6.10d)$$

$$\mathbf{Q}_l = \text{diag} \left(\frac{1}{J_l}, \frac{1}{J_{P,l}}, \frac{1}{C_{P,l}} \right)$$

and nonlinear damping function

$$\mathcal{R}_l \left(\frac{\partial H_l}{\partial \mathbf{x}_l}(\mathbf{x}_l) \right) = \begin{bmatrix} \lambda_l(q_l) \\ 0 \\ 0 \end{bmatrix}. \quad (6.10e)$$

DGUs and consumers (6.5) The ISO-PHS model is given by (3.9) with state and co-state

$$\mathbf{x}_l = \begin{bmatrix} J_l q_l \\ J_{P,l} q_{P,l} \\ C_{P,l} p_{P,l} \end{bmatrix}, \quad \frac{\partial H_l}{\partial \mathbf{x}_l}(\mathbf{x}_l) = \begin{bmatrix} q_l \\ q_{P,l} \\ p_{P,l} \end{bmatrix}, \quad (6.11a)$$

control port pair

$$\mathbf{u}_l = \begin{bmatrix} u_{v,l} \\ u_{P,l} \end{bmatrix}, \quad y_l = \begin{bmatrix} -\tilde{\mu}_l(q_l) q_l \\ q_{P,l} \end{bmatrix}, \quad (6.11b)$$

uncontrolled interaction (coupling) port pair

$$d_l = - \sum_{i \in \mathcal{V}} b_{il} p_i, \quad z_l = q_l, \quad (6.11c)$$

matrices

$$\mathbf{J}_l = \begin{bmatrix} 0 & 0 & 1 \\ 0 & 0 & -1 \\ -1 & 1 & 0 \end{bmatrix}, \quad \mathbf{R}_l = \begin{bmatrix} 0 & 0 & 0 \\ 0 & R_{P,l} & 0 \\ 0 & 0 & 0 \end{bmatrix}, \quad \mathbf{G}_l(\mathbf{x}_l) = \begin{bmatrix} -\tilde{\mu}_l(q_l) & 0 \\ 0 & 1 \\ 0 & 0 \end{bmatrix}, \quad \mathbf{K}_l = \begin{bmatrix} 1 \\ 0 \\ 0 \end{bmatrix},$$

$$\mathbf{Q}_l = \text{diag} \left(\frac{1}{J_l}, \frac{1}{J_{P,l}}, \frac{1}{C_{P,l}} \right) \quad (6.11d)$$

and nonlinear damping function

$$\mathcal{R}_l \left(\frac{\partial H_l}{\partial \mathbf{x}_l}(\mathbf{x}_l) \right) = \begin{bmatrix} \lambda_l(q_l) \\ 0 \\ 0 \end{bmatrix}. \quad (6.11e)$$

Mixing connections (6.6) The ISO-PHS model is given by (3.9) with state and co-state

$$x_l = J_l q_l, \quad \frac{\partial H_l}{\partial x_l}(x_l) = q_l, \quad (6.12a)$$

control port pair

$$u_l = u_{v,l}, \quad y_l = -\tilde{\mu}_l(q_l) q_l, \quad (6.12b)$$

uncontrolled interaction (coupling) port pair

$$d_l = - \sum_{i \in \mathcal{V}} b_{il} p_i, \quad z_l = q_l, \quad (6.12c)$$

scalars (instead of matrices)

$$\mathbf{J}_l = 0, \quad \mathbf{R}_l = R_l, \quad \mathbf{G}_l(x_l) = -\tilde{\mu}_l(q_l), \quad \mathbf{K}_l = 1, \quad \mathbf{Q}_l = \frac{1}{J_l}, \quad (6.12d)$$

and nonlinear damping function

$$\mathcal{R}_l \left(\frac{\partial H_l}{\partial x_l}(x_l) \right) = \lambda_l(q_l). \quad (6.12e)$$

Capacitor nodes (6.8) The ISO-PHS model is given by (3.9) with state and co-state

$$x_i = C_i p_i, \quad \frac{\partial H_i}{\partial x_i}(x_i) = p_i, \quad (6.13a)$$

uncontrolled interaction (coupling) port pair

$$d_i = \sum_{l \in \mathcal{V}} b_{il} q_l, \quad z_i = p_i, \quad (6.13b)$$

and scalars (instead of matrices)

$$\mathbf{J}_i = 0, \quad \mathbf{R}_i = R_i, \quad \mathbf{G}_i = 0, \quad \mathbf{K}_i = 1, \quad \mathbf{Q}_i = \frac{1}{C_i}. \quad (6.13c)$$

6.1.6 Interconnection Structure

The interconnection of the pressure holding and capacitor subsystems on the nodes $i \in \mathcal{V}$ with the DGU, consumer, pipe, and mixing connection subsystems on the edges $l \in \mathcal{E}$ is clearly defined by the interaction (coupling) ports (6.9c), (6.10c), (6.11c), (6.12c), and (6.13b) arising from their respective PHS representations. In particular, it holds that

$$d_i = \sum_{l \in \mathcal{E}} b_{il} q_l = \sum_{i \in \mathcal{V}} b_{il} z_l, \quad (6.14a)$$

$$d_l = - \sum_{i \in \mathcal{V}} b_{il} p_i = - \sum_{i \in \mathcal{V}} b_{il} z_i, \quad (6.14b)$$

and (cf. (3.1e))

$$\begin{bmatrix} \mathbf{d}_{\mathcal{V}} \\ \mathbf{d}_{\mathcal{E}} \end{bmatrix} = \begin{bmatrix} \mathbf{0}_{|\mathcal{V}| \times |\mathcal{V}|} & \mathbf{B} \\ -\mathbf{B}^T & \mathbf{0}_{|\mathcal{E}| \times |\mathcal{E}|} \end{bmatrix} \begin{bmatrix} \mathbf{z}_{\mathcal{V}} \\ \mathbf{z}_{\mathcal{E}} \end{bmatrix} =: \mathbf{M} \begin{bmatrix} \mathbf{z}_{\mathcal{V}} \\ \mathbf{z}_{\mathcal{E}} \end{bmatrix}, \quad (6.15)$$

with $(\cdot)_{\mathcal{V}} = \text{stack}((\cdot)_i)_{i \in \mathcal{V}}$ and $(\cdot)_{\mathcal{E}} = \text{stack}((\cdot)_l)_{l \in \mathcal{E}}$ denoting the respective, stacked vectors of the subsystems.

6.2 Asymptotic Stability Conditions and Control Problems

With the DHN formalized as a digraph and its model established, research questions (Q3.2) and (Q3.3) can now formally be addressed. Firstly, in Section 6.2.1, decentralized asymptotic stability conditions are derived by application of Theorem 3.1 and Corollary 3.1. Subsequently, in Section 6.2.2, the unactuated DHN subsystems are shown to fulfill the derived, decentralized stability conditions. Lastly, in Section 6.2.3, the remaining control problems for the actuated DHN subsystems are formulated. Their solution in Section 6.3 will provide answers to research question (Q3.3).

6.2.1 Decentralized Asymptotic Stability Conditions

The DHN model outlined in Section 6.1 is similar to that of an autonomous, networked system given in Definition 3.1. So far, however, the control ports (u_k, y_k) associated with the actuated subsystems $k \in \mathcal{D} \cup \mathcal{L} \cup \mathcal{P}_{\text{boost}} \cup \mathcal{M} \cup \mathcal{H}$ (see Section 6.1.5) are open, i.e., the models are of the form (3.2). In order to conduct an equilibrium stability analysis, it is thus assumed that each actuated subsystem is in closed loop with some pump and/or valve controller, respectively (see Remark 3.2).

Then, by direct application of Theorem 3.1 and Corollary 3.1 to the now autonomous DHN model, decentralized, analytical conditions can be obtained, which, if satisfied, ensure asymptotic stability of any feasible, hydraulic DHN equilibrium $\bar{x}_{\text{DHN}} =$

$\text{stack}(\bar{\mathbf{x}}_k)_{k \in \mathcal{V} \cup \mathcal{E}}$. The vectors $\bar{\mathbf{x}}_k$ are the respective equilibrium state vectors of the subsystems that are proportional to the steady-state pressures and volume flow rates of the DHN (cf. (6.10a), (6.11a), (6.12a), (6.9), (6.13a)).⁴⁷

Theorem 6.1 (Decentralized, asymptotic stability conditions for DHNs)

Consider an autonomous DHN as described in Section 4.1 with some controller u_k at each subsystem $k \in \mathcal{D} \cup \mathcal{L} \cup \mathcal{P}_{\text{boost}} \cup \mathcal{M} \cup \mathcal{H}$ which is actuated with a pump and/or a valve. Any feasible, hydraulic equilibrium $\bar{\mathbf{x}}_{\text{DHN}} = \text{stack}(\bar{\mathbf{x}}_k)_{k \in \mathcal{V} \cup \mathcal{E}}$ of such an autonomous DHN is asymptotically stable, if the following two conditions hold:

(DHN 1) each subsystem at a node $i \in \mathcal{V}$ is

- strictly EIP w.r.t. the supply rate $(d_i - \bar{d}_i)(z_i - \bar{z}_i)$ and a continuously differentiable, positive definite storage function $S_i(\mathbf{x}_i, \bar{\mathbf{x}}_i)$, or
- EIP w.r.t. the supply rate $(d_i - \bar{d}_i)(z_i - \bar{z}_i)$ and a continuously differentiable, positive definite storage function $S_i(\mathbf{x}_i, \bar{\mathbf{x}}_i)$, and such that no solution other than $\mathbf{x}_i(t) = \bar{\mathbf{x}}_i$ can stay in $\mathbb{E}_i = \{\mathbf{x}_i \in \mathcal{X}_i \subseteq \mathbb{R}^{n_i} \mid \dot{S}_i(\mathbf{x}_i, \bar{\mathbf{x}}_i) = 0, d_i = \bar{d}_i\}$ for all time.

(DHN 2) each subsystem at an edge $l \in \mathcal{E}$ is

- strictly EIP w.r.t. the supply rate $(d_l - \bar{d}_l)(z_l - \bar{z}_l)$ and a continuously differentiable, positive definite storage function $S_l(\mathbf{x}_l, \bar{\mathbf{x}}_l)$, or
- OSEIP w.r.t. the supply rate $(d_l - \bar{d}_l)(z_l - \bar{z}_l)$ and a continuously differentiable, positive definite storage function $S_l(\mathbf{x}_l, \bar{\mathbf{x}}_l)$, and either EIO or such that no solution other than $\mathbf{x}_l(t) = \bar{\mathbf{x}}_l$ can stay in $\mathbb{E}_l = \{\mathbf{x}_l \in \mathcal{X}_l \subseteq \mathbb{R}^{n_l} \mid \dot{S}_l(\mathbf{x}_l, \bar{\mathbf{x}}_l) = 0, d_l = \bar{d}_l\}$ for all time.

Proof:

The proof follows directly by application of Theorem 3.1 and Corollary 3.1 to the DHN model established in Section 4.1 with some controller u_k at each subsystem $k \in \mathcal{D} \cup \mathcal{L} \cup \mathcal{P}_{\text{boost}} \cup \mathcal{M} \cup \mathcal{H}$. \square

The conditions (DHN 1) and (DHN 2) of Theorem 6.1 answer research question (Q3.2). Next, it has to be ensured that the DHN subsystems modeled in Section 6.1 fulfill the respective conditions.

⁴⁷ Note that $\bar{\mathbf{x}}_k$ for $k \in \mathcal{D} \cup \mathcal{L} \cup \mathcal{P}_{\text{boost}} \cup \mathcal{M} \cup \mathcal{H}$ possibly implies a slight abuse of notation as in the case of dynamic controllers the original state vectors \mathbf{x}_k are augmented by additional controller states.

6.2.2 Properties of the Unactuated Systems

For the unactuated subsystems without control ports, i.e, capacitor nodes $i \in \mathcal{C}$ (see (6.13)) and pipe edges without booster pumps $l \in \mathcal{P} \setminus \mathcal{P}_{\text{boost}}$ (see (6.10) and Remark 6.4), requirements on the model parameters have to be established such that conditions (DHN 1) and (DHN 2) are met.

Capacitor Nodes

The capacitor node models (6.8) can be represented as linear ISO-PHSs with constant matrices (see (6.13)). According to Lemma 3.1, the capacitor node subsystem (6.8) is thus EIP w.r.t. the supply rate $(d_i - \bar{d}_i)(z_i - \bar{z}_i)$ and the shifted Hamiltonian as continuously differentiable, positive definite storage function $S_i(x_i, \bar{x}_i) = \frac{1}{2C_i} \|x_i - \bar{x}_i\|^2$, $\bar{x}_i = C_i \bar{p}_i$.

Next, it is shown that no solution other than \bar{x}_i can stay in $\mathbb{E}_i = \{x_i \in \mathcal{X}_i \subseteq \mathbb{R} \mid \dot{S}_i(x_i, \bar{x}_i) = 0, d_i = \bar{d}_i\}$ for all time. For $d_i = \bar{d}_i$, it directly follows from (6.8) that $C_i \dot{p}_i = 0$, implying $p_i \equiv \bar{p}_i$ and $x_i \equiv \bar{x}_i$, respectively. Thus, the capacitor node models (6.8) fulfill condition (DHN 1) for all model parameters.

Pipes without Booster Pumps

The model of each pipe $l \in \mathcal{P} \setminus \mathcal{P}_{\text{boost}}$ without booster pumps is given by (see Remark 6.4)

$$\underbrace{J_l \dot{q}_l}_{\dot{x}_l} = - \underbrace{\lambda_l(q_l)}_{\mathcal{R}_l(x_l)} - \underbrace{\sum_{i \in \mathcal{V}} b_{il} p_i}_{d_l}, \quad (6.16a)$$

$$z_l = q_l, \quad (6.16b)$$

$$H_l(x_l) = \frac{1}{2J_l} x_l^2. \quad (6.16c)$$

The model (6.16) constitutes an ISO-PHS of the form (3.9) with strictly increasing, nonlinear damping function $\mathcal{R}_l(x_l)$ (see Property 6.1) and $G(x) = G = 0$. According to Lemma 3.1, (6.16) is thus strictly EIP w.r.t. the supply rate $(d_i - \bar{d}_i)(z_i - \bar{z}_i)$ and the shifted Hamiltonian as continuously differentiable, positive definite storage function $S_l(x_l, \bar{x}_l) = \frac{1}{2J_l} \|x_l - \bar{x}_l\|^2$, $\bar{x}_l = J_l \bar{p}_l$. Consequently, the models of pipes without booster pumps fulfill condition (DHN 2) for all model parameters.

6.2.3 Control Problems

For the actuated DHN subsystems $k \in \mathcal{D} \cup \mathcal{L} \cup \mathcal{P}_{\text{boost}} \cup \mathcal{M} \cup \mathcal{H}$, decentralized controllers for the pumps and/or valves are to be designed such that the closed-loop systems fulfill (DHN 1) and (DHN 2), respectively. Furthermore, the respective closed-loop equilibrium state vectors \tilde{x}_k should be such that desired pressures $\bar{p}_{P,k} = p_{P,k}^*$ and volume flow rates $\bar{q}_k = q_k^*$ are established in steady state (see research question (Q3.3)).

In the following, the individual control problems for each of the actuated subsystems are specified and subsequently summarized in Problem 6.1.

DGUs DGUs $l \in \mathcal{D}$ may operate in two modes: pressure-controlled or volume flow rate-controlled. From a generalized modeling perspective, these modes are similar to grid-forming voltage control and grid-feeding current control of DGUs in electrical power systems (cf. Table A.1). To highlight this similarity, the *grid-forming* and *grid-feeding* terminology from electrical power systems is used in the following to describe the operating modes of DGUs in a DHN.⁴⁸

DGUs in grid-forming mode $l \in \mathcal{D}_{\text{form}}$ actively form the hydraulic conditions required to operate DHNs by regulating the differential pressure generated by their circulation pumps to desired setpoints $p_{P,l}^*$ [Nussbaumer et al., 2020, pp. 47–48]. In this case, the control valves in their circulation circuits are fully open, i.e., $\bar{u}_{v,l} = u_{v,l}(s_{v,l} = 1)$ (see (6.2)). DGUs in grid-feeding mode $l \in \mathcal{D}_{\text{valve}} \subseteq \mathcal{D}_{\text{feed}}$ regulate the volume flow rate through their circulation circuits to desired setpoints q_l^* by means of their control valves. Under approximately constant water temperature, this is equivalent to controlling the thermal energy they feed into a DHN (see Lennermo et al. [2014], Lennermo et al. [2019], and Krug et al. [2021, Section 2.3]). Note that for a proper functioning of the control valve, the circulation pump still introduces some differential pressure $p_{P,l}^*$, which is then throttled by the control valve such that the desired volume flow rate q_l^* is reached.

Consumers Consumers $l \in \mathcal{L}$ regulate the thermal energy they consume by controlling their volume flow rates to desired setpoints q_l^* [Li et al., 2017, p. 29]; [Nussbaumer et al., 2020, pp. 143–145, 151]. Traditionally, this volume flow rate control is conducted by control valves only. The set of consumers for which $u_{v,l}(s_{v,l})$ is the main control input is thus denoted by $\mathcal{L}_{\text{valve}} \subseteq \mathcal{L}$. However, as discussed in Section 6.1.3, booster pumps might be added to some consumer circuits. These consumers are identified by the set $\mathcal{L}_{\text{boost}} \subseteq \mathcal{L}$. In each consumer $l \in \mathcal{L}_{\text{boost}}$, the pump pressure is controlled

⁴⁸ Although this perspective is not yet established in the DHN community, hints regarding this parallel can already be found in the literature. Lennermo et al. [2014] and Lennermo et al. [2019], for example, compare the principle of regulating the heat power in feed of decentralized solar-thermal power plants via the fed-in volume flow rate with that of photovoltaic power plants that operate in grid-feeding mode.

to some desired setpoint $p_{P,l}^*$, which is then throttled by the control valve such that the desired volume flow rate q_l^* is reached.

Remark 6.8. *In some DHN setups with DVSPs (see, e.g., Yan et al. [2013] and Wang et al. [2017a]), it is suggested to directly conduct the volume flow rate control in grid-feeding DGUs $l \in \mathcal{D}_{\text{VSP}} \subseteq \mathcal{D}_{\text{feed}}$ and consumers $l \in \mathcal{L}_{\text{VSP}} \subseteq \mathcal{L}$ by pumps without including any control valves in the respective hydraulic circuits (cf. Figures 6.9 and 6.11). Gong et al. [2019] propose a hybrid DVSP setup in which all DGUs and some consumers have only pumps, while some consumers have only control valves. Consequently, it is apparent that depending on the topology and producer-consumer configuration, different hydraulic designs of DGU and consumer circuits might be beneficial. Thus, in this thesis, all possible combinations of designs (see Problem 6.1 below) are considered.*

Pipes For pipes $l \in \mathcal{P}$, as introduced in Remark 6.4, $\mathcal{P}_{\text{boost}} \subseteq \mathcal{P}$ denotes the subset of pipes that have a booster pump connected in series. These pumps are in charge of counteracting the differential pressure loss over the corresponding pipe by introducing a differential pressure $p_{P,l}^*$.

Mixing connections Mixing connections $l \in \mathcal{M}$ control their volume flow rates to desired setpoints q_l^* such that a desired mixing ratio of high- and medium-temperature water is achieved (see Section 6.1.3).

Pressure holding units Pressure holding units $i \in \mathcal{H}$ are located at the suction sides of DGUs $l \in \mathcal{D}$. Regardless of the operation mode of the DGU they are associated with, pressure holding units control the pressure at their nodes to desired setpoints $p_{P,i}^*$. This pressure also serves as the static pressure in a DHN (see Nussbaumer et al. [2020, p. 55] and Buffa et al. [2021, Figure 1]).

In summary, it can be seen that the control tasks amount to *pressure and volume flow rate control of pumps* and *volume flow rate control of valves* in the respective subsystems. Consequently, in order to achieve decentralized stabilization in DHNs as per Definition 2.5 and provide answers to research question (Q3.3), the following control problem is left to be addressed:

Problem 6.1 (Decentralized pressure and volume flow rate control)

Consider a DHN as described in Section 4.1. For the pump and/or control valve in each actuated subsystem $k \in \mathcal{D} \cup \mathcal{L} \cup \mathcal{P}_{\text{boost}} \cup \mathcal{M} \cup \mathcal{H}$, design decentralized controllers of the form

$$\dot{\mathbf{x}}_{c,k} = \mathbf{f}_{c,k}(\mathbf{x}_k, \mathbf{x}_{c,k}), \quad \mathbf{u}_k = \begin{bmatrix} u_{v,k} \\ u_{p,k} \end{bmatrix} = \hat{\mathbf{u}}_k(\mathbf{x}_k, \mathbf{x}_{c,k}), \quad (6.17)$$

with controller states $\mathbf{x}_{c,k} \in \mathbb{R}^2$ such that the resulting closed-loop system fulfills (DHN 1) or (DHN 2), respectively. Furthermore, the respective control inputs and the closed-loop equilibrium state vector $\tilde{\mathbf{x}}_k = [\tilde{\mathbf{x}}_k^\top, \tilde{\mathbf{x}}_{c,k}^\top]^\top$ shall fulfill the following characteristics:

- (a) For each DGU $l \in \mathcal{D}_{\text{form}}$, $u_{v,l}(s_{v,l} = 1) = 1 = \bar{u}_{v,l}$ is fixed and $u_{p,l}$ is such that $p_{p,l} = p_{p,l}^* > 0$ in $\tilde{\mathbf{x}}_l$.
- (b) For each DGU $l \in \mathcal{D}_{\text{valve}}$, $u_{v,l}$ and $u_{p,l}$ are such that $\bar{q}_l = q_l^* > 0$ and $p_{p,l} = p_{p,l}^* > 0$ in $\tilde{\mathbf{x}}_l$.
- (c) For each DGU $l \in \mathcal{D}_{\text{VSP}}$, $u_{v,l}(s_{v,l} = 1) = 1 = \bar{u}_{v,l}$ is fixed and $u_{p,l}$ is such that $\bar{q}_l = q_l^* > 0$ in $\tilde{\mathbf{x}}_l$.
- (d) For each consumer $l \in \mathcal{L}_{\text{boost}}$, $u_{v,l}$ and $u_{p,l}$ are such that $\bar{q}_l = q_l^* > 0$ and $p_{p,l} = p_{p,l}^* > 0$ in $\tilde{\mathbf{x}}_l$.
- (e) For each consumer $l \in \mathcal{L}_{\text{valve}}$, $u_{p,l} = 0$ and $u_{v,l}$ is such that $\bar{q}_l = q_l^* > 0$ in $\tilde{\mathbf{x}}_l$.
- (f) For each consumer $l \in \mathcal{L}_{\text{VSP}}$, $u_{v,l}(s_{v,l} = 1) = 1 = \bar{u}_{v,l}$ is fixed and $u_{p,l}$ is such that $\bar{q}_l = q_l^* > 0$ in $\tilde{\mathbf{x}}_l$.
- (g) For each pipe $l \in \mathcal{P}_{\text{boost}}$ with booster pump, $u_{p,l}$ is such that $p_{p,l} = p_{p,l}^* > 0$ in $\tilde{\mathbf{x}}_l$.
- (h) For each mixing connection $l \in \mathcal{M}$, $u_{v,l}$ is such that $\bar{q}_l = q_l^* > 0$ in $\tilde{\mathbf{x}}_l$.
- (i) For each pressure holding unit $i \in \mathcal{H}$, $u_{p,i}$ is such that $p_{p,i} = p_{p,i}^* > 0$ in $\tilde{\mathbf{x}}_i$.

Remark 6.9 (Notation). To avoid cluttering the notation, it is assumed that the valves in the circuits of DGUs $l \in \mathcal{D}_{\text{form}} \cup \mathcal{D}_{\text{VSP}}$ and consumers $l \in \mathcal{L}_{\text{VSP}}$ physically remain, but are fully open, i.e., $u_{v,l}(s_{v,l} = 1) = 1 = \bar{u}_{v,l}$ is fixed (see (6.2)).

Remark 6.10. In line with the hierarchical control structure discussed in Section 2.3.2, the setpoints $p_k^* > 0$, $k \in \mathcal{D}_{\text{form}} \cup \mathcal{D}_{\text{valve}} \cup \mathcal{L}_{\text{boost}} \cup \mathcal{P}_{\text{boost}} \cup \mathcal{H}$, and $q_k^* > 0$, $k \in \mathcal{D}_{\text{valve}} \cup \mathcal{D}_{\text{VSP}} \cup \mathcal{L} \cup \mathcal{M}$, are assumed to be known and specified by a higher-level control ensuring that these setpoints constitute feasible, hydraulic DHN equilibria $\tilde{\mathbf{x}}_{\text{DHN}}$ within the operational constraints. A preliminary analysis regarding the degrees of freedom in choosing the operating modes of the DHN subsystems outlined in Problem 6.1 can be found in Appendix C.1.

6.3 Passivity-Based Control Design

In this section, Problem 6.1 is addressed. Following a classical divide-and-conquer approach, firstly, the controllers for pumps and for valves in series with a pipe element are designed. Subsequently, these controllers are assigned to the respective models of the actuated subsystems $k \in \mathcal{D} \cup \mathcal{L} \cup \mathcal{P}_{\text{boost}} \cup \mathcal{M} \cup \mathcal{H}$.

6.3.1 Pressure Control of Pumps

Instrumental to solving Problem 6.1 is the ability to regulate the pressure $p_{P,k}$ of a given pump in each subsystem $k \in \mathcal{D}_{\text{form}} \cup \mathcal{D}_{\text{valve}} \cup \mathcal{L}_{\text{boost}} \cup \mathcal{P}_{\text{boost}} \cup \mathcal{H}$ towards a desired constant setpoint $p_{P,k}^*$. For the design of the pump pressure controller, recall that the pump model (6.1) constitutes a linear second-order system represented by a generalized RLC equivalent circuit (see Figure 6.5). The pump pressure $p_{P,k}$ is the actual output of the linear, second-order system, which constitutes the interaction output $z_k = p_{P,k}$ from a ISO-PHS model perspective (see (B.8c), (6.9c)). Consequently, the generalized results from Section B.2, i.e., the combined algebraic IDA and integral action design applied to linear, second-order systems, can be used for the pressure control design.

Proposition 6.1 (Pressure controller for pumps)

Consider a pump in open loop described by (6.1). Assign the control input $u_k = u_{P,k}$ as

$$Q_{I,k} \dot{r}_k = p_{P,k} - p_{P,k}^*, \quad (6.18a)$$

$$u_k = p_{P,k}^* + (R_{P,k} - \hat{R}_k)q_{P,k} - \hat{R}_k r_k + \frac{J_{P,k}}{Q_{I,k}}(p_{P,k}^* - p_{P,k}), \quad (6.18b)$$

where $p_{P,k}^* > 0$ is a desired pressure setpoint and $\hat{R}_k, Q_{I,k} > 0$ are control parameters. Then, with the change of coordinates from $q_{P,k}$ to

$$\chi_k := q_{P,k} + r_k, \quad (6.19)$$

the closed-loop system can be written as

$$\frac{d}{dt} \underbrace{\begin{bmatrix} J_{P,k} \chi_k \\ C_{P,k} p_{P,k} \\ Q_{I,k} r_k \end{bmatrix}}_{\mathbf{x}_k^P} = \underbrace{\begin{bmatrix} -\hat{R}_k \chi_k - (p_{P,k} - p_{P,k}^*) \\ \chi_k - r_k \\ p_{P,k} - p_{P,k}^* \end{bmatrix}}_{\mathbf{f}_k^P(\mathbf{x}_k^P)} + \underbrace{\begin{bmatrix} 0 \\ 1 \\ 0 \end{bmatrix}}_{\mathbf{K}_k^P} d_k, \quad (6.20a)$$

$$z_k = p_{P,k}. \quad (6.20b)$$

Moreover, (6.20) is EIP w.r.t. the supply rate $(d_k - \bar{d}_k)(z_k - \bar{z}_k)$ and the continuously differentiable, positive definite storage function

$$S_k^p = \frac{1}{2} \|\mathbf{x}_k^p - \bar{\mathbf{x}}_k^p\|_{\mathbf{Q}_k^p}, \quad (6.21a)$$

$$\mathbf{Q}_k^p = \text{diag} \left(\frac{1}{J_{P,k}}, \frac{1}{C_{P,k}}, \frac{1}{Q_{I,k}} \right) \quad (6.21b)$$

for any (feasible) equilibrium pair (\bar{d}_k, \bar{z}_k) and associated equilibrium state vector

$$\bar{\mathbf{x}}_k^p = [J_{P,k}\bar{\chi}_k, C_{P,k}p_{P,k}^*, Q_{I,k}\bar{r}_k]^\top. \quad (6.22)$$

Furthermore, no solution other than $\mathbf{x}_k^p = \bar{\mathbf{x}}_k^p$ as in (6.22) can stay in $\mathbb{E}_k = \{\mathbf{x}_k^p \in \mathcal{X}_k^p \subseteq \mathbb{R}^3 \mid \dot{S}_k^p(\mathbf{x}_k^p, \bar{\mathbf{x}}_k^p) = 0, d_k = \bar{d}_k\}$ for all time.

Proof:

The proof follows directly from Proposition B.1 by comparing (B.8) with (6.9) and substituting $K = 1, T_1 = J_{P,k}, T_2 = C_{P,k}, x_1 = J_{P,k}q_{P,k}, x_2 = C_{P,k}p_{P,k}, \frac{x_1}{T_1} = q_{P,k}, \frac{x_2}{T_2} = p_{P,k}$, and $2D\sqrt{\frac{T_1}{T_2}} = R_{P,k}$. \square

Remark 6.11. Note that the controller (6.18) is composed of a setpoint feedforward $p_{P,k}^*$, a static state feedback proportional to $q_{P,k}$ for damping assignment, and a PI term acting on the control error $p_{P,k}^* - p_{P,k}$ to ensure zero steady-state errors under parameter uncertainties and unknown, steady-state interaction inputs \bar{d} . All these building blocks are available as industrial standard, off-the-shelf control functions. However, in contrast to the current I_i in the DC voltage controller (4.26), the volume flow rate $q_{P,k}$ does not represent a measurable, physical quantity (see also Section 6.1.2). Thus, for a practical implementation, either the damping assignment has to be neglected, i.e., $\hat{R}_k = R_{P,k}$, or the variable $q_{P,k}$ has to be estimated.

6.3.2 Volume Flow Rate Control via Pumps

In each DGU or consumer subsystem $k \in \mathcal{D}_{VSP} \cup \mathcal{L}_{VSP}$, the volume flow rate q_k through the pipes of the circulation circuit has to be regulated via pumps to a desired constant setpoint q_k^* . In fact, the dynamics (6.5) of DGUs and consumers are, excluding the control valve, equivalent to the dynamics (6.4) of a pipe element in series with a pump. Thus, the following control design focuses on the model of a pump in series with a pipe element, i.e., (6.4), (6.10), but with d_k treated as an arbitrary external input.

Proposition 6.2 (Volume flow rate controller for pumps)

Consider a pump in open loop in series with a pipe element (see (6.4)). Assign the control input $u_k = u_{P,k}$ as

$$Q_{I,k}\dot{r}_k = q_k - q_k^*, \quad (6.23a)$$

$$u_k = -\bar{K}_{P,k}p_{P,k} - r_k, \quad (6.23b)$$

where $q_k^* > 0$ is a desired volume flow rate setpoint and $Q_{I,k}, K_{P,k}$ are control parameters satisfying

$$Q_{I,k} > 0, \quad 0 < Q_{I,k}(K_{P,k} + 1) - C_{P,k} =: \kappa_k^f. \quad (6.24)$$

Then, the closed-loop system can be written as

$$\frac{d}{dt} \underbrace{\begin{bmatrix} J_k q_k \\ J_{P,k} q_{P,k} \\ C_{P,k} p_{P,k} \\ Q_{I,k} r_k \end{bmatrix}}_{\mathbf{x}_k^f} = \underbrace{\begin{bmatrix} p_{P,k} - \lambda_k(q_k) \\ -p_{P,k} - R_{P,k} q_{P,k} - K_{P,k} p_{P,k} - r_k \\ q_{P,k} - q_k \\ q_k - q_k^* \end{bmatrix}}_{\mathbf{f}_k^f(\mathbf{x}_k^f)} + \underbrace{\begin{bmatrix} 1 \\ 0 \\ 0 \\ 0 \end{bmatrix}}_{\mathbf{K}_k^f} d_k, \quad (6.25a)$$

$$z_k = q_k. \quad (6.25b)$$

Moreover, (6.25) is OSEIP w.r.t. the supply rate $(d_k - \bar{d}_k)(z_k - \bar{z}_k)$ and the continuously differentiable, positive definite storage function

$$S_k^f = \frac{1}{2} \|\mathbf{x}_k^f - \bar{\mathbf{x}}_k^f\|_{\mathbf{Q}_k^f}, \quad (6.26a)$$

$$\mathbf{Q}_k^f = \begin{bmatrix} \frac{1}{J_k} & 0 & 0 & 0 \\ 0 & \frac{Q_{I,k}}{J_{P,k}\kappa_k^f} & 0 & 0 \\ 0 & 0 & \frac{1}{C_{P,k}} + \frac{1}{\kappa_k^f} & \frac{1}{\kappa_k^f} \\ 0 & 0 & \frac{1}{\kappa_k^f} & \frac{1}{\kappa_k^f} \end{bmatrix}, \quad (6.26b)$$

for any (feasible) equilibrium pair (\bar{d}_k, \bar{z}_k) and associated equilibrium state vector

$$\bar{\mathbf{x}}_k^f = [J_k q_k^*, J_{P,k} q_{P,k}^*, C_{P,k} \bar{p}_{P,k}, Q_{I,k} \bar{r}_k]^\top. \quad (6.27)$$

Furthermore, no solution other than $\mathbf{x}_k^f = \bar{\mathbf{x}}_k^f$ as in (6.27) can stay in $\mathbb{E}_k = \{\mathbf{x}_k^f \in \mathcal{X}_k^f \subseteq \mathbb{R}^4 \mid \dot{S}_k^f(\mathbf{x}_k^f, \bar{\mathbf{x}}_k^f) = 0, d_k = \bar{d}_k\}$ for all time.

Proof:

The proof is similar to that of Proposition 4.2. By combining (6.4) with the controller (6.23), the closed-loop system (6.25) follows directly.

To show that (6.25) is OSEIP, consider the time derivative of S_k^f , i.e.,

$$\dot{S}_k^f(\mathbf{x}_k^f, \bar{\mathbf{x}}_k^f) = \underbrace{(\mathbf{x}_k^f - \bar{\mathbf{x}}_k^f)^\top \mathbf{Q}_k^f (\mathbf{f}_k^f(\mathbf{x}_k^f) - \mathbf{f}_k^f(\bar{\mathbf{x}}_k^f))}_{-\psi_k^f(\mathbf{x}_k^f, \bar{\mathbf{x}}_k^f)} + \underbrace{(\mathbf{x}_k^f - \bar{\mathbf{x}}_k^f)^\top \mathbf{Q}_k^f \mathbf{K}_k^f}_{(z_k - \bar{z}_k)} (d_k - \bar{d}_k). \quad (6.28)$$

With (6.25) and (6.27), the dissipation rate can be written as

$$\psi_k^f(\mathbf{x}_k^f, \bar{\mathbf{x}}_k^f) = (q_k - q_k^*) (\lambda_k(q_k) - \lambda_k(q_k^*)) + 2 \frac{R_{P,k} Q_{I,k}}{\kappa_k^f} (q_{P,k} - \bar{q}_{P,k})^2 \quad (6.29a)$$

$$\stackrel{(6.25b)}{=} (z_k - z_k^*) (\lambda_k(z_k) - \lambda_k(z_k^*)) + 2 \frac{R_{P,k} Q_{I,k}}{\kappa_k^f} (q_{P,k} - \bar{q}_{P,k})^2. \quad (6.29b)$$

Since $\lambda_k(z_k)$ is strictly increasing (see Property 6.1) and (6.24) holds, the closed-loop system (6.25) is OSEIP w.r.t. the supply rate $(d_k - \bar{d}_k)(z_k - \bar{z}_k)$ and the continuously differentiable, positive definite storage function S_k^f as in (6.26) (see Definition 3.2).

From

$$\psi_k^f(\mathbf{x}_k^f, \bar{\mathbf{x}}_k^f) \equiv 0 \stackrel{(6.29)}{\implies} q_k \equiv q_k^*, q_{P,k} \equiv \bar{q}_{P,k} \equiv q_k^* \quad (6.30)$$

follows that the shifted dynamics of (6.25) confined to $\mathbb{E}_k = \{\mathbf{x}_k^f \in \mathcal{X}_k^f \subseteq \mathbb{R}^4 \mid \dot{S}_k^f(\mathbf{x}_k^f, \bar{\mathbf{x}}_k^f) = 0, d_k = \bar{d}_k\}$ are given by

$$\begin{aligned} 0 &= p_{P,k} - \bar{p}_{P,k}, \\ 0 &= -(1 + K_{P,k})(p_{P,k} - \bar{p}_{P,k}) - (r_k - \bar{r}_k), \\ C_{P,k} \dot{p}_{P,k} &= 0, \\ Q_{I,k} \dot{r}_k &= 0, \end{aligned} \quad (6.31)$$

whose unique solution is $p_{P,k} \equiv \bar{p}_{P,k}$, $r_k \equiv \bar{r}_k$. Thus, no solution other than $\bar{\mathbf{x}}_k^f$ as in (6.27) can stay in \mathbb{E}_k for all time. \square

Remark 6.12. Note that the controller (6.23) and particularly the structuring of the positive definite matrix \mathbf{Q}_k^f for the storage function in (6.26) is inspired by Nahata et al. [2020, Theorem 2], which provides an analytical solution to a similarly structured storage function (compare (4.44) and (6.26)).

6.3.3 Volume Flow Rate Control via Valves

Problem 6.1 also considers the regulation of volume flow rates q_k through DGUs, consumers, and mixing connections, $k \in \mathcal{D}_{\text{feed}} \cup \mathcal{L}_{\text{boost}} \cup \mathcal{L}_{\text{valve}} \cup \mathcal{M}$ via control valves. Similar to the volume flow rate control via pumps, the valve controller design is conducted by means of the model of a valve in series with a pipe element, i.e., (6.6) and (6.12), but with d_k treated as an arbitrary external input.

Proposition 6.3 (Volume flow rate controller for valves)

Consider a control valve in open loop in series with a pipe element (see (6.6)). Let

$$\hat{y}_{v,k} = -\tilde{\mu}_k(q_k)(q_k - q_k^*) \quad (6.32)$$

and assign the control input $u_k = u_{v,k}$ as

$$Q_{I,k}\dot{r}_k = -\hat{y}_{v,k}, \quad (6.33a)$$

$$u_k = -K_{P,k}\hat{y}_{v,k} + r_k, \quad (6.33b)$$

where $q_k^* > 0$ is a desired volume flow rate setpoint and $Q_{I,k}, K_{P,k} > 0$ are control parameters. Then, the closed-loop system can be written as

$$\frac{d}{dt} \underbrace{\begin{bmatrix} J_k q_k \\ Q_{I,k} r_k \end{bmatrix}}_{\mathbf{x}_k^v} = \underbrace{\begin{bmatrix} -\lambda_k(q_k) - \tilde{\mu}_k(q_k)(-K_{P,k}\hat{y}_{v,k} + r_k) \\ -\hat{y}_{v,k} \end{bmatrix}}_{\mathbf{f}_k^v(\mathbf{x}_k^v)} + \underbrace{\begin{bmatrix} 1 \\ 0 \end{bmatrix}}_{\mathbf{K}_k^v} d_k, \quad (6.34a)$$

$$z_k = q_k. \quad (6.34b)$$

Moreover, (6.25) is OSEIP w.r.t. the supply rate $(d_k - \bar{d}_k)(z_k - \bar{z}_k)$ and the continuously differentiable, positive definite storage function

$$S_k^v = \frac{1}{2} \|\mathbf{x}_k^v - \bar{\mathbf{x}}_k^v\|_{\mathbf{Q}_k^v}, \quad (6.35a)$$

$$\mathbf{Q}_k^v = \text{diag} \left(\frac{1}{J_k}, \frac{1}{Q_{I,k}} \right), \quad (6.35b)$$

for any (feasible) equilibrium pair (\bar{d}_k, \bar{z}_k) , and associated equilibrium state vector

$$\bar{\mathbf{x}}_k^v = \begin{cases} [J_k q_k^*, Q_{I,k} \bar{r}_k]^\top, & \bar{d}_k \neq 0, \\ [0, Q_{I,k} \bar{r}_k]^\top, & \bar{d}_k = 0. \end{cases} \quad (6.36)$$

Proof:

The proof is similar to that of Proposition 6.2. By combining (6.6) with the controller (6.33), the closed-loop system (6.34) follows directly. Furthermore, the equilibrium state vector $\bar{\mathbf{x}}_k^v$ in (6.36) follows directly from (6.34) in steady-state.

Next, by using the identity $\bar{u}_k = \bar{r}_k$ and adding and subtracting $\tilde{\mu}_k(q_k)\bar{r}_k$, (6.25) can equivalently be written as

$$\begin{aligned} J_k \dot{q}_k &= -(\lambda_k(q_k) - \lambda_k(\bar{q}_k)) + \tilde{\mu}_k(q_k)K_{P,k}\hat{y}_k - \tilde{\mu}_k(q_k)(r_k - \bar{r}_k) \\ &\quad - \bar{r}_k(\tilde{\mu}_k(q_k) - \tilde{\mu}_k(\bar{q}_k)) + (d_k - \bar{d}_k), \end{aligned} \quad (6.37a)$$

$$Q_{I,k}\dot{r}_k = \tilde{\mu}_k(q_k)(q_k - \bar{q}_k). \quad (6.37b)$$

with $\bar{q}_k = q_k^*$ for $\bar{d}_k \neq 0$ and $\bar{q}_k = 0$ for $\bar{d}_k = 0$. For the time derivative of S_k^v in (6.35a), it

holds that

$$\dot{S}_k^v(\mathbf{x}_k^v, \bar{\mathbf{x}}_k^v) = \underbrace{(\mathbf{x}_k^v - \bar{\mathbf{x}}_k^v)^\top \mathbf{Q}_k^v (\mathbf{f}_k^v(\mathbf{x}_k^v) - \mathbf{f}_k^v(\bar{\mathbf{x}}_k^v))}_{-\psi_k^v(\mathbf{x}_k^v, \bar{\mathbf{x}}_k^v)} + \underbrace{(\mathbf{x}_k^v - \bar{\mathbf{x}}_k^v)^\top \mathbf{Q}_k^v \mathbf{K}_k^v (d_k - \bar{d}_k)}_{(z_k - \bar{z}_k)}. \quad (6.38)$$

With (6.34), (6.36), and (6.37), the dissipation rate can be written as

$$\psi_k^v(\mathbf{x}_k^v, \bar{\mathbf{x}}_k^v) = (q_k - \bar{q}_k) (\lambda_k(q_k) - \lambda_k(\bar{q}_k)) + \bar{r}_k (q_k - \bar{q}_k) (\tilde{\mu}_k(q_k) - \tilde{\mu}_k(\bar{q}_k)) \quad (6.39a)$$

$$\stackrel{(6.34b)}{=} (z_k - \bar{z}_k) (\lambda_k(z_k) - \lambda_k(\bar{z}_k)) + \bar{r}_k (z_k - \bar{z}_k) (\tilde{\mu}_k(z_k) - \tilde{\mu}_k(\bar{z}_k)). \quad (6.39b)$$

Since $\lambda_k(z_k)$ and $\tilde{\mu}_k(z_k)$ are strictly increasing (see (6.2b) and Property 6.1) and $\bar{u}_{v,k} = \bar{r}_k > 0$ per definition (see Section 6.1.2), the closed-loop system (6.34) is OSEIP w.r.t. the supply rate $(d_k - \bar{d}_k)(z_k - \bar{z}_k)$ and the continuously differentiable, positive definite storage function S_k^v as in (6.35a) (see Definition 3.2). \square

Remark 6.13. *The design of the PI controller (6.33) is based on the observation that the dynamics of a control valve in series with a pipe element, i.e., (6.6) and (6.12), respectively, are EIP with respect to the supply rate $(u_{v,k} - \bar{u}_{v,k})(\hat{y}_k - \tilde{y}_k)$ and the continuously differentiable, positive definite storage function S_k^v in (6.35a). The definition of the output \hat{y}_k originates from the fact that the input matrix $G_k(\mathbf{x}_k)$ as in (6.12d) is state-dependent. This circumstance complicates the use of a standard PI controller around the shifted, natural passive output $y - \bar{y}$ (see also Arcak et al. [2016, p. 26], van der Schaft [2017, p. 137], and Monshizadeh et al. [2019]). Following Monshizadeh et al. [2019, Equation (8)], a new passive output \hat{y}_k as in (6.32) can be proposed, which is obtained from a suitable, shifted representation of the dynamics.*

As state in the proof above, $\hat{y}_k = 0$ allows for either $\bar{q}_k = q_k^*$ or $\bar{q}_k = 0$ (see (6.32) and (6.34)). However, $\bar{q}_k = 0$ implies $\lambda_k(0) = 0$, $\tilde{\mu}_k(0) = 0$ (see (6.2b) and Property 6.1) and thus $\bar{d}_k = 0$, where d_k is the pressure difference over the serial connection of valve and pipe element (cf. (6.6)). This makes sense from a practical perspective, as a control valve with zero differential pressure available is not functional. Since valves can only function as variable, nonlinear flow resistors, the assembly of control valve and pipe requires a sufficient positive differential pressure $d_k > 0$ to establish a desired volume flow rate setpoint $\bar{q}_k = q_k^*$ in steady state (see Remark 6.3). In practice, sufficient positive differential pressure is ensured by a proper assignment of the pump pressure setpoints $p_{P,k}^*$ via a higher-level control (see Remark 6.10), which motivates the following assumption:

Assumption 6.3 (Positive differential pressure for valves)

Any control valve in series with a pipe element has a positive differential pressure $d_l > 0$ for all time. This implies for DGUs and consumer circuits $l \in \mathcal{D} \cup \mathcal{L}$ that $p_i + p_{P,l} - p_j > 0$ (see (6.11c) and Figures 6.9 and 6.11) and for mixing connections $l \in \mathcal{M}$ that $p_i - p_j > 0$ (see (6.12c) and Figure 6.13).

6.3.4 Properties of the Closed-Loop Systems

In this section, the controlled pumps and valves from Propositions 6.1–6.3 are deployed in the corresponding actuated subsystems $k \in \mathcal{D} \cup \mathcal{L} \cup \mathcal{P}_{\text{boost}} \cup \mathcal{M} \cup \mathcal{H}$. It is shown that the resulting closed-loop systems fulfill the requirements set in Problem 6.1.

Proposition 6.4 (Properties of the closed-loop DHN subsystems)

Assign the pump controllers (6.18), (6.23), and the valve controller (6.33) to the respective edge and node subsystems $k \in \mathcal{D} \cup \mathcal{L} \cup \mathcal{P}_{\text{boost}} \cup \mathcal{M} \cup \mathcal{H}$ according to the control tasks in Problem 6.1. Then, the resulting closed-loop subsystems can be written as

$$\dot{\hat{\mathbf{x}}}_k = \hat{\mathbf{f}}_k(\hat{\mathbf{x}}_k) + \hat{\mathbf{K}}_k d_k, \quad (6.40a)$$

$$z_k = \hat{\mathbf{K}}_k^\top \hat{\mathbf{Q}}_k \hat{\mathbf{x}}_k, \quad (6.40b)$$

with appropriate vectors and matrices. For each actuated edge subsystem $k \in \mathcal{D} \cup \mathcal{L} \cup \mathcal{P}_{\text{boost}} \cup \mathcal{M}$, the closed loop (6.40) is OSEIP w.r.t. the supply rate $(d_k - \bar{d}_k)(z_k - \bar{z}_k)$ and the continuously differentiable, positive definite storage function

$$\hat{S}_k(\hat{\mathbf{x}}_k, \bar{\mathbf{x}}_k) = \frac{1}{2} \|\hat{\mathbf{x}}_k - \bar{\mathbf{x}}_k\|_{\hat{\mathbf{Q}}_k}^2, \quad (6.41)$$

where $\hat{\mathbf{Q}}_k$ is a suitable positive definite diagonal matrix, and $\bar{\mathbf{x}}_k$ is any (feasible) equilibrium value of $\hat{\mathbf{x}}_k$ with associated (\bar{d}_k, \bar{z}_k) . In addition, under Assumption 6.3, $\bar{\mathbf{x}}_k$ is such that $\bar{q}_k = \bar{q}_{\text{P},k} = q_k^*$ and $\bar{p}_{\text{P},k} = p_{\text{P},k}^*$ in accordance with Problem 6.1.

For each actuated node subsystem $k \in \mathcal{H}$, the closed loop (6.40) is EIP w.r.t. the supply rate $(d_k - \bar{d}_k)(z_k - \bar{z}_k)$, the continuously differentiable, positive definite storage function as in (6.41), and any (feasible) equilibrium value $\hat{\mathbf{x}}_k = \left[J_{\text{P},k} \bar{\chi}_k, C_{\text{P},k} p_{\text{P},k}^*, Q_{1,k} \bar{r}_k \right]^\top$ with associated (\bar{d}_k, \bar{z}_k) .

Furthermore, for each $k \in \mathcal{D} \cup \mathcal{L} \cup \mathcal{P}_{\text{boost}} \cup \mathcal{M} \cup \mathcal{H}$, no solution other than $\hat{\mathbf{x}}_k = \bar{\mathbf{x}}_k$ can stay in $\mathbb{E}_k = \{\hat{\mathbf{x}}_k \in \hat{\mathcal{X}}_k \subseteq \mathbb{R}^{\hat{n}_k} \mid \hat{S}_k(\hat{\mathbf{x}}_k, \bar{\mathbf{x}}_k) = 0, d_k = \bar{d}_k\}$ for all time.

Proof:

The proof follows similar steps than the proofs of Propositions 6.1–6.3. To avoid disrupting the reading flow, the straightforward yet lengthy proof is provided in Appendix C.2. \square

6.4 Simulation

This section demonstrates the stabilizing properties, plug-and-play capabilities, and disturbance rejection behavior of the proposed pressure and volume flow rate controllers via simulations in MATLAB/SIMULINK using SIMSCAPE components. In Section 6.4.1, a scenario with plug-and-play operations and varying reference values is presented. In Section 6.4.2, the first scenario is repeated, albeit with parameter uncertainties and a saturation to the valve input.

The simulations are conducted by means of the DHN depicted in Figures 6.1 and 6.2 which shows all structural features discussed in Section 6.1. Furthermore, all control problems outlined in Problem 6.1 are covered by assigning appropriate DGU, consumer, and pressure holding configurations, i.e., $\mathcal{D}_{\text{form}} = \{1\}$, $\mathcal{D}_{\text{valve}} = \{2\}$, $\mathcal{D}_{\text{VSP}} = \{3\}$, $\mathcal{L}_{\text{boost}} = \{7\}$, $\mathcal{L}_{\text{valve}} = \{4, 5, 6\}$, $\mathcal{L}_{\text{VSP}} = \{8\}$, $\mathcal{P}_{\text{boost}} = \{15\}$, $\mathcal{M} = \{25\}$, $\mathcal{H} = \{4\}$. Additionally, all requirements posed by the operation mode analysis in Proposition C.1 are fulfilled, i.e., there is at least one grid-forming DGU (at edge 1) between the two hydraulic layers constituted by the high-temperature pipe network (red) and the combination of the medium- and low-temperature network (orange, blue) (compare Figure 6.2 with Figure 6.4).

The model and controller parameters are given in Tables 6.1 and 6.2.

The pump parameters follow from Goppelt et al. [2018, Equation (42)] by considering that $\frac{R_{P,k}}{J_{P,k}} \approx 7.2878$, $\frac{1}{J_{P,k} C_{P,k}} \approx 341.4283$, and setting $R_{P,k} = 1 \cdot 10^6 \text{ Pa s/m}^3$ for pressure-controlled pumps, $k \in \mathcal{D}_{\text{form}} \cup \mathcal{D}_{\text{valve}} \cup \mathcal{L}_{\text{boost}} \cup \mathcal{P}_{\text{boost}} \cup \mathcal{H}$ and $R_{P,k} = 1 \cdot 10^{10} \text{ Pa s/m}^3$ for volume flow rate-controlled pumps, $k \in \mathcal{D}_{\text{VSP}} \cup \mathcal{L}_{\text{VSP}}$.⁴⁹

The flow capacity of the control valves is obtained by considering a maximum volume flow rate of $k_{vs} = 90 \text{ m}^3/\text{h} = 0.025 \text{ m}^3/\text{s}$ at full valve opening $s_{v,k} = 1$, for which follows $f_{v,k}(s_{v,k} = 1) = 1$ and $\mu_k(s_{v,k} = 1, k_{vs} = 0.025 \text{ m}^3/\text{s}) = 1 \cdot 10^5 \text{ Pa}$ valve pressure (see also Nussbaumer et al. [2020, p. 144]). The value in Table 6.1 then follows from

$$C_{v,k} = \frac{k_{vs}}{\sqrt{1 \cdot 10^5 \text{ Pa}}}. \quad (6.42)$$

Any pipe resistance $\lambda_l(q_l)$ and fluid inertia J_l , $l \in \mathcal{E}$, are modeled by using the hydraulic pipe resistance and hydraulic fluid inertia SIMSCAPE components with standard values and no elevation. The diameters, roughness, and lengths given in Tables 6.1 and 6.2 are in line with typical values (see, e.g., Liu et al. [2016] and Machado et al. [2022b]) and correspond to diameter nominal (DN) 32 and DN 80 pipes, respectively.

The elasticities lumped into the capacitive nodes $i \in \mathcal{C}$ are chosen according to exemplary values for one-family installations given in Stræde [1995] and Boysen and Thorsen [2003].

⁴⁹ Note that these hydraulic resistance values are in the order of magnitude of DN 80 and DN 20 pipes, respectively, for a length of 1 m and an external pressure of $1 \cdot 10^5 \text{ Pa}$.

Following Remark 6.11, the pressure controllers (6.18) of pumps do not comprise any damping assignment, i.e., $R_k^P = R_{P,k}$, to avoid dependency on the non-physical, auxiliary variable $q_{P,k}$. Additionally, preliminary simulations have shown that neglecting the reference feedforward of $p_{P,k}^*$ in (6.18) yields a better control performance. Thus, the pressure controllers implemented and simulated in the following scenarios are only PI controllers⁵⁰

$$Q_{I,k} \dot{r}_k = p_{P,k} - p_{P,k}^*, \quad (6.43a)$$

$$u_k = -R_{P,k} r_k + \frac{J_{P,k}}{Q_{I,k}} (p_{P,k} - p_{P,k}^*). \quad (6.43b)$$

Table 6.1: Simulation parameter values for the DHN simulation












Pressure-controlled pumps (6.1)	$R_{P,k} = 1 \cdot 10^6 \text{ Pa s/m}^3$ $J_{P,k} = 1.37 \cdot 10^5 \text{ Pa s}^2/\text{m}^3$ $C_{P,k} = 2.13 \cdot 10^{-8} \text{ m}^3/\text{Pa}$
Flow-controlled pumps (6.1)	$R_{P,k} = 1 \cdot 10^{10} \text{ Pa s/m}^3$ $J_{P,k} = 1.37 \cdot 10^9 \text{ Pa s}^2/\text{m}^3$ $C_{P,k} = 2.13 \cdot 10^{-12} \text{ m}^3/\text{Pa}$
Control valves (6.2)	$C_{v,k} = 7.9 \cdot 10^{-5} \text{ m}^3/(\text{s Pa}^{0.5})$
DGUs & consumers (6.5) (DN 32)	length = 25 m diameter = 0.0359 m roughness = $4.5 \cdot 10^{-5} \text{ m}$
Pipes (6.4) (DN 80)	diameter = 0.0825 m roughness = $4.5 \cdot 10^{-5} \text{ m}$
Mixing connection (6.6) (DN 80)	length = 25 m diameter = 0.0825 m roughness = $4.5 \cdot 10^{-5} \text{ m}$
Capactive nodes (6.6)	$C_j = 5 \cdot 10^{-10} \text{ m}^3/\text{Pa}$
Pressure controller pump (6.43)	$Q_{I,k}^{-1} = 3.64 \cdot 10^{-7}$ $R_k^P = R_{P,i}$
Flow controller pump (6.23)	$K_{P,k} = 2 \cdot 10^6$ $Q_{I,k}^{-1} = 2 \cdot 10^{10}$
Flow controller valve (6.33)	$K_{P,k} = 1 \cdot 10^4$ $Q_{I,k}^{-1} = 1 \cdot 10^4$

⁵⁰ Note that the statements of Proposition 6.1 are not undermined by these changes. To see this, consider the equivalent proof of the DC voltage controller and set $V_i^* = 0$, $\hat{R}_i = R_i$ in (4.28a), (4.31), and (4.35). The resulting controller has a PI structure and the following steps are as before with $\hat{R}_i = R_i$.

Table 6.2: Pipe lengths

Pipe	Length	Pipe	Length	Pipe	Length
9	350 m	15	50 m	20	100 m
10	300 m	16	400 m	21	100 m
11	300 m	17	100 m	22	100 m
12	200 m	18	100 m	23	100 m
13	200 m	19	100 m	24	100 m
14	50 m				

Table 6.3: Pressure and volume flow rate setpoints for the DGUs, consumers, the pipe with booster pump, the mixing connection, and the pressure holding unit. The values in the brackets indicated the setpoint variations throughout Scenario A and B.

Edges		$p_{P,k}^*$ in 10^5 Pa	q_k^* in 10^{-3} m ³ /s
DGU 1		15	—
DGU 2		10	3.5 (4.5)
DGU 3		—	3
Consumer 4		—	2
Consumer 5		—	2
Consumer 6		—	2 (4)
Consumer 7		6	2.5 (5)
Consumer 8		—	3 (6)
Pipe 15		5	—
Mixing connection 25		—	1 (3)
Nodes			
Pressure holding 4		2	—

6.4.1 Scenario A: Plug-and-Play and Setpoint Changes

In this scenario, the simulation starts with DGU 3 disconnected. The pressure and volume flow rate setpoints for the pumps and valves are assigned as in Table 6.3. At the indicated times, the following events occur (see Figure 6.2 for the DHN):

- $t = 5$ s – 10 s: Consumers $l \in \{6, 7, 8\}$ increase their volume flow rates by 100 %.
- $t = 20$ s: To help cover the increased demand, DGU 3 connects and the mixing connection 23 increases its volume flow rate to $3 \cdot 10^{-3}$ m³/s.
- $t = 30$ s: DGU 2 increases its input volume flow rate to $4.5 \cdot 10^{-3}$ m³/s.
- $t = 40$ s: Consumer 4 disconnects.

The pressure and volume flow rate trajectories shown in Figures 6.14 and 6.15 confirm the theoretical stability statements. Despite plug-and-play operations and changing operating conditions, the pressures of pressure-controlled pumps and the volume flow rates of flow-controlled pumps and valves are asymptotically stabilized at their desired setpoints. For the pressures, the maximum deviations resulting from the events at $t \in \{5 \text{ s}, 20 \text{ s}, 30 \text{ s}, 40 \text{ s}\}$ remain within a 1% band with respect to the setpoints and subside below 0.2% within approximately 5 s. For the volume flow rates, larger deviations can be observed. In particular at $t = 20 \text{ s}$ and $t = 30 \text{ s}$ during the connection of DGU 3 and the setpoint changes the error plots in Figure 6.15 shows large outliers. However, from a practical perspective, this is natural as abrupt setpoint changes cannot be realized instantly by the respective volume flow rate controllers. More importantly, except for the load ramps at $t \in [5 \text{ s}; 10 \text{ s}]$, the volume flow rates settle to within a 1.5% band with respect to the setpoints after at most 5 s. During the load ramps, the errors are higher, but remain below 8%. This shows that the volume flow rate controllers for both pumps and valves, although not specifically designed for it, are sufficiently fast to track setpoints that vary on a time scale of seconds.

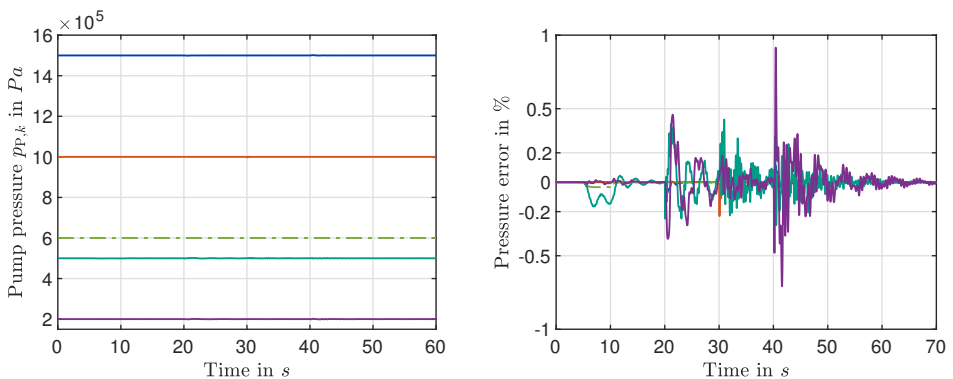


Figure 6.14: Scenario A: simulated pump pressures in DGUs $l \in \{1, 2\}$, consumer $l \in \{7\}$, booster pump $l \in \{15\}$, and dynamic pressure holding unit at node $i \in \{4\}$ with corresponding deviations from the references. The line colors are as per Table 6.3.

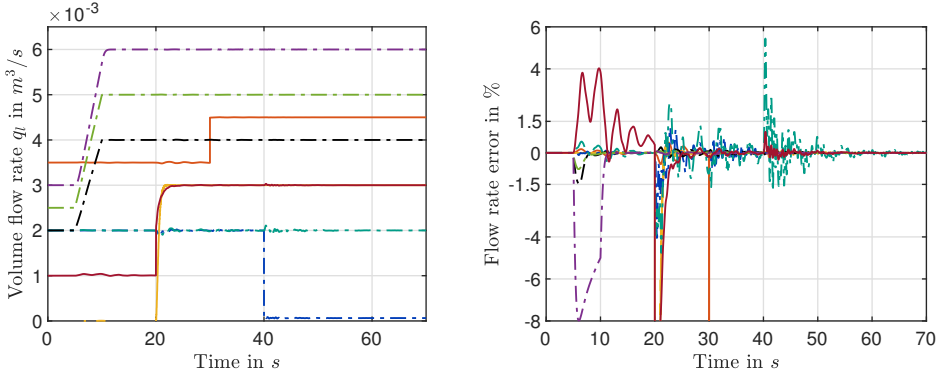


Figure 6.15: Scenario A: simulated volume flow rates through DGUs $l \in \{2, 3\}$, consumers $l \in \{4, 5, 6, 7, 8\}$, and mixing valve $l \in \{25\}$ with corresponding deviations from the references. The line colors are as per Table 6.3.

6.4.2 Scenario B: Parameter Uncertainty and Valve Saturation

Scenario B is similar to Scenario A except for two modifications: firstly, a 10% uncertainty is added to the pump parameters $R_{P,k}$, $J_{P,k}$, $C_{P,k}$ and the valve parameters $C_{v,i}$. Secondly, the virtual valve control input of all valves is saturated to $u_v \in [1, u_{v,i}^{\max}]$ (see Assumption 6.2).⁵¹

The resulting pressure and volume flow rate trajectories shown in Figures 6.16 and 6.17 are similar to those shown in Figures 6.14. The main difference introduced by the valve saturation is an impaired convergence performance of the volume flow rate control via valves, particularly at DGU 2 and Consumer 6 (see the orange and black lines in Figure 6.17). In practice, the control performance can be improved by an appropriate redesign of the valves or by increasing the available pressure, e.g., via the booster pump in Pipe 15 or a separate booster pump in the respective consumer.

Overall, the results of the two scenarios illustrate that the passivity-based pressure and volume flow rate controllers indeed asymptotically stabilize the hydraulic variables while allowing for plug-and-play operations of the different DHN subsystems. Furthermore, the integral parts of the proposed controllers ensure zero steady-state errors in the presence of parameter uncertainties and changing hydraulic conditions naturally occurring during the operation of DHNs.

This concludes the presentation of the unifying stabilization framework for DHNs. In the next section, the presented model, decentralized stability conditions, and controller designs are discussed with respect to the main research questions (Q3.1), (Q3.2), and

⁵¹ In line with classical feedback control design, the possibility of control input saturation is not considered explicitly during the control design stage in Section 6.3. Instead, its impact on the performance is analyzed by means of the numerical simulation in this section.

(Q3.3) related to stabilization in DHNs. Additionally, the results from this chapter are compared to those of the passivity-based works that have been published in parallel to this thesis (see Section 2.4.1).

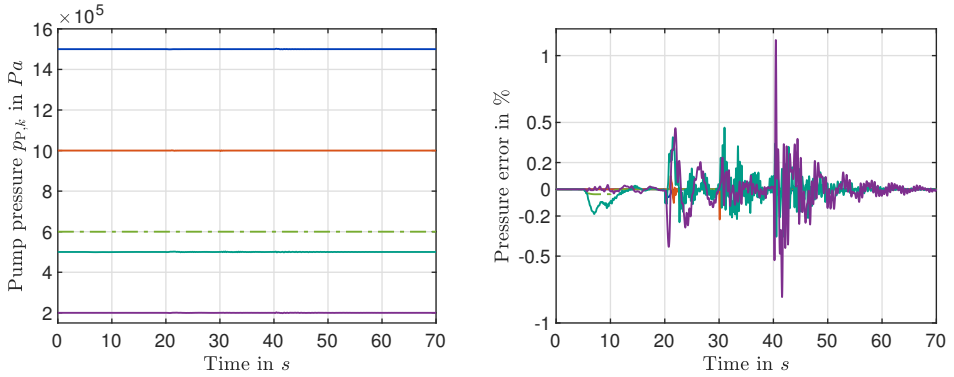


Figure 6.16: Scenario B: simulated pump pressures in DGUs $l \in \{1, 2\}$, consumer $l \in \{7\}$, booster pump $l \in \{15\}$, and dynamic pressure holding unit at node $i \in \{4\}$ with corresponding deviations from the references. The line colors are as per Table 6.3

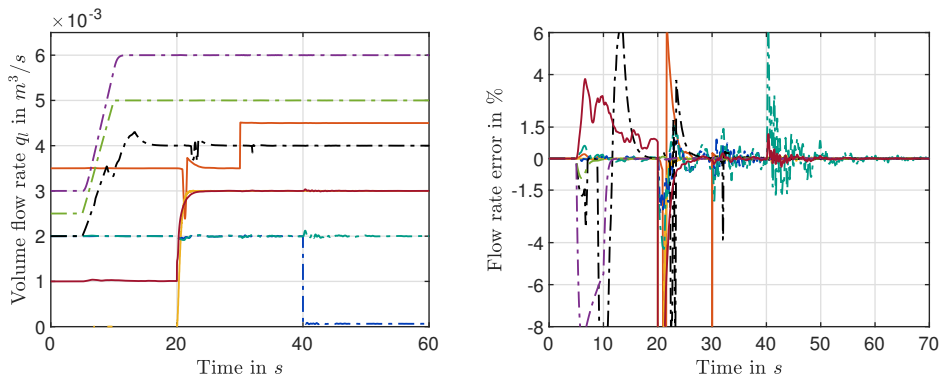


Figure 6.17: Scenario B: simulated volume flow rates through DGUs $l \in \{2, 3\}$, consumers $l \in \{4, 5, 6, 7, 8\}$, and mixing valve $l \in \{25\}$ with corresponding deviations from the references. The line colors are as per Table 6.3

6.5 Discussion

The first main result of this chapter is the comprehensive dynamic, hydraulic DHN model provided in Section 6.1. In contrast to the current state of research (see the discussion in Section 2.3.2), the presented model covers 2nd, 3rd, and 4th generation DHNs as well as intermediate development stages. In particular, the model allows for DHNs with asymmetric, meshed topologies, multiple temperature layers (temperature cascading), multiple DGUs, pressure holding units, booster pumps at consumers and pipes, DVSP configurations, as well as mixing connections used to increase the water temperature in topologies with multiple temperature layers. Moreover, opposed to the ideal pressure source consideration in the literature (see Section 2.3.2), pumps are described by dynamic design models to improve control design and system analysis in the face of increasing numbers of pump interactions. Furthermore, instead of as mere nonlinear hydraulic resistances, control valves are explicitly considered as actuators. In summary, the presented DHN model thus enables the unifying description of the hydraulic dynamics of flexible DHN configurations spanning different DHN generations and designs.

The second main result are the decentralized, asymptotic stability conditions (DHN 1) and (DHN 2) in Theorem 6.1, which answer research question (Q3.2). Similar to the power system conditions in Theorems 4.1 and 5.1, the conditions (DHN 1) and (DHN 2) provide model- and technology-independent system and control design requirements for the decentralized stabilization in DHNs. Other subsystem models and decentralized control solutions can thus readily be integrated into the presented DHN model, if they adhere to the requirements posed by (DHN 1) and (DHN 2). Note that such other subsystem models or controllers may be required to account for modifications to the presented subsystems types, e.g., due to different pump technologies, valve designs (like pressure-independent control valves [Nussbaumer et al., 2020, p. 146]) or new components such as thermal energy storages. Besides the presented hydraulic circuit designs for DGUs, consumers, and mixing connections, which represent the most commonly used structures, there also exists a variety of other circuit designs (see, e.g., Lamaison et al. [2017] and Lennermo et al. [2019] for DGUs and Köfinger et al. [2017], Volkova et al. [2020], and Volkova et al. [2022] for temperature cascading and mixing connections). Furthermore, there exist also altogether new subsystem types such as prosumers which can both produce and consume thermal energy [Brand et al., 2014].

By comparing (DHN 1) and (DHN 2) with the conditions in Theorems 4.1 and 4.1, it can be seen that the asymptotic stability conditions in the various energy systems are in fact identical. Consequently, despite the technical and physical differences between power systems and DHNs, passivity theory can serve as a unifying tool for providing technology- and domain-independent system and control design requirements for the decentralized stabilization in various networked energy systems. On the one hand, this allows for a transfer of passivity-based results between different engineering fields as demonstrated with the pump controller in Proposition 6.1. On the other hand, this

provides a system-theoretic basis for establishing a unifying, technology- and domain-independent framework for the decentralized stabilization in NMESs.⁵²

The third main result are the decentralized pump and valve control designs in Propositions 6.1, 6.2, 6.3, and 6.4, which provide explicit solutions for research question (Q3.3). Similar to the decentralized DC and AC controllers from Chapters 4 and 5, the developed pump and valve controllers are simple and use standard, off-the-shelf control functions such as a setpoint feedforward, a static state feedback, and a PI term (see (6.18), (6.23), and (6.33)). However, note that for a proper functioning of the control valves, it is crucial that the differential pressure over each control valve is sufficiently high (see Remark 6.3 and Assumption 6.3). An insufficient differential pressure at best impairs the convergence performance of the respective valve and at worst leads to a complete loss of functionality with a large offset from the desired volume flow rate and a fully open valve. In such cases, the established volume flow rate only depends on the hydraulic conditions of the remaining DHN and cannot be influenced. In the light of the emerging trends and challenges discussed in Section 2.3, this motivates to develop new coordination methods in addition to the presented decentralized, hydraulic stabilization solution. Due to the outlined parallels between DC power systems and DHNs and their generalized models presented in this thesis, it seems promising to transfer existing DC coordination solutions such as consensus algorithms (see, e.g., Cucuzzella et al. [2019b], Malan et al. [2022], and Nahata et al. [2022]) to the coordination in DHNs.

6.5.1 Comparison with Parallel Works

In contrast to electrical DC and AC power systems, DHNs and particularly the hydraulic stabilization problem have so far not received much attention by the systems and control community. The most noteworthy works regarding the hydraulic control in DHNs with topology changes and multiple distributed pumps revolve around the research activities supervised and lead by De Persis (see Section 2.3.1). In particular, Jensen [2012] is the first to explicitly elaborate on using passivity properties for the design of pressure controllers in such a setup. Despite providing valuable insights, the obtained results are more of a first approach due to the very limited DHN model allowing only for one heat source, the requirement of pumps and valves at every producer and consumers, as well as the need for communication to implement the controllers.

Machado et al. [2022a] and Machado et al. [2022b] are the first to take up the above works and elaborate a decentralized, passivity-based approach for hydraulic stabilization problems. In fact, these are the only works published in parallel to this thesis to address hydraulic stabilization problems in DHNs by a decentralized, passivity-based approach. In Machado et al. [2022b], the model setup from De Persis and Kallešøe [2011] and Jensen [2012], respectively, is extended to account for the main emerging DHN trend, i.e., multiple heat producers/DGUs. Additionally, storage tanks at producers are

⁵² This implication will be elaborated in more detail the next chapter.

considered. Subsequently, a detailed passivity analysis and an outlook on how these passivity properties might be used for a decentralized pressure and volume flow rate design is given. Based on these insights, Machado et al. [2022a] propose a decentralized pump controller which combines elements from backstepping, adaptive, and passivity-based control to regulate both the volume flow rates in a DHN and the storage volumes in the storage tanks at the producers.

While the addition of storage tanks and the controller designs are promising extensions to the results developed in this chapter, the DHN model considered by Machado et al. [2022a] and Machado et al. [2022b] exhibits a number of restrictions compared to the model presented in Section 6.1: symmetric DHN topologies⁵³, two temperature layers only, static pump models, no pressure holding units, and valves modeled as non-actuated components. Furthermore, pumps are assumed to be installed at every producer and every consumer, which excludes traditional DHNs in which consumers regulate their volume flow rates only via control valves.

Additionally, similar to the parallel works in DC power systems (see Section 4.5.1), Machado et al. [2022b] and Machado et al. [2022a] follow a constructive procedure of modeling, control design, and stability analysis. The (shifted) passivity properties of their closed-loop models are merely used to facilitate the stability statement. However, no inferences are drawn on how the passivity properties can be translated into general system and control design guidelines.

The results of this chapter are thus the first to provide a unifying, technology-independent framework for the decentralized, hydraulic stabilization in DHNs.

6.6 Summary and Contributions

Future DHN stabilization is confronted with increasing numbers of interacting units which comprise a variety of deployed technologies and control strategies. This chapter provides a passivity-based framework for DHN stabilization which makes large numbers of units manageable by means of decentralized methods and ensures interoperability across different technologies and control strategies. The results of this chapter are the first to provide such a decentralized, cross-technology stabilization framework for DHNs. In summary, the main contributions of this chapter are:

- a comprehensive dynamic, hydraulic DHN model which covers different DHN generations and is represented in a generalized networked system form (Section 6.1);

⁵³ In symmetric DHN topologies, supply and return pipes are laid in parallel. This excludes practically relevant cases with meshed supply pipe networks and tree-like return pipe networks or more complex structures arising in multi-layer topologies.

- decentralized, EIP-based conditions that provide model- and technology-independent system and control design requirements for ensuring asymptotic stability of any feasible, hydraulic DHN equilibrium (Theorem 6.1);
- decentralized pump and valve controllers that ensure the EIP-based asymptotic stability conditions are met and desired pressure and volume flow rate setpoints are asymptotically stabilized (Propositions 6.1, 6.2, 6.3, and 6.4).

Together, these contributions answer the research questions (Q3.1), (Q3.2), and (Q3.3) formulated in Section 2.3.2. Simulation studies based on realistic DHN data demonstrate the functionality of the developed decentralized stabilization framework and illustrate its unifying nature.

In addition to these DHN-related main contributions, the results of this chapter further demonstrate the domain-unifying capabilities of a passivity-based, decentralized stabilization framework. The identical, general formulation of the decentralized stability conditions in Theorems 4.1, 5.1, and 6.1 in particular provides direct indications for establishing a unifying, technology- and domain-independent framework for the decentralized stabilization in NMESs.

7 Towards a Unifying Framework for Decentralized Stabilization in Networked Multi-Energy Systems

In this chapter, it is shown how the passivity-based approach from the previous chapters naturally extends to the NMES case providing a unifying, decentralized stabilization perspective not only across different technologies and control strategies within individual energy systems, but also across different energy system domains. While a detailed modeling and controller synthesis for NMESs is outside the scope of this thesis, the following sections establish the necessary foundation for such an endeavor and showcase the basic ideas. In particular, some fundamental concepts such as *stability* of and *decentralized stabilization* in NMESs are formally defined by combining the insights from the previous chapters. Furthermore, decentralized asymptotic stability conditions for the equilibria in NMESs are derived. Such conditions form the foundation of a unifying, decentralized stabilization framework for NMESs and answer research question (Q4.1).

7.1 Modeling

In Chapters 4 to 6, it has been shown that various network energy systems can be represented by the graph-based description of an autonomous networked system introduced in Definition 3.1. Consequently, their combination in NMESs can also be represented in such a way (see, e.g., Strehle et al., [2018] for coupled gas and AC power systems, Maurer [2023, Figure 2.1] for coupled DHNs and AC power systems, Malan et al., [2023] for gas networks, and Shahbakhsh and Nieße [2019] for a conceptual work on NMESs).

Thus, in the following, consider NMESs described by a weakly connected digraph $\mathcal{G} = (\mathcal{V}, \mathcal{E})$ without self-loops with subsystems on the nodes $i \in \mathcal{V}$ and edges $l \in \mathcal{E}$. The subsystems may represent various producers/DGUs, consumers/loads, storage devices, pipes, power lines, various other units necessary for the operation (e.g., pressure holding units, pressure regulating stations, transformers, FACTSs, etc.), as well as converters between the energy system domains such as heat pumps, combined heat and power plants, gas turbines, or power-to-gas stations. Furthermore, it is assumed that each of the subsystems is represented by a generalized state-space model of the form (3.1b), if unactuated, and (3.2), if actuated. Consequently, the domain-specific variables (voltages, pressures, currents, volume flow rates) are represented by their effort (voltage, pressure)

and flow (current, volume flow rate) counterparts as given in Table A.1. Then, the orientation of the edges in \mathcal{G} represents the arbitrary reference direction of positive, generalized flow. Furthermore, the digraph \mathcal{G} is completely specified by its incidence matrix $\mathbf{B} \in \mathbb{R}^{|\mathcal{V}| \times |\mathcal{E}|}$ with elements b_{il} (cf. (1.1)).

Remark 7.1. *Note that for clarity of presentation, the domain-specific effort (voltage, pressure) and flow (current, volume flow rate) variables are used in Chapters 4 to 6. However, one can straightforwardly replace them with their generalized counterparts and use the obtained generalized models for composing an NMES model.*

7.2 Stability and Decentralized Stabilization

In this section, initial suggestions for the definition of *NMES stability* and *decentralized stabilization* in NMESs are developed. Such definitions are essential for developing holistic, integrated operation strategies for NMESs and pave the way for a systematic, system-theoretical treatment of NMESs. While there are conceptual statements on what is required for the “stable” operation of NMESs (see, e.g., Mancarella [2014], Shahbakhsh and Nieße [2019], O’Malley et al. [2020], and Martínez Ceseña et al. [2020]), a clear systems and control perspective on this topic is missing in the current state of research.

Remark 7.2. *In fact, there is little work regarding the modeling and analysis of integrated NMESs as a whole (see also Chicco et al. [2020]). The majority of works focus on coordination topics such as enabling flexibility in the framework of energy hubs or extensions thereof (see, e.g., Geidl [2007], Mancarella [2014], Martínez Ceseña et al. [2020], Chicco et al. [2020], and the references therein).⁵⁴ In particular, there exists no analysis and control design model of NMESs which combines the network variables, their constitutive relations, and system dynamics that go beyond simple storage elements. Consequently, a comprehensive system-theoretical treatment of stability and stabilization in NMESs is, to the best of the author’s knowledge, missing in the literature.*

To begin with, recall from the introduction in Chapter 1 and the overviews in Sections 2.1, 2.2, and 2.3 that the operation of different energy systems comprises two main tasks which can be approached by a hierarchical control structure: firstly, at the lowest control layer, different energy system equilibria comprising the system variables (efforts, flows) have to be asymptotically stabilized via decentralized controllers. Subsequently, feasibility of such equilibria within the operational constraints has to be ensured at

⁵⁴ The energy hub framework represent an aggregated perspective on NMESs in which the main resources, i.e., producers, consumers, and converters are lumped together in so-called energy hubs. The main focus is on obtaining an input-output perspective on a power flow level, which is then used, e.g., for optimal power flow coordination or flexibility provision (see Geidl [2007], Martínez Ceseña et al. [2020], and Chicco et al. [2020] for further details).

higher control layers by appropriate coordination of generation, transportation, and consumption.

Together, decentralized stabilization and coordination have to ensure what may be referred to as the *stability* of an energy system, i.e., despite disturbances, the necessary amount of energy can be provided in the right place at the right time within the operational constraints. However, note that the term “stability” only has a clear, standardized definition in an AC power system context (see Sections 2.1). As discussed in Sections 2.2 and 2.3, there exist no standardized stability definitions for DC power systems and DHNs. Nevertheless, the requirements posed on their “stable” operation can be categorized into *decentralized stabilization* and *coordination* as well.

Motivated by these insights, it is proposed to define *NMES stability* based on a generalized formulation of AC power system stability as provided in Farrokhhabadi et al. [2020].

Definition 7.1 (Stability of NMESs)

Consider an NMES which is operating in equilibrium with state variables taking on appropriate steady-state values satisfying operational constraints, such as acceptable ranges of efforts and flows. Such an NMES is stable if, after being subjected to a disturbance, all state variables recover without the occurrence of involuntary load shedding to (possibly new) steady-state values satisfying operational constraints.

To ensure NMESs stability as in Definition 7.1, it is suggested to follow the insights established for the individual energy systems and employ a hierarchical asymptotic stabilization-coordination control structure. Following Definitions 2.3, 2.4, and 2.5, decentralized stabilization in NMESs can then be defined as follows:

Definition 7.2 (Decentralized stabilization in NMESs)

Decentralized stabilization in NMESs refers to the basic control task conducted by decentralized controllers at the lowest control layer of an hierarchical stabilization-coordination control structure for NMESs. It ensures that such NMES equilibria are asymptotically stabilized that efforts and flows of actuated subsystems are at desired setpoints.

In order to ensure decentralized stabilization as per Definition 7.2, two main problems are to be addressed: firstly, decentralized, analytical conditions are to be provided which ensure asymptotic stability of any feasible NMES equilibrium. Secondly, parameter specifications for the unactuated subsystems are to be established and appropriate decentralized controllers for the actuated subsystems are to be designed such that the asymptotic stability conditions are satisfied.

The following section focuses on the first of the two above problems which lays the

groundwork for a unifying, decentralized stabilization framework in NMESs. That is, it provides decentralized, analytical conditions that ensure asymptotic stability of any feasible NMES equilibrium across different technologies, control strategies, and physical domains.

7.3 Asymptotic Stability Conditions

Following the reasoning established in Sections 4.2, 5.2, and 6.2, decentralized asymptotic stability conditions can be derived by means of Theorem 3.1 and Corollary 3.1.

Starting point is the NMES model outlined in Section 7.1, which is similar to that of an autonomous, networked system given in Definition 3.1. So far, however, the control ports $(\mathbf{u}_k, \mathbf{y}_k)$ of the actuated subsystems $k \in \mathcal{V}_{\text{Act}} \cup \mathcal{E}_{\text{Act}} \subseteq \mathcal{V} \cup \mathcal{E}$ are open, i.e., their models are of the form (3.2). In order to conduct an equilibrium stability analysis, it is thus assumed that each actuated subsystem is in closed loop with some static or dynamic controller (see also Remark 3.2).

Then, by direct application of Theorem 3.1 and Corollary 3.1 to the now autonomous NMES model, decentralized, analytical conditions can be obtained, which, if satisfied, ensure asymptotic stability of any feasible NMES equilibrium $\bar{\mathbf{x}}_{\text{NMES}} = \text{stack}(\bar{\mathbf{x}}_k)_{k \in \mathcal{V} \cup \mathcal{E}}$. The vectors $\bar{\mathbf{x}}_k$ are the respective equilibrium state vectors of the subsystems that are proportional to the steady-state efforts and flows.⁵⁵

⁵⁵ Note that $\bar{\mathbf{x}}_k$ possibly implies a slight abuse of notation as in the case of dynamic controllers the original state vector \mathbf{x}_k is augmented by additional controller states.

Theorem 7.1 (Decentralized, asymptotic stability conditions for NMESs)

Consider an autonomous NMES as described in Section 7.1 with some controller \mathbf{u}_k at each actuated subsystem $k \in \mathcal{V}_{\text{Act}} \cup \mathcal{E}_{\text{Act}}$. Any feasible equilibrium $\bar{\mathbf{x}}_{\text{NMES}} = \text{stack}(\bar{\mathbf{x}}_k)_{k \in \mathcal{V} \cup \mathcal{E}}$ of such an autonomous NMES is asymptotically stable, if the following two conditions hold:

(NMES 1) each subsystem at a node $i \in \mathcal{V}$ is

- strictly EIP w.r.t. the supply rate $(\mathbf{d}_i - \bar{\mathbf{d}}_i)^\top (\mathbf{z}_i - \bar{\mathbf{z}}_i)$ and a continuously differentiable, positive definite storage function $S_i(\mathbf{x}_i, \bar{\mathbf{x}}_i)$, or
- EIP w.r.t. the supply rate $(\mathbf{d}_i - \bar{\mathbf{d}}_i)^\top (\mathbf{z}_i - \bar{\mathbf{z}}_i)$ and a continuously differentiable, positive definite storage function $S_i(\mathbf{x}_i, \bar{\mathbf{x}}_i)$, and such that no solution other than $\mathbf{x}_i(t) = \bar{\mathbf{x}}_i$ can stay in $\mathbb{E}_i = \{\mathbf{x}_i \in \mathcal{X}_i \subseteq \mathbb{R}^{n_i} \mid \dot{S}_i(\mathbf{x}_i, \bar{\mathbf{x}}_i) = 0, \mathbf{d}_i = \bar{\mathbf{d}}_i\}$ for all time.

(NMES 2) each subsystem at an edge $l \in \mathcal{E}$ is

- either strictly EIP w.r.t. the supply rate $(\mathbf{d}_l - \bar{\mathbf{d}}_l)^\top (\mathbf{z}_l - \bar{\mathbf{z}}_l)$ and a continuously differentiable, positive definite storage function $S_l(\mathbf{x}_l, \bar{\mathbf{x}}_l)$, or
- OSEIP w.r.t. the supply rate $(\mathbf{d}_l - \bar{\mathbf{d}}_l)^\top (\mathbf{z}_l - \bar{\mathbf{z}}_l)$ and a continuously differentiable, positive definite storage function $S_l(\mathbf{x}_l, \bar{\mathbf{x}}_l)$, and either EIO or such that no solution other than $\mathbf{x}_l(t) = \bar{\mathbf{x}}_l$ can stay in $\mathbb{E}_l = \{\mathbf{x}_l \in \mathcal{X}_l \subseteq \mathbb{R}^{n_l} \mid \dot{S}_l(\mathbf{x}_l, \bar{\mathbf{x}}_l, \mathbf{d}_l = \bar{\mathbf{d}}_l) = 0\}$ for all time.

Proof:

The proof follows directly by application of Theorem 3.1 and Corollary 3.1 to the graph-based NMES model from Section 7.1 with some controller \mathbf{u}_i at each actuated subsystem $k \in \mathcal{D} \cup \mathcal{E}$. \square

The conditions (NMES 1) and (NMES 2) of Theorem 7.1 answer research question (Q4.1). Next, it has to be ensured that the NMES subsystems satisfy the respective conditions. Furthermore, for the actuated subsystems, the respective closed-loop equilibrium state vectors $\bar{\mathbf{x}}_k$ should be such that desired effort and flow setpoints are established in steady state.

Recalling the results from Chapters 4, 5, and 6, the following guidelines can be established on how to proceed:

- if a subsystem is unactuated, i.e, it has no control port $(\mathbf{u}_k, \mathbf{y}_k)$, its system design (parameter specifications, model structure) has to ensure that condition (NMES 1) or (NMES 2), respectively, are satisfied.
- if a subsystem is accessible for control, the design of a decentralized controller

together with system design measures (parameter specifications, model structure) has to ensure that the closed-loop subsystem satisfies its respective condition (NMES 1) or (NMES 2). Furthermore, the closed-loop equilibrium state vector \bar{x}_k should be such that desired effort and/or flow setpoints are established in steady state.

- if an unactuated subsystem cannot fulfill condition (NMES 1) or (NMES 2), respectively, via system design alone, the decomposition of the overall NMES model into subsystems can be revised. Alternatively, actuators for passivation can be added.⁵⁶

7.4 Summary and Contributions

The increase in interacting units and deployed technologies resulting from the sustainable energy transition is calling for decentralized, cross-technology stabilization frameworks in power systems and DHNs. However, in light of a growing networking between energy systems of different domains towards integrated NMESs, it is also of interest to explore the possibilities of a framework that provides a unifying basis for decentralized stabilization solutions across different technologies, control strategies, and energy system domains. This chapter establishes the foundation of such a unifying, decentralized stabilization framework for NMESs by the following main contributions:

- formal, system-theoretical definitions for *stability of NMESs* (Definition 7.1) and *decentralized stabilization in NMESs* (Definition 7.2);
- decentralized, EIP-based conditions that provide model-, technology-, and domain-independent system and control design requirements for ensuring asymptotic stability of any feasible NMES equilibrium (Theorem 7.1).

Together, these contributions answer the research question (Q4.1) formulated in Section 2.4.

The results of this chapter are the first to approach the topics of NMES stability and NMES stabilization from a systems and control perspective. Together with the findings of Chapters 4 to 6, these first results provide solid, system-theoretical starting points for the future development of holistic, integrated system and control solutions for NMESs.

⁵⁶ See for example the recent results by Ferguson et al. [2023] which provide first ideas on how this can be done in a DC power system context.

8 Conclusion

The strive for a climate neutral energy supply fundamentally changes the dynamics, behavior, and network structures of energy systems, particularly of power systems and district heating networks (DHNs). Most prominently and impactful among these changes are the increasing number of dynamically interacting subsystems, both controllable and uncontrollable, and more flexible system configurations due to volatile generation/demand situations. Additionally, promoted by societal and engineering advantages, individual energy systems with different physical domains are increasingly developing into networked multi-energy systems (NMEs). To retain a secure and efficient energy supply in light of these changes, new operation strategies are required with the stabilization at the lowest control layer as a necessary foundation. From a systems and control viewpoint, the stabilization challenges and requirements in the various networked energy systems show similarities.⁵⁷ Scalability and interoperability via decentralized, cross-technology stabilization solutions, in particular, are of paramount importance to address the increasing number and variety of subsystems and allow for flexible system configurations.

This thesis develops a unifying, passivity-based framework for the decentralized stabilization in networked energy systems that provides such scalability and ensures interoperability across different technologies, control strategies, and energy system domains. The main idea is to use the input-output property of equilibrium-independent passivity (EIP) to establish decentralized, analytical conditions that ensure—independent of specific technologies, control strategies, or physical domains—asymptotic stability of any feasible networked energy system equilibrium. Subsequently, stabilization amounts to ensuring that these EIP-based conditions are satisfied by the individual subsystems that constitute the energy system in question. For unactuated subsystems, satisfying the EIP-based conditions entails an appropriate system design, while actuated subsystems can use both system and control design measures.

Along the lines of this basic idea, the thesis at hand answers the research questions stated in Chapter 2 with the following main contributions:

1. Firstly, comprehensive, unifying system descriptions for DC power systems, AC power systems, and DHNs have been presented which combine a graph-based, networked system representation with the domain-unifying framework of port-Hamiltonian systems (PHSs). The results of this thesis are the first to adopt such a

⁵⁷ Note the dual meaning of networked in this context covering both the increased network aspect in power systems and DHNs due to the increasing numbers of interacting units as well as the growing networking between energy systems of different domains towards integrated NMEs.

generalized perspective in an energy system context and project the generalized effort-flow modeling paradigm onto various networked energy systems.

2. Secondly, an EIP-based stability theorem has been developed which provides decentralized, technology- and domain-independent conditions for the asymptotic stability of general networked system equilibria. In contrast to the asymptotic stability conditions that can be deduced by combining results from the literature, the developed theorem is not limited to strict EIP properties, which significantly extends its practical applicability. By application of this theorem to DC power systems, AC power systems, and DHNs, a unifying, EIP-based framework has been established that ensures—*independent of specific technologies, control strategies, or physical domains*—decentralized stabilization. In addition, elaborating on the results from the individual energy systems, stability and decentralized stabilization definitions for NMESs as well as decentralized, analytical conditions for the asymptotic stability of any feasible NMES equilibrium have been developed. The presented stability conditions lay the foundation for establishing a unifying, decentralized stabilization framework for NMESs and provide clear system and control design guidelines.
3. Thirdly, for DC power systems, AC power systems, and DHNs, parameter specifications and decentralized component controllers have been provided that ensure the EIP-based, asymptotic stability conditions are satisfied and desired voltage, current, frequency, pressure, and volume flow rate setpoints are asymptotically stabilized. The validity of the developed stabilization framework together with its unifying nature has been demonstrated by various, simulative case studies based on benchmark networks and realistic network data.

The unifying, technology- and domain-independent nature of the established, decentralized stabilization framework can serve as common ground between the engineering communities and practitioners within and across the various networked energy systems. The results for NMESs presented in Chapter 7, in particular, present a first step towards realizing holistic system and control solutions for the operation of NMESs. Besides scalability and interoperability, the decentralized and unifying perspective on stabilization provides further practically appealing engineering advantages such as flexibility and adaptability in the control architectures of energy system operators. Together, these benefits also establish the technical foundation for realizing, *e.g.*, novel, liberalized energy market concepts with active customer involvement or cross-domain ancillary services (*e.g.*, where DHNs provide flexibility services for power systems).

Outlook

A natural direction for future, practically-oriented research is to evaluate the theoretical benefits of the proposed frameworks in field applications and compare them to the currently implemented methods and heuristics. As demonstrated for example by

Watson et al. [2019] for AC power systems, it is to be expected that several of the state-of-the-art controllers and components can, possibly with minimal adaptations, be shown to fulfill some kind of passivity condition. A natural direction for future, methodological-focused research is to complement the stabilization framework presented in this thesis by a unifying framework for the coordination in energy systems. Moreover, it seems promising to explore the possibilities of relaxing the conservativeness of the presented EIP-based, asymptotic stability conditions. Such conservativeness is inherent to any decentralized, passivity-based stability conditions and is related to the fact that if there is a single subsystem which, after system and/or control design measures, still does not fulfill the specified passivity/EIP conditions, no statement can be made about the asymptotic stability of the considered system equilibrium. One way of overcoming this limitation seems to be via appropriate control designs. Recent results by Ferguson et al. [2023], for example, showcase in a DC power system context how appropriate control of actuated subsystems can be used to passivate inherently non-passive subsystems. Another way of reducing conservativeness are more differentiated passivity notions which allow to quantify the lack or excess of passivity/EIP via passivity indices. Under appropriate interconnection structures, lack and excess can compensate each other and allow for decentralized, asymptotic stability statements even with non-passive subsystems (see, e.g., Bao and Lee [2007, p. 24ff.] and the references therein).

In summary, this thesis is the first to provide a **unifying, technology- and domain-independent framework for the decentralized stabilization** in networked energy systems such as DC power systems, AC power systems, DHNs, and NMESs.

A Appendices to Chapter 3

A.1 Passivity and Stability of Networked Systems

To recapitulate the basic ideas behind the passivity-based approach of this thesis, this section presents selected content regarding passivity theory and its use for the compositional stability analysis of the origin $\bar{x} = \mathbf{0}_n$, $\mathbf{0}_n = \mathbf{f}(\bar{x})$, of an autonomous, networked system (3.1a).

To begin with, different elementary passivity properties are introduced. The following definition is condensed from Khalil [1996, Definition 10.4], Khalil [2002, Definition 6.3], and van der Schaft [2017, Definition 4.1.1].

Definition A.1 (Passivity, strict passivity, output strict passivity (OSP))

A state-space system (3.1b) is **passive** w.r.t. the supply rate $\mathbf{d}_k^\top \mathbf{z}_k$, if there exists a continuously differentiable, positive semidefinite storage function $S_k : \mathcal{X}_k \rightarrow \mathbb{R}_{\geq 0}$, $S_k(\mathbf{0}_{n_k}) = 0$, and a positive semidefinite dissipation rate $\psi_k : \mathcal{X}_k \rightarrow \mathbb{R}_{\geq 0}$, $\psi_k(\mathbf{0}_{n_k}) = 0$, such that the differential passivity inequality

$$\dot{S}_k = -\psi_k(\mathbf{x}_k) + \mathbf{d}_k^\top \mathbf{z}_k \leq \mathbf{d}_k^\top \mathbf{z}_k, \quad \forall (\mathbf{x}_k, \mathbf{d}_k) \in \mathcal{X}_k \times \mathbb{R}^m. \quad (\text{A.1})$$

holds. Moreover, system (3.1b) is **strictly passive** w.r.t. $\mathbf{d}_k^\top \mathbf{z}_k$, if the dissipation rate is positive definite, i.e., $\psi_k(\mathbf{x}_k) > 0, \forall \mathbf{x}_k \neq \mathbf{0}, \psi_k(\mathbf{0}_{n_k}) = 0$. If

$$\dot{S}_k = -\psi_k(\mathbf{x}_k) - \mathbf{z}_k^\top \boldsymbol{\rho}_k(\mathbf{z}_k) + \mathbf{d}_k^\top \mathbf{z}_k \leq \mathbf{d}_k^\top \mathbf{z}_k, \quad \forall (\mathbf{x}_k, \mathbf{d}_k) \in \mathcal{X}_k \times \mathbb{R}^m, \quad (\text{A.2})$$

with positive semidefinite dissipation rate $\psi_k : \mathcal{X}_k \rightarrow \mathbb{R}_{\geq 0}$, $\psi_k(\mathbf{0}_{n_k}) = 0$, and strictly monotone function $\boldsymbol{\rho}_k(\mathbf{z}_k) : \mathbb{R}^m \rightarrow \mathbb{R}^m$, $\mathbf{z}_k^\top \boldsymbol{\rho}_k(\mathbf{z}_k) > 0, \forall \mathbf{z}_k \neq \mathbf{0}_m$, then system (3.1b) is **output strictly passive (OSP)** w.r.t. $\mathbf{d}_k^\top \mathbf{z}_k$.

Next, different passivity requirements for the subsystems (3.1b) are combined for specific interconnection structures to make stability statements about the origin. Of particular interest within this thesis is the skew-symmetric interconnection of passive subsystems which naturally arises in autonomous, networked systems (see (3.1e)) and other control engineering applications.⁵⁸

⁵⁸ The elementary negative feedback interconnection of two SISO subsystems of the form (3.1b) with $m = 1$ is for example a skew-symmetric interconnection with $\begin{bmatrix} d_1 \\ d_2 \end{bmatrix} = \begin{bmatrix} 0 & -1 \\ 1 & 0 \end{bmatrix} \begin{bmatrix} z_1 \\ z_2 \end{bmatrix}$ [Arcak et al., 2016, p. 17].

The following lemma is condensed from Khalil [2002, p. 242–243], Arcak et al. [2016, p. 13–17], and van der Schaft [2017, pp.49,50,77].

Lemma A.1 (Stability of networked, passive systems)

Consider an autonomous, networked system as in Definition 3.1. If each subsystem (3.1b) is passive w.r.t. the supply rate $\mathbf{d}_k^\top \mathbf{z}_k$ and a continuously differentiable, positive definite storage function $S_k(\mathbf{x}_k) > 0, \forall \mathbf{x}_k \neq \mathbf{0}, S_k(\mathbf{0}_{n_k}) = 0$, then the origin $\bar{\mathbf{x}} = \mathbf{0}_n$ is a stable equilibrium of the autonomous, networked system (3.1a). If each subsystem (3.1b) is strictly passive w.r.t. $\mathbf{d}_k^\top \mathbf{z}_k$ and a continuously differentiable, positive definite storage function, then the origin is an asymptotically stable equilibrium.

Proof:

Choose the storage function $S : \mathcal{X} \rightarrow \mathbb{R}_{\geq 0}$ of the autonomous, networked system (3.1a) as the sum of the subsystem storage functions $S(\mathbf{x}) = \sum_{i=1}^N S_k(\mathbf{x}_k)$. Since each $S_k(\mathbf{x}_k)$ is continuously differentiable and positive definite, $S(\mathbf{x})$ is continuously differentiable and positive definite. Due to the skew symmetry of the interconnection structure (3.1e), it holds that $\mathbf{z}^\top \mathbf{d} = \mathbf{z}^\top \mathbf{M} \mathbf{z} = 0$. Thus, the time derivative of $S(\mathbf{x})$ is given by

$$\dot{S}(\mathbf{x}) = - \sum_{k=1}^N \psi_k(\mathbf{x}_k) \leq 0, \quad \forall \mathbf{x} \in \mathcal{X}, \quad (\text{A.3})$$

which makes $S(\mathbf{x})$ a Lyapunov function for the origin $\bar{\mathbf{x}} = \mathbf{0}_n$ and proves its stability (see [van der Schaft, 2017, p. 44]). From strict passivity of each subsystem (3.1b), it follows that

$$\dot{S}(\mathbf{0}_n) = 0, \quad \dot{S}(\mathbf{x}) = - \sum_{k=1}^N \psi_k(\mathbf{x}_k) < 0, \quad \forall \mathbf{x} \neq \mathbf{0}_n, \quad (\text{A.4})$$

which proves asymptotic stability of $\bar{\mathbf{x}} = \mathbf{0}_n$ (see van der Schaft [2017, p. 44]). \square

A.2 Port-Hamiltonian Systems

This section provides a short overview about selected fundamentals of PHS theory that are relevant in the context of this thesis. In Section A.2.1, the concept of generalized modeling is shortly recapitulated. In Section A.2.2 some of the main class of ISO-PHS models are introduced. A combination of these ISO-PHS models is used throughout this thesis to model the subsystems in the various networked energy systems.

A.2.1 Generalized Modeling

The PHS framework follows the power- and energy-based perspective used in the Lagrangian and Hamiltonian modeling of multi-domain physical systems (see, e.g., Wellstead [1979], Jeltsema and Scherpen [2009], and Duindam et al. [2009] for a comprehensive introduction). The general idea behind such an energy-based approach is to use energy as the universally conserved quantity across different physical domains. In particular, the instantaneous exchange of energy, i.e., power flow $P = \frac{dE}{dt}$, formally equals the inner product of two physical quantities in the various physical domains. Hence, two time-dependent, generalized variables can be introduced, viz. an effort $e \in \mathbb{R}^n$ and a flow $f \in \mathbb{R}^n$, whose inner product $P = e^\top f$ has the unit of power.

For different physical domains, effort and flow have straightforward correspondences to the respective domain-specific variables. Within this thesis, the relevant correspondences in the electrical and hydraulic domains are given in Table A.1. Note that these correspondences follow the so-called thermodynamic framework in which the (generalized) state results from the time integral over the flow, i.e., $x = \int f dt$.

Table A.1: Correspondences between the generalized and physical variables of the electrical and hydraulic domain in the thermodynamic framework (cf. Duindam et al. [2009, p. 24])

	f flow	e effort	x state
electric	I current	V voltage	Q charge
magnetic	V voltage	I current	Ψ flux linkage
elastic hydraulic	q volume flow	p pressure	Λ volume
kinetic hydraulic	p pressure	q volume flow	Γ momentum of a fluid

Under the roof of such an energy-based generalization, systems within different physical domains can formally be represented by structurally identical equations. Furthermore, generalized equivalent circuit diagrams can be used to represent different physical domains in the familiar schematics from electrical circuit theory (see, e.g., the hydraulic DHN subsystem models in Section 6.1 and the examples in Wellstead [1979, pp. 178–179] and Pfeifer [2022, Example 2.14]). In addition to facilitating and unifying the model representation over different physical domains, such generalized equivalent circuit diagrams directly enable the transfer of established methods from electrical circuit theory such as Kirchhoff's laws to other physical domains. Among others, these benefits are used to develop the DHN results in Chapter 6.

A.2.2 Input-State-Output Port-Hamiltonian Systems

In this thesis, an important subclass of PHSs, so-called ISO-PHSs, are used to model the different subsystems within the networked energy systems. ISO-PHSs are explicit

state-space models with a specific structure and represent the starting point for most of the control engineering methods that exploit PHS theory (see, e.g., Ortega and García-Cansco [2004], Jayawardhana et al. [2007], Donaire and Junco [2009], and van der Schaft [2017, Chapter 7]). A comprehensive theoretical introduction into PHS theory and explicit ISO-PHSs can be found in the textbooks of Duindam et al. [2009], van der Schaft and Jeltsema [2014], and van der Schaft [2017]. For an illustrative summary, see Pfeifer [2022, Section 2.2].

The following definition is based on Duindam et al. [2009, p. 69].

Definition A.2 (ISO-PHS without feedthrough)

An ISO-PHS without feedthrough is an explicit state-space model of the form

$$\dot{\mathbf{x}} = [\mathbf{J}(\mathbf{x}) - \mathbf{R}(\mathbf{x})] \frac{\partial H}{\partial \mathbf{x}}(\mathbf{x}) + \mathbf{G}(\mathbf{x})\mathbf{u} + \mathbf{K}(\mathbf{x})\mathbf{d}, \quad (\text{A.5a})$$

$$\mathbf{y} = \mathbf{G}(\mathbf{x})^\top \frac{\partial H}{\partial \mathbf{x}}(\mathbf{x}), \quad (\text{A.5b})$$

$$\mathbf{z} = \mathbf{K}(\mathbf{x})^\top \frac{\partial H}{\partial \mathbf{x}}(\mathbf{x}), \quad (\text{A.5c})$$

with state vector $\mathbf{x} \in \mathcal{X} \subseteq \mathbb{R}^n$, co-state vector $\frac{\partial H}{\partial \mathbf{x}}(\mathbf{x}) \in \mathbb{R}^n$, control port pair $(\mathbf{u}, \mathbf{y}) \in \mathbb{R}^{m_u} \times \mathbb{R}^{m_u}$, and uncontrolled interaction (coupling) port pair $(\mathbf{d}, \mathbf{z}) \in \mathbb{R}^m \times \mathbb{R}^m$. The Hamiltonian H is a continuously differentiable, positive semidefinite function $H : \mathcal{X} \rightarrow \mathbb{R}_{\geq 0}$. The matrices $\mathbf{J}(\mathbf{x}), \mathbf{R}(\mathbf{x}) \in \mathbb{R}^{n \times n}$ satisfy $\mathbf{J}(\mathbf{x}) = -\mathbf{J}(\mathbf{x})^\top$ and $\mathbf{R}(\mathbf{x}) = \mathbf{R}(\mathbf{x})^\top \succcurlyeq 0$. Furthermore, $\mathbf{G}(\mathbf{x}) \in \mathbb{R}^{n \times m_u}$ and $\mathbf{K}(\mathbf{x}) \in \mathbb{R}^{n \times m}$.

Remark A.1. Note that in contrast to the ISO-PHS definitions commonly found in the literature, for example in van der Schaft and Jeltsema [2014, p. 56] or van der Schaft [2017, Definition 6.1.1], Definition A.2 makes a precise distinction between inputs \mathbf{u} that are accessible for control and (uncontrolled) inputs \mathbf{d} that arise from the interaction (coupling) with the system environment or other subsystems. Particularly in the context of networked systems, such a distinction is helpful for control design and a modular stability analysis.

For some practical applications, e.g., for nonlinear loads in power systems (see Sections 4.1.2 and 5.1.2) or pressure drops in hydraulic networks (see Section 6.1.5), the relation describing dissipation effects cannot be brought into an expression of the form $\mathbf{R}(\mathbf{x}) \frac{\partial H}{\partial \mathbf{x}}(\mathbf{x})$ as in (A.5a). In such cases, the ISO-PHS definition has to be extended to nonlinear resistive structures⁵⁹ expressed by a general nonlinear damping function (cf.

⁵⁹ Note that the term *nonlinear* in the context of the resistive structure does not refer to a nonlinearity with respect to \mathbf{x} , which can already occur in expressions of the form $\mathbf{R}(\mathbf{x}) \frac{\partial H(\mathbf{x})}{\partial \mathbf{x}}$. Instead, the nonlinearity refers to the so-called resistive port variables. For a detailed discussion see van der Schaft and Jeltsema [2014, p. 24] and Pfeifer [2022, pp. 28–29].

van der Schaft [2017, p. 115])

$$\mathcal{R}(x, \cdot) : \mathbb{R}^n \rightarrow \mathbb{R}^n, \left(\frac{\partial H}{\partial x}(x) \right)^\top \mathcal{R} \left(x, \frac{\partial H}{\partial x}(x) \right) \geq 0, \quad \forall \frac{\partial H}{\partial x}(x) \in \mathbb{R}^n, x \in \mathcal{X}. \quad (\text{A.6})$$

On the other end of the spectrum, an important subclass of ISO-PHS models constitute linear state-space models. Such linear ISO-PHSs are given by (A.5) with quadratic, positive semidefinite Hamiltonians $H(x) = \frac{1}{2}x^\top Qx$, $Q = Q^\top \succcurlyeq 0$ and constant matrices $J, R \in \mathbb{R}^{n \times n}$, $G \in \mathbb{R}^{n \times m_u}$, $K \in \mathbb{R}^{n \times m}$ with $J = -J^\top$ and $R = R^\top \succcurlyeq 0$ [van der Schaft, 2017, p. 116].

B Appendices to Chapters 4 and 5

B.1 Nonlinear Static Load Models

The most common nonlinear static load models are polynomial and exponential models. In the case of AC power system, they are described by the active and reactive powers $P_L(V)$ and $Q_L(V)$ as voltage-dependent functions [van Cutsem and Vournas, 1998, pp. 95ff]; [Machowski et al., 2008, pp. 111-112]; [Farrokhabadi et al., 2018, pp. 33–34]. Polynomial models comprise constant impedance (a_Z), constant current (a_I) and constant power (a_P) coefficients, leading to the ZIP load equations

$$P_L = P_0 \left[a_{Z,P} \left(\frac{V}{V_0} \right)^2 + a_{I,P} \left(\frac{V}{V_0} \right) + a_{P,P} \right], \quad (\text{B.1a})$$

$$Q_L = Q_0 \left[a_{Z,Q} \left(\frac{V}{V_0} \right)^2 + a_{I,Q} \left(\frac{V}{V_0} \right) + a_{P,Q} \right], \quad (\text{B.1b})$$

where $V \geq 0$ is the amplitude of any instantaneous, complex voltage vector (see (5.2)),⁶⁰ $V_0 > 0$ is the nominal phase-to-phase RMS value (e.g., 400 V or 20 kV), and $P_0 > 0$ and $Q_0 > 0$ are the nominal active and reactive powers, respectively. By grouping the coefficients and nominal values in (B.1) into the model parameters

$$Y_P = \frac{a_{Z,P}}{V_0^2}, \quad I_P = \frac{a_{I,P}P_0}{V_0}, \quad P_P = a_{P,P}P_0, \quad (\text{B.2a})$$

$$Y_Q = \frac{a_{Z,Q}Q_0}{V_0^2}, \quad I_Q = \frac{a_{I,Q}Q_0}{V_0}, \quad P_Q = a_{P,Q}Q_0, \quad (\text{B.2b})$$

the simplified ZIP load equations

$$P_L(V) = Y_P V^2 + I_P V + P_P, \quad (\text{B.3a})$$

$$Q_L(V) = Y_Q V^2 + I_Q V + P_Q, \quad (\text{B.3b})$$

are obtained. Note that the constant impedances (Z) are expressed as admittances (Y).

Exponential load models, on the other hand, are given by

$$P_L(V) = P_0 \left(\frac{V}{V_0} \right)^{n_P}, \quad (\text{B.4a})$$

$$Q_L(V) = Q_0 \left(\frac{V}{V_0} \right)^{n_Q}, \quad (\text{B.4b})$$

⁶⁰ Recall from Property 5.1 that under a power-invariant dq transformation, V in steady-state equals the phase-to-phase RMS voltage.

where V_0, P_0, Q_0 as above and $n_P \geq 0$ and $n_Q \geq 0$ are the voltage indices of the active and reactive power, respectively.

As per Machowski et al. [2008, pp. 110-112], the models in (B.3) and (B.4) are only accurate above $0.7 V_0$. Below $0.7 V_0$, real loads typically exhibit a rapid power drop and approximately behave like constant impedances

$$P_L(V) = P_0 \left[a_{z,P} \left(\frac{V}{V_0} \right)^2 \right] = \tilde{Y}_P V^2, \quad (\text{B.5a})$$

$$Q_L(V) = Q_0 \left[a_{z,Q} \left(\frac{V}{V_0} \right)^2 \right] = \tilde{Y}_Q V^2. \quad (\text{B.5b})$$

From continuity considerations, i.e., by comparing (B.3) and (B.4) with (B.5a) and (B.5b) at $V = 0.7 V_0$, it follows for ZIP loads that

$$\tilde{Y}_P = Y_P + \frac{I_P}{0.7 V_0} + \frac{P_P}{(0.7 V_0)^2}, \quad \tilde{Y}_Q = Y_Q + \frac{I_Q}{0.7 V_0} + \frac{P_Q}{(0.7 V_0)^2}. \quad (\text{B.5c})$$

For exponential loads, it follows that

$$\tilde{Y}_P = \frac{P_0 0.7^{n_P}}{(0.7 V_0)^2}, \quad \tilde{Y}_Q = \frac{Q_0 0.7^{n_Q}}{(0.7 V_0)^2}. \quad (\text{B.5d})$$

The combination of (B.5) for $V < 0.7 V_0$ and (B.3) and (B.4), respectively, for $V \geq 0.7 V_0$ is referred to as *two-tier load model* [Machowski et al., 2008, p. 112].

In DC power systems, the reactive power equations are not needed. Thus, ZIP and exponential DC loads are simply modeled by (B.3a) and (B.4a), respectively, for $V \geq 0.7 V_0$ and by (B.5a) for $V < 0.7 V_0$.

B.2 Passivity-Based Output Control of Linear Second-Order Systems

In many practical engineering problems (e.g., second-order generator models [Ajala et al., 2020], dynamics in multi-agent systems [Yu et al., 2010], RLC circuits and filters [Desoer and Khu, 1969, Chapter 5]), it is sufficient for the control design to describe the dynamics of the systems in question by linear, second-order dynamics of the form

$$\frac{Y(s)}{U(s)} = \frac{K}{T^2 s^2 + 2DTs + 1} \quad (\text{B.6})$$

with $\dot{y}(t=0) = 0, y(t=0) = 0, u(t=0) = 0$, time constant $T > 0$, damping factor $D > 0$, and gain $K > 0$. A typical control problem is then to asymptotically stabilize the output y to some desired setpoint y^* .

However, the ‘control input u to measured and controlled output y' ’-perspective of linear, second-order models (B.6) hampers their integration into physically networked system models such as the energy system models considered in this thesis. This is due to the fact that in contrast to models obtained from first-principle physics (see, e.g., the DC power system modeling in Section 4.1), the interfaces, i.e., the control and interaction (coupling) ports, of subsystems modeled as transfer functions (B.6) are not automatically well-defined. Instead, to recover a suitable network model and conduct an overall system analysis, the definition of the ports over which the transfer function models interact with the network has to be given careful consideration.

In the following, it is shown how suitable control and interaction ports can be defined for general linear, second-order systems of the form (B.6) such that they can be represented as linear ISO-PHSs. Subsequently, it is shown how the voltage controller design from Proposition 4.3 that combines algebraic IDA-PBC and integral action can be applied to ensure $\bar{y} = y^*$ while providing additional EIP properties and confined dynamics behavior as required per Theorem 3.1. Moreover, it is demonstrated that the insight from Remark 4.7 extends to general linear second-order systems of the form (B.6), i.e., the resulting controller amounts to a combination of standardized setpoint feedforward, state-feedback, and PI control functions.

To begin with, the linear, second-order system (B.6) is rewritten without loss of generality as

$$\frac{Y(s)}{U(s)} = \frac{K}{T_1 T_2 s^2 + 2D\sqrt{T_1 T_2} s + 1}, \quad (\text{B.7})$$

where the time constant T is expressed by two auxiliary variables $T_1, T_2 > 0$ as $T = \sqrt{T_1 T_2}$. Subsequently, by introducing a suitable interaction input d , (B.7) can be represented as a linear ISO-PHSs [van der Schaft, 2017, p. 116].

Lemma B.1 (ISO-PHS model of a linear, second-order transfer function)

Consider a linear, second-order system of the form (B.7) with $\dot{y}(t=0) = 0, y(t=0) = 0, u(t=0) = 0$. By introducing a suitable interaction input d , (B.7) can be written as linear ISO-PHS of the form

$$\begin{bmatrix} \dot{x}_1 \\ \dot{x}_2 \end{bmatrix} = \begin{bmatrix} -2D\sqrt{\frac{T_1}{T_2}} & -1 \\ 1 & 0 \end{bmatrix} \begin{bmatrix} \frac{x_1}{T_1} \\ \frac{x_2}{T_2} \end{bmatrix} + \begin{bmatrix} K \\ 0 \end{bmatrix} u + \begin{bmatrix} 0 \\ 1 \end{bmatrix} d, \quad (\text{B.8a})$$

$$y_p = [K, 0] \begin{bmatrix} \frac{x_1}{T_1} \\ \frac{x_2}{T_2} \end{bmatrix} = \frac{K}{T_1} x_1, \quad (\text{B.8b})$$

$$z = [0, 1] \begin{bmatrix} \frac{x_1}{T_1} \\ \frac{x_2}{T_2} \end{bmatrix} = \frac{x_2}{T_2} = y, \quad (\text{B.8c})$$

with quadratic, positive definite Hamiltonian $H : \mathbb{R}^2 \rightarrow \mathbb{R}_{\geq 0}$

$$H(\mathbf{x}) = \frac{1}{2} \mathbf{x}^\top \begin{bmatrix} \frac{1}{T_1} & 0 \\ 0 & \frac{1}{T_2} \end{bmatrix} \mathbf{x}, \quad (\text{B.8d})$$

states $x_1 = T_1 T_2 \dot{y} \in \mathbb{R}$, $x_2 = T_2 y \in \mathbb{R}$, control port pair $(u, y_p) \in \mathbb{R} \times \mathbb{R}$, and interaction port pair $(d, z) \in \mathbb{R} \times \mathbb{R}$.

Proof:

By choosing the states as $x_1 = T_1 T_2 \dot{y}$, $x_2 = T_2 y$, and the Hamiltonian as in (B.8d), (B.7) can be written in the time domain as

$$\begin{bmatrix} \dot{x}_1 \\ \dot{x}_2 \end{bmatrix} = \begin{bmatrix} -2D\sqrt{\frac{T_1}{T_2}} & -1 \\ 1 & 0 \end{bmatrix} \begin{bmatrix} \frac{x_1}{T_1} \\ \frac{x_2}{T_2} \end{bmatrix} + \begin{bmatrix} K \\ 0 \end{bmatrix} u, \quad (\text{B.9a})$$

$$y_p = [K, 0] \begin{bmatrix} \frac{x_1}{T_1} \\ \frac{x_2}{T_2} \end{bmatrix} = \frac{K}{T_1} x_1, \quad (\text{B.9b})$$

with y_p the passive output of relative degree one with respect to the control input u [Sepulchre et al., 1997, pp. 61,63]. Next, the interaction port pair (d, z) is defined. Firstly, consider that with the state definition used in (B.9), the actual output y of the second-order transfer function (B.7) is given by

$$y = \frac{x_2}{T_2} = [0 \ 1] \begin{bmatrix} \frac{x_1}{T_1} \\ \frac{x_2}{T_2} \end{bmatrix} \quad (\text{B.10})$$

Since system (B.7) interacts via output y with other subsystems (in the networked case) or the environment, define the interaction output as $z := y$ to obtain (B.8c). Lastly, the corresponding passive input d is introduced by using $[0, 1]^\top$ as suitable interaction input matrix such that z has a relative degree of one with respect to d . \square

Remark B.1. Note that since $y_p = K T_2 \dot{y} = K T_2 \dot{z}$ holds, $z = y$ has a relative degree of two with respect to the control input u .

Remark B.2. From the second-order transfer function (B.7), one can directly recover the transfer function

$$\frac{Y(s)}{U(s)} = \frac{1}{LCs^2 + RCs + 1} \quad (\text{B.11})$$

of a generalized RLC equivalent circuit as illustrated in Figure B.1 by identifying $K = 1$, $T_1 = L$, $T_2 = C$, and $R = 2D\sqrt{\frac{T_1}{T_2}}$. Note in order to obtain a transfer function as in (B.11) from an RLC equivalent circuit, the interaction flow is set to zero, i.e. $d = -f_N = 0$. If an RLC equivalent circuit is connected to a larger network, i.e. with $f_N \neq 0$, it can directly be represented as a linear ISO-PHS as in (B.8) with $K = 1$, $T_1 = L$, $T_2 = C$, $R = 2D\sqrt{\frac{T_1}{T_2}}$, control port pair $(u = e_S, y_p = f)$, and interaction port pair $(d = -f_N, z = e)$.

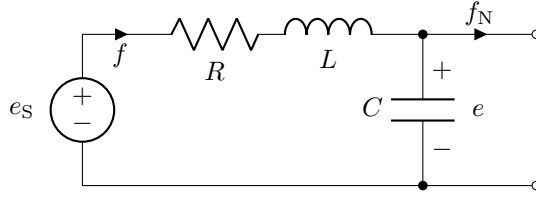


Figure B.1: Linear, generalized RLC equivalent circuit diagram with generalized voltage source

Based on the ISO-PHS model in Lemma B.1, the combined algebraic IDA and integral action design from Proposition 4.3 can now be applied. The resulting controller ensures that the non-passive, relative-degree-two output⁶¹ $z = y$ reaches some desired setpoint $\bar{z} = \bar{y} = y^*$ in steady-state while additional EIP properties and confined dynamics behavior are provided as required by Theorem 3.1.

Proposition B.1 (EIP-based output controller for linear second-order systems)

Consider a linear second-order system (B.8). Assign the control input u as

$$Q_1 \dot{r} = y - y^*, \quad (\text{B.12a})$$

$$u = \frac{1}{K} \left[y^* + \left(2D\sqrt{\frac{T_1}{T_2}} - \hat{R} \right) \frac{x_1}{T_1} - \hat{R}r + \frac{T_1}{Q_1} (y^* - y) \right], \quad (\text{B.12b})$$

where $y^* = \frac{x_2^*}{T_2} > 0$ is a desired output setpoint and $\hat{R}, Q_1 > 0$ are control parameters. Then, with the change of coordinates from $\frac{x_1}{T_1}$ to

$$\chi := \frac{x_1}{T_1} + r, \quad (\text{B.13})$$

the closed-loop system can be written as

$$\frac{d}{dt} \underbrace{\begin{bmatrix} T_1 \chi \\ x_2 \\ Q_1 r \end{bmatrix}}_{\hat{x}} = \underbrace{\begin{bmatrix} -\hat{R}\chi - (y - y^*) \\ \chi - r \\ y - y^* \end{bmatrix}}_{\hat{f}(\hat{x})} + \underbrace{\begin{bmatrix} 0 \\ 1 \\ 0 \end{bmatrix}}_{\hat{K}} d, \quad (\text{B.14a})$$

$$z - \bar{z} = y - y^*. \quad (\text{B.14b})$$

⁶¹ Note that the relative degree and the non-passivity refer to the control input u .

Moreover, (B.14) is EIP w.r.t. the supply rate $(d - \bar{d})(z - \bar{z})$ and the continuously differentiable, positive definite storage function

$$\hat{S}(\hat{\mathbf{x}}, \bar{\mathbf{x}}) = \frac{1}{2} \|\hat{\mathbf{x}} - \bar{\mathbf{x}}\|_{\hat{Q}}^2, \quad (\text{B.15a})$$

$$\hat{Q} = \text{diag} \left(\frac{1}{T_1}, \frac{1}{T_2}, \frac{1}{Q_I} \right), \quad (\text{B.15b})$$

for any (feasible) equilibrium pair (\bar{d}, \bar{z}) and associated equilibrium state vector

$$\bar{\mathbf{x}} = [T_1 \bar{\chi}, T_2 y^*, Q_I \bar{r}]^\top. \quad (\text{B.16})$$

Lastly, no solution other than $\hat{\mathbf{x}} = \bar{\mathbf{x}}$ as in (B.16) can stay in $\mathbb{E} = \{\hat{\mathbf{x}} \in \hat{\mathcal{X}} \subseteq \mathbb{R}^3 \mid \dot{\hat{S}}(\hat{\mathbf{x}}, \bar{\mathbf{x}}) = 0, d = \bar{d}\}$ for all time.

Proof:

The proof is similar to that of Proposition 4.3. In particular, substitute $T_1 = L_i, T_2 = C_i, x_1 = L_i I_i, x_2 = C_i V_i, \frac{x_1}{T_1} = I_i, \frac{x_2}{T_2} = V_i$, and set $I_{L,i}(V_i) = 0$. The factor $\frac{1}{K}$ in the controller (B.12b) arises by noting that Ku instead of u_i in (4.34) and (4.35). \square

C Appendices to Chapter 6

C.1 Operating Modes of District Heating Network Subsystems

In this section, a preliminary investigation is conducted regarding the degrees of freedom that are available in choosing the operating modes of the DHN subsystems. In particular, it is to be determined (i) if DGUs are subject to any restrictions on their choice of operating modes, i.e., grid-forming or grid-feeding, and (ii) whether all consumers and mixing connections can in principle, i.e., disregarding any technical constraints, independently control their volume flow rates to desired steady-state values.

Proposition C.1 (Operating modes of DHN subsystems)

Consider a DHN as modeled in Section 6.1 with $D \geq 1$ DGUs, $L \geq 1$ consumers, $P \geq 2$ pipes, $M \geq 0$ mixing connections, and two hydraulic layers $\mathcal{G}_1, \mathcal{G}_2$ (see Definition 6.1). Then, the following holds:

- (i) there must be at least one grid-forming DGU $l \in \mathcal{D}_{\text{form}}$ connecting the two hydraulic layers $\mathcal{G}_1, \mathcal{G}_2$.
- (ii) each steady-state volume flow rate $\bar{q}_l, l \in \mathcal{D}_{\text{feed}} \cup \mathcal{L} \cup M \cup \mathcal{P}_{\text{loop}}$, is an independent variable where each $\mathcal{P}_{\text{loop}} \subseteq \mathcal{P}$ forms an independent loop within \mathcal{G}_1 or \mathcal{G}_2 .

Proof:

Following Desoer and Khu [1969, pp. 477–482], the subsequent proof makes use of the fundamental loop analysis of circuit theory. Firstly, note that since the digraph \mathcal{G} representing a DHN is weakly connected, it admits a generally non-unique spanning tree \mathcal{T} (see, e.g., De Persis and Kallæsø [2011] and Wang et al. [2017b]). The spanning tree \mathcal{T} is a weakly connected subgraph of \mathcal{G} that contains all nodes of \mathcal{G} and no loops [Desoer and Khu, 1969, p. 477]. Any edge of \mathcal{G} not in \mathcal{T} is referred to as *chord* and creates a (fundamental) loop when added to \mathcal{T} . For $\mathcal{G} = (\mathcal{N}, \mathcal{E})$, there are $|\mathcal{E}| - |\mathcal{N}| + 1$ chords and loops, respectively. By applying KCL, it can be shown that each steady-state flow through an edge in \mathcal{T} is the superposition of one or more of the steady-state loop flows [Desoer and Khu, 1969, p. 482]. By setting the loop flows equal to the chord flows, it thus follows that the $|\mathcal{E}| - |\mathcal{N}| + 1$ chord flows form a complete set of independent variables.

To prove (i), note that per Definition 6.1, only DGU, consumer, or mixing edges may connect the two hydraulic layers \mathcal{G}_1 and \mathcal{G}_2 (see also Figures 6.3 and 6.4). Additionally,

the hydraulic layers may have a meshed structure. Thus, in order to create a spanning tree \mathcal{T} of \mathcal{G} , \mathcal{G}_1 and \mathcal{G}_2 have to be connected via exactly one edge in the union $\mathcal{D} \cup \mathcal{L} \cup \mathcal{M}$. Furthermore, some pipe edges in $\mathcal{P}_{\text{loop}} \subseteq \mathcal{P}$ that form loops within \mathcal{G}_1 and \mathcal{G}_2 , respectively, may have to be removed. From the fundamental loop analysis follows that the steady-state flow through the single edge connecting \mathcal{G}_1 and \mathcal{G}_2 is not independent. Thus, this edge must be a pressure-controlled subsystem in $\mathcal{D} \cup \mathcal{L} \cup \mathcal{M}$, which can only be fulfilled by a grid-forming DGU $l \in \mathcal{D}_{\text{form}}$.

In turn, the set of chords can be chosen such that it contains all DGU edges except one, all consumer edges, possibly some pipe edges that form loops within a meshed, hydraulic layer \mathcal{G}_1 or \mathcal{G}_2 , respectively, and all mixing edges. Consequently, the steady-state flows through these edges are independent variables, which proves (ii). \square

Remark C.1. *The independent steady-state pipe flows $\bar{q}_l, l \in \mathcal{P}_{\text{loop}}$, provide additional degrees of freedom that might be used, e.g., to minimize pumping costs (see Wang et al. [2017b, Section 2.2]).*

C.2 Proof of Proposition 6.4

In the following, the closed-loop systems are considered successively according to their order in Problem 6.1 (a)–(i).

$k \in \mathcal{D}_{\text{form}}$ By combining the open-loop DGU model (6.5), (6.11) with $u_{P,k}$ as in (6.18) and fixing $u_{v,k}(s_{v,k} = 1) = \bar{u}_{v,k} = 1 > 0$, the closed loop can be written as in (6.40) with

$$\frac{d}{dt} \underbrace{\begin{bmatrix} J_k q_k \\ J_{P,k} \chi_k \\ C_{P,k} p_{P,k} \\ Q_{I,k} r_k \end{bmatrix}}_{\hat{\mathbf{x}}_k} = \underbrace{\begin{bmatrix} p_{P,k} - \lambda_k(q_k) - \tilde{\mu}_k(q_k) \bar{u}_{v,k} \\ -\hat{R}_k \chi_k - (p_{P,k} - p_{P,k}^*) \\ \chi_k - r_k \\ p_{P,k} - p_{P,k}^* \end{bmatrix}}_{\hat{\mathbf{f}}_k(\hat{\mathbf{x}}_k)} + \underbrace{\begin{bmatrix} 1 \\ 0 \\ 0 \\ 0 \end{bmatrix}}_{\hat{\mathbf{K}}_k} d_k, \quad (\text{C.1a})$$

$$z_i = \underbrace{\begin{bmatrix} \frac{1}{J_i} & 0 & 0 & 0 \end{bmatrix}}_{\hat{\mathbf{K}}_k^\top \hat{\mathbf{Q}}_k} \hat{\mathbf{x}}_k. \quad (\text{C.1b})$$

To show that (C.1) is OSEIP, write (C.1) equivalently as

$$\dot{\hat{\mathbf{x}}}_k = \hat{\mathbf{f}}_k(\hat{\mathbf{x}}_k) - \hat{\mathbf{f}}_k(\tilde{\mathbf{x}}_k) + \hat{\mathbf{K}}_k(d_k - \bar{d}_k), \quad (\text{C.2a})$$

$$z_k - \bar{z}_k = \hat{\mathbf{K}}_k^\top \hat{\mathbf{Q}}_k(\hat{\mathbf{x}}_k - \tilde{\mathbf{x}}_k), \quad (\text{C.2b})$$

and take the storage function \hat{S}_k as in (6.41) with

$$\hat{Q}_k = \text{diag}^{-1}(J_k, J_{P,k}, C_{P,k}, Q_{I,k}). \quad (\text{C.3})$$

For the time derivative of $\hat{S}_k(\hat{\mathbf{x}}_k, \bar{\mathbf{x}}_k)$, it holds that

$$\dot{\hat{S}}_k(\hat{\mathbf{x}}_k, \bar{\mathbf{x}}_k) = \underbrace{(\hat{\mathbf{x}}_k - \bar{\mathbf{x}}_k)^\top \hat{Q}_k (\hat{\mathbf{f}}_k(\hat{\mathbf{x}}_k) - \hat{\mathbf{f}}_k(\bar{\mathbf{x}}_k))}_{-\hat{\psi}_k(\hat{\mathbf{x}}_k, \bar{\mathbf{x}}_k)} + \underbrace{(\hat{\mathbf{x}}_k - \bar{\mathbf{x}}_k)^\top \hat{Q}_k \hat{K}_k}_{(z_k - \bar{z}_k)} (d_k - \bar{d}_k). \quad (\text{C.4})$$

With (C.1) and (C.3), the dissipation rate can be written as

$$\begin{aligned} \hat{\psi}_k(\hat{\mathbf{x}}_k, \bar{\mathbf{x}}_k) &= (q_k - \bar{q}_k) (\lambda_k(q_k) - \lambda_k(\bar{q}_k)) + \bar{u}_{v,k} (q_k - \bar{q}_k) (\tilde{\mu}_k(q_k) - \tilde{\mu}_k(\bar{q}_k)) \\ &\quad + \hat{R}_k (\chi_k - \bar{\chi}_k)^2 \end{aligned} \quad (\text{C.5a})$$

$$\begin{aligned} &= (z_k - \bar{z}_k) (\lambda_k(z_k) - \lambda_k(\bar{z}_k)) + (z_k - \bar{z}_k) \bar{u}_{v,k} (\tilde{\mu}_k(z_k) - \tilde{\mu}_k(\bar{z}_k)) \\ &\quad + \hat{R}_k (\chi_k - \bar{\chi}_k)^2. \end{aligned} \quad (\text{C.5b})$$

Since $\lambda_k(z_k)$ and $\tilde{\mu}_k(z_k)$ are strictly increasing and $\bar{u}_{v,k}, \hat{R}_k > 0$, the closed-loop system (C.1) is OSEIP w.r.t. the supply rate $(d_k - \bar{d}_k)(z_k - \bar{z}_k)$ and the continuously differentiable, positive definite storage function (6.41) with \hat{Q}_k as in (C.3). Then, from (C.4), it follows that set \mathbb{E}_k is characterized by

$$\hat{\psi}_k(\hat{\mathbf{x}}_k, \bar{\mathbf{x}}_k) \equiv 0 \xrightarrow{(\text{C.5})} q_k \equiv \bar{q}_k, \chi_k \equiv \bar{\chi}_k. \quad (\text{C.6})$$

Now consider the evolution of a solution of (C.2) starting in \mathbb{E}_k . Confine the dynamics (C.2) to \mathbb{E}_k for any future time by inserting (C.6). This yields the set of equations

$$\begin{aligned} 0 &= p_{P,k} - p_{P,k}^*, \\ 0 &= -(p_{P,k} - p_{P,k}^*), \\ C_{P,k} \dot{p}_{P,k} &= -(r_k - \bar{r}_k), \\ Q_{I,k} \dot{r}_k &= p_{P,k} - p_{P,k}^*, \end{aligned} \quad (\text{C.7})$$

whose unique solution is $p_{P,k} \equiv p_{P,k}^*, r_k \equiv \bar{r}_k$. Thus, no solution other than

$$\bar{\mathbf{x}}_k = [J_k \bar{q}_k, J_{P,k} \bar{\chi}_k, C_{P,k} p_{P,k}^*, Q_{I,k} \bar{r}_k]^\top. \quad (\text{C.8})$$

can stay in \mathbb{E}_k for all time.

$k \in \mathcal{D}_{\text{valve}}$ By combining the open-loop DGU model (6.5), (6.11) with $u_{P,k}$ and $u_{v,k}$ as in (6.18) and (6.33), respectively, the closed loop can be written as in (6.40) with

$$\frac{d}{dt} \underbrace{\begin{bmatrix} J_k q_k \\ J_{P,k} \chi_k \\ C_{P,k} p_{P,k} \\ Q_{I,k}^\alpha r_k^\alpha \\ Q_{I,k}^\beta r_k^\beta \end{bmatrix}}_{\hat{\mathbf{x}}_k} = \underbrace{\begin{bmatrix} p_{P,k} - \lambda_k(q_k) - \tilde{\mu}_k(q_k)(-K_{v,k} \hat{y}_k + r_k^\beta) \\ -\hat{R}_k \chi_k - (p_{P,k} - p_{P,k}^*) \\ \chi_k - r_k^\alpha \\ p_{P,k} - p_{P,k}^* \\ \tilde{\mu}_k(q_k)(q_k - q_k^*) \end{bmatrix}}_{\hat{\mathbf{f}}_k(\hat{\mathbf{x}}_k)} + \underbrace{\begin{bmatrix} 1 \\ 0 \\ 0 \\ 0 \\ 0 \end{bmatrix}}_{\mathbf{K}_k} d_k, \quad (\text{C.9a})$$

$$z_k = \underbrace{\begin{bmatrix} \frac{1}{J_k} & 0 & 0 & 0 & 0 \end{bmatrix}}_{\mathbf{K}_k^\top \hat{\mathbf{Q}}_k} \hat{\mathbf{x}}_k. \quad (\text{C.9b})$$

Note that the indices α and β are used to distinguish between the integral actions of (6.18) and (6.33), respectively. The remaining steps are similar as before. From (C.9) and the storage function \hat{S}_k as in (6.41) with

$$\hat{\mathbf{Q}}_k = \text{diag}^{-1}(J_k, J_{P,k}, C_{P,k}, Q_{I,k}^\alpha, Q_{I,k}^\beta) \quad (\text{C.10})$$

follows the dissipation rate

$$\begin{aligned} \hat{\psi}_k(\hat{\mathbf{x}}_k, \bar{\hat{\mathbf{x}}}_k) &= (q_k - \bar{q}_k)(\lambda_k(q_k) - \lambda_k(\bar{q}_k)) + \bar{r}_k^\beta (q_k - \bar{q}_k)(\tilde{\mu}_k(q_k) - \tilde{\mu}_k(\bar{q}_k)) \\ &\quad + \hat{R}_k (\chi_i - \bar{\chi}_i)^2 + K_{v,k} \hat{y}_k^2 \end{aligned} \quad (\text{C.11a})$$

$$\begin{aligned} &= (z_k - \bar{z}_k)(\lambda_k(z_k) - \lambda_k(\bar{z}_k)) + (z_k - \bar{z}_k) \bar{u}_{v,k} (\tilde{\mu}_k(z_k) - \tilde{\mu}_k(\bar{z}_k)) \\ &\quad + \hat{R}_k (\chi_i - \bar{\chi}_i)^2 + K_{v,k} \hat{y}_k^2. \end{aligned} \quad (\text{C.11b})$$

Since $\lambda_k(z_k)$ and $\tilde{\mu}_k(z_k)$ are strictly increasing, $\bar{u}_{v,k} = \bar{r}_k^\beta > 0$ per definition (see Section 6.1.2), and $K_{v,k}, \hat{R}_k > 0$, the closed-loop system (C.9) is OSEIP w.r.t. the supply rate $(d_k - \bar{d}_k)(z_k - \bar{z}_k)$ and the continuously differentiable, positive definite storage function \hat{S}_k . Under Assumption 6.3, it holds that

$$\hat{\psi}_k(\hat{\mathbf{x}}_k, \bar{\hat{\mathbf{x}}}_k) \equiv 0 \xrightarrow{(\text{C.11})} \chi_k \equiv \bar{\chi}_k, \hat{y}_k \equiv 0 \implies q_k \equiv \bar{q}_k \equiv q_k^* \quad (\text{C.12})$$

and the shifted dynamics of (C.9) confined to \mathbb{E}_k are given by

$$\begin{aligned} 0 &= p_{P,k} - p_{P,k}^* - \tilde{\mu}_k(q_k^*) (r_k^\beta - \bar{r}_k^\beta), \\ 0 &= -(p_{P,k} - p_{P,k}^*), \\ C_{P,k} \dot{p}_{P,k} &= -(r_k^\alpha - \bar{r}_k^\alpha), \\ Q_{I,k}^\alpha \dot{r}_k^\alpha &= p_{P,k} - p_{P,k}^*, \\ Q_{I,k}^\beta \dot{r}_k^\beta &= 0, \end{aligned} \quad (\text{C.13})$$

whose unique solution is $p_{P,k} \equiv p_{P,k}^*$, $r_k^\alpha \equiv \bar{r}_k^\alpha$, $r_k^\beta \equiv \bar{r}_k^\beta$. Thus, no solution other than

$$\bar{\hat{\mathbf{x}}}_k = \left[J_k q_k^*, J_{P,k} \bar{\chi}_k, C_{P,k} p_{P,k}^*, Q_{I,k}^\alpha \bar{r}_k^\alpha, Q_{I,k}^\beta \bar{r}_k^\beta \right]^\top \quad (\text{C.14})$$

can stay in \mathbb{E}_k for all time.

$k \in \mathcal{D}_{\text{VSP}}$ By combining the open-loop DGU model (6.5), (6.11) with $u_{\text{P},k}$ as in (6.23) and fixing $u_{\text{v},k}(s_{\text{v},k} = 1) = \bar{u}_{\text{v},k} = 1 > 0$, the closed loop can be written as in (6.40) with

$$\frac{\text{d}}{\text{d}t} \underbrace{\begin{bmatrix} J_k q_k \\ J_{\text{P},k} \chi_k \\ C_{\text{P},k} p_{\text{P},k} \\ Q_{\text{I},k} r_k \end{bmatrix}}_{\hat{\mathbf{x}}_k} = \underbrace{\begin{bmatrix} p_{\text{P},k} - \lambda_k(q_k) - \tilde{\mu}_k(q_k) \bar{u}_{\text{v},k} \\ -(1 + K_{\text{P},k}) p_{\text{P},k} - R_{\text{P},k} q_{\text{P},k} - t_k \\ q_{\text{P},k} - q_k \\ q_k - q_k^* \end{bmatrix}}_{\hat{\mathbf{f}}_k(\hat{\mathbf{x}}_k)} + \underbrace{\begin{bmatrix} 1 \\ 0 \\ 0 \\ 0 \end{bmatrix}}_{\hat{\mathbf{K}}_k} d_k, \quad (\text{C.15a})$$

$$z_k = \underbrace{\begin{bmatrix} \frac{1}{J_k} & 0 & 0 & 0 \end{bmatrix}}_{\hat{\mathbf{K}}_k^\top \hat{\mathbf{Q}}_k} \hat{\mathbf{x}}_k. \quad (\text{C.15b})$$

The remaining steps are similar as before. From (C.15) and the storage function \hat{S}_k as in (6.41) with $\hat{\mathbf{Q}}_k = \mathbf{Q}_k^{\text{f}}$ (see (6.26b)) follows the dissipation rate

$$\begin{aligned} \hat{\psi}_k(\hat{\mathbf{x}}_k, \bar{\mathbf{x}}_k) &= (q_k - q_k^*) (\lambda_k(q_k) - \lambda_k(q_k^*)) + \bar{u}_{\text{v},k} (q_k - q_k^*) (\tilde{\mu}_k(q_k) - \tilde{\mu}_k(q_k^*)) \\ &\quad + 2 \frac{R_{\text{P},k} Q_{\text{I},k}}{\kappa_i^{\text{f}}} (q_{\text{P},k} - \bar{q}_{\text{P},k})^2 \end{aligned} \quad (\text{C.16a})$$

$$\begin{aligned} &= (z_k - z_k^*) (\lambda_k(z_k) - \lambda_k(z_k^*)) + \bar{u}_{\text{v},k} (z_k - z_k^*) (\tilde{\mu}_k(z_k) - \tilde{\mu}_k(z_k^*)) \\ &\quad + 2 \frac{R_{\text{P},k} Q_{\text{I},k}}{\kappa_i^{\text{f}}} (q_{\text{P},k} - \bar{q}_{\text{P},k})^2. \end{aligned} \quad (\text{C.16b})$$

Since $\lambda_k(z_k)$ and $\tilde{\mu}_k(z_k)$ are strictly increasing, $\bar{u}_{\text{v},k} = 1 > 0$, and (6.24) holds, the closed-loop system (C.15) is OSEIP w.r.t. the supply rate $(d_k - \bar{d}_k)(z_k - \bar{z}_k)$ and the continuously differentiable, positive definite storage function \hat{S}_k . From

$$\hat{\psi}_k(\hat{\mathbf{x}}_k, \bar{\mathbf{x}}_k) \equiv 0 \stackrel{(\text{C.16})}{\implies} q_k \equiv q_k^*, q_{\text{P},k} \equiv \bar{q}_{\text{P},k} \equiv q_k^* \quad (\text{C.17})$$

follows that the shifted dynamics of (C.15) confined to \mathbb{E}_k are given by

$$\begin{aligned} 0 &= (p_{\text{P},k} - \bar{p}_{\text{P},k}), \\ 0 &= -(1 + K_{\text{P},k})(p_{\text{P},k} - \bar{p}_{\text{P},k}) - (r_k - \bar{r}_k), \\ C_{\text{P},k} \dot{p}_{\text{P},k} &= 0, \\ Q_{\text{I},k} \dot{r}_k &= 0, \end{aligned} \quad (\text{C.18})$$

whose unique solution is $p_{\text{P},k} \equiv \bar{p}_{\text{P},k}$, $r_k \equiv \bar{r}_k$. Thus, no solution other than

$$\bar{\mathbf{x}}_k = [J_k q_k^*, J_{\text{P},k} q_k^*, C_{\text{P},k} \bar{p}_{\text{P},k}, Q_{\text{I},k} \bar{r}_k]^\top \quad (\text{C.19})$$

can stay in \mathbb{E}_k for all time.

$k \in \mathcal{L}$ Recall that the open-loop model of any consumer $k \in \mathcal{L}$ is identical to that of any DGU $k \in \mathcal{D}$, i.e., to (6.5), (6.11). For any $k \in \mathcal{L}_{\text{boost}}$, assigning $u_{\text{P},k}$ and $u_{\text{v},k}$ as

in (6.18) and (6.33) thus yields a closed loop equivalent to (C.9) and the proof follows as above. For any $k \in \mathcal{L}_{\text{valve}}$, the associated pump can either be turned off or is not present. Thus, the open-loop model is equivalent to that of a control valve in series with a pipe element, i.e., to (6.34) and OSEIP follows directly by Proposition 6.3. Additionally, under Assumption 6.3, it holds that

$$\hat{\psi}_k(\hat{\mathbf{x}}_k, \bar{\mathbf{x}}_k) \equiv 0 \xrightarrow{(6.39)} q_k \equiv \bar{q}_k \equiv q_k^* \quad (\text{C.20})$$

and the shifted dynamics of (6.34) confined to \mathbb{E}_k are given by

$$\begin{aligned} 0 &= (r_k - \bar{r}_k), \\ Q_{I,k} \dot{r}_k^\beta &= 0, \end{aligned} \quad (\text{C.21})$$

whose unique solution is $r_k \equiv \bar{r}_k$. Thus, no solution other than

$$\bar{\mathbf{x}}_k = [J_k q_k^*, Q_{I,k} \bar{r}_k]^\top \quad (\text{C.22})$$

can stay in \mathbb{E}_k for all time. For any $k \in \mathcal{L}_{\text{VSP}}$, fixing $u_{v,k}(s_{v,k} = 1) = \bar{u}_{v,k} = 1 > 0$ and assigning $u_{p,k}$ as in (6.23) yields a closed loop equivalent to (C.15) and the proof follows as above.

$k \in \mathcal{P}_{\text{boost}}$ The open-loop model (6.4), (6.10) of any pipe $k \in \mathcal{P}_{\text{boost}}$ with booster pump can be obtained from the open-loop DGU model (6.5), (6.11) by setting $u_{v,k} = 0$. Thus, assigning $u_{p,k}$ as in (6.18) to the open-loop pipe model (6.4), (6.10) results in a closed loop as in (C.1) except with $\bar{u}_{v,k} = 0$. Thus, the proof follows analogously as above for $k \in \mathcal{D}_{\text{form}}$ by setting $\bar{u}_{v,k} = 0$ in the respective equations.

$k \in \mathcal{M}$ Combining the open-loop model (6.6), (6.12) with $u_{v,k}$ as in (6.33) yields a closed loop equivalent to (6.34). Thus, the proof is identical to that of $k \in \mathcal{L}_{\text{valve}}$.

$k \in \mathcal{H}$ The open-loop model (6.7) is identical to (6.1) and thus the proof follows directly from Proposition 6.1.

Abbreviations and Symbols

Abbreviations

CIGRE	Conseil International des Grands Réseaux Électriques
DGU	distributed generation unit (electrical)/ distributed heat generation unit (heat)
DHN	district heating network
DN	diameter nominal
DVSP	distributed variable-speed pump
EIO	equilibrium-independent observable/observability
EIP	equilibrium-independent passive/passivity
FACTS	flexible alternating current transmission system
GPS	global positioning system
IDA	interconnection and damping assignment
ISO	input-state-output
KCL	Kirchhoff's current law
KVL	Kirchhoff's voltage law
NMES	networked multi-energy system
ODE	ordinary differential equation
OSEIP	output strictly equilibrium-independent passive/ output strict equilibrium-independent passivity
OSP	output strictly passive/output strict passivity
PBC	passivity-based control
PDE	partial differential equation
PHS	port-Hamiltonian system
PI	proportional-integral
RES	renewable energy source
RMS	root-mean-square
SISO	single-input single-output
VSC	voltage-source converter
VSI	voltage-source inverter
w.r.t.	with respect to
ZIP	constant impedance, constant current, constant power
ZSO	zero-state observable

Latin Letters

Symbol	Description
b_{il}	element of the incidence matrix of a digraph \mathcal{G}
B	incidence matrix of a digraph \mathcal{G}
C	capacitance
C_v	flow capacity of a valve
d	interaction (coupling) input variable
\mathbf{d}	interaction (coupling) input vector
f_0	nominal frequency of an AC power system
f_v	valve characteristic
\mathbf{f}	system dynamics
G	input matrix of a port-Hamiltonian system
h	interaction output function
H	Hamiltonian of a port-Hamiltonian system
I_i	filter current of a distributed generation unit at node i
$I_{L,i}$	load current of a load at node i
$I_{N,i}$	net-current injected at node i into a power system
I_P	constant current load parameter for active power
I_Q	constant current load parameter for reactive power
\mathbf{I}^{dq}	dq current vector
J	volume inertia of water in a pipe/pump
\mathbf{J}	interconnection matrix of a port-Hamiltonian system
k_1	state feedback control parameter (see also k_2, k_3)
k_p	proportional control parameter for a converter controller
K_p	proportional control parameter for a pump controller
\mathbf{K}	interaction matrix of a port-Hamiltonian system
\mathbf{K}_{11}	multivariable state feedback control parameter matrix (see also $\mathbf{K}_{12}, \mathbf{K}_{13}$)
L	inductance
m	number of interaction inputs/outputs
\mathbf{M}	interconnection matrix of an autonomous, networked system
n	number of states
n_P	voltage index parameter of an exponential for active power
n_Q	voltage index parameter of an exponential for reactive power
N	number of subsystems
p	pressure
P	active power
P_P	constant power load parameter for active power
P_Q	constant power load parameter for reactive power
q	volume flow rate
Q	reactive power
Q_I	integrator control parameter

Symbol	Description
Q	state weight matrix used in a quadratic storage function
r	integrator co-state variable
\mathbf{r}	integrator co-state vector
R	resistance
\hat{R}	assigned filter resistance
R^{P}	assigned pump resistance
\mathbf{R}	dissipation matrix of a port-Hamiltonian system
s	valve stem position
S	storage function
S_{L}	instantaneous complex power of a load
t	time
u	control input variable
u_{v}	virtual control input of a valve
\mathbf{u}	control input vector
V	DC voltage or amplitude of an instantaneous voltage vector in dq coordinates
V_0	nominal voltage (DC) or nominal phase-to-phase RMS voltage (three-phase AC)
V_i	voltage at node i
$V_{\text{S},i}$	converter output voltage of the distributed generation unit at node i
\mathbf{V}^{dq}	dq voltage vector
x	state variable
\mathbf{x}	state vector
$\hat{\mathbf{x}}$	closed-loop equilibrium state vector
\mathbf{X}	auxilliary voltage controller matrix [Nahata and Ferrari-Trecate, 2019]
y	output variable
\mathbf{y}	output vector
Y_{P}	active power constant impedance load parameter
\tilde{Y}_{P}	active power constant impedance load parameter for voltages below $0.7 V_0$
Y_{Q}	reactive power constant impedance load parameter
\tilde{Y}_{Q}	reactive power constant impedance load parameter for voltages below $0.7 V_0$
z	interaction (coupling) output variable
\mathbf{z}	interaction (coupling) output vector
\mathbf{Z}	auxilliary voltage controller matrix [Nahata and Ferrari-Trecate, 2019]

Greek Letters

Symbol	Description
λ	pressure losses inside pipes
μ	pressure losses due to valves
ρ	output function for OSP/OSEIP
χ	state variable after coordinate transformation
\mathcal{X}	state vector after coordinate transformation
ψ	dissipation rate
ω_0	rotating frequency of a dq coordinate frame

Calligraphic and Blackboard Bold

Symbol	Description
\mathcal{C}	set of capacitor nodes
\mathcal{D}	set of distributed generation units (electrical)/ distributed heat generation units (heat)
\mathcal{E}	set of edges of a digraph \mathcal{G}
\mathbb{E}	set where the time derivative of the storage function/Lyapunov function is zero
\mathcal{G}	digraph
\mathcal{H}	set of pressure holding units
\mathcal{L}	set of loads/consumers
\mathcal{M}	set of mixing connections
\mathbb{M}	largest invariant set contained in \mathbb{E}
\mathbb{N}	set of natural numbers
\mathcal{P}	set of power lines/pipes
\mathcal{R}	nonlinear damping function of a port-Hamiltonian system
\mathbb{R}	set of real numbers
\mathcal{V}	set of nodes of a digraph \mathcal{G}
\mathcal{X}	state space
$\bar{\mathcal{X}}$	state equilibrium set

Indices and Exponents

Symbol	Description
\square_{AC}	variable/function/etc. corresponding to the complete AC power system under consideration
\square_{boost}	set related to pipes/consumers with booster pumps
\square_c	variable/function/etc. corresponding to a controller
\square^d	d-component of a vector/function in dq coordinates
\square^{dq}	vector/function in dq coordinates or set related to variables in dq coordinates
\square_{DC}	variable/function/etc. corresponding to the complete DC power system under consideration
\square_{DHN}	variable/function/etc. corresponding to the complete district heating network under consideration
$\square_{\mathcal{E}}$	variable/function/etc. corresponding to all edge subsystems of a digraph
\square_{EXP}	set related to exponential loads
\square^f	variable/function/etc. related to a flow-controlled pump
\square_{feed}	set related to distributed (heat) generation units in grid-feeding mode
\square_{form}	set related to distributed (heat) generation units in grid-forming mode
\square_i	variable/function/etc. corresponding to a node subsystem i
\square_k	variable/function/etc. corresponding to a general (edge or node) subsystem k
\square_l	variable/function/etc. corresponding to an edge subsystem l
\square_L	variable/function/etc. related to a load
\square_{NMES}	variable/function/etc. corresponding to the complete networked multi-energy system under consideration
\square^P	variable/function/etc. related to a pressure-controlled pump
\square_P	load parameter related to active power
\square_P	variable/function/etc. related to a pump
\square^q	q-component of a vector/function in dq coordinates
\square_Q	load parameter related to reactive power
\square_{SEIP}	set of subsystems that are strictly EIP
\square_{Th}	set of subsystems that fulfill the conditions of Theorem 3.1
\square^v	variable/function/etc. related to a flow-controlled valve
\square_v	variable/function/etc. related to a valve
\square_{valve}	set related to distributed heat generation units/consumers with valve-based volume flow regulation
\square_{VSP}	set related to distributed heat generation units/consumers with volume flow regulation based on variable-speed pumps
\square_v	variable/function/etc. corresponding to all node subsystems of a digraph
\square_{ZIP}	set related to ZIP loads
\square_0	nominal (e.g., power, voltage, pressure, etc.)

Symbol	Description
$\square_{\geq 0}$	set of positive real/natural numbers
$\square_{> 0}$	set of strictly positive real/natural numbers
$\bar{\square}$	steady-state variable/vector
\square^*	desired setpoint or vector of setpoints to be established in steady state
$\dot{\square}$	time derivative
$\hat{\square}$	variable/function/etc. related to a closed-loop (sub)-system
$\tilde{\square}$	auxiliary superscript to avoid unclear overloading of notation

List of Figures

1.1	Thesis outline	6
4.1	Digraph of a DC power system based on a CIGRE AC benchmark network	47
4.2	Circuit diagram of a DGU in a DC power system	48
4.3	Circuit diagram of a load node in a DC power system	49
4.4	DC simulation: node voltages in Scenario A	70
4.5	DC simulation: DGU and load currents in Scenario A	70
4.6	DC simulation: zoomed in voltage and current errors in Scenario A	71
4.7	DC simulation: power line currents in Scenario A	71
4.8	DC simulation: node voltages in Scenario B	73
4.9	DC simulation: DGU and load currents in Scenario B	73
4.10	DC simulation: zoomed in voltage and current errors in Scenario B	74
4.11	DC simulation: power line currents in Scenario B	74
5.1	Digraph of an AC power system based on a CIGRE AC benchmark network	81
5.2	Circuit diagram of a DGU in an AC power system	83
5.3	Circuit diagram of a load node in an AC power system	84
5.4	AC simulation: node voltages in Scenario A	112
5.5	AC simulation: DGU and load currents in Scenario A	113
5.6	AC simulation: power line currents in Scenario A	114
5.7	AC simulation: DGU output and load currents in Scenario A	114
5.8	AC simulation: node voltages in Scenario B	117
5.9	AC simulation: DGU and load currents in Scenario B	118
5.10	AC simulation: power line currents in Scenario B	119
6.1	Hydraulic schematic of a DHN with multiple DGUs and three temperature layers	129
6.2	Digraph of the exemplary DHN from Figure 6.1	129
6.3	Temperature and hydraulic layers of 2 nd , 3 rd , and 4 th generation DHNs	130
6.4	Illustration of a DHN with three temperature and two hydraulic layers	130
6.5	Equivalent circuit of a linear, second-order approximation of pump dynamics	132
6.6	Hydraulic schematic of a pipe with optional booster pump	135
6.7	Equivalent circuit of a hydraulic pipe model with optional booster pump	135
6.8	Hydraulic schematic of a DGU with pressure holding unit	136
6.9	Equivalent circuit of the hydraulic model of a DGU	136
6.10	Hydraulic schematic of a consumer with optional pump	137

6.11	Equivalent circuit of the hydraulic model of a consumer with optional pump	137
6.12	Hydraulic schematic of a mixing connection	138
6.13	Equivalent circuit of the hydraulic model of a mixing connection	138
6.14	DHN simulation: pump pressures in Scenario A	159
6.15	DHN simulation: controlled volume flow rates in Scenario A	160
6.16	DHN simulation: pump pressures in Scenario B	161
6.17	DHN simulation: controlled volume flow rates in Scenario B.	161
B.1	Generalized RLC equivalent circuit diagram	187

List of Tables

4.1	Simulation parameters for the DC power system simulation	68
4.2	Setpoints for the DC power system simulation	68
4.3	ZIP load parameters for the DC power system simulation	68
4.4	Exponential load parameters for the DC power system simulation	69
5.1	Simulation parameters for the AC power system simulation	108
5.2	Setpoints for the AC power system simulation	109
5.3	ZIP load parameters for the AC power system simulation	109
5.4	Exponential load parameters for the AC power system simulation	109
6.1	Simulation parameter values for the DHN simulation	157
6.2	Pipe lengths for the DHN simulation	158
6.3	Pressure and volume flow rate setpoints for the DHN simulation	158
A.1	Correspondences between generalized and physical variables	179

References

- Ajala, O., Domínguez-García, A., Sauer, P., and Liberzon, D. (2020). A library of second-order models for synchronous machines. *IEEE Transactions on Power Systems*, 35(6):4803–4814.
- Akagi, H., Watanabe, E. H., and Aredes, M. (2007). *Instantaneous Power Theory and Applications to Power Conditioning*. John Wiley & Sons, Inc., Hoboken, New Jersey.
- Andreasson, M., Tegling, E., Sandberg, H., and Johansson, K. H. (2017). Performance and scalability of voltage controllers in multi-terminal hvdc networks. In *2017 American Control Conference (ACC)*, pages 3029–3034.
- Arcak, M., Meissen, C., and Packard, A. (2016). *Networks of Dissipative Systems: Compositional Certification of Stability, Performance, and Safety*. SpringerBriefs in Control, Automation and Robotics. Springer, New York, NY, USA.
- Arghir, C., Jouini, T., and Dörfler, F. (2018). Grid-forming control for power converters based on matching of synchronous machines. *Automatica*, 95:273–282.
- Avila-Becerril, S., Montoya, O. D., Espinosa-Pérez, G., and Garcés, A. (2018). Control of a detailed model of microgrids from a hamiltonian approach. *IFAC-PapersOnLine*, 51(3):187–192.
- Avila-Becerril, S., Silva-Martínez, D., and Espinosa-Pérez, G. (2017). On the robustness of a passivity-based controller for microgrids. *IFAC-PapersOnLine*, 50(1):6648–6653.
- Babazadeh, M. and Karimi, H. (2013). A robust two-degree-of-freedom control strategy for an islanded microgrid. *IEEE Transactions on Power Delivery*, 28(3):1339–1347.
- Baimel, D., Belikov, J., Guerrero, J. M., and Levron, Y. (2017). Dynamic modeling of networks, microgrids, and renewable sources in the dq0 reference frame: A survey. *IEEE Access*, 5:21323–21335.
- Bao, J. and Lee, P. L. (2007). *Process Control: The Passive Systems Approach*. Springer London.
- Beck, H.-P. and Hesse, R. (2007). Virtual synchronous machine. In *2007 9th International Conference on Electrical Power Quality and Utilisation*, pages 1–6.
- Boysen, H. and Thorsen, J. E. (2003). How to avoid pressure oscillations in district heating systems. Danfoss A/S, Nordborg, Denmark.

- Braess, D., Nagurney, A., and Wakolbinger, T. (2005). On a paradox of traffic planning. *Transportation Science*, 39(4):446–450. Translated from the original German: Braess, Dietrich. 1968. Über ein Paradoxon aus der Verkehrsplanung. *Unternehmensforschung* 12 258—268.
- Brand, L., Calvén, A., Englund, J., Landersjö, H., and Lauenburg, P. (2014). Smart district heating networks – a simulation study of prosumers’ impact on technical parameters in distribution networks. *Applied Energy*, 129:39–48.
- Buffa, S., Fouladfar, M. H., Franchini, G., Lozano Gabarre, I., and Andrés Chicote, M. (2021). Advanced control and fault detection strategies for district heating and cooling systems—a review. *Applied Sciences*, 11(1):455.
- Bundesverband der Energie- und Wasserwirtschaft (2023). Redispatch in Deutschland—Auswertung der Transparenzdaten April 2013 bis einschließlich Dezember 2022 [Redispatch in Germany—Evaluation of transparency data from April 2013 until December 2022]. Technical report.
- Bürger, M., Zelazo, D., and Allgöwer, F. (2014). Duality and network theory in passivity-based cooperative control. *Automatica*, 50(8):2051–2061.
- Caliskan, S. Y. and Tabuada, P. (2014). Compositional transient stability analysis of multimachine power networks. *IEEE Transactions on Control of Network Systems*, 1(1):4–14.
- Chandorkar, M., Divan, D., and Adapa, R. (1993). Control of parallel connected inverters in standalone AC supply systems. *IEEE Transactions on Industry Applications*, 29(1):136–143.
- Chertkov, M. and Novitsky, N. N. (2019). Thermal transients in district heating systems. *Energy*, 184:22–33.
- Chicco, G., Riaz, S., Mazza, A., and Mancarella, P. (2020). Flexibility from distributed multienergy systems. *Proceedings of the IEEE*, 108(9):1496–1517.
- Chiniforoosh, S., Jatskevich, J., Yazdani, A., Sood, V., Dinavahi, V., Martinez, J. A., and Ramirez, A. (2010). Definitions and applications of dynamic average models for analysis of power systems. *IEEE Transactions on Power Delivery*, 25(4):2655–2669.
- Council and Parliament of the European Union (2021). Regulation (EU) 2021/1119 of the European Parliament and of the Council of 30 June 2021 establishing the framework for achieving climate neutrality and amending Regulations (EC) No 401/2009 and (EU) 2018/1999 (‘European Climate Law’). *Official Journal of the European Union*, 64(L 243):1–17.
- Cucuzzella, M., Kosaraju, K. C., and Scherpen, J. M. A. (2020). Passivity-based voltage control of DC microgrids: addressing the stability issue of ZIP loads. In *2020 European Control Conference (ECC)*, pages 298–301.

- Cucuzzella, M., Kosaraju, K. C., and Scherpen, J. M. A. (2023). Voltage control of DC microgrids: Robustness for unknown ZIP-loads. *IEEE Control Systems Letters*, 7:139–144.
- Cucuzzella, M., Lazzari, R., Kawano, Y., Kosaraju, K. C., and Scherpen, J. M. A. (2019a). Robust passivity-based control of boost converters in DC microgrids. In *2019 IEEE 58th Conference on Decision and Control (CDC)*, pages 8435–8440.
- Cucuzzella, M., Trip, S., De Persis, C., Cheng, X., Ferrara, A., and van der Schaft, A. (2019b). A robust consensus algorithm for current sharing and voltage regulation in DC microgrids. *IEEE Transactions on Control Systems Technology*, 27(4):1583–1595.
- De Persis, C., Jensen, T. N., Ortega, R., and Wisniewski, R. (2014). Output regulation of large-scale hydraulic networks. *IEEE Transactions on Control Systems Technology*, 22(1):238–245.
- De Persis, C. and Kallešøe, C. S. (2011). Pressure regulation in nonlinear hydraulic networks by positive and quantized controls. *IEEE Transactions on Control Systems Technology*, 19(6):1371–1383.
- Desoer, C. A. and Khu, E. S. (1969). *Basic Circuit Theory*. McGraw-Hill, New York.
- Deutscher Bundestag (2022). Gesetz zu Sofortmaßnahmen für einen beschleunigten Ausbau der erneuerbaren Energien und weiteren Maßnahmen im Stromsektor [Act on Immediate Measures for Accelerated Expansion of Renewable Energies and Further Measures in the Electricity Sector]. *Bundesgesetzblatt I*, 28:1237–1324.
- Donaire, A. and Junco, S. (2009). On the addition of integral action to port-controlled hamiltonian systems. *Automatica*, 45(8):1910–1916.
- Dörfler, F., Bolognani, S., Simpson-Porco, J. W., and Grammatico, S. (2019). Distributed control and optimization for autonomous power grids. In *2019 18th European Control Conference (ECC)*, pages 2436–2453.
- Dörfler, F. and Groß, D. (2023). Control of low-inertia power systems. *Annual Review of Control, Robotics, and Autonomous Systems*, 6(1):415–445.
- Dragičević, T., Lu, X., Vasquez, J. C., and Guerrero, J. M. (2016). DC microgrids – part I: A review of control strategies and stabilization techniques. *IEEE Transactions on Power Electronics*, 31(7):4876–4891.
- Duindam, V., Macchelli, A., Stramigioli, S., and Bruyninckx, H. (2009). *Modeling and Control of Complex Physical Systems*. Springer Berlin Heidelberg.
- Dörfler, F., Simpson-Porco, J. W., and Bullo, F. (2014). Plug-and-play control and optimization in microgrids. In *53rd IEEE Conference on Decision and Control (CDC)*, pages 211–216.

- D'Arco, S., Suul, J. A., and Fosso, O. B. (2015). A virtual synchronous machine implementation for distributed control of power converters in smartgrids. *Electric Power Systems Research*, 122:180–197.
- Etemadi, A. H., Davison, E. J., and Iravani, R. (2012a). A decentralized robust control strategy for multi-DER microgrids—part I: Fundamental concepts. *IEEE Transactions on Power Delivery*, 27(4):1843–1853.
- Etemadi, A. H., Davison, E. J., and Iravani, R. (2012b). A decentralized robust control strategy for multi-DER microgrids—part II: Performance evaluation. *IEEE Transactions on Power Delivery*, 27(4):1854–1861.
- Farrokhhabadi, M., Cañizares, C. A., Simpson-Porco, J. W., Nasr, E., Fan, L., Mendoza-Araya, P. A., Tonkoski, R., Tamrakar, U., Hatziargyriou, N., Lagos, D., Wies, R. W., Paolone, M., Liserre, M., Meegahapola, L., Kabalan, M., Hajimiragha, A. H., Peralta, D., Elizondo, M. A., Schneider, K. P., Tuffner, F. K., and Reilly, J. (2018). Microgrid stability definitions, analysis, and modeling. Technical report, IEEE Power & Energy Society.
- Farrokhhabadi, M., Cañizares, C. A., Simpson-Porco, J. W., Nasr, E., Fan, L., Mendoza-Araya, P. A., Tonkoski, R., Tamrakar, U., Hatziargyriou, N., Lagos, D., Wies, R. W., Paolone, M., Liserre, M., Meegahapola, L., Kabalan, M., Hajimiragha, A. H., Peralta, D., Elizondo, M. A., Schneider, K. P., Tuffner, F. K., and Reilly, J. (2020). Microgrid stability definitions, analysis, and examples. *IEEE Transactions on Power Systems*, 35(1):13–29.
- Federal Ministry for Economic Affairs and Energy (2018). Innovations for the energy transition: 7th energy research programme of the federal government. Technical report, Federal Government of Germany.
- Ferguson, J., Cucuzzella, M., and Scherpen, J. M. (2023). Increasing the region of attraction in DC microgrids. *Automatica*, 151:110883.
- Ferguson, J., Cucuzzella, M., and Scherpen, J. M. A. (2021). Exponential stability and local ISS for DC networks. *IEEE Control Systems Letters*, 5(3):893–898.
- Fiaz, S., Zonetti, D., Ortega, R., Scherpen, J. M. A., and van der Schaft, A. (2013). A port-hamiltonian approach to power network modeling and analysis. *European Journal of Control*, 19(6):477–485.
- Floriduz, A., Tucci, M., Rivero, S., and Ferrari-Trecate, G. (2018). Approximate kron reduction methods for electrical networks with applications to plug-and-play control of AC islanded microgrids. *IEEE Transactions on Control Systems Technology*, pages 1–14. early access.
- Geidl, M. (2007). *Integrated Modeling and Optimization of Multi-Carrier Energy Systems*. PhD thesis, ETH Zürich.

- Glover, J. D., Sarma, M. S., and Overbye, T. (2012). *Power System Analysis & Design, SI Version*. Cengage Learning, 5th edition.
- Gómez-Expósito, A., Conejo, A. J., and Cañizares, C. A., editors (2018). *Electric Energy Systems: Analysis and Operation*. CRC Press, Boca Raton, Florida, U.S., 2nd edition.
- Gong, E., Wang, N., You, S., Wang, Y., Zhang, H., and Wei, S. (2019). Optimal operation of novel hybrid district heating system driven by central and distributed variable speed pumps. *Energy Conversion and Management*, 196:211–226.
- Goppelt, F., Hieninger, T., and Schmidt-Vollus, R. (2018). Modeling centrifugal pump systems from a system-theoretical point of view. In *2018 18th International Conference on Mechatronics – Mechatronika (ME)*, pages 1–8.
- Gu, Y., Li, W., and He, X. (2015). Passivity-based control of DC microgrid for self-disciplined stabilization. *IEEE Transactions on Power Systems*, 30(5):2623–2632.
- Guerrero, J. M., Chandorkar, M., Lee, T., and Loh, P. C. (2013). Advanced control Architectures for intelligent microgrids—part I: decentralized and hierarchical control. *IEEE Transactions on Industrial Electronics*, 60(4):1254–1262.
- Guerrero, J. M., Vasquez, J. C., Matas, J., de Vicuna, L. G., and Castilla, M. (2011). Hierarchical control of droop-controlled AC and DC microgrids—a general approach toward standardization. *IEEE Transactions on Industrial Electronics*, 58(1):158–172.
- Gui, Y., Wei, B., Li, M., Guerrero, J. M., and Vasquez, J. C. (2018). Passivity-based coordinated control for islanded AC microgrid. *Applied Energy*, 229:551–561.
- Han, R., Tucci, M., Martinelli, A., Guerrero, J. M., and Ferrari-Trecate, G. (2019). Stability analysis of primary plug-and-play and secondary leader-based controllers for DC microgrid clusters. *IEEE Transactions on Power Systems*, 34(3):1780–1800.
- Harnefors, L., Wang, X., Yepes, A. G., and Blaabjerg, F. (2016). Passivity-based stability assessment of grid-connected VSCs—an overview. *IEEE Journal of Emerging and Selected Topics in Power Electronics*, 4(1):116–125.
- Hassine, I. B. and Eicker, U. (2014). Control aspects of decentralized solar thermal integration into district heating networks. *Energy Procedia*, 48:1055–1064.
- Hatzargyriou, N., Milanovic, J., Rahmann, C., Ajarapu, V., Cañizares, C., Erlich, I., Hill, D., Hiskens, I., Kamwa, I., Pal, B., Pourbeik, P., Sanchez-Gasca, J., Stankovic, A., Van Cutsem, T., Vittal, V., and Vournas, C. (2021). Definition and classification of power system stability — revisited & extended. *IEEE Transactions on Power Systems*, 36(4):3271–3281.
- Hauschild, S.-A., Marheineke, N., Mehrmann, V., Mohring, J., Badlyan, A. M., Rein, M., and Schmidt, M. (2020). Port-hamiltonian modeling of district heating networks. In *Progress in Differential–Algebraic Equations II*, Differential-Algebraic Equations Forum, pages 333–355, Cham. Springer International Publishing.

- He, X., Zhang, H., and Zahar, A., editors (2020). *Climate Change Law in China in Global Context*. Routledge, Abingdon, New York. (Routledge Advances in Climate Change Research).
- Hertle, H., Pehnt, M., Gugel, B., Dingeldey, M., and Müller, K. (2015). *Wärmewende in Kommunen: Leitfaden für den klimafreundlichen Umbau der Wärmeversorgung [Heat transition in municipalities: Guideline for a climate friendly change of heat supply]*, volume 41 of *Schriften zur Ökologie*. Heinrich-Böll-Stiftung, Berlin, 3 edition.
- Hines, G. H., Arcak, M., and Packard, A. K. (2011). Equilibrium-independent passivity: A new definition and numerical certification. *Automatica*, 47(9):1949 – 1956.
- IEEE 1588 (2008). IEEE standard for a precision clock synchronization protocol for networked measurement and control systems. *IEEE Std 1588-2008 (Revision of IEEE Std 1588-2002)*, pages 1–269.
- IEEE 1588 (2017). IEEE standard profile for use of IEEE 1588 precision time protocol in power system applications. *IEEE Std C37.238-2017 (Revision of IEEE Std C37.238-2011)*, pages 1–42.
- International Energy Agency (2020). *India 2020 Energy Policy Review*. OECD Publishing, Paris.
- Jayawardhana, B., Ortega, R., García-Canseco, E., and Castañós, F. (2007). Passivity of nonlinear incremental systems: Application to PI stabilization of nonlinear RLC circuits. *Systems & Control Letters*, 56(9):618 – 622.
- Jeltsema, D. and Scherpen, J. M. (2009). Multidomain modeling of nonlinear networks and systems. *IEEE Control Systems Magazine*, 29(4):28–59.
- Jensen, T. N. (2012). *Plug and play control of hydraulic networks*. PhD thesis, Aalborg University.
- Johnson, B. B., Dhople, S. V., Hamadeh, A. O., and Krein, P. T. (2014). Synchronization of parallel single-phase inverters with virtual oscillator control. *IEEE Transactions on Power Electronics*, 29(11):6124–6138.
- Jouini, T., Arghir, C., and Dörfler, F. (2016). Grid-friendly matching of synchronous machines by tapping into the DC storage. *IFAC-PapersOnLine*, 49(22):192–197. 6th IFAC Workshop on Distributed Estimation and Control in Networked Systems (NECSYS) 2016.
- Justo, J. J., Mwasilu, F., Lee, J., and Jung, J.-W. (2013). AC-microgrids versus DC-microgrids with distributed energy resources: A review. *Renewable and Sustainable Energy Reviews*, 24:387–405.
- Khalil, H. K. (1996). *Nonlinear Systems*. Prentice Hall, Upper Saddle River, NJ, 2nd edition.

- Khalil, H. K. (2002). *Nonlinear Systems*. Prentice Hall, Upper Saddle River, NJ, 3rd edition.
- Knudsen, T., Trangbaek, K., and Kallesøe, C. S. (2008). Plug and play process control applied to a district heating system. *IFAC Proceedings Volumes*, 41(2):325–330. 17th IFAC World Congress.
- Köfinger, M., Basciotti, D., and Schmidt, R.-R. (2017). Reduction of return temperatures in urban district heating systems by the implementation of energy-cascades. *Energy Procedia*, 116:438–451. 15th International Symposium on District Heating and Cooling, DHC15-2016, 4–7 September 2016, Seoul, South Korea.
- Kolluri, R., Mareels, I., T., A., Brazil, M., de Hoog, J., and Thomas, D. (2018). Stability and active power sharing in droop controlled inverter interfaced microgrids: Effect of clock mismatches. *Automatica*, 93:469 – 475.
- Kölsch, L. (2022). *Dynamic Incentives for Optimal Control of Competitive Power Systems*. PhD thesis, Karlsruher Institut für Technologie (KIT).
- Kosaraju, K. C., Cucuzzella, M., Scherpen, J. M. A., and Pasumathy, R. (2021). Differentiation and passivity for control of brayton–moser systems. *IEEE Transactions on Automatic Control*, 66(3):1087–1101.
- Kosaraju, K. C., Kawano, Y., and Scherpen, J. M. (2019). Krasovskii’s passivity. *IFAC-PapersOnLine*, 52(16):466–471.
- Krug, R., Mehrmann, V., and Schmidt, M. (2021). Nonlinear optimization of district heating networks. *Optimization and Engineering*, 22(2):783–819.
- KSB Aktiengesellschaft (2006). Pump control / system automation.
- Kundur, P. (1994). *Power System Stability and Control*. McGraw-Hill, New York.
- Kundur, P., Paserba, J., Ajarapu, V., Andersson, G., Bose, A., Canizares, C., Hatziargyriou, N., Hill, D., Stankovic, A., Taylor, C., Van Cutsem, T., and Vittal, V. (2004). Definition and classification of power system stability IEEE/CIGRE joint task force on stability terms and definitions. *IEEE Transactions on Power Systems*, 19(3):1387–1401.
- Kwasinski, A. and Krein, P. T. (2007). Passivity-based control of buck converters with constant-power loads. In *2007 IEEE Power Electronics Specialists Conference*, pages 259–265.
- Kwasinski, A. and Onwuchekwa, C. N. (2011). Dynamic behavior and stabilization of dc microgrids with instantaneous constant-power loads. *IEEE Transactions on Power Electronics*, 26(3):822–834.
- Lamaison, N., Bavière, R., Cheze, D., and Paulus, C. (2017). A multi-criteria analysis of bidirectional solar district heating substation architecture. In *Proceedings of SWC2017/SHC2017*, pages 1–11.

- Lasseter, B. (2001). Microgrids [distributed power generation]. In *2001 IEEE Power Engineering Society Winter Meeting*, volume 1, pages 146–149.
- Lennermo, G., Lauenburg, P., and Brand, L. (2014). Decentralised heat supply in district heating systems: Implications of varying differential pressure. In *Proceedings from the 14th International Symposium on District Heating and Cooling*.
- Lennermo, G., Lauenburg, P., and Werner, S. (2019). Control of decentralised solar district heating. *Solar Energy*, 179:307–315.
- Levron, Y., Belikov, J., and Baimel, D. (2018). A tutorial on dynamics and control of power systems with distributed and renewable energy sources based on the dq0 transformation. *Applied Sciences*, 8(9):1661.
- Li, H., Svendsen, S., Gudmundsson, O., Kuosa, M., Rämä, M., Sipilä, K., Blesl, M., Broydo, M., Stehle, M., Pesch, R., Pietruschka, D., Huther, H., Grajcar, M., Jentsch, A., Kallert, A., Schmidt, D., Nord, N., Tereshchenko, T., Park, P., Im, Y., Liu, J., Dag, S., Wiltshire, R., and Bevilacqua, C. (2017). *Future low temperature district heating design guidebook: Final Report of IEA DHC Annex TS1. Low Temperature District Heating for Future Energy Systems*. International Energy Agency.
- Liu, T., Song, Y., Zhu, L., and Hill, D. J. (2022). Stability and control of power grids. *Annual Review of Control, Robotics, and Autonomous Systems*, 5(1):689–716.
- Liu, X., Wu, J., Jenkins, N., and Bagdanavicius, A. (2016). Combined analysis of electricity and heat networks. *Applied Energy*, 162:1238–1250.
- Lund, H., Østergaard, P. A., Chang, M., Werner, S., Svendsen, S., Sorknæs, P., Thorsen, J. E., Hvelplund, F., Mortensen, B. O. G., Mathiesen, B. V., Bojesen, C., Duic, N., Zhang, X., and Möller, B. (2018). The status of 4th generation district heating: Research and results. *Energy*, 164:147–159.
- Lund, H., Werner, S., Wiltshire, R., Svendsen, S., Thorsen, J. E., Hvelplund, F., and Mathiesen, B. V. (2014). 4th generation district heating (4GDH): Integrating smart thermal grids into future sustainable energy systems. *Energy*, 68:1–11.
- Lunze, J. (1992). *Feedback Control of Large-Scale Systems*. Prentice Hall, Upper Saddle River, NJ, USA.
- Machado, J. E., Cucuzzella, M., Pronk, N., and Scherpen, J. M. A. (2022a). Adaptive control for flow and volume regulation in multi-producer district heating systems. *IEEE Control Systems Letters*, 6:794–799.
- Machado, J. E., Cucuzzella, M., and Scherpen, J. M. (2022b). Modeling and passivity properties of multi-producer district heating systems. *Automatica*, 142:110397.
- Machowski, J., Bialek, J. W., and Bumby, J. R. (2008). *Power System Dynamics: Stability and Control*. John Wiley & Sons, Ltd., Chichester, United Kingdom, 2nd edition.

- Malan, A. J., Pfeifer, M., and Hohmann, S. (2022). Distributed coordination of physically-interconnected multi-agent systems with actuated and unactuated agents. *European Journal of Control*, 68:100673. 2022 European Control Conference Special Issue.
- Mancarella, P. (2014). MES (multi-energy systems): An overview of concepts and evaluation models. *Energy*, 65:1–17.
- Martinelli, A., Nahata, P., and Ferrari-Trecate, G. (2018). Voltage stabilization in MVDC microgrids using passivity-based nonlinear control. In *2018 IEEE Conference on Decision and Control (CDC)*, pages 7022–7027.
- Martínez Ceseña, E. A., Loukarakis, E., Good, N., and Mancarella, P. (2020). Integrated electricity-heat-gas systems: Techno-economic modeling, optimization, and application to multienergy districts. *Proceedings of the IEEE*, 108(9):1392–1410.
- Matevosyan, J., Badrzadeh, B., Prevost, T., Quitmann, E., Ramasubramanian, D., Urdal, H., Achilles, S., MacDowell, J., Huang, S. H., Vital, V., O’Sullivan, J., and Quint, R. (2019). Grid-forming inverters: Are they the key for high renewable penetration? *IEEE Power and Energy Magazine*, 17(6):89–98.
- Maurer, J. (2023). *Transactive Control of Coupled Electric Power and District Heating Networks*. PhD thesis, Karlsruher Institut für Technologie (KIT).
- Meng, L., Shafiee, Q., Ferrari-Trecate, G., Karimi, H., Fulwani, D., Lu, X., and Guerrero, J. M. (2017). Review on control of DC microgrids and multiple microgrid clusters. *IEEE Journal of Emerging and Selected Topics in Power Electronics*, 5(3):928–948.
- Milano, F., Dörfler, F., Hug, G., Hill, D. J., and Verbič, G. (2018). Foundations and challenges of low-inertia systems (invited paper). In *2018 Power Systems Computation Conference (PSCC)*, pages 1–25.
- Mohring, J., Linn, D., Eimer, M., Rein, M., and Siedow, N. (2021). District heating networks—dynamic simulation and optimal operation. In *Mathematical Modeling, Simulation and Optimization for Power Engineering and Management*, pages 303–325. Springer.
- Monshizadeh, P., De Persis, C., Stegink, T., Monshizadeh, N., and van der Schaft, A. (2017). Stability and frequency regulation of inverters with capacitive inertia. In *2017 IEEE 56th Annual Conference on Decision and Control (CDC)*, pages 5696–5701.
- Monshizadeh, P., Machado, J. E., Ortega, R., and van der Schaft, A. (2019). Power-controlled hamiltonian systems: Application to electrical systems with constant power loads. *Automatica*, 109:108527.
- Nahata, P. (2021). *Hierarchical Control of Islanded Microgrids with Flexible Structures*. PhD thesis, École Polytechnique Fédérale de Lausanne (EPFL).
- Nahata, P. and Ferrari-Trecate, G. (2019). Passivity-based voltage and frequency stabilization in AC microgrids. In *2019 18th European Control Conference (ECC)*, pages 1890–1895.

- Nahata, P., Soloperto, R., Tucci, M., Martinelli, A., and Ferrari-Trecate, G. (2020). A passivity-based approach to voltage stabilization in DC microgrids with ZIP loads. *Automatica*, 113:108770.
- Nahata, P., Turan, M. S., and Ferrari-Trecate, G. (2022). Consensus-based current sharing and voltage balancing in DC microgrids with exponential loads. *IEEE Transactions on Control Systems Technology*, 30(4):1668–1680.
- Novitsky, N. N., Shalaginova, Z. I., Alekseev, A. A., Tokarev, V. V., Grebneva, O. A., Lutsenko, A. V., Vanteeva, O. V., Mikhailovsky, E. A., Pop, R., Vorobev, P., and Chertkov, M. (2020). Smarter smart district heating. *Proceedings of the IEEE*, 108(9):1596–1611.
- Nussbaumer, T., Thalmann, S., Jenni, A., and Ködel, J. (2020). Handbook on planning of district heating networks. QM Fernwärme and EnergieSchweiz.
- Ojo, Y. and Schiffer, J. (2017). Towards a time-domain modeling framework for small-signal analysis of unbalanced microgrids. In *2017 IEEE Manchester PowerTech*, pages 1–6.
- Ojo, Y., Watson, J. D., Laib, K., and Lestas, I. (2021). A decentralized frequency and voltage control scheme for grid-forming inverters. In *2021 IEEE PES Innovative Smart Grid Technologies Europe (ISGT Europe)*, pages 1–5.
- Olivares, D. E., Mehrizi-Sani, A., Etemadi, A. H., Cañizares, C. A., Iravani, R., Kazerani, M., Hajimiragha, A. H., Gomis-Bellmunt, O., Saeedifard, M., Palma-Behnke, R., Jimeénez-Estévez, G., and Hatziargyriou, N. D. (2014). Trends in microgrid control. *IEEE Transactions on Smart Grid*, 5:1905–1919.
- Ortega, R. and García-Canseco, E. (2004). Interconnection and damping assignment passivity-based control: A survey. *European Journal of Control*, 10(5):432–450.
- Osiadacz, A. J. and Chaczykowski, M. (2020). Modeling and simulation of gas distribution networks in a multienergy system environment. *Proceedings of the IEEE*, 108(9):1580–1595.
- O'Malley, M. J., Anwar, M. B., Heinen, S., Kober, T., McCalley, J., McPherson, M., Muratori, M., Orths, A., Ruth, M., Schmidt, T. J., and Tuohy, A. (2020). Multicarrier energy systems: Shaping our energy future. *Proceedings of the IEEE*, 108(9):1437–1456.
- Paap, G. (2000). Symmetrical components in the time domain and their application to power network calculations. *IEEE Transactions on Power Systems*, 15(2):522–528.
- Pan, Z., Guo, Q., and Sun, H. (2016). Interactions of district electricity and heating systems considering time-scale characteristics based on quasi-steady multi-energy flow. *Applied Energy*, 167:230–243.
- Parliament of Canada (2021). Canadian net-zero emissions accountability act (s.c. 2021, c. 22). <https://laws-lois.justice.gc.ca/eng/acts/C-19.3/>.

- Perez, M., Ortega, R., and Espinoza, J. R. (2004). Passivity-based pi control of switched power converters. *IEEE Transactions on Control Systems Technology*, 12(6):881–890.
- Pfeifer, M. (2022). *Automated Model Generation and Observer Design for Interconnected Systems: A Port-Hamiltonian Approach*. PhD thesis, Karlsruher Institut für Technologie (KIT).
- Riccobono, A. and Santi, E. (2014). Comprehensive review of stability criteria for DC power distribution systems. *IEEE Transactions on Industry Applications*, 50(5):3525–3535.
- Riverso, S., Sarzo, F., and Ferrari-Trecate, G. (2015). Plug-and-play voltage and frequency control of islanded microgrids with meshed topology. *IEEE Transactions on Smart Grid*, 6(3):1176–1184.
- Rocabert, J., Capó-Misut, R., Muñoz-Aguilar, R. S., Candela, J. I., and Rodriguez, P. (2019). Control of energy storage system integrating electrochemical batteries and supercapacitors for grid-connected applications. *IEEE Transactions on Industry Applications*, 55(2):1853–1862.
- Rocabert, J., Luna, A., Blaabjerg, F., and Rodríguez, P. (2012). Control of power converters in ac microgrids. *IEEE Transactions on Power Electronics*, 27(11):4734–4749.
- Rockafellar, R. T. and Wets, R. (1998). *Variational Analysis*. Springer, Berlin.
- Rugh, W. J. (1996). *Linear System Theory*. Prentice-Hall, Inc., Upper Saddle River, NJ, USA, 2nd edition.
- Sadabadi, M. S. and Shafiee, Q. (2020a). Scalable PI voltage stabilization in DC microgrids. *IFAC-PapersOnLine*, 53(2):12882–12887. 21st IFAC World Congress.
- Sadabadi, M. S. and Shafiee, Q. (2020b). Scalable robust voltage control of DC microgrids with uncertain constant power loads. *IEEE Transactions on Power Systems*, 35(1):508–515.
- Sadabadi, M. S., Shafiee, Q., and Karimi, A. (2017). Plug-and-play voltage stabilization in inverter-interfaced microgrids via a robust control strategy. *IEEE Transactions on Control Systems Technology*, 25(3):781–791.
- Sadabadi, M. S., Shafiee, Q., and Karimi, A. (2018). Plug-and-play robust voltage control of DC microgrids. *IEEE Transactions on Smart Grid*, 9(6):6886–6896.
- Schäfer, B., Pesch, T., Manik, D., Gollenstede, J., Lin, G., Beck, H.-P., Witthaut, D., and Timme, M. (2022). Understanding braess’ paradox in power grids. *Nature Communications*, 13, 5396.
- Schiffer, J., Ortega, R., Astolfi, A., Raisch, J., and Sezi, T. (2014). Conditions for stability of droop-controlled inverter-based microgrids. *Automatica*, 50(10):2457–2469.

- Schiffer, J., Zonetti, D., Ortega, R., Stanković, A. M., Sezi, T., and Raisch, J. (2016). A survey on modeling of microgrids—from fundamental physics to phasors and voltage sources. *Automatica*, 74:135–150.
- Scholten, T., De Persis, C., and Tesi, P. (2017a). Modeling and control of heat networks with storage: The single-producer multiple-consumer case. *IEEE Transactions on Control Systems Technology*, 25(2):414–428.
- Scholten, T., Trip, S., and De Persis, C. (2017b). Pressure regulation in large scale hydraulic networks with input constraints. *IFAC-PapersOnLine*, 50(1):5367–5372.
- Sepulchre, R., Janković, M., and Kokotović, P. (1997). *Constructive Nonlinear Control*. Springer London.
- Serra, F. M., Angelo, C. H. D., and Forchetti, D. G. (2017). IDA-PBC control of a DC–AC converter for sinusoidal three-phase voltage generation. *International Journal of Electronics*, 104(1):93–110.
- Shafiee, Q., Dragicevic, T., Vasquez, J. C., and Guerrero, J. M. (2014). Modeling, stability analysis and active stabilization of multiple DC-microgrid clusters. In *2014 IEEE International Energy Conference (ENERGYCON)*, pages 1284–1290.
- Shafiee-Rad, M., Shafiee, Q., Sadabadi, M. S., and Jahed-Motlagh, M. R. (2021). Decentralized voltage stabilization and robust performance satisfaction of islanded inverter-interfaced microgrids. *IEEE Systems Journal*, 15(2):1893–1904.
- Shahbakhsh, A. and Nieße, A. (2019). Modeling multimodal energy systems. *at - Automatisierungstechnik*, 67(11):893–903.
- Simpson-Porco, J. W. (2019). Equilibrium-independent dissipativity with quadratic supply rates. *IEEE Transactions on Automatic Control*, 64(4):1440–1455.
- Simpson-Porco, J. W., Dörfler, F., and Bullo, F. (2013). Synchronization and power sharing for droop-controlled inverters in islanded microgrids. *Automatica*, 49(9):2603–2611.
- Simpson-Porco, J. W., Dörfler, F., and Bullo, F. (2017). Voltage stabilization in microgrids via quadratic droop control. *IEEE Transactions on Automatic Control*, 62(3):1239–1253.
- Sinha, M., Dörfler, F., Johnson, B. B., and Dhople, S. V. (2015). Virtual oscillator control subsumes droop control. In *2015 American Control Conference (ACC)*, pages 2353–2358.
- Sira-Ramirez, H., Perez-Moreno, R., Ortega, R., and Garcia-Esteban, M. (1997). Passivity-based controllers for the stabilization of dc-to-dc power converters. *Automatica*, 33(4):499–513.
- Soloperto, R., Nahata, P., Tucci, M., and Ferrari-Trecate, G. (2018). A passivity-based approach to voltage stabilization in DC microgrids. In *2018 Annual American Control Conference (ACC)*, pages 5374–5379.

- Sommer, T., Mennel, S., and Sulzer, M. (2019). Lowering the pressure in district heating and cooling networks by alternating the connection of the expansion vessel. *Energy*, 172:991–996.
- Spanias, C., Aristidou, P., and Michaelides, M. (2020). A passivity-based framework for stability analysis and control including power network dynamics. *IEEE Systems Journal (Early Access)*, pages 1–11.
- Spanias, C. and Lestas, I. (2019). A system reference frame approach for stability analysis and control of power grids. *IEEE Transactions on Power Systems*, 34(2):1105–1115.
- Stan, G. and Sepulchre, R. (2007). Analysis of interconnected oscillators by dissipativity theory. *IEEE Transactions on Automatic Control*, 52(2):256–270.
- Stræde, B. (1995). Pressure oscillation in district heating installations. Danfoss A/S, Nordborg, Denmark.
- Strunz, K., Abbasi, E., Abbey, C., Andrieu, C., Annakkage, U., Barsali, S., Campbell, R. C., Fletcher, R., Gao, F., Gaunt, T., Gole, A., Hatziargyriou, N., Iravani, R., Joos, G., Konishi, H., Kuschke, M., Lakervi, E., Liu, C., Mahseredjian, J., Mosallat, F., Muthumuni, D., Orths, A., Papathanassiou, S., Rudion, K., Styczynski, Z., and Verma, S. C. (2014). Benchmark systems for network integration of renewable and distributed energy resources. Technical report, CIGRE, Paris, France. C6.04.02.
- The European Commission (2020). Powering a climate-neutral economy: An EU strategy for energy system integration. In *Communication from the Commission to the European Parliament, the Council, the European Economic and Social Committee and Committee of the Regions*, pages 1–21.
- Trangbaek, K., Knudsen, T., and Kallesøe, C. S. (2009). Plug and play process control of a district heating system. In *2009 European Control Conference (ECC)*, pages 4084–4089.
- Trip, S., Scholten, T., and De Persis, C. (2019). Optimal regulation of flow networks with transient constraints. *Automatica*, 104:141–153.
- Tucci, M. and Ferrari-Trecate, G. (2017). Voltage and frequency control in AC islanded microgrids: a scalable, line-independent design algorithm. *IFAC-PapersOnLine*, 50(1):13922–13927. 20th IFAC World Congress.
- Tucci, M. and Ferrari-Trecate, G. (2020). A scalable, line-independent control design algorithm for voltage and frequency stabilization in AC islanded microgrids. *Automatica*, 111:108577.
- Tucci, M., Floriduz, A., Rivero, S., and Ferrari-Trecate, G. (2016a). Plug-and-play control of AC islanded microgrids with general topology. In *2016 European Control Conference (ECC)*, pages 1493–1500.
- Tucci, M., Rivero, S., and Ferrari-Trecate, G. (2018). Line-independent plug-and-play controllers for voltage stabilization in DC microgrids. *IEEE Transactions on Control Systems Technology*, 26(3):1115–1123.

- Tucci, M., Rivero, S., Vasquez, J. C., Guerrero, J. M., and Ferrari-Trecate, G. (2016b). A decentralized scalable approach to voltage control of DC islanded microgrids. *IEEE Transactions on Control Systems Technology*, 24(6):1965–1979.
- United States Congress (2022). Inflation Reduction Act of 2022 (P.L. 117-169). <https://www.congress.gov/bill/117th-congress/house-bill/5376/text>.
- van Cutsem, T. and Vournas, C. (1998). *Voltage Stability of Electric Power Systems*. Kluwer Academic Publishers, Boston, USA.
- van der Heijde, B., Fuchs, M., Tugores, C. R., Schweiger, G., Sartor, K., Basciotti, D., Müller, D., Nytsch-Geusen, C., Wetter, M., and Helsen, L. (2017). Dynamic equation-based thermo-hydraulic pipe model for district heating and cooling systems. *Energy Conversion and Management*, 151:158–169.
- van der Schaft, A. (2017). *L2-Gain and Passivity Techniques in Nonlinear Control*. Springer International Publishing AG, 3rd edition.
- van der Schaft, A. and Jeltsema, D. (2014). Port-hamiltonian systems theory: an introductory overview. *Foundations and Trends in Systems and Control*, 1(2–3):173–378.
- van der Schaft, A. and Stegink, T. (2016). Perspectives in modeling for control of power networks. *Annual Reviews in Control*, 41:119–132.
- Vandermeulen, A., van der Heijde, B., and Helsen, L. (2018). Controlling district heating and cooling networks to unlock flexibility: A review. *Energy*, 151:103–115.
- Volkova, A., Krupenski, I., Ledvanov, A., Hlebnikov, A., Lepiksaar, K., Latšov, E., and Mašatin, V. (2020). Energy cascade connection of a low-temperature district heating network to the return line of a high-temperature district heating network. *Energy*, 198:117304.
- Volkova, A., Reuter, S., Puschnigg, S., Kauko, H., Schmidt, R.-R., Leitner, B., and Moser, S. (2022). Cascade sub-low temperature district heating networks in existing district heating systems. *Smart Energy*, 5:100064.
- Wang, H., Wang, H., and Zhu, T. (2017a). A new hydraulic regulation method on district heating system with distributed variable-speed pumps. *Energy Conversion and Management*, 147:174–189.
- Wang, Y., You, S., Zhang, H., Zheng, W., Zheng, X., and Miao, Q. (2017b). Hydraulic performance optimization of meshed district heating network with multiple heat sources. *Energy*, 126:603–621.
- Watson, J. (2021). *Control and optimization of modern power networks: hybrid AC/DC networks and inverter-based microgrids*. PhD thesis, University of Cambridge.
- Watson, J. D., Ojo, Y., Laib, K., and Lestas, I. (2021). A scalable control design for grid-forming inverters in microgrids. *IEEE Transactions on Smart Grid*, 12(6):4726–4739.

- Watson, J. D., Ojo, Y., Lestas, I., and Spanias, C. (2019). Stability of power networks with grid-forming converters. In *2019 IEEE Milan PowerTech*.
- Wellstead, P. E. (1979). *Introduction to Physical System Modelling*. Academic Press, London.
- Yan, A., Zhao, J., An, Q., Zhao, Y., Li, H., and Huang, Y. J. (2013). Hydraulic performance of a new district heating systems with distributed variable speed pumps. *Applied Energy*, 112:876–885.
- Yu, W., Chen, G., and Cao, M. (2010). Some necessary and sufficient conditions for second-order consensus in multi-agent dynamical systems. *Automatica*, 46(6):1089–1095.
- Zeng, J., Zhang, Z., and Qiao, W. (2014). An interconnection and damping assignment passivity-based controller for a dc–dc boost converter with a constant power load. *IEEE Transactions on Industry Applications*, 50(4):2314–2322.
- Zhang, M., Wu, Q., Wen, J., Lin, Z., Fang, F., and Chen, Q. (2021). Optimal operation of integrated electricity and heat system: A review of modeling and solution methods. *Renewable and Sustainable Energy Reviews*, 135:110098.
- Zhao, J. and Dörfler, F. (2015). Distributed control and optimization in DC microgrids. *Automatica*, 61:18–26.
- Zhong, Q. (2013). Robust droop controller for accurate proportional load sharing among inverters operated in parallel. *IEEE Transactions on Industrial Electronics*, 60(4):1281–1290.
- Zhong, Q. and Stefanello, M. (2017). Port-hamiltonian control of power electronic converters to achieve passivity. In *2017 IEEE 56th Annual Conference on Decision and Control (CDC)*, pages 5092–5097.
- Zonetti, D., Ortega, R., and Benchaib, A. (2015). Modeling and control of HVDC transmission systems from theory to practice and back. *Control Engineering Practice*, 45:133–146.
- Zonetti, D., Saoud, A., Girard, A., and Fribourg, L. (2019). Decentralized monotonicity-based voltage control of dc microgrids with zip loads. *IFAC-PapersOnLine*, 52(20):139–144. 8th IFAC Workshop on Distributed Estimation and Control in Networked Systems (NECSYS) 2019.

List of Publications and Supervised Theses

Journal Articles

- **Felix Strehle**, Pulkit Nahata, Albertus J. Malan, Sören Hohmann, and Giancarlo Ferrari-Trecate (2022b), *A unified passivity-based framework for control of modular islanded AC microgrids*, IEEE Transactions on Control Systems Technology, 30(5):1960–1976
- Lukas Kölsch, Pol Jané Soneira, **Felix Strehle**, and Sören Hohmann (2021), *Optimal control of port-hamiltonian systems: A continuous-time learning approach*, Automatica, 130:109725

Refereed Conference Articles

- Albertus J. Malan, Lukas Rausche, **Felix Strehle**, and Sören Hohmann (2023), *Port-Hamiltonian modelling for analysis and control of gas networks*, 22nd IFAC World Congress, Yokohama, Japan
- **Felix Strehle**, Juan E. Machado, Michele Cucuzzella, Albertus J. Malan, Jacquélien M.A. Scherpen, and Sören Hohmann (2022a), *Port-hamiltonian modeling of hydraulics in 4th generation district heating networks*, 2022 IEEE 61st Conference on Decision and Control (CDC), Cancún, Mexico
- **Felix Strehle**, Jonathan Vieth, Martin Pfeifer, and Sören Hohmann (2021), *Passivity-based stability analysis of hydraulic equilibria in 4th generation district heating networks*, 7th IFAC Workshop on Lagrangian and Hamiltonian Methods for Nonlinear Control, Berlin, Germany
- Martin Pfeifer, Sven Caspart, **Felix Strehle**, and Sören Hohmann (2021), *Full-order observer design for a class of nonlinear port-Hamiltonian systems*, 7th IFAC Workshop on Lagrangian and Hamiltonian Methods for Nonlinear Control, Berlin, Germany
- Oliver Stark, **Felix Strehle**, and Sören Hohmann (2021), *Convergence analysis of the short-memory principle for fractional models*, 2021 European Control Conference, 2021, Delft, The Netherlands
- **Felix Strehle**, Albertus J. Malan, Stefan Krebs, and Sören Hohmann (2020a), *Passivity conditions for plug-and-play operation of nonlinear static AC loads*, 21st IFAC World Congress, Berlin, Germany

- **Felix Strehle**, Albertus J. Malan, Stefan Krebs, and Sören Hohmann (2020b), *A scalable port-Hamiltonian approach to plug-and-play voltage stabilization in DC microgrids*, 2020 IEEE Conference on Control Technology and Applications (CCTA), Montreal, Canada
- **Felix Strehle**, Albertus J. Malan, Stefan Krebs, and Sören Hohmann (2019), *A port-hamiltonian approach to plug-and-play voltage and frequency control in islanded inverter-based AC microgrids*, 2019 IEEE 58th Conference on Decision and Control (CDC), 2019, Nice, France
- **Felix Strehle**, Martin Pfeifer, Lukas Kölsch, Charlotte Degünther, Johannes Ruf, Lisa Andresen, and Sören Hohmann (2018), *Towards port-Hamiltonian modeling of multi-carrier energy systems: a case study for a coupled electricity and gas distribution system*, 9th Vienna International Conference on Mathematical Modelling (MATHMOD), 2018, Vienna, Austria

Invited Talks and Sessions

- **Felix Strehle**, Sören Hohmann, Juan E. Machado, Michele Cucuzzella, and Jacquélien M.A. Scherpen, *Recent advances in modeling and control of networked energy systems*, Invited session at the 22nd IFAC World Congress, 2023, Yokohama, Japan
- **Felix Strehle**, Juan E. Machado, Michele Cucuzzella, Albertus J. Malan, Jacquélien M.A. Scherpen, and Sören Hohmann, *A Unifying passivity-based framework for hydraulic control in district heating networks*, VDI/VDE GMA-Fachausschuss 1.40 "Systemtheorie und Regelungstechnik", 2022, Anif, Austria
- **Felix Strehle**, Albertus J. Malan, Stefan Krebs, and Sören Hohmann, *Passivitätsbasierte Plug-and-Play Spannungs- und Frequenzregelung in inverterbasierten Stromnetzen, Zukünftige Stromnetze*, 2020, Berlin, Germany
- **Felix Strehle**, *Passivity-based plug-and-play voltage and frequency control in islanded inverter-based microgrids*, Seminar talk at the Automatic Control Laboratory, 2019, EPFL, Switzerland
- **Felix Strehle**, Martin Pfeifer, Stefan Krebs, and Sören Hohmann, *A scalable port-Hamiltonian approach to plug-and-play voltage stabilization in DC microgrids*, 2nd International Conference on Future Electric Power Systems and the Energy Transition (FEPSET), 2019, Champéry, Switzerland

Supervised Student Theses

- Jonathan Vieth, *Modular Stability Analysis of Interconnected System: a Port-Hamiltonian Approach*, Master's thesis, Institute of Control Systems (IRS), Karlsruhe Institute of

Technology (KIT), 2022

- Raphael Stöckner, *Hydraulic Modeling and Passivity-Based Control of Next Generation District Heating Networks*, Bachelor's thesis, Institute of Control Systems (IRS), Karlsruhe Institute of Technology (KIT), 2022
- Mohamed Fares Radouche *Modular Stability Analysis and System Design via Passivity Indices*, Bachelor's thesis, Institute of Control Systems (IRS), Karlsruhe Institute of Technology (KIT), 2021
- Stephan Zeitvogel, *Passivity-Based Stability Analysis and Voltage Tracking Control of AC Microgrids*, Master's thesis, Institute of Control Systems (IRS), Karlsruhe Institute of Technology (KIT), 2020
- Chidan Zhu, *Actuator Saturation of Passivity-Based Plug-and-Play Controllers in AC Microgrids*, Master's thesis, Institute of Control Systems (IRS), Karlsruhe Institute of Technology (KIT), 2019
- Albertus Johannes Malan, *Plug-and-Play Control and Stability Analysis of Inverter-Based AC Microgrids*, Master's thesis, Institute of Control Systems (IRS), Karlsruhe Institute of Technology (KIT), 2019
- Patrick Armbruster, *Passivitätsbasierte Plug-and-Play Spannungsregelung von DC Microgrid Clustern*, Bachelor's thesis, Institute of Control Systems (IRS), Karlsruhe Institute of Technology (KIT), 2019
- Manuel Dupuis, *Regelungstechnische Analyse und Modellierung von Systemdienstleistungen für sektorgekoppelte Energiesysteme*, Bachelors's thesis, Institute of Control Systems (IRS), Karlsruhe Institute of Technology (KIT), 2018

